Turbulent Flows and Simple Behaviours. Their effect on Strategic Determinations of Population Persistence.

Steven John Holmes

Submitted for

Degree of Doctor of Philosophy,

Department of Statistics and Modelling Science,

University of Strathclyde.

November 2001

Acknowledgements

My supervisor throughout this thesis has been Professor Bill Gurney. I have learnt much and his guidance and enthusiasm has been constant. Also special mention should go to Dougie Speirs. His work on persistence in systems with net advection became the basis on which this thesis was built. It was also Dougie who first arrived at the analytic solution to the one dimensional problem with clinging.

Many thanks to Ian Thurlbeck who showed great restraint and good humour on those occasions when it was discovered I had been unwittingly thrashing the network. Further, he was willing to postpone his dream of hardware rationalisation until after this project was finished. Also to Roy Veitch, who was always willing to offer support of the humanitarian kind.

I have thoroughly enjoyed the company of fellow members within the department. Special mention must go those with whom I shared a room; Colin Selfridge, Glenn Marion, (who heard his name so often just before some dumb maths question), Richard Hedger and Sotirios Sabanis. Beyond this I name no names for fear of neglecting someone but thank all for their companionship.

I was supported in this work by a studentship from the Natural Environment Research Council and I am thankful to the STAMS department for offering that studentship to myself.

Above all I wish to thank family. To my parents, who have always let me follow my own path and to my wife Minori. She has shown much patience and trust and for her quiet and unheralded support and sacrifices I wish to express my gratitude.

Abstract

All non-oceanic lotic habitats, chiefly streams, rivers, estuaries and fjords, have a net seaward water movement. If individuals from a population have no means of upstream movement, either through their own actions or from some other mechanism, then any advection, (no matter how small), will result in that population being moved downstream and eventual removal from the system. Many organisms with little or no swimming ability, however, manage to persist in such systems. This phenomenon has been termed the drift paradox.

Organisms in a one dimensional domain are considered initially, using an advection, diffusion population balance equation with exponential in situ growth in the absence of movement. Building upon the results of Speirs and Gurney (2001) new analytic results were obtained for an extension to the model which considered the effect of organisms repeatedly transferring between the drift and a static benthic state, an approximation to the case for benthic stream invertebrates. Numerical modelling, through use of a discrete space-time approach, was employed to investigate swimming against the flow. For constant upstream swimming it was found possible to use the previously developed analytic results with minor modification. Movement against a time average of prior net water movement was found a considerably less successful strategy.

Rivers with non-chaotic flow will exhibit a well defined vertical gradient in their downstream advection due to bottom friction and viscosity. This presents the possibility of a near benthic flow refugia in systems where the upper water column flows too fast to allow persistence. The refugia can only exist, however, so long as vertical turbulent diffusion does not remove individuals from this region at too fast a rate. Virtually all fresh water organisms meanwhile, have a negative buoyancy. Semi-analytic results were derived to determine the extent to which a constant advection toward the bottom could increase the value of 'critical' vertical diffusion at which mixing becomes too rapid for persistence. Results were compared to a two dimensional version of the discrete space-time numerical model. Predictions

of the extent of a benthic refugia were made for the River Meuse Belgium, a river considered to contain a resident population of phytoplankton, using the semi-analytic results. Predictions of critical vertical diffusion were contrasted with hydraulic engineering approximations of vertical turbulent diffusion over a range of river discharge values.

In tidal bodies it is the net advections over a tidal cycle that become important to the issue of persistence. Strategic representations of both a coastal plain estuary and a fjord were investigated. Additional parameters become significant in determining the net advection of these systems. In particular the magnitude and gradient of density differences caused by the interaction of fresh water river runoff and saline coastal water. To determine the flow fields for these complex systems a primitive equation fluid dynamics model, the Princeton Ocean Model (POM), was used and particle tracking was employed to establish redistribution matrices for two dimensional, (x,z), slices through these systems. Assuming that parameters affecting the vertical movement of organisms relative to the deterministic flow field are likely to be of greatest significance to persistence, results were investigated for a range of organismal vertical diffusion believed to bracket values to be found in the field. The degree of persistence was re-evaluated on introduction of a constant sinking velocity and depth dependent growth rate, both individually and in combination.

Contents

List of Symbols

The following table provides a list of symbols where the symbols are used a number of times or where the symbol is quite standard within the literature. Other symbols are defined locally in the text. Bold typeface denotes vectors.

A_M	Coefficient of horizontal kinematic eddy viscosity used within computational fluid dynamics package.
B	Width of a river.
$B_{x',t}$	Redistribution matrix term: number of survivors and descendents of the population of quadrant x' at time t who are present at time $t + \Delta t$.
C	Mass concentration.
$C(\tau)$	Coefficient of variation for a normal distribution over the time τ.
C_g	Coefficient of variation for a normal distribution over the time required for a population experiencing exponential growth to increase by a factor of $\sqrt{e} \approx 65\%$.
C_p	Specific heat capacity of a fluid at constant pressure.
c_i	Phase speed of internal gravity wave.
D	Time dependent total depth below the free surface.
D	Coefficient of diffusion used when describing Fikian diffusion.
d_{mx}	Displaced tent distribution parameter: associated with diffusion in x direction.
d_{mz}	Displaced tent distribution parameter: associated with diffusion in z direction.
d_{ox}	Displaced tent distribution parameter: associated with advection in x direction.
d_{oz}	Displaced tent distribution parameter: associated with advection in z direction.
F_m	Densimetric Froude number.
g	Acceleration due to gravity.
H	Mean depth below the free surface.

H'	Rate of change of surface elevation with distance due to river flow.
$\mathbf{J}(x, y, z, t)$	Net rate of flow of individuals past the position (x, y, z).
$I(z)$	Light intensity at a depth z below the surface.
I_o	Light intensity at the surface.
K_M	Coefficient of vertical kinematic eddy viscosity used within computational fluid dynamics package.
K_H	Coefficient of vertical kinematic scalar diffusivity used within computational fluid dynamics package.
K_x, K_y, K_z	Coefficient of eddy diffusion of scalars in x, y and z directions.
k	Population carrying capacity.
L	Length of a system/domain.
L_c	Critical system length – For given per-capita growth rate, advection rate and diffusion constant, length of system at which population transitional between persistence and washout.
L_c(Ch6)	$\equiv H - z_c$ – Distance form the benthos to the critical depth.
L_D	$\equiv \sqrt{2\Phi\Delta t}$ – The root mean square diffusive dispersal distance travelled by an individual during the update increment of the discrete space-time population model.
L_b	Length of water column nearest benthos in which a population will persist in the absence of vertical diffusion.
L_d	$\equiv \sqrt{\Phi r^{-1}}$ – The root mean square diffusive dispersal distance travelled by an individual during the time required for a population experiencing exponential growth to increase by $\approx 65\%$.
$m(x, t)$	Population in the benthos at location x and time t.
N	Number of tracks, (from a given cell), used by particle tracking program.
$N(x, t)$	Total population at location x and time t if population is split between the benthos and drift.
N_x, N_y, N_z	Coefficient of eddy viscosity in x, y and z directions – turbulent equivalent to absolute, (dynamic), viscosity.
n_x, n_y, n_z	Coefficient of eddy viscosity in x, y and z directions – turbulent equivalent to kinematic viscosity.

n_{man}	Manning roughness coefficient.
$n(x,t)$	Population in the drift at location x and time t.
$\mathbf{n}(x,y,z)$	Normal to a geometrical surface element within a fluid.
P	$p - \rho g z$ – Modified pressure term.
P_w	Wetted perimeter of a river channel.
p	Local pressure force acting on a fluid element.
$p(n)$	Per-capita growth rate of a population n.
$p(w)$	Probability of an individual being in the water column. Also proportion of a population in water column at any one time.
psu	Practical salinity units, (salinity concentration).
$\mathbf{p}(x,y,z)$	Position vector.
Q_F	Total fresh water discharge.
Q_f	Fresh water discharge, (per unit width).
q	Mass flux.
Ri_E	Estuarine Richardson number.
$R_{p\prime,p}$	Redistribution matrix term: proportion of population starting in cell centred on position vector $p\prime$ that move to a cell with centre p over a time interval Δt.
$R_{x\prime,x}$	Redistribution matrix term(1D): proportion of population in quadrant x' that move to quadrant x over a time interval Δt.
r	Population intrinsic growth rate.
S	Salinity.
S_o	Mean salinity in an estuarine cross section.
T	Tidal period.
t	Time.
Δt	Time interval of discrete space-time representation of population model.
δt	Time step of particle tracking algorithm.
U_*	Shear velocity, (in some texts known as friction velocity and denoted U_f).
U_f	Cross-sectionally averaged net velocity due to fresh water discharge.

U_R	Eulerian residual velocity.
U_s	Net surface current (in a tidal estuary).
U_T	Root mean squared (rms) tidal velocity.
V_d	$\equiv 2rL_d \equiv 2\sqrt{\Phi r}$ – The equivalent velocity if an organism travels a diffusive dispersal distance L_d during the time required for a population experiencing exponential growth to increase by $\approx 65\%$.
V_c	Critical velocity – For given per-capita growth rate, system length and diffusion constant, advection rate at which population transitional between persistence and washout.
V_R	Water velocity at the free surface due to river run-off; river surface velocity.
$\hat{V}_R$	Mean river velocity.
V_r	Horizontal velocity generated by river flow.
V_s	Swimming velocity; 1D simulations.
V_s	Sinking velocity; 2D simulations.
V_T	Maximum water velocity at the free surface due to tidal action.
V_t	Horizontal velocity generated by tidal flow.
V_x	Water velocity in x direction.
V_z	Water velocity in z direction.
$\mathbf{V}(x, y, z)$	Velocity vector in Cartesian co-ordinates.
x'	Source cell of redistribution matrix.
z_c	Critical depth. Depth at which the 1D population model indicates the transition from persistence to washout when applied to unconnected horizontal slices in a 2D domain with vertical advection gradient.
z_{eu}	Euphotic depth; depth below surface at which the gross photosynthetic rate becomes zero.
z_{rc}	Depth at which depth dependent intrinsic growth rate becomes zero.
$< >$	Averaging of a measured quantity over the period of a tidal cycle.

Greek symbols

α	Rate of movement from the benthos to the drift.
β	Rate of movement from the drift to the benthos.
Δt	Time interval of discrete space-time representation of population model.
δt	Time step of particle tracking algorithm.
Δx	Size of cell (x direction) in fluid dynamics, particle tracking or population model.
Δ_x	Net displacement in x direction of a neutrally buoyant particle over a tidal period.
Δz	Size of cell (z direction) in fluid dynamics, particle tracking or population model.
Δ_z	Net displacement in z direction of a neutrally buoyant particle over a tidal period.
ε	Light attenuation, (extinction) coefficient.
ζ	$\equiv e^{-r\Delta t}$ – Term in solution to the logistic growth equation.
η	Distance above mean free surface level; surface elevation.
η_r	Surface elevation associated with river flow.
η_t	Surface elevation associated with tidal flow.
θ	Ratio between population density in the benthos and that in the drift at any given longitudinal location.
κ	von Karman constant.
Λ	Long term growth rate.
Λ_{br}	Long term growth rate in the benthic region of a river.
Λ_{sr}	Long term growth rate in the surface region of a river.
λ	Scaled long term growth rate.
μ	Coefficient of absolute, (dynamic), viscosity of a fluid.
ν	$\equiv \mu/\rho$ – Coefficient of kinematic viscosity of a fluid.
	Correction factor applied to diffusion coefficient used in particle tracking.

ρ	Fluid density.
σ	Co-ordinate expressing depth as the proportional distance from the free surface to the bottom.
π	Ratio circumference/diameter.
τ	Stress tensor.
Φ_T	Diffusion coefficient provided to a tracking algorithm such that tracking a large ensemble of particles over the period Δt, (modelling diffusive displacement as a white noise velocity with power spectral density $\sqrt{2\Phi_T}$), and binning the resulting end locations into discrete cells, results in redistribution kernel with variance $2\Phi\Delta t$.
Φ_x	Coefficient of (particle or organismal) diffusion/dispersion in longitudinal direction.
Φ_z	Coefficient of (particle or organismal) diffusion/dispersion in vertical direction.
ϕ	Displaced tent distribution parameter: Ensures $\sum_{\mathbf{p}} R_{\mathbf{p}\prime,\mathbf{p}} = 1$.
ϕ	z dependent component of horizontal tidal velocity.
∇	The gradient operator $\left(\frac{\partial}{\partial x}, \frac{\partial}{\partial y}, \frac{\partial}{\partial z}\right)$.
$\nabla\cdot$	The divergence operator.
$\nabla\times$	The curl operator.
∇^2	The Laplacian operator $\left(\frac{\partial^2}{\partial x^2}, \frac{\partial^2}{\partial y^2}, \frac{\partial^2}{\partial z^2}\right)$.
D/Dt	$\equiv \frac{\partial}{\partial t} + V_x\frac{\partial}{\partial x} + V_y\frac{\partial}{\partial y} + V_z\frac{\partial}{\partial z}$ – Rate of change 'following the fluid'. Also known as the 'substantive derivative', 'particle derivative' or 'material derivative'.

Part I

Introduction

Chapter 1

The problem of persistence; the 'Drift Paradox'

1.0.1 The problem of the 'Drift Paradox'

All non-oceanic lotic habitats, chiefly streams, rivers, estuaries and fjords, have a net seaward water movement. If individuals from a population have no real means of upstream movement, either through their own actions or from some other mechanism, then any advection, (no matter how small), will result in that population being moved downstream and eventual removal from the system. Many organisms with little or no swimming ability, however, manage to persist in systems with such a continuous net advection. This phenomenon has been termed the drift paradox, (Hershey, Pastor, Peterson, and Kling 1993). Most obviously, this paradox applies to organisms living permanently in the water column, (the pelagic environment), such as free floating phytoplankton and zooplankton in estuaries and fjords. The issue, however, also affects bottom dwelling organisms with planktonic developmental stages. Accidental dislodgement or active drift entry of benthic species - particularly stream invertebrates - again means population persistence in the face of downstream advection must be considered.

1.0.2 Suggested resolutions: streams and rivers

Various resolutions to the drift paradox have been put forward. In relation to streams and benthic insects, Waters (1972) proposed that for a given section of stream, drift represented only excess production beyond that required to to replace the local population. This production hypothesis implies that drifting is simply a source of mortality. In the absence of active upstream movement, this would require individuals to hold station at all locations at least long enough to reproduce, over indefinite generations. Any instance of total loss of population from the upstream end of the system would lead to permanent loss from that location. Such events are plausible, especially as streams can experience 'catastrophic drift' events where a large fraction of the biota are transported downstream, (Allan 1995).

A more recent hypothesis similarly independent of upstream movement has been proposed by Anholt (1995). Anholt added the idea of density-dependent population growth to the production hypothesis. As such, areas subjected to greater losses from drift experience a higher rate of population increase. Using a strategic computer simulation in which a series of stream segments with local density dependent growth were linked by random downstream drift events and adults dispersing randomly both downstream and upstream, he was able to show that persistence was more likely when density dependence was stronger. However, extinction almost always occurred in the absence of the random adult dispersal. Although density dependent growth rates may well have the ability to enhance persistence, the experiment seems to have shown that some degree of upstream movement is the essential component for true long term survival.

In respect to stream insects the idea of adult compensation for downstream drift of larvae was encapsulated by Müller (1954, 1982). Müller suggested that drift entry was primarily behavioural and a response to competition for resources amongst larvae. Drifting allowed colonisation of unexploited downstream reaches. Washout from the system was avoided by upstream flight of adults prior to ovipo-

sition. Müller termed this pattern the colonisation cycle. Various studies suggest that adults of some stream insects do move upstream, (Williams and Williams 1993) and Hershey et al. (1993) conclude that such movements can be sufficient to compensate for drift. Recently, this form of species persistence has been shown to occur for other than insects. March, Benstead, Pringle, and Scatena (1998) were able to demonstrate the cycle in tropical freshwater shrimps.

If the downstream drift and upstream flight are viewed as purely deterministic processes, the colonisation cycle cannot, however, ensure population persistence. If drift exceeds upstream movement then net downstream movement is simply reduced. If there is net upstream movement then the population is still removed from the system, only in the opposite direction. Considering the problem at a population level, however, with its associated degree of random variability, several workers have pointed out that no upstream bias in adult dispersal is necessary for maintaining populations when fecundity is high, (Brittain and Eikeland 1988; Allan 1995) or if reproduction or drift is locally density dependent, (Waters 1972; Waters 1981; Allan 1995), there simply exists a requirement for sufficient adults to compensate for drift. Two recent strategic studies lend further support to the hypothesis as, while not contradicting the above studies they suggest there is evolutionary advantage in both upstream bias to dispersion and exact compensation of downstream drift. Anholt (1995) found that genotypes with upstream biased dispersal drove randomly dispersing competitors to extinction. Using the framework developed by Anholt, Kopp, Jeschke, and Gabriel (2001) conducted an invasion analysis in order to determine the evolutionarily stable dispersion strategy. They concluded that exact compensation by the population as a whole, that is a mean net movement of individuals from birth to reproduction of zero, was the optimal strategy.

The colonisation cycle is only applicable to species where at least one developmental stage is capable of overcoming downstream advection. This is certainly not true of all species that exist in lotic systems, obvious examples being river dwelling phytoplankton, (potamoplankton) and zooplankton. Recent studies of

streams and rivers have focused on the fact that the flow is not uniform. Natural channels often contain areas of very low flow, which may act as refugia for organisms, (Reckendorfer, Keckeis, Winkler, and Schiemer 1999). The residence time organisms can achieve in these areas is important. Small areas, or those with high exchange with the main flow can act to reduce drift by effectively reducing the average velocity of the water body as a whole. The drift paradox is only overcome once the characteristic residence time in the refuge allows reproduction.

Floodplain habitats have been cited as stores of plankton population such that floodplain inundation can significantly influence plankton densities in the river, (Saunders and Lewis 1988). More generally it has been proposed that riverine zooplankton are imports from adjacent lentic areas such as the flood plain or river margins and side channels, (Saunders and Lewis 1989). These areas, however, are probably best considered as separate subsystems, in the same way as lakes are in general. As with the studies of Waters and Anholt, without a means of placing some individuals back upstream, studies of short term refugia, (Lancaster and Hildrew 1993; Robertson, Lancaster, and Hildrew 1995) fail to resolve the paradox, although for insects with an airborne adult stage they do provide a way in which the required upstream compensation can be reduced.

With respect to the issue of persistence, most studies had focused on the deterministic aspects of drift[1]. This was noted by Speirs and Gurney (2001) who, in their approach to the issue considered random motion, due both to turbulent water movement and to the randomly directed movements of individual organisms, as a potential source of upstream re-colonisation and therefore as a candidate mechanism for population persistence. Rather than attempt to approximate a given system strategic models were developed. Models were cast in the form of advection-diffusion equations with the advective term representing deterministic drift and the diffusive term approximating random motion. Models progressed in complexity from a simple one dimensional system with constant advection and population intrinsic growth rate through to a two dimensional model incorporat-

[1]A notable exception is that of Anholt (1995)

ing the features of bottom friction and shearing, density dependent growth rate and a superimposed tidal oscillation. The one-dimensional linear system allowed semi-analytical results to be obtained with respect to the conditions required for persistence through diffusion to operate. These results could be contrasted with those from the more complex scenarios, which could not be treated analytically and for which a discrete space and time simulation strategy was developed. This strategy, which was adopted by this thesis, is described in chapter 3.

For rivers, Speirs and Gurney (2001) performed simulations on two dimensional domains incorporating bottom friction and shearing. They concluded that the more complex flow environments produced only moderate effects on the conclusions drawn from the simplest (and analytically tractable) model. All models, however, assumed organismal motion to be unbiased. This may be of particular importance in the vertical as, in the absence of strong organismal random motion, this effectively assumes organisms of neutral buoyancy with random movement due to the vertical component of turbulence. In general, for larger rivers velocity gradients are much greater in the vertical than they are in the horizontal. Shearing leads to water at greater depths moving more slowly which, as Speirs and Gurney pointed out, introduces a form of flow refugia and the possibility of near benthic persistence. This in turn suggests some form of directed motion toward the benthos may well enhance persistence. Work on the investigation of organismal sinking and its impact on persistence in this domain are presented in chapter 7.

Prior to this, the one dimensional semi-analytic model of Speirs and Gurney (2001) is expanded to consider organisms spending part of their time on or in the substrate. Speirs and Gurney took account of this factor through a simple multiplication of the advection term by the fraction of time spent in the drift. In chapter 6, however, a new analytic solution is obtained from first principles.

1.0.3 Suggested resolutions: tidal systems

In systems where tidal flows are superimposed upon seaward flowing river run-off, (estuaries and fjords), the net cross sectionally averaged flow over a tidal cycle will correspond to the cross sectionally averaged flow of the river discharge. The pattern of net velocities over the length of the system - and vertically for the same horizontal location - can vary considerably however. The issue of net tidal cycle movement becomes more complicated still in that any particle or organism moving within the fluid experiences many of these different velocity cycles. The issues of residual flow patterns and net tidal cycle movements are discussed in chapter 2. These variations present the possibility of diffusive movement through turbulence, in combination with spatially varying advective flows, providing greater opportunities for persistence to planktonic organisms than in the purely gravity driven flows of streams and rivers.

The idea of the net motion in estuaries in itself being sufficient to ensure the persistence of passive organisms has been put forward with respect to larvae, (Wolf 1973; Jager 1999). Species of flat fish are even known to spawn in the coastal oceans but for the pelagic larval phase to migrate into estuaries before settling to become benthic dwelling. Of more widespread significance, almost all estuaries and fjords carry significant populations of phytoplankton species with no means of swimming and at best only limited buoyancy control.

Chen, Shaw, and Wolcott (1997) reduced the fluid dynamic equations representing tidal flow in a uniform domain to a linear form such that analytic solutions for velocities could be obtained. With specific combinations of bottom drag and vertical diffusion coefficient they demonstrated how phase and magnitude differences between near benthic and near surface flows could enhance the retention of larval crabs. Speirs and Gurney (2001) were able to extend the analytical solutions to include a river flow component. With this net seaward flow in place their investigations found that the underlying requirements for persistence in terms of the relative magnitude of vertical diffusion, horizontal diffusion, advection and

system length were only moderately changed from the case of river flow.

The analytic treatment of the tidal flows, however, require the assumption of uniform density and the absence of buoyancy driven flow. As discussed in chapter 2 density gradients are considered a very major contributing factor in the net circulations observed in estuaries and fjords often leading to landward flowing 'compensatory currents'. In considering tidal regimes in this work a numerical package for solution of oceanographic fluid dynamics equations was employed such that the effect of density variations could be incorporated. Such an approach also allows the adoption of non-uniform bathymetry, which is necessary for investigations involving fjords. This package, the Princeton ocean model, (POM), is outlined and discussed in chapter 5.

Results for both neutrally buoyant and negatively buoyant organisms in estuarine flow with density induced currents as an additional mechanism for persistence are considered in chapter 8. Results for the more complex bathymetry of a fjord are presented in chapter 9. Light is essential to the maintenance and reproduction of phytoplankton. Given the importance of phytoplankton in these two habitats, investigations also contrasted results for when growth rates are uniform over depth to those where growth rates declined in line with attenuation of daylight.

Alternative to organismal motion directed exclusively toward the benthos is the idea of active vertical migration. Larvae possess the ability to swim, in the order of one to several $cm\ s^{-1}$, not enough to swim against tidal flows but enough to influence their depth in the water column. An alternative to purely passive transport allowing colonisation was postulated by Creutzberg (1961) and termed 'selective tidal stream transport' (STST). In this hypothesis larvae ascend actively in the water column during flood and return to the bottom when the tide turns. For this behaviour to be most effective vertical movements need to be in phase with the tidal cycle, requiring cues for timing. Candidate synchronising cues have been suggested by Boehlert and Mundy (1988). Field evidence for such behaviour has potentially been found for the larvae of some species, (Christy

1989). Interestingly, the examples appear to be restricted to larvae that will not reproduce before the need for persistence in planktonic form has ended.

A more common form of vertical migration pattern amongst plankton is a light dependent diel ($24h$ period) migration. Except for a few world locations this migration pattern is not synchronised with the main tidal constituent. In most locations the dominant tidal constituent is the lunar semi-diurnal M_2 tidal current. Hill (1995) combined vertical migration, (in the form of a square wave), with a purely oscillatory and spatially uniform tidal velocity. When migration and tide were out of phase, integration over time led to no net transport over seasonal time scales but a basically sinusoidal pattern of displacement with amplitude of up to several kilometres (for modest tidal currents) and a period related to the difference in period between migration pattern and tide. These results are from a quite abstract model and Hill freely concedes that many factors such as the non-uniformity of tidal currents due to bottom friction and shear, turbulent diffusion and net circulations from density gradients are not represented.

Chapter 2

Complex flows and simple behaviours

2.1 Rivers, estuaries and fjords

A simple definition of a river is 'a channel of flowing water, whose movement is determined by gravity and is therefore downhill', (Dobson and Frid 1998). A widely adopted definition of an estuary, (which also encompasses fjords), is that of Cameron and Pritchard (1963) who state that 'An estuary is a semi-enclosed coastal body of water which has a free connection with the open sea and within which sea water is measurably diluted with fresh water derived from land drainage.' using these definitions, two major differences are of significance to this work. Firstly, the mean flow of a river is always in one direction if averaged over any time long enough to account for random fluctuations. An estuary has both the uni-directional river component and an oscillating tidal flow. A mean seaward flow (averaged over the estuary cross section) is only seen if the flow is averaged over the length of one tidal cycle. Secondly, the density of rivers is effectively uniform whereas the mixing of river water and saline water from beyond the mouth of an estuary causes variations of salinity, and as a consequence density, that can affect the tidally averaged mean flow patterns.

There is an additional form of water body that fails to fall into the above categories. The rivers feeding estuaries can be given a tidal component while re-

maining free of salt intrusion. These sections of river can be called tidal rivers, although they are sometimes referred to as the homogeneous portion, or homogeneous fresh water zone, of estuaries, (Holley, Harleman, and Fischer 1970; McDowell and O'Connor 1977).

2.1.1 Rivers

When considering idealised non-tidal rivers, (those of a uniform cross section), the only upstream water movement provided is that of turbulent diffusion. The degree of turbulence and the length scales over which it operates depend on the character of river being considered, and this character variation is often more significant between zones of the same river than between rivers. In general a river system can be divided into three zones, (Dobson and Frid 1998). The erosion zone comprises mainly headwater streams. Channel slope is steep and sediment is generally eroded rather than deposited. The eroding nature of the stream ensures that substrate particle size is generally large (cobbles and boulders), although sometimes the river may have eroded to the bedrock. The steep slope and coarse substrate is likely to lead to high turbulence and riffles and rapids are likely to be present.

The second zone is called the sediment transfer zone because gradient is reduced and sediment is transported with little net loss or gain. In this zone substrate particle size is dominated by sand and gravel. The smaller gravitational force driving the flow and the smoother nature of the substrate will reduce the degree of turbulence generated in the flow and it is more likely that the vertical profiles of velocity caused by the viscosity of the fluid will become apparent.

The deposition zone is where a river deposits its sediment load, typically as it approaches the sea. A tidal river is likely to be such a zone, or deposition may not occur until a river has already entered an estuary. Conversely, such a zone may occur well inland. The substrate again becomes smoother, being dominated by fine silt and a deposition zone has normally been brought about by a further

reduction in river gradient. As such, the factors causing turbulence are reduced compared to the sediment transfer zone.

Diffusion lengths are generally small in comparison to the mean advection for both the vertical and horizontal elements of diffusion. However, the horizontal spread of fluid elements, and any passive and neutrally buoyant particles that travel with the fluid, can be much greater than that which would result from diffusion. Termed dispersion, this spreading is caused by the interaction of the random diffusive motion and the non-uniform nature of the time averaged velocity within a river cross section. Bottom friction creates non-uniform vertical profiles, while other factors include varying depths across a river transect and the influence of bends. As discussed below, the nature of the spreading can be regarded as analogous to turbulent diffusion. Therefore, such effects can be taken into account by the equations describing the motion of particles in idealised rivers by retaining the same form of equation but substituting a much larger coefficient to describe the degree of horizontal spread.

2.1.2 Estuaries and fjords

The definition of an estuary given above is a very general definition covering systems from shallow, bar-built estuaries to deep, narrow sea fjords (known as sea lochs in Scotland), and a very wide range of flow regimes. Many different classification schemes are possible to further sub-divide estuaries into those with similar characteristics but most useful to this project is a division based on a combination of topography and salinity structure.

Topography is used to distinguish sea fjords from drowned river valley estuaries. Fjords are found in areas where river valleys were over-deepened and widened by ice sheets during the last ice age. In general fjords are deep, up to several hundred metres, with a small width-depth ratio, steep sides and an almost rectangular cross section[1]. The intersection between fjords, and the mouths of sea fjords are,

[1] Their plan view is also in general rectangular.

by contrast, usually shallow at the point where the ice sheet deposited material to form sills. Sometimes such sills are very shallow compared to the main body of the fjord and they can also be constricted. River discharge is small compared to the total fjord volume, but, as many sea fjords have restricted tidal ranges inland of their mouths, the river flow is often large with respect to the tidal prism, the volume between high and low water levels, (Dyer 1973). Drowned river valley estuaries, also known as coastal plain estuaries, were formed when the rising sea waters after the last ice age flooded normal river valleys. The estuarine topography is still much like a river valley, deepening toward their mouths, but with maximum depths seldom exceeding 30 metres, and usually considerably less. The width-depth ratio is usually large although not always. River flow is generally small compared to the tidal prism, (Dyer 1973). There are other estuaries that do not fit into these two types of topographic description but these are the types of concern in this thesis. For convenience, from this point coastal plain estuaries are simply referred to as estuaries.

Salinity structure is important in estuaries as it affects their flow regimes. The flows in a tidal body tend to be dominated at any one instant by the tidal component of the flow itself. Measured at any one location over a regular tidal period however, a tidal flow of inviscid water taking place in a channel of regular cross section will have a net flow of zero. If a river discharge is introduced, the net flow over a tidal cycle at any location becomes equal to that of the river. When considering the persistence of planktonic organisms it is this residual movement, from the same point in one tidal cycle to the next, that is important. In addition to the effects of viscosity, friction and turbulence, salinity structure alters the simple picture of net flows. It does this by introducing differences in water density that in combination with the acceleration due to gravity, produces new forces acting in the direction of lower density. While salinity differences affect currents, in their turn currents affect salinity distribution. Given constant forcing variables, (chiefly tidal motion over a tidal period and river discharge), however, an equilibrium will be established. Dyer (1973), however, questions whether real

estuaries ever really establish true steady states as, amongst other factors, tidal regimes are complex, river discharge constantly variable and the topography of an estuary often alters in response to a different flow regime.

Salt, as well as being important in altering water densities, can also be regarded as a passive tracer. The distribution and movement of salt can and is used as an indication of the spread and steady state distribution of other passive and neutrally buoyant particles. In terms of their salinity distributions there are four main classifications of estuary.

Highly stratified, 'salt wedge' estuaries

In all estuaries the water from river inflow will tend to flow over the top of the more saline (and denser) water in the body of the estuary. Because of the sloping nature of the estuary this tends to form a thin surface flow of low salinity over a wedge shaped body of saline water. Frictional forces will tend to drag the top layer of the salt water seawards and if shear is sufficient internal waves form and break at the interface, causing salt water to be mixed into the fresh water. This process is known as entrainment. Turbulent forces, caused mainly by tidal motion, will also mix the layers of lesser and higher salinity. In a highly stratified estuary, however, the ratio of river flow to tidal flow is relatively large such that only minimal mixing due to turbulence occurs and the salinity in the wedge is virtually constant along the estuary. In general, salt wedge estuaries tend to have relatively small width to depth ratios. The layer of very rapid change in salinity with depth is known as the halocline. Salinity is often the most important factor in determining water density, such that the halocline is often coexistent with a pycnocline, a layer of rapid density change.

The entrainment of salt water into the fresh water heading seawards leads to a compensating landward flow in the salt wedge. Because the degree of recruitment, (entrainment plus turbulent mixing), into the surface seaward flow is modest, however, so is the compensatory flow. A simple diagram characterising this type

of estuary is given in Fig. 2.1

The combination of seaward flow of less dense water and landward flow of more dense water is often referred to as the gravitational circulation within the estuary. The removal of denser water from lower down the water column and the reduction in density of remaining water through turbulent mixing causes a pressure gradient in the opposite direction to that in the surface layer. It is the horizontal variation in density, combined with the force of gravity that causes the reverse pressure gradient and so the currents may be referred to as density, as well as gravity, currents. Except in the case of near vertically homogeneous and wide estuaries (see below) gravitational circulations are distributed vertically.

Tidal flow can also be termed tidal action. In terms of stratification the tidal prism is as important as velocities generated by the tidal motion at the estuary mouth. A smaller volume of water moving in and out of the estuary provides less energy for turbulent mixing and this can be caused by a small tidal range and/or a steeply sloping bathymetry (McDowell and O'Connor 1977, page 15).

Partially mixed estuaries

As the tidal flow of an estuary increases so does its energy. Most of this energy is transferred into turbulence which in turn is dissipated by acting against the density gradients in the estuary. If the turbulent eddies are sufficiently strong to mix significant amounts of water across the halocline, then the estuary can be considered partially mixed. The salinity of the seaward surface flow is considerably raised but so too is its volume. This in turn causes an increase in the volume of the compensating landward flow. In the James estuary, Virginia, USA the seaward flow in the upper layer is 20 times the river flow and the compensating inflow near the bottom is 19 times river flow, (Dyer 1973, page 9). This flow pattern is known as a two layer flow system.

In a partially mixed estuary the surface salinity increases much more steadily

down the estuary and undiluted fresh water only occurs very near the head of the estuary. Within the more saline water there is also a longitudinal gradient in salinity. Horizontal salinity gradients have become almost linear but in the vertical there is still a zone of high salinity gradient, often at about mid depth. Fig. 2.2 gives a characterisation of this type of estuary.

Well mixed – vertically homogeneous – estuaries

Well mixed estuaries occur when the tidal current is much larger than the river flow. The turbulence from velocity shear needs to be sufficient to overcome density stratification. This is normally only possible in estuaries with small cross-sections. If the width of the estuary is sufficiently small that lateral shear is enough to create laterally homogeneous conditions, salinity increases evenly toward the mouth and there is no compensatory flow. The salt balance, in terms of tidally averaged flow, is maintained solely by turbulent exchange due to bottom friction or topographic irregularities. An intra tidal effect also helps to maintain the salt balance, however. Well mixed estuaries are likely to be subject to high bottom friction. This implies the tidal wave is likely to have a large progressive component, that is the maximum of the flood and ebb flows are likely to coincide quite closely to the high and low tide points at different locations along the estuary, but these times vary along the estuary. With maximum flood occurring near high water, when the cross sectional area is large, and maximum ebb occurring near low water, small cross section, there is a larger transport of salt on the flood than on the ebb. Fig. 2.3 gives a characterisation of this type of estuary.

Net upstream flows can occur in a well mixed estuary if it is sufficiently wide. The Coriolis force, (due to the Earth's rotation), will cause horizontal separation of the flow. In the northern hemisphere this leads to net seaward flow down the right hand side (looking seaward) and a compensatory flow along the left hand side of the estuary.

Dyer (1973) contends that it is difficult to be sure that vertically homogeneous

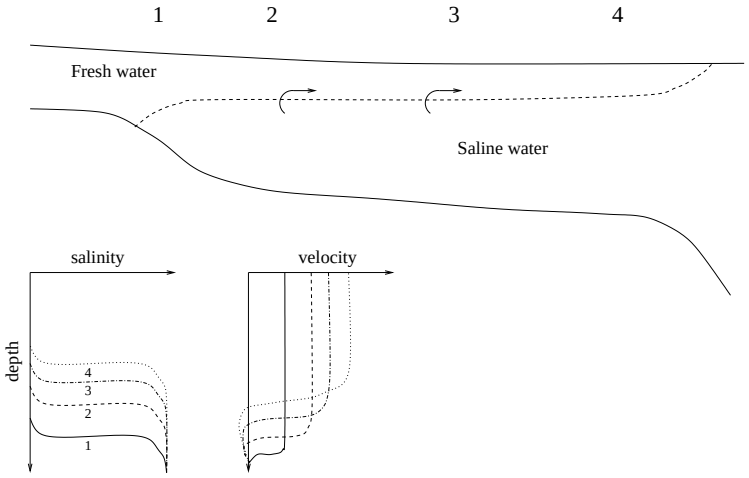

Figure 2.1: *Schematic of a salt wedge estuary, together with net tidal cycle characteristic salinity and velocity profiles.*

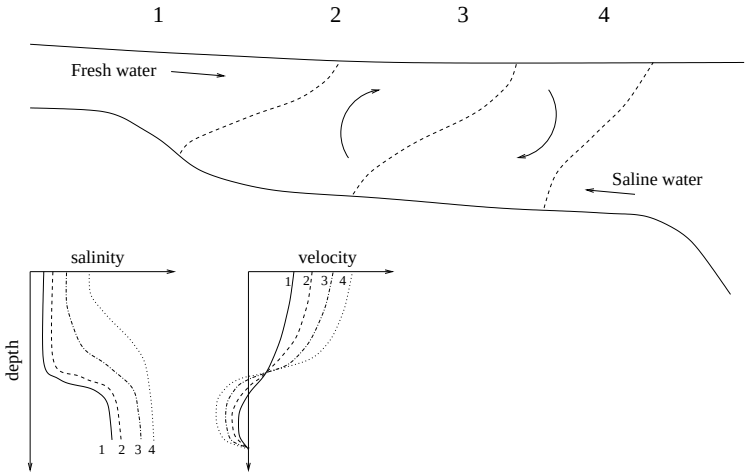

Figure 2.2: *Schematic of a partially mixed estuary, together with net tidal cycle characteristic salinity and velocity profiles.*

estuaries really exist. Even very well mixed estuaries may still retain small vertical variations that may get lost due to imperfect data collection.

Fjords

The flow patterns in fjords is generally similar to that in salt wedge estuaries. If they possess the typical sill structure at their mouth then, because of the restrictions of the sill, river flow tends to be large compared to the volume of water input and extracted by the tide. Entrainment is the main cause of mixing between the fresh water inflow and the saline water below. This upper layer is commonly of virtually constant thickness from head to mouth and sometimes this thickness is restricted to a depth equal to the sill. Where river discharge is high, the surface layer is virtually of uniform salinity, but when discharge is lower maximum salinity gradients can occur at the surface. This can also happen near to the sill. Tidal velocities are greater over the sill and the water is less stratified. There is generally much stronger vertical mixing in this region and the circulation pattern over the sill can be viewed as quite separate to that in the main body of the fjord. The inflow of water into the fjord is composed of a mixture of coastal water and the outflow water. Fig. 2.4 gives a characterisation of a fjord.

Uncertainty of classification and variation within an estuary

The classification of estuary types is only very general and the point at which an estuary changes from being highly stratified to partially mixed or from partially mixed to well mixed is somewhat arbitrary. In addition, a given estuary may show traits of different classifications of estuary at different points along its length, (Dyer 1973). For example, near the head of an estuary where tidal amplitude may be reduced, river flow can dominate and a salt wedge structure may be present. If tidal velocities increase downstream causing eddy diffusion of salt to become more active then a partially mixed structure may occur.

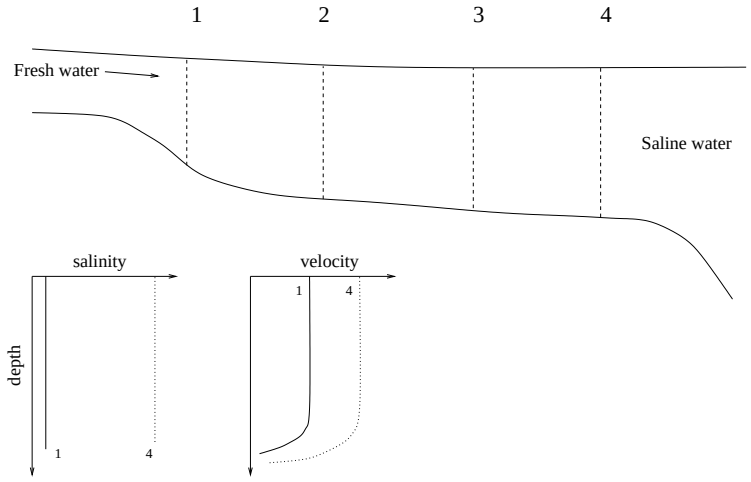

Figure 2.3: *Schematic of a well mixed estuary, together with net tidal cycle characteristic salinity and velocity profiles.*

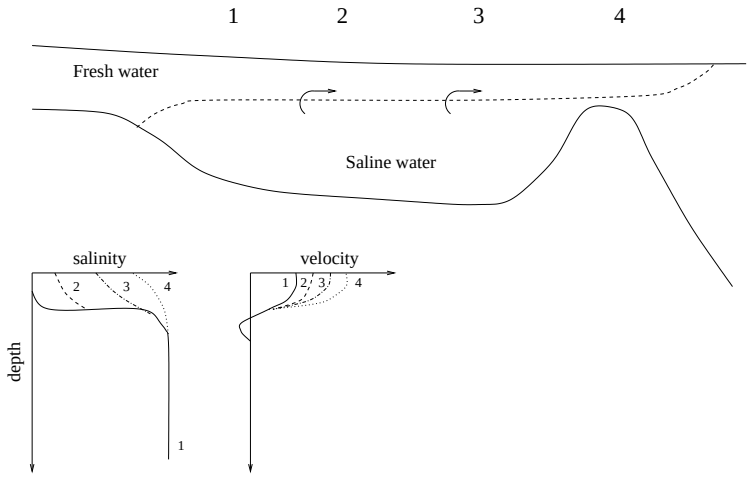

Figure 2.4: *Schematic of a sea fjord, together with net tidal cycle characteristic salinity and velocity profiles.*

Variations in topography along an estuary can affect the flow structure. For a given river discharge and tidal forcing, a large increase in width will increase the tidal volume to river flow ratio. This acts in a similar way to a reduction in river flow for an estuary of constant width, leading to a more mixed structure. Increasing the depth with other parameters fixed again increases tidal flow compared to river flow. The greater depth, however, is likely to decrease the effectiveness of vertical mixing and the river flow becomes more confined to the surface, thereby increasing the degree of stratification.

Finally, the character of an estuary can change temporally. If an estuary experiences much higher river runoff in one season than in another it can become more stratified in nature. The variation in tidal amplitude over the spring, neap tidal cycle can be enough to change an estuary from having a partially mixed character to that of a highly stratified estuary, (McDowell and O'Connor 1977).

Classification using a stratification-circulation diagram

A useful quantitative means of classifying and comparing estuaries was developed by Hansen and Rattray (1966). They used two dimensionless parameters to characterise estuaries. Firstly a stratification parameter $\delta S/S_o$, defined as the ratio of the surface to bottom salinity difference δS to the mean cross sectional salinity S_o. secondly a circulation parameter U_s/U_f, defined as the ratio of the net surface current U_s to the net mean cross sectional velocity U_f. Net current, in this instance, refers to the current averaged over a tidal cycle. The net mean cross sectional velocity U_f is effectively the cross sectional average of the river flow, as without river flow net mean cross sectional velocity would be zero.

A version of the classification diagram as used by Hansen and Rattray (1966) is shown in Fig. 2.5. This diagram distinguishes four main types of estuary, but further sub-divides types 1 to 3 according to the value of the stratification parameter. Estuaries of Type 1 have net flow that is seaward at all depths. Type 1a has only slight stratification as would be expected for a well mixed estuary.

Type 1b, however, can have an appreciable degree of stratification even though no net upstream counter current is generated. Maintenance of a horizontal salinity gradient is by diffusive effects alone. In Type 2 estuaries there is a flow reversal at depth. Upstream salt flux is due to a combination of diffusion and advection. These estuaries fit the pattern of partially mixed estuaries. Type 3 estuaries differ from Type 2 in that advection dominates upstream salt transfer, (accounting for over 99%). In Type 3b estuaries, the lower layer is sufficiently deep that in effect the salinity gradient and the circulation do not extend to the bottom. Sea fjords are generally of Type 3b. Type 4 estuaries are the salt wedge type. A vertical, (and tidally averaged), cross section of such a flow should show a thick upper layer flowing over a thin lower layer at the estuary head, graduating to a thin upper layer flowing over a thick lower layer, with the two layers being little influenced by the other. As indicated in the figure, there is a region at the top of the diagram bounded by the conditions found for freshwater outflow over a stagnant saline layer.

The demarcation between estuary types is again somewhat arbitrary. In particular Hansen and Rattray note that the transition between Types 3 and 4 has little observational or theoretical basis. Because of the variation in character of estuaries over their length, whole estuaries for any given set of conditions, (river discharge, tidal flow and, potentially, wind mixing), are represented by lines on the diagram rather than points. It is perfectly possible for the line of one estuary to cross class boundaries.

Hansen and Rattray (1966) found that U_s/U_f was related to the ratio between forced river flow and the potential for density induced internal circulation. This ratio is known as the 'densimetric Froude number' and is defined by

$$F_m = \frac{U_f}{\sqrt{gH\Delta\rho/\rho}} \tag{2.1}$$

where g is the acceleration due to gravity, H is the depth of the estuary, $\Delta\rho$ is

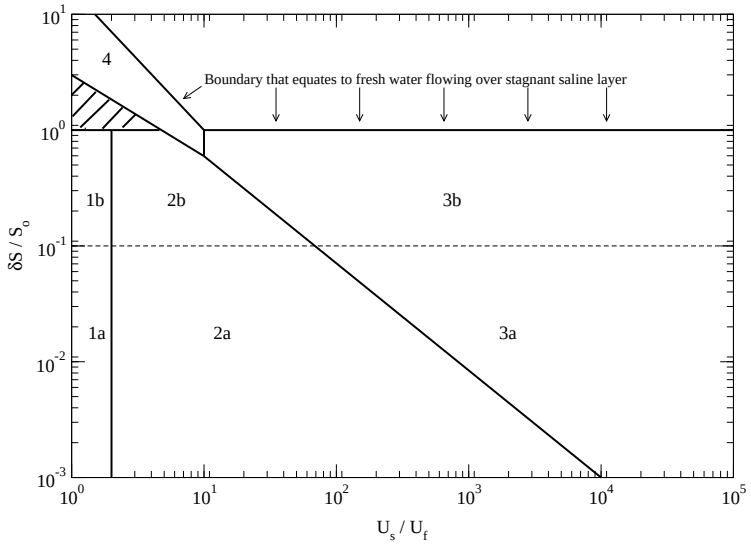

Figure 2.5: *Stratification-circulation diagram, after Hansen and Rattray (1966).*

the density difference between river and sea water and ρ is the mean density of the estuary at that point in its length. Fischer (1976) found that $\delta S/S_o$ depends primarily on a form of Richardson number termed the 'estuarine Richardson number' Ri_E which is defined by

$$Ri_E = \frac{g\Delta\rho Q_F}{\rho B U_T^3} \tag{2.2}$$

where Q_F is the total fresh water discharge, B is the width of the estuary and U_T is the root mean squared (rms) tidal velocity. This form of Richardson number is a bulk number reflecting the characteristics of the whole flow. It is essentially a comparison of the buoyancy force introduced by the river per unit width, $(g\Delta\rho Q_F)/(\rho B)$, to the tidal velocities, (Dyer 1973). The relationship between Richardson number and the degree of turbulent diffusion of salt is discussed further in chapter 5.

By performing a perturbation solution on a width averaged and nondimensionalised set of governing equations, including the salt balance equation, (see section 5.2), citeNoey:84 found expressions for both U_s/U_f and $\delta S/S_o$ in terms of F_m and Ri_E as follows

$$\delta S/S_o \sim Ri_E^{1/3} F_m^{1/15} + \text{terms of higher order} \quad (2.3)$$

$$U_s/U_f \sim Ri_E^{1/6} F_m^{-29/30} + \text{terms of higher order} \quad (2.4)$$

Equation (2.3) implies that any density difference between the head and mouth of an estuary will always induce some degree of vertical stratification while Equation (2.4) shows this stratification will always drive a gravitational circulation. They also indicate, as expected, that for a tidal body with truly homogeneous vertical density, gravitational circulation can not exist. Oey (1984) also concluded that Hansen and Rattray's method for determination of the relative importance of gravitational circulation compared to diffusive forces in salt transport – and therefore the transport of any passive and neutrally buoyant particle – was remarkably general and applicable to many estuaries of various shapes.

The gravitational circulation is best seen by considering vertical profiles of velocity averaged over a tidal cycle. If the stratification is sufficient, however, an actual landward flow in the vertical profile might be present if flows are integrated over the ebb tide. Fig. 2.6 shows the contrast between vertical flow profiles for a highly stratified and a well mixed estuary.

2.1.3 Plume fronts

In estuaries with pronounced stratification the distinct band of lower salinity water moving seaward over more saline water can be termed a plume. These plumes tend to end in fairly sharp fronts. The fronts are noticeable as they are associated with marked changes in colour or turbidity and perhaps a line of foam or other detritus, (O'Donnell 1993). These are visual evidence to the front being a zone of convergence toward which the buoyant water moves and at which it sinks. If river inflow is relatively modest plumes will only appear for a few hours during an ebb tide. If river inflow is high, the plume front will only appear in the estuary during the flood tide and is swept out through the mouth of the

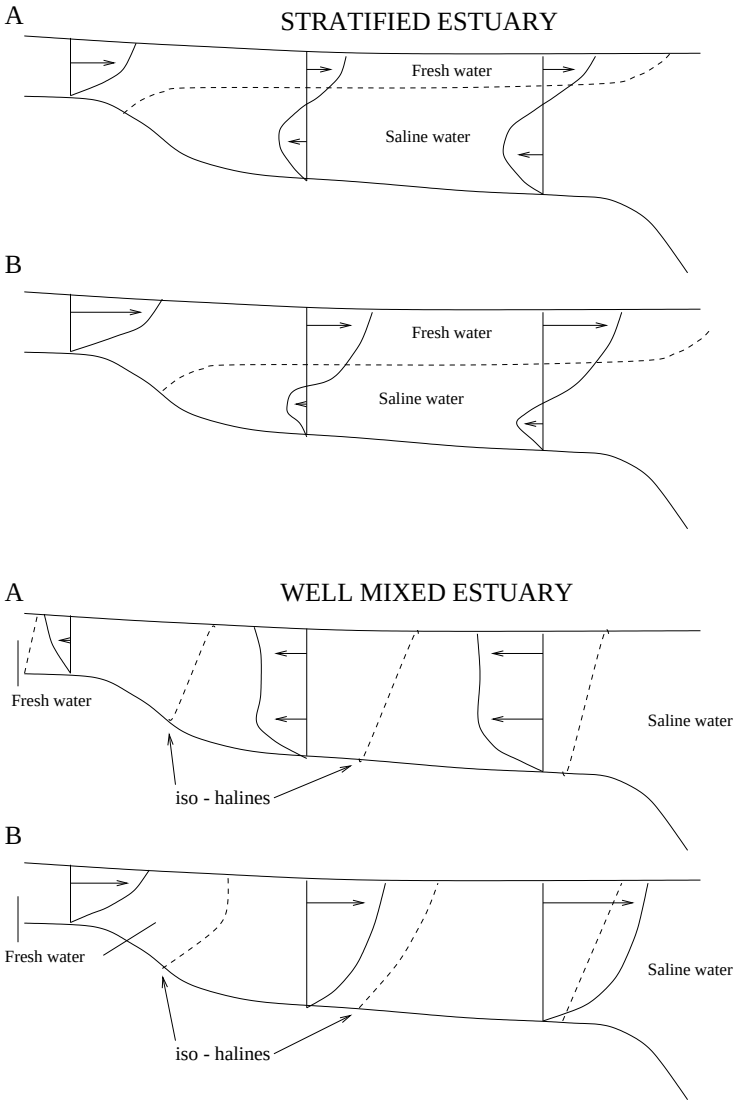

Figure 2.6: *Schematic of a stratified estuary and a well mixed estuary showing the contrast in velocity profiles during A) flood tide and B) ebb tide, after McDowell and O'Connor (1977).*

estuary during the ebb tide or even as the flood tide current diminishes from its maximum, (Dyer 1987). Garvine (1977), from observations in the Connecticut River, concluded that a well developed plume will exist during the ebb tide when the ratio of the mean freshwater discharge velocity to the root mean squared tidal velocity exceeds about 0.75 and will be present during a flood tide when the ratio exceeds 2.

2.1.4 Tidally averaged residual movement: 'residual velocity'

Observed residual flows within systems result from oscillatory tidal currents, the effects of surface wind stress, horizontal density gradients and river discharges. As indicated earlier, one can compute expected 'steady' residual velocities, that is residual velocities expected to remain constant between tidal cycles, by imposing similarly steady states on the driving forces. The residual velocities as described above are for velocities defined at a point in space (Longuet and Higgins 1969)

$$\mathbf{U_R} = \frac{1}{T}\int_0^T \mathbf{V}dt$$

where T is the duration of the tidal cycle. Such residual velocities are called Eulerian residual velocities[2]. Taking a particle starting at the point where the residual velocity was measured and determining that its end point corresponds to the direction and magnitude of the U_R value after one tidal cycle is incorrect, however. If the values of U_R vary spatially then as a particle moves it will sample brief instances of flows that constitute many different residual currents. To establish the true residual velocity of a particle the frame of reference must travel with the particle. Such a residual movement is known as a Lagrangian residual.

As outlined in Chapter 3, determination of persistence in this thesis is performed using a discrete space-time approach. To apply this approach to flows experiencing tidal forcing, any method determining the redistribution matrix must supply the net, or residual, movement of a passive and neutrally buoyant particle over the period of a tidal cycle. A redistribution matrix representing Lagrangian residual movement will result if the movement over a tidal cycle is determined by using a combination of a fluid dynamics package, (solving flow governing equations in their continuous form), and a tracking algorithm.

[2]Euler pioneered the work determining the equations of motion for fluid using a fixed frame of reference.

The fluid dynamics package is used to produce snap shots of the instantaneous flow fields. Tracking of tracers could be incorporated into the fluid dynamics program. To allow greater flexibility, tracking of particles with different characteristics using the same flow fields, a separate discrete time tracking algorithm was developed, (see also section 3.3.1). This tracking algorithm uses small intervals, δt, to update the position of a particle, using the snapshots of instantaneous flow fields. A new velocity to be applied to the particle is then determined taking account of the particle's new position in time *and* space.

If a vector is drawn from a particle's starting position to its finishing position then an imaginary velocity can be considered. When residual velocities are discussed in relation to particle movements determined from particle tracking, it is this imaginary velocity related to the Lagrangian residual movement that is being considered.

2.1.5 Diffusion versus dispersion

Turbulence within fluid flows is not yet fully understood and direct numerical modelling of turbulence is very expensive computationally, (Ferziger and Peric 1999). As detailed in chapter 4.2.1, a widely practised approach to dealing with turbulent motion is to consider it analogous to molecular diffusion, the result of the random movements of a substance's molecules. Molecular diffusion is governed by Fick's law of diffusion which states that the mass of a substance crossing a unit area per unit time in a given direction is proportional to the gradient of mass concentration in that direction. In one dimension, Fick's law can be stated mathematically as

$$q = -D\frac{\partial C}{\partial x} \tag{2.5}$$

where q is the mass flux, C the mass concentration and D a coefficient of proportionality. The minus sign is to indicate transport is from high to low concentra-

tions. Considering the relationship between q and C and applying the law of the conservation of mass in addition to Fick's law gives two more equations known as diffusion equations.

$$\frac{\partial C}{\partial t} = D\frac{\partial^2 C}{\partial x^2} \tag{2.6}$$

$$\frac{\partial q}{\partial t} = -D\frac{\partial^2 q}{\partial x^2} \tag{2.7}$$

When considering the spread of a point source of concentration the pattern of concentration at subsequent points in time will conform to a Gaussian distribution centred on the starting position. For general diffusion equations, or advection-diffusion equations if a mean advection is super-imposed on the 'mass' movement, the coefficient of proportionality, D is known as the coefficient of diffusion. When describing the effect of molecular diffusion in fluid flows it is known as the coefficient of kinematic viscosity, ν and when the effect of turbulence is described in an analogous fashion to diffusion the coefficient takes the name of coefficient of kinematic eddy viscosity, N. Kinematic eddy viscosity describes the transfer of momentum by this process. Diffusive transport of passive tracers can be considerably different to that of momentum. This can be especially true in the vertical direction, depending on the degree of density stratification. Thus a third coefficient, K, is used called the coefficient of eddy diffusivity.

Dispersion arises when a fluid has advection in a given direction but this advection has a gradient in a second dimension. Considering a two dimensional river flow, if the downstream direction is x with advective component V_x and the coordinate from river bottom to surface z, then dispersion arises when $\partial V_x/\partial z \neq 0$ which, because of bottom friction and the viscosity of the fluid itself, is the situation in all rivers and estuaries. The phenomenon arises because a fluid element in the river flow will move randomly vertically (because of molecular diffusion and possibly turbulence) and so sample at random all the advective velocities. Therefore, if a long enough averaging time is available, the element's time-averaged

velocity becomes equal to the instantaneous cross-sectional average of all the velocities. In other words, after some long enough forgetting time the velocity has become independent of the fluid element's initial position and velocity. The horizontal motion over this period can be considered a series of independent steps of random length. This makes the motion analogous to molecular diffusion and so an advection-diffusion equation should describe the changing mean position and spread of any particles moving with the fluid. The difference is that the step lengths and time steps of the 'random walk' are very different to that of the diffusion that caused the vertical motion and a different value is required for the coefficient of proportionality. This coefficient is then termed the dispersion coefficient.

Flows with velocity gradients are often referred to as 'shear flows' and the mechanism of dispersion is often known as the 'shear effect', (Fischer, List, Koh, Imberger, and Brooks 1979). For some simple steady shear flows, analytic relationships have been derived between the dispersion coefficient, Φ and the kinematic viscosity ν in laminar flows and between Φ and the eddy diffusivity K in turbulent flows. The relationship most directly applicable to that for a river is given for turbulent flow down an inclined plane, where Φ is given by

$$\Phi = I \frac{H^2 \overline{V_x'^2}}{\overline{K_z}} \tag{2.8}$$

where I is a dimensionless integral given by

$$I = -\int_0^1 V_x'' \int_0^{z'} \frac{1}{K_z'} \int_0^{z'} V_x'' dz' dz' dz' \tag{2.9}$$

and

$$V_x'' = \frac{V_x'}{\sqrt{\overline{V_x'^2}}} \tag{2.10}$$

where $K_z' \equiv K_z(z')/\overline{K_z}$, $V_x' \equiv V_x(z') - \overline{V_x}$, an over-bar denotes a cross sectional

average and $z' \equiv z/H$ is the dimensionless measure of the distance up the water column given that H is the overall water depth. Alternatively, if dimensional terms are retained in the multiple integral, the dispersion coefficient is given by

$$\Phi = -\frac{1}{H}\int_0^H V_x' \int_0^z \frac{1}{K_z}\int_0^z V_x' dz dz dz \tag{2.11}$$

Natural channels tend to have a variation of depth across the channel. This in turn leads to transverse shear. Fischer (1967) applied the same reasoning that leads to Equation (2.11) to the transverse direction of river cross sections and obtained

$$\Phi^t = -\frac{1}{A}\int_0^B q' \int_0^y \frac{1}{K_y}\int_0^y q' dy dy dy \tag{2.12}$$

where A is cross sectional area, K_y an eddy diffusivity in the transverse direction and $q' \equiv HV_{x_b}'$ represents the deviation of the local flow per unit width from the mean discharge per unit width. He concluded that for rivers with a large width to depth ratio the longitudinal dispersion caused by transverse shear, Φ^t, was more significant than that caused by shear in the vertical.

The problem with estuaries and fjords is that flow is not steady but oscillatory. This places limits on the applicability of the above equations, the important consideration being whether the time scale of the tidal cycle is much greater than the time for turbulence to diffuse a substance across the vertical and transverse distances of the estuary. Holley, Harleman, and Fischer (1970) considered tidal mean dispersion caused by vertical diffusion, Φ^{zT} for systems with neutral stability, that is without stratification. They derived expressions relating this quantity to the value, Φ^z, that would be obtained by using Equation (2.11) and Eulerian residual velocities. They found the relationship reduced to a simple function for two ranges of a dimensionless mixing time scale τ^z, namely

$$\Phi^{zT} = 3\Phi^{z}(\tau^{z})^{2} \qquad for\ \tau^{z} \leq 0.2 \tag{2.13}$$

and

$$\Phi^{zT} = \Phi^{z} \qquad for\ \tau^{z} \geq 1 \tag{2.14}$$

where τ^{z} is given by

$$\tau^{z} = \frac{T}{T^{z}} = \frac{TK_{z}}{H^{2}} \tag{2.15}$$

where H is a tidal mean value and $T^{z} \equiv H^{2}/K_{z}$ can be considered a turbulent mixing time scale. They suggested the above equations were applicable to reasonably straight channels that were also well defined such that the channel geometry does not vary significantly during a tidal cycle. With these assumptions and a reasonably wide estuary a turbulent mixing time-scale in the transverse direction relating half width to transverse diffusion coefficient becomes large and a transverse dimensionless mixing time scale much less than one. In effect, because of the oscillatory nature of the flow, dispersion due to transverse velocity variation decreases as estuary width increases, and for sufficiently wide estuaries this allows consideration of dispersion due to vertical shear and diffusion coefficient only.

The above conclusion was reached even though tidal flow is understood to introduce new mechanisms for dispersion, even in homogeneous conditions. The first mechanism was termed 'tidal pumping' by Fischer et al. (1979). It describes residual circulation set up by the interaction of the oscillating flow and the irregular bathymetry found in most estuaries. Estuaries with a narrow mouth can receive a flood tide as a confined jet type flow, while the ebb flow originates from all around the mouth. Averaging over a tidal cycle shows a net landward flow in the area of the jet but a net seaward flow elsewhere. More generally, combinations of channel geometry and separation at corners can induce large scale gyres in the

residual flow. Such residual vortices can be created in the vertical as well as the horizontal if the tidal current flows over irregular bottom topography, (Fischer et al. 1979, page 239). The horizontal separation of flow caused by the Coriolis force in wide estuaries is also considered a component of tidal pumping.

A second mechanism has been referred to as the 'storing basin', 'tidal trapping' or 'dispersion by non-local mixing' mechanism. It considers the net mass transport caused by the variation of cross-sectional shape, salinity and velocity at different points in the cross section during a tidal cycle. An illustration of tidal trapping is to consider an estuary with a main channel and a shallow side channel. In the main channel, tidal elevations and velocities are likely to not be in phase. This is because the momentum of the flow is sufficient to cause the current to continue to flow against an opposing pressure gradient, resulting in high and low slack tides lagging behind high and low water respectively. The side channel is likely to have flow with less momentum and a smaller phase difference. If the flood tide carries a patch of tracer up both main and side channel then, as the tide turns, the tidal flow will reverse sooner in the side channel and the tracer it held may well return to the main channel downstream from that part of the patch which stayed in the main channel. Winterwerp (1983) determined mixing by the sea beyond the mouth of an estuary to be important in maintaining the salt balance in an estuary. For estuarine water that leaves the estuary on each ebb tide, the more it is well mixed outside of the estuary mouth, (such that the salinity becomes effectively that of the sea water), then the greater the salinity intrusion during the next flood tide. Whether this last effect can be included when considering animal persistence in an estuary depends on whether the animal is considered able to survive for any period outside of the estuary.

For systems with buoyancy effects, gravitational circulation can be a significant or even dominant mechanism of dispersion. Several studies have concluded that, even in narrow estuaries, mass transport (and therefore longitudinal dispersion coefficients) are determined predominantly by the vertical gradients in velocity and salinity, (Fischer 1972; Dyer 1974; Dyer 1977; Hughes and Rattray 1980).

Abraham, Karelse, and Lases (1975), however, concluded that dispersion coefficients in estuaries are dependent on time and also vary with distance along an estuary and this was confirmed by Winterwerp (1983) for longitudinal two dimensional slices of the Rotterdam Waterway. West and Mangat (1986), analysed data from the Conwy estuary and concluded that on average the dispersion coefficient was larger on the ebb tide than on the flood tide. They suggested that if buoyancy effects are weak, a value for one dimensional dispersion due to both shear effects and the secondary circulation induced by buoyancy Φ^{sc} could be given to a first approximation by

$$\Phi^{sc} \sim \frac{k_1 B^2 |V_A|}{H} \tag{2.16}$$

In this instance H represents the maximum depth along a transverse cross section and B represents the half width, while V_A is the cross sectionally averaged velocity. The term k_1 is a coefficient which West and Mangat (1986) suggested could take the value of $k_1 = 0.1$ during an ebb tide and $k_1 = 0.025$ for the flood tide. Equation (2.16) is a simplification of Equation (2.12) with an empirical alteration to take account of stratification. As such it requires explicit consideration of domain width. Its derivation was possible because the ratio of transverse diffusion coefficient, K_y, predicted by Equation (2.12) to that derived from the field data was consistent for each half tidal cycle. Unfortunately, a similar approach could not be applied to Equation (2.11) as it was found that the ratio of predicted to measured vertical diffusion coefficient, K_z, varied throughout each half tidal cycle.

(McDowell and O'Connor 1977, page78) consider that predicting dispersion coefficients for real estuaries with stratification from semi-empirical formulae can only provide order-of-magnitude estimates because of the unique velocity structure of each system. The only way to obtain true dispersion coefficients is from field data. Winterwerp (1983), considering mass transport due to variations in the vertical only, sets out the calculation of both a 'real time' dispersion coefficient

Φ^{scz} and a coefficient, $\tilde{\Phi}^{scz}$ to be used for tidally averaged advection diffusion equations. In general the value of Φ^{scz} averaged over a tidal cycle is not equal to $\tilde{\Phi}^{scz}$, in large part because the dispersion in the tidally averaged advection diffusion equation implicitly describes net mass transport by tidal flows. Both values can be obtained by breaking down velocity and concentration terms into averaged values and the deviation of a value at a given point from that average. The value of $\tilde{\Phi}^{scz}$ is given by

$$\begin{aligned} -H_o\tilde{\Phi}^{scz}\frac{\partial \overline{C}_o}{\partial x} &= \left\langle H\overline{U}_t\overline{C}_t\right\rangle + \overline{U}_o\left\langle H_t\overline{C}_t\right\rangle + H_o\overline{U}_o'\overline{C}_o' \\ &\quad + \left\langle H\overline{U}_o'\overline{C}_t'\right\rangle + \left\langle H\overline{U}_t'\overline{C}_o'\right\rangle + \left\langle H\overline{U}_t'\overline{C}_t'\right\rangle \end{aligned} \tag{2.17}$$

Here an over-line denotes a vertically averaged quantity and a prime a deviation from that vertical average. The subscript o denotes a tidally averaged quantity and the subscript t denotes the deviation from this tidal average. An H with no subscript is simply the water depth at a given point in time and the angular brackets denote tidally averaged products. The various terms making up Equation (2.17) represent the different mechanisms of dispersion as follows

- $H_o\overline{U}_o'\overline{C}_o'$ – shear dispersion from the net gravitational circulation.
- $\left\langle H\overline{U}_t'\overline{C}_t'\right\rangle$ – vertical shear dispersion from the non-steady velocity and concentration profiles.
- $\left\langle H\overline{U}_o'\overline{C}_t'\right\rangle$ and $\left\langle H\overline{U}_t'\overline{C}_o'\right\rangle$ – shear dispersion from the correlation between the steady and oscillating components of the vertical shear.
- $\left\langle H\overline{U}_t\overline{C}_t\right\rangle$ – dispersion by non-local mixing, (tidal trapping).
- $\overline{U}_o\left\langle H_t\overline{C}_t\right\rangle$ – dispersion by the correlation between the steady and oscillating components of the flow.

Winterwerp (1983) compared measurements taken from three tidal flume experiments and from the Rotterdam Water-way. The three flume tests represented

highly stratified, partially mixed and well mixed conditions respectively, while the Rotterdam Water-way was found to be highly stratified. In all cases it was found that the three terms representing correlation effects provided a negligible contribution. It was also found that the contribution from the net gravitational circulation, $H_o\overline{U_o'C_o'}$ increased in magnitude as conditions became more stratified. In the flume tests its contribution went from being less than that from the non-steady vertical shear term $\left\langle H\overline{U_t'C_t'}\right\rangle$ under well mixed conditions, to comparable under partially mixed conditions to considerably greater under stratified conditions. Unsurprisingly therefore, the contribution from the net gravitational circulation was somewhat greater than that from non-steady vertical shear in the Rotterdam Water-way.

A more traditional, and much simpler approach, of using salinity field measurements to determine a longitudinal dispersion coefficient, is to use the equation describing the 'salt balance' in an estuary

$$\Phi\frac{\partial S}{\partial x} = U_f S \tag{2.18}$$

where S is salinity at a point along an estuary, $\partial S/\partial x$ the longitudinal gradient and U_f the cross sectionally averaged net velocity due to fresh water discharge. The equation effectively assumes the salinity profile to be in steady state from one tidal cycle to the next such that Φ represents the dispersion, by all relevant mechanisms, that allows an equal and opposite net tidal flux of salinity to the seaward flux represented by the term $U_f S$ at that location. Fischer et al. (1979) point out that Equation (2.18) has been used with salinity values observed at low slack water, high slack water or with values averaged over a tidal cycle and that the result is highly dependent on which approach is used. Also, some estuaries do not conform well with the assumption that their salinity distribution is cyclic. This latter problem, however, also affects any estimation made using Equation (2.17).

Fischer et al. (1979) compiled a table of different estuaries and their observed

dispersion coefficients. Values range from $10m^2s^{-1}$ to approximately $1000m^2s^{-1}$ with the bulk of values falling in the range $100-300m^2s^{-1}$. They noted that such values were considerably smaller than values observed in even moderately sized rivers and concluded the reason was the limited ability of shear flow to cause dispersion in estuaries, as indicated by Equation (2.13). Low values, in the range $10-60m^2s^{-1}$, were generally found in very well mixed or homogeneous portions of estuaries where shear flow dispersion is the dominant mechanism.

2.2 Planktonic animals and behaviour relevant to persistence

Plankton can be defined as, (Reynolds 1984)

> the community of plants and animals adapted to suspension in the sea or in fresh waters and which is liable to passive movement by wind and current.

As such it is distinct from the 'nekton' (e.g. fish), that have the ability to substantially regulate their own distribution through swimming. This is not to say some plankton can not swim or otherwise influence their movement by the surrounding water to a certain extent, but under normal circumstances they are unable to overcome advective movements imposed on them by the flow.

The most obvious form of plankton are those that spend their whole life cycle in suspension and which have morphological and behavioural adaptations to survive in the pelagic habitat. However, there are animals which spend part or even most of their life cycle in the littoral habitat at the bottom of the water column. For example, the larvae of crabs and flat fish, (commercially important species), are planktonic. There are still other organisms that are benthic dwellers but which can be found in the drift for short periods. Although not conforming fully with the

definition of plankton given above, they are certainly subject to passive movement by the current when they enter the drift. Many stream invertebrates fall into this last category. A considerable number of field studies have measured the numbers of bottom dwelling invertebrates found in the drift. A review of these is given in Brittain and Eikeland (1988).

There is much debate as to the reasons for individuals entering the drift. Some studies support the idea of animals being involuntarily swept into the water column by the rapidly and strongly varying forces of the near bed turbulent flow, (Poff and Ward 1991). Other studies[3] suggest drift entry is deliberate and cite many potential triggers including food depletion, (Kohler 1985), predator avoidance, (Peckarsky 1980; Malmqvist and Sjostrom 1987), density dependence, (Corkum and Clifford 1980) and indeed reductions in flow velocity as the reasons for such action, (Minshall and Winger 1968; Poff and Ward 1991; Fonseca and Hart 1996). The reasons are almost certainly different for different taxa. Results from Degani et al. (1993) indicate that many invertebrates may prefer the highly turbulent flows characteristic of the shallow and high velocity areas characteristic of riffles in upland streams, while Growns and Davis (1994) describe a number of 'flow avoiders'.

Behaviour can also be passive or active once in the drift. Individuals have been found to actively reduce their time in the water column, (Elliott 1971a; Ciborowski and Corkum 1980). Some studies cite changes of behaviour by individuals of a given species in response to the strength of the flow, acting to minimise drift time when flow is strong but to increase drift time and distance when velocities fall below a certain threshold, (Campbell 1985; Allan and Feifarek 1989). Even with in-drift behaviour, it seems likely that the rate at which drifting individuals return to the benthos is strongly dependent on the degree of turbulence, (vertical mixing), in the flow, (Smith 1982; McNair, Newbold, and Hart 1997). Regardless of the means of drift entry and exit, chapter 6 demonstrates that if rates of drift entry and exit can be determined and can be considered ap-

[3]Or results for different taxa within the same study.

proximately constant, then the critical flow parameters for persistence in a given length of system can be determined semi-analytically.

The work of Speirs and Gurney (2001) considered problems in which organisms could effectively be considered as neutrally buoyant. Persistence in the more complicated flow regimes of chapters 8 and 9 is also initially considered for such organisms. Such considerations are very instructive, not least because it is then possible to make comparison to results where vertical movement is also due to factors other than entrainment in the surrounding flow. A very simple form of 'behaviour' for plankton can be considered that of sinking. There are few planktonic organisms that are consistently buoyant. Most are often or always more dense than the water they inhabit, (Reynolds 1984). Phytoplankton are no exception to this general rule. Terminal sinking speeds in quiescent water have been measured for various marine and fresh water diatom phytoplankton. Chapters 8 and 9 investigate whether or not simple, constant sinking can enhance the persistence of populations in estuaries and fjords. This is appropriate to diatoms as they possess no mechanism for swimming. Even so, it seems they are not totally incapable of influencing their position in the water column. Live phytoplankton are able to control their density to a certain extent. A number of studies have found that several species of live phytoplankton demonstrate lower settling velocities in quiescent water than dead or senescent individuals from the same population, (Reynolds 1984, page 77). In the presence of turbulence, elimination time from the water column is also influenced by the 'form resistance' of each species. Those with higher form resistance achieved longer times in the water column. Form resistance is a non-dimensional measure of the degree to which an organism's shape increases its drag. It is therefore also a measure of how readily an organism can be entrained by random water movements.

If organisms possess a quiescent settling velocity the theory of settling in the presence of turbulence implies that turbulence will only delay the settling of individuals in the water column, by a factor directly related to their settling velocity and form resistance. If only random motion is present in the vertical, eventual

settling is inevitable, (Reynolds 1984, page 50). Phytoplankton derive their energy from sunlight. Sinking may enhance physical persistence by transferring individuals from net seaward flowing waters into the net landward flowing compensating currents but the attenuation of sunlight in water is often quite rapid. The influence of light dependent growth rates upon both neutrally buoyant and sinking populations is considered. In this way the effect of both added elements of realism can be assessed independently and in combination.

Other forms of phytoplankton possess flagella which allow them to become motile. It is now well established that phytoplanktonic organisms will adjust their position in a water column by means of vertical migration, (Figueroa, Niell, Figueiras, and Villarino 1998). They have been shown to respond to gravity, chemical and thermal gradients, the magnetic field of the Earth as well as to light. This last factor can stimulate both positive and negative phototactic responses, (Nultsch and Hader 1988), although the basic pattern is one of a diurnal migration leading to maximum concentrations at depth during the night and near the surface during the day. For the well stratified system they studied, Figueroa, Niell, Figueiras, and Villarino (1998) found the pycnocline was significant in that only some species studied were able to migrate through.

Zooplankton are also known to make diurnal migrations, although the pattern is in reverse with individuals rising during the night and moving to deeper water during the day. This behaviour has been found in the open ocean, fjords and estuaries. Migration to the surface in estuaries, however, has been seen to be inhibited by high stratification. Sampling of the estuarine section of the River Test, Southampton, found concentrations of zooplankton just below the low-salinity surface water at times of high stratification, but zooplankton all the way to the surface when the salinity gradient was not present. In controlled experiments Grindley (1964) showed that *Pseudodiaptomus* in an estuary migrated downwards during the day and upwards at night. However, upward movement was halted by salinities in the range 8.5-19.0 parts per thousand. He suggested that at times of normal river run-off the full migration allowed persistence in the

estuary. At times of river flood the animals prevented wash out by their avoidance of low salinities.

Part II

Methodologies

Chapter 3

Methods for determining the persistence of spatially structured populations

3.1 Population balance equation

The balance equation for a spatially structured population represented in continuous space and time has the general form (Gurney and Nisbet 1998)

$$\frac{\partial n}{\partial t} = (\beta - \delta)n - \frac{\partial J_x}{\partial x} - \frac{\partial J_y}{\partial y} - \frac{\partial J_z}{\partial z} \tag{3.1}$$

where $n(x, y, z, t)$ represents the population density at a point (x, y, z), $\beta(x, y, z, t)$ and $\delta(x, y, z, t)$ are local per-capita birth and death rates, and $\mathbf{J}(x, y, z, t)$ represents the net flux densities of individuals past the position (x, y, z).

This thesis is concerned with the possibility for persistence provided by the fact that fluid flows with a net advection experience shear, turbulence and, (in later chapters), are influenced by varying topography and salinity. Reducing the problem to one dimension in the first instance, (the x direction), if there were only

advection present, moving all individuals at the speed V_x past a given point, then the net flow rate term would be given by $J(x,t) = V_x n(x,t)$. The motion imparted by turbulence is considered random. Random motions produce a net flow rate which is proportional to the spatial gradient of any concentration. The constant of proportionality, the diffusion coefficient, when used in relation to population balance equations is denoted by Φ_x. The subscript denotes the possibility for coefficients with different values in the other directions for models that consider more dimensions. The net flow takes individuals from regions of higher density to lower density. The diffusion constant is always regarded as positive by convention, such that a net flow rate caused by solely diffusion becomes $J(x,t) = -\Phi_x \partial n/\partial x$. Taking the overall net flow rate to be a combination of advection and diffusion, and replacing $(\beta - \delta)$ by $p(n)$, the net per-capita growth rate, the balance (or conservation) equation for a population in one dimension becomes

$$\frac{\partial n}{\partial t} = p(n)n - V_x \frac{\partial n}{\partial x} + \Phi_x \frac{\partial^2 n}{\partial x^2} \tag{3.2}$$

where the value of $p(n)$ is now considered to, potentially, depend on the population density n.

3.2 Analytic technique for 1D problems

3.2.1 1D problem

Speirs and Gurney (2001) considered the case of Equation (3.2) representing a turbulent stream, where the turbulence has enabled the water to become well mixed vertically and transversely. The advection velocity and diffusion coefficient are also assumed constant throughout the domain. The term Φ_x can be considered analogous to the coefficient of eddy diffusion seen in the conservation equations for passive tracers found in fluid dynamics, (for example see Equations (5.9), (5.13)

and (5.16) that determine the evolution of salinity in a turbulent 3D system). These quantities are not equivalent, however, as the term in Equation (3.2) can be regarded as representing motion induced by fluid movements but of different magnitude and/or random movement generated by individuals themselves.

The point $x = 0$ was assumed to represent the source of the river at which water containing zero organisms enters at velocity V_x. It was further assumed that no individuals could pass upstream of the source, so the population flux at $x = 0$ is zero. That is, there exists a reflecting boundary given by

$$V_x n(0,t) - \Phi_x \left(\frac{\partial n}{\partial x}\right)_{x=0} = 0 \tag{3.3}$$

At the opposite end of the domain ($x = L$) the river flows into an environment which the organisms can enter but from which they can not return. This is represented by an absorbing boundary at which the population is always zero

$$n(L,t) = 0 \tag{3.4}$$

If $p(n)$ is assumed to be a constant, that is involving no density dependence, then the problem defined by Equations (3.2) to (3.4) is linear and the only possibilities for the overall population are for exponential growth or decay over time, (Gurney and Nisbet 1998). Following the analysis for the case when diffusion only is present, (Gurney and Nisbet 1975), Speirs and Gurney (2001) assumed that after initial transients have died away, the solution takes the form of a static spatial pattern with each point in the pattern growing, or decaying, exponentially with time. This meant solutions were sought in the form

$$n(x,t) = e^{\Lambda t} f(x) \tag{3.5}$$

where Λ is the long term exponential growth rate and $f(x)$ is the function determining the spatial pattern. For species which do not exhibit an Allee effect,

(Allee 1931), p is normally a decreasing function of the local population density. Its maximum value is therefore when n is effectively zero. If $p(n)$ is set to this maximum value, the 'intrinsic growth rate' denoted by r, the population can be thought of as one invading a given system. Because r is a maximum value a population which can not invade a given system is also incapable of persisting in that system after being introduced as a finite population.

Speirs and Gurney (2001) were able to show that solutions are only possible if the long term growth rate Λ is related to r, V_x, Φ_x and the system length L by

$$\tan\left(\kappa\frac{L}{L_d}\right) = -\frac{V_d}{V_x}\kappa \tag{3.6}$$

where

$$L_d \equiv \sqrt{\Phi_x r^{-1}}, \qquad V_d \equiv 2\sqrt{\Phi_x r}, \qquad \kappa \equiv \sqrt{1 - \frac{\Lambda}{r} - \left(\frac{V_x}{V_d}\right)^2} \tag{3.7}$$

Intermediate working leading to this result is given in Appendix A. The implications for population persistence of the above result are covered in chapter 6.

3.2.2 $1\frac{1}{2}$D problem

The method of Speirs and Gurney (2001) can be extended to consider the case where organisms spend some of their time in the drift and the rest resident on or in the benthos. To attain an analytic solution organisms are assumed to be static while in their benthic 'state'. A further simplification is to assume that the times spent in the drift and benthos are independent of the river velocity and diffusion coefficient. If, in addition, organisms are assumed to have exponential decay distributions for the benthic and water column residence times then the rate of transfer between states are simple constants. The details of this extension

to the above method are detailed in chapter 6, section 6.3.1. Chapter 6 then considers the difference 'clinging' to the benthos makes compared to the scenario of individuals permanently in the drift.

Failure of solution technique when there is benthic movement

The key element to being able to extend the solution technique of Speirs and Gurney (2001) to the case when individuals spend time on the bottom is the assumption that these organisms are non-moving while on the bottom. This in turn permits non-trivial solutions in which the population density in the benthos, $m(x,t)$, is a constant proportion of the population density in the drift, $n(x,t)$, at all points. Once movement is introduced in the benthos then the possibility of a constant ratio between $m(x,t)$ and $n(x,t)$ breaks down.

3.3 Numerical techniques

As discussed in the previous section, analytic solutions can be found for the long term growth rate of a population if the per-capita growth rate of the population is assumed to be constant. Such solutions provide valuable insights into the limiting conditions for potential persistence. Non-linear representations of per-capita growth rate are more realistic of real populations, however, and their introduction makes it impossible to apply the analytic approach so far described.

Analytic solutions for certain two dimensional problems are possible, (Richards 1996), but the assumptions necessary to simplify the problem are quite restrictive. If realistic hydrodynamics, or other factors, such as animal behaviour, are to be incorporated then it is necessary to turn to numerical techniques. One approach is to solve the continuous version of the equations specifying the model in question. There are a number of distinct schemes that can be applied, (finite differences, finite elements, finite volumes, method of characteristics), and no one scheme has

proven the best choice for all possible problems. As an alternative to numerical solution of the continuous model, a discrete space-time representation can be adopted, as outlined for one dimensional problems in Gurney and Nisbet (1998), with extensions to two dimensional problems described in Speirs and Gurney (2001).

3.3.1 Discrete space-time approach

Considering a one dimensional model in the first instance, the domain is divided into a contiguous series of equally spaced intervals of width Δx and the average population density in quadrant x at time t is denoted by $n_{x,t}$. This density distribution is updated at intervals Δt according to

$$n_{x,t+\Delta t} = \sum_{x'} R_{x',x} B_{x',t} \tag{3.8}$$

The term $R_{x',x}$ represents a redistribution matrix and $B_{x',t}$ represents the number of survivors and descendants of the population of quadrant $x^{'}$ at time t who are present at time $t + \Delta t$. In this work all non-linear per capita growth rates are represented by the logistic growth rate

$$p(n) = r\left(1 - \frac{n}{k}\right) \tag{3.9}$$

where k represents the carrying capacity of the population. Therefore, following (Gurney and Nisbet 1998), $B_{x',t}$ is equated with the solution to the logistic equation, so that

$$B_{x',t} = \frac{k n_{x',t}}{n_{x',t} + \xi(k - n_{x',t})}, \quad \xi \equiv e^{-r\Delta t} \tag{3.10}$$

The redistribution matrix must be properly normalised such that it produces a mean displacement of $V_x \Delta t$ and a displacement variance of $2\Phi_x \Delta t$. That is

$$\begin{aligned}\sum_x R_{x',x} &= 1 \\ \sum_x (x-x')R_{x',x} &= V_x \Delta t \\ \sum_x (x-x')^2 R_{x',x} &= 2\Phi_x \Delta t + (V_x \Delta t)^2 \end{aligned} \tag{3.11}$$

Speirs and Gurney (2001) used a displaced tent distribution to represent $R_{x',x}$. Such a distribution is given by

$$R_{x',x} = \phi \left(1 - \frac{|x - x' - d_{ox}|}{d_{mx}} \right)^+ \tag{3.12}$$

where the + symbol denotes taking the value of the expression on the right hand side if it is positive, or zero otherwise. The coefficients ϕ, d_{ox} and d_{mx} are chosen so that the conditions of Equation (3.11) are satisfied. To conform to the conditions of Equations (3.3) and (3.4) at the boundaries, the method of images is used to define an appropriately modified redistribution matrix. Using this technique to model a logistically regulated population living in a 1D domain, (representing a well mixed river), Speirs and Gurney (2001) demonstrated that this form of discrete space-time model demonstrated good agreement with the results of a continuous model obtained by standard numerical methods, but with a computational cost approximately two orders of magnitude lower. The comparison of results is shown in Fig. 3.1.

The discrete space-time representation can be readily generalised to higher dimensions by denoting position by a vector, $\mathbf{p} \equiv (x, z)$, for a vertical slice, or $\mathbf{p} \equiv (x, y, z)$ for a full three dimensional model. The domain is now split into a contiguous series of rectangular (2D), or cuboidal (3D) cells. Equation (3.8) generalises to

$$n_{\mathbf{p},t+\Delta t} = \sum_{\mathbf{p}'} R_{\mathbf{p}',\mathbf{p}} B_{\mathbf{p}',t} \tag{3.13}$$

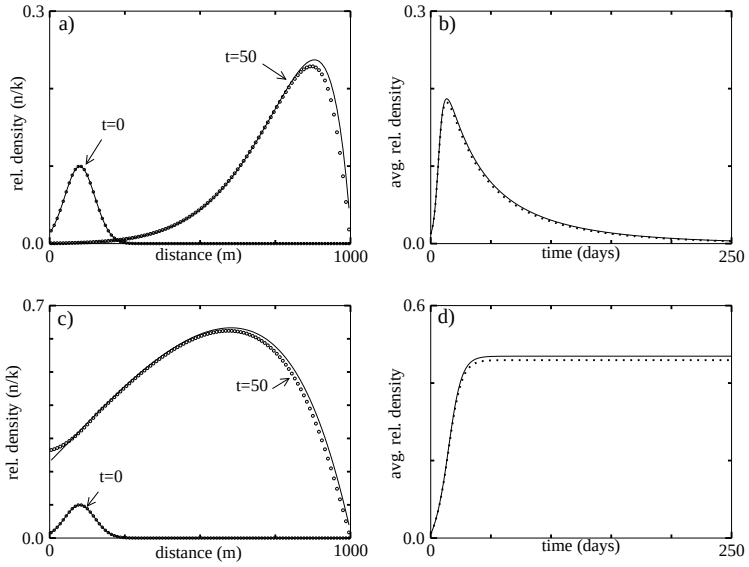

Figure 3.1: *Temporal development of a logistically regulated population with an intrinsic growth rate of* $0.39day^{-1}$*, being advected along a 1 km river with a velocity of* $0.001ms^{-1}$*. Upper frames have* $\Phi_x = 0.06m^2s^{-1}$*. Lower frames have* $\Phi = 0.25m^2s^{-1}$*. Right hand frames show the time history of average population density. Left hand frames show the spatial distributions at* $t = 0$ *and the predicted distribution at* $t = 50days$*. Solid lines represent the continuous time numerical model implementations, circles represent the discrete model. Discrete model: displaced tent redistribution matrix (3.12),* $\Delta t = 0.1day$*. From Speirs and Gurney (2001), with permission.*

The local growth function is still given by Equation (3.10). In a 2D system with constant rates of advection and diffusion, the requirements on the redistribution matrix become

$$\begin{aligned}
\sum_{\mathbf{p}} R_{\mathbf{p}',\mathbf{p}} &= 1 \\
\sum_{\mathbf{p}} (x - x') R_{\mathbf{p}',\mathbf{p}} &= V_x \Delta t \\
\sum_{\mathbf{p}} (x - x')^2 R_{\mathbf{p}',\mathbf{p}} &= 2\Phi_x \Delta t + (V_x \Delta t)^2 \\
\sum_{\mathbf{p}} (z - z') R_{\mathbf{p}',\mathbf{p}} &= V_z \Delta t \\
\sum_{\mathbf{p}} (z - z')^2 R_{\mathbf{p}',\mathbf{p}} &= 2\Phi_z \Delta t + (V_z \Delta t)^2
\end{aligned} \tag{3.14}$$

where $V_z \Delta t$ and $2\Phi_z \Delta t$ are the mean displacement and displacement variance in the vertical respectively.

For such a system the generalisation of the displaced tent distribution is given by

$$R_{\mathbf{p}',\mathbf{p}} = \phi \left(1 - \frac{|x - x' - d_{ox}|}{d_{mx}} - \frac{|z - z' - d_{oz}|}{d_{mz}} \right)^{+} \tag{3.15}$$

The coefficients ϕ, d_{ox}, d_{mx}, d_{oz} and d_{mz} are chosen so that the conditions of Equation (3.14) are satisfied. Speirs and Gurney (2001) used a recursive bi-linear interpolation algorithm to determine these coefficients for each run using a new combination of model parameters. This satisfied a penalty function imposed on each of the conditions in turn, repeating the exercise if satisfying one condition re-invalidated a previously satisfied condition, until all penalty functions were satisfied simultaneously. For this work the parameters were found by making use of a NAG software library routine and combining separate penalty functions for each of the conditions of Equation (3.14) in to one overall penalty function. That is if ψ_1, ψ_2, ψ_3, ψ_4 and ψ_5 are defined as

$$\begin{aligned}
\psi_1 &= \sum_{\mathbf{p}} R_{\mathbf{p}',\mathbf{p}} - 1 \\
\psi_2 &= \sum_{\mathbf{p}} (x - x') R_{\mathbf{p}',\mathbf{p}} - V_x \Delta t \\
\psi_3 &= \sum_{\mathbf{p}} (x - x')^2 R_{\mathbf{p}',\mathbf{p}} - [2\Phi_x \Delta t + (V_x \Delta t)^2] \\
\psi_4 &= \sum_{\mathbf{p}} (z - z') R_{\mathbf{p}',\mathbf{p}} - V_z \Delta t \\
\psi_5 &= \sum_{\mathbf{p}} (z - z')^2 R_{\mathbf{p}',\mathbf{p}} - [2\Phi_z \Delta t + (V_z \Delta t)^2]
\end{aligned} \tag{3.16}$$

then the NAG routine is used to minimise Ψ, where

$$\Psi = \psi_1^2 + \psi_2^2 + \psi_3^2 + \psi_4^2 + \psi_5^2 \tag{3.17}$$

This approach was found to work most efficiently if the component penalty functions, ψ_1 etc., were weighted according to the relative magnitudes of the right hand sides of the separate conditions shown in Equation 3.14.

Space dependent displaced tent distributions

The parameters of a displaced tent distribution are dependent on the velocities and diffusion coefficients found at the point in space and time at which it is to be applied. For work considering a 2D domain of a weakly mixed river, velocities and diffusion constants are considered constant in time but river velocity varies with depth. In this instance a unique tent distribution is required for each depth representing a cell centre in the model. If z' represents the vertical component of the source cell position vector, then the formula for each tent becomes

$$R_{\mathbf{p}',\mathbf{p}} = \phi(z') \left(1 - \frac{|x - x' - d_{ox}(z')|}{d_{mx}(z')} - \frac{|z - z' - d_{oz}(z')|}{d_{mz}(z')}\right)^{+} \tag{3.18}$$

and each tent is subject to the conditions as in Equation (3.14), but with a uniform value of V_x now replaced by $V_x(z')$.

Speirs and Gurney (2001) showed how use of tent distributions could be extended to tidally driven habitats. In such habitats the deterministic flow fields vary with time and it is therefore expected that the redistribution matrix $R_{\mathbf{p}',\mathbf{p}}$ also becomes time dependent. If, however, the update increment, Δt is set equal to one tidal cycle, $R_{\mathbf{p}',\mathbf{p}}$ then represents the residual motion over one tidal cycle. It is necessary to ignore the spring-neap cycle, but if this is done $R_{\mathbf{p}',\mathbf{p}}$ becomes time-independent. Assuming a tidal period of 12 hours, this is the size required for the update increment of the population model. Speirs and Gurney (2001) found that results obtained from simulations of the river scenarios, (using $\Delta t = 0.1 day$), were weakly affected by the increase in timestep.

With Δt set equal to the tidal period the population model is defined by Equation (3.13) while each redistribution matrix is given by

$$R_{\mathbf{p}',\mathbf{p}} = \phi(x', z') \left(1 - \frac{|x - x' - d_{ox}(x', z')|}{d_{mx}(x', z')} - \frac{|z - z' - d_{oz}(x', z')|}{d_{mz}(x', z')}\right)^{+} \tag{3.19}$$

and the coefficients of each redistribution matrix are chosen so that

$$\begin{aligned}
\sum_{\mathbf{p}} R_{\mathbf{p}',\mathbf{p}} &= 1 \\
\sum_{\mathbf{p}} (x - x') R_{\mathbf{p}',\mathbf{p}} &= \Delta_x(x', z') \\
\sum_{\mathbf{p}} (x - x')^2 R_{\mathbf{p}',\mathbf{p}} &= 2\Phi_x \Delta t + (\Delta_x(x', z'))^2 \\
\sum_{\mathbf{p}} (z - z') R_{\mathbf{p}',\mathbf{p}} &= \Delta_z(x', z') \\
\sum_{\mathbf{p}} (z - z')^2 R_{\mathbf{p}',\mathbf{p}} &= 2\Phi_z \Delta t + (\Delta_z(x', z'))^2
\end{aligned} \tag{3.20}$$

In the above equations, Δ_x and Δ_z represent the x and z components of the net displacement of a neutrally buoyant particle, starting at position (x', z'), over exactly one tidal cycle. In other words they are Lagrangian residual movements, as outlined in section 2.1.4. These values are derived by performing particle tracking on such a particle using a fourth order Runge-Kutta algorithm and snap shots of instantaneous flow fields. The x and z components of velocity in the flow fields can be defined by an analytic solution of a simplified set of fluid dynamic equations, or via numerical solution of the full equations. These two means of determining the velocity fields are described in chapters 4 and 5 respectively.

The Δ_x and Δ_z values are very likely to be different for each cell used in a model. Potentially a unique tent distribution is required for each cell. Application of tent distributions in a tidal situation also relies on organismal diffusion being divorced from the flow fields in that its application is unaffected by the locations and movements of the tracked particle during a tidal cycle. The issue of dispersion caused by an interaction of advective and random motion at sub-tidal timescales raises doubts about the validity of diffusion imposed only at the end of deterministic tracking. This is certainly the case if the flow fields are strongly divergent. It would again be true if animal behaviour in the form of reaction to changes in the flow field or some other factor, (such as salinity), were to be modelled. A further

complication arises when the bathymetry is no longer straight sided. The method of images at a reflecting boundary, effectively folding the distribution about the boundary, becomes complicated.

Redistribution matrices from particle tracking

To accommodate scenarios where the use of displaced tent distributions is less convenient or inapplicable, the work of this thesis also generated redistribution matrices obtained from particle tracking. In its simplest form the particle tracking algorithm uses the same discrete spatial representation of the domain as the population model. From the centre of each cell the program tracks a specified number of particles, N, over Δt, the time step used for the population model. Assuming velocities within the domain can vary with space and time, particle tracking is performed over timesteps, δt, much smaller than those used for the population model. The average velocity over each period δt is obtained using a fourth order Runge-Kutta algorithm. In the same way as particle tracking used to produce the most general form of displaced tent distribution, the values of instantaneous velocity used by the Runge-Kutta algorithm were derived from snap shots of flow fields, defined either by solution to a simplified set of fluid dynamic equations, or via numerical solution to the full set of equations. Because a particle's position at any particle tracking timestep is unlikely to coincide with a velocity data value position, instantaneous velocity values are interpolated in space. If the timesteps δt are smaller than the time gaps between snap shot velocity data files the instantaneous velocity values are also interpolated in time. Organismal diffusion is added at the end of each tracking timestep by assuming it is a white noise velocity with power spectral density $\sqrt{2\Phi_x}; \sqrt{2\Phi_z}$, that is the displacement variances over the time interval δt are defined as $2\Phi_x \delta t$ and $2\Phi_z \delta t$ in the x and z directions respectively.

In this approach $R_{p',p}$ is given by

$$R_{\mathbf{p}',\mathbf{p}} = \frac{\text{number of tracks from } \mathbf{p}' \text{ to } \mathbf{p}}{\text{number of repetitions, } N}$$

There is additional computing overhead in the need to run the particle tracking program, compared to generating displaced tent distributions. Once a redistribution matrix is completed, however, the population model runs exactly as before. Indeed, whereas the population model must handle any tent distributions that attempt to place population beyond reflecting boundaries, the population model using a redistribution matrix from a particle tracking program is free from such issues, as they have been dealt with by the tracking algorithm.

Regardless of how the redistribution matrix is formed, if investigating the effect of parameters that do not alter the spatial redistribution of population, the redistribution matrix only need be formed once and its calculation can be considered 'off line'. The most important parameter in this respect is the per-capita growth of the population, either through changes in the intrinsic growth rate, or the whole growth regime. Overall, use of a tracking algorithm combined with a discrete population model can still be more computationally efficient than numerical solution of the partial differential equations.

In Fig. 3.2 the numerical solutions to a continuous model representing a logistically regulated population, as shown in Fig. 3.1 are reproduced from (Speirs and Gurney 2001). Super-imposed on these results are ones obtained using particle tracking and the discrete space-time population model. The discrete model is able to match the continuous model very closely. The approximation is better than that achieved using the displaced tent redistribution matrix while using comparable, or even greater values of Δt. Use of particle tracking performs better close to the boundaries.

A good match of the continuous solution was obtained over a range of values for Δt and interval size Δx. With $\Phi = 0.06$, a Δt value of $6hrs \sim 0.1r^{-1}$ worked well. With $\Phi = 0.25$, the peak values of the population distribution could only be

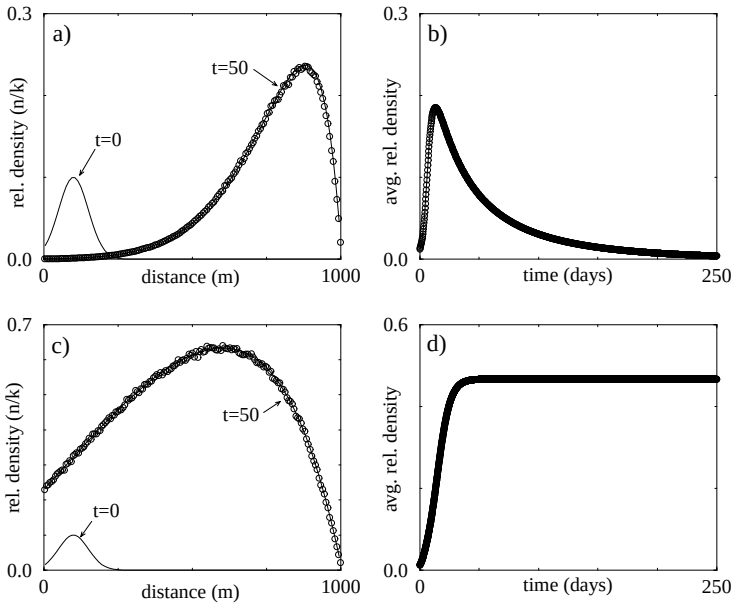

Figure 3.2: *Temporal development of a logistically regulated population with an intrinsic growth rate of* $0.39day^{-1}$*, being advected along a 1 km river with a velocity of* $0.001ms^{-1}$*. Upper frames have* $\Phi_x = 0.06m^2s^{-1}$*. Lower frames have* $\Phi = 0.25m^2s^{-1}$*. Right hand frames show the time history of average population density. Left hand frames show the spatial distributions at* $t = 0$ *and the predicted distribution at* $t = 50days$*. Solid lines represent the continuous time numerical model implementations, circles represent the discrete model. Discrete model: redistribution matrix from particle tracking. Upper frames:* $\Delta x = 6m$*,* $\Delta t = 6hrs$*, Particles tracked per cell 10000; Lower frames:* $\Delta x = 6m$*,* $\Delta t = 2hrs$*, Particles tracked per cell 12000; All frames* $\delta t = 30s$*.*

repeated with $\Delta t = 2hrs$. This is possibly due to the higher relative densities of the latter case, such that population growth within an update increment is more likely to be affected by the non-linear growth term.

As would be expected, the fidelity of the discrete model is affected as N is reduced. In Fig. 3.3 the lower frames show runs with Φ_x, Δt and Δx values as used in the upper frames of Fig. 3.2 but with decreasing values of N.

Conditions requiring corrections to diffusion coefficients

Gurney, Speirs, Wood, Clarke, and Heath (2001) identified a source of potential error when using particle tracking to form redistribution matrices, depending on the combination of cell size, diffusion coefficient and update increment, Δt.

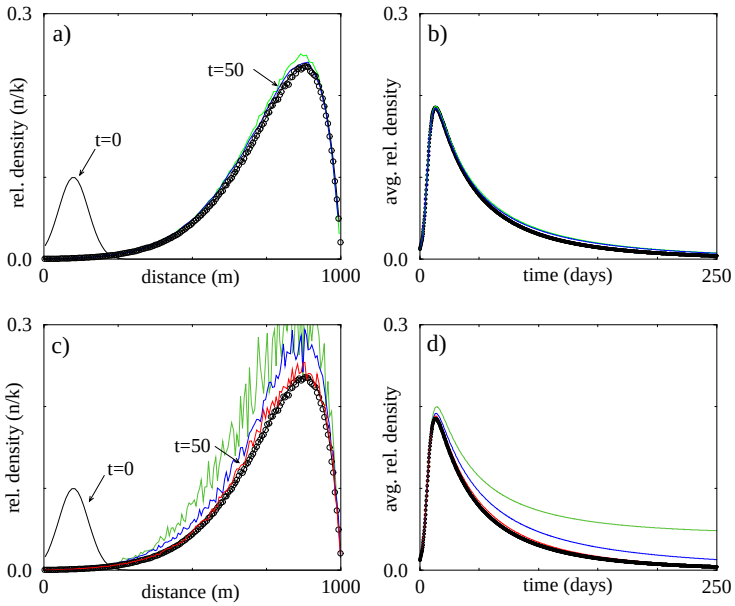

Figure 3.3: *Logistically regulated population with an intrinsic growth rate of* $0.39day^{-1}$*, being advected along a* $1km$ *river with a velocity of* $0.001ms^{-1}$*,* $\Phi_x = 0.06m^2s^{-1}$*.* $\Delta t = 6hrs$*. Upper frames: Particles tracked per cell 10000,* $\Delta x = 6m$*(circles),* $10m$*(blue),* $20m$*(green); Lower frames:* $\Delta x = 6m$*, Particles tracked per cell* 10000*(circles),* 1000*(red),* 500*(blue),* 100*(green).*

Considering the x direction only, and assuming a population is only subject to diffusion, the redistribution matrix is required to satisfy

$$\sum_x (x - x')^2 R_{x',x} = 2\Phi_x \Delta t \tag{3.21}$$

If we name the diffusion coefficient used by the tracking algorithm, Φ_T, then the tracking operation produces a distribution of particle positions at Δt which is normal with a zero mean and variance $2\Phi_T \Delta t$. R_{x',x_j} represents the fraction of the tracked ensemble whose final position lies in the cell centred at $(j - \frac{1}{2})\Delta x$, where Δx represents the cell size. Therefore, in the limit of a very large ensemble

$$R_{x',x_j} = \frac{1}{\sqrt{4\pi\Phi_T \Delta t}} \int_{(j-1)\Delta x}^{j\Delta x} \exp\left(-\frac{x^2}{4\Phi_T \Delta t}\right) dx \tag{3.22}$$

The value of Φ_T should be such that when the component parts of the redistribution matrix given by Equation (3.22) are summed, they satisfy Equation (3.21).

By defining $y \equiv x/L_D$ where $L_D \equiv \sqrt{2\Phi_x \Delta t}$ and $\nu \equiv \Phi_T/\Phi_x$, and combining Equations (3.21) and (3.22) the problem becomes one of choosing ν such that

$$1 = \frac{1}{\sqrt{2\pi\nu}} \sum_x \left(\frac{x - x'}{L_D} \right)^2 \int_{(j-1)\frac{\Delta x}{L_D}}^{j\frac{\Delta x}{L_D}} \exp\left(-\frac{y^2}{2\nu} \right) dy \tag{3.23}$$

Solving Equation (3.23) for ν numerically allows the appropriate value of ν to be applied for any given combination of Δt, Δx and desired Φ_x. Gurney et al. (2001) showed that for $\Delta x < 0.1 L_D$ no correction to the target diffusion constant is necessary. For the approximate range $0.1 L_D \leq \Delta x \leq 3.5 L_D$, tracking with the target diffusion constant produces redistribution matrices which imply excess diffusion, that is ν is a number less than one. Once the normalised cell size exceeds $3.5 L_D$ the situation is reversed, with use of the target diffusion constant producing matrices which underestimate the required diffusion.

Gurney, Speirs, Wood, Clarke, and Heath (2001) went on to consider situations where particles are subject to both constant advection and diffusion. The correction factor ν was calculated from Equation (3.23), that is as if there were zero advection. It was found that for $\Delta x < 1.5 L_D$ both the advection and diffusion were rendered accurately, (errors $< 1\%$), by the corrected tracking process. A value of $\Delta x/L_D$ of up to 2 could be used for an error of approximately 10% but if the ratio of cell size to diffusion length were larger, error increased rapidly and became sensitively dependent on advection velocity.

The upper frames of Fig. 3.3 shows results for the case where $\Phi_x = 0.06 m^2 s_{-1}$ and $\Delta t = 6hrs$, with the black line showing the solution to the continuous model. The circles represent the result using $\Delta x = 6m$, giving $\Delta x/L_D \approx 0.1$. The green line represents the result using an uncorrected value of Φ_x and $\Delta x = 20m$, giving $\Delta x/L_D \approx 0.4$.

Chapter 4

Analytically derived flow fields

4.1 Equations of motion for a Newtonian viscous fluid

The equations of motion for a fluid are given by a combination of a conservation of mass, or continuity equation, and a conservation of momentum equation. If an assumption of incompressibility is used, together with that of constant density, then the conservation of mass equation can be written as

$$\frac{\partial v_1}{\partial x_1} + \frac{\partial v_2}{\partial x_2} + \frac{\partial v_3}{\partial x_3} \equiv \nabla \cdot \mathbf{v} = 0 \tag{4.1}$$

where x_1, x_2, x_3 represent the Cartesian axes, v_1, v_2, v_3 are the components of velocity along the x_1, x_2 and x_3 directions, $\mathbf{v}$ is the velocity components in vector form and $\nabla\cdot$ is known as the divergence operator.

The momentum equation states that for an elementary volume of fluid, the product of its mass and acceleration equals the total force acting upon it, that is

$$\rho \frac{D\mathbf{v}}{Dt} = \rho \mathbf{F} + \nabla \cdot \tau \tag{4.2}$$

where the 'body force', $\mathbf{F}$ is the force per unit mass acting on the body of the fluid and the 'stress tensor', τ is a tensor quantity whose elements, τ_{ij}, represent the force per unit area acting in the j direction on a surface with its normal in the i direction. The term $\nabla \cdot \tau$ is used in the sense that

$$(\nabla \cdot \tau)_i = \frac{\partial \tau_{i1}}{\partial x_1} + \frac{\partial \tau_{i2}}{\partial x_2} + \frac{\partial \tau_{i3}}{\partial x_3} \tag{4.3}$$

A Newtonian viscous fluid is defined such that

$$\tau_{ij} = -p\delta_{ij} + \mu \left(\frac{\partial v_j}{\partial x_i} + \frac{\partial v_i}{\partial x_j} \right) \tag{4.4}$$

where μ is the coefficient of absolute viscosity of the fluid. It is a quantity describing the amount of random molecular motion within the fluid, (and as such is a property of the fluid). The term δ_{ij} is the Kronecker delta which takes the value zero unless $i = j$ in which case it is unity[1]. If we assume the absolute viscosity to be constant then the equation of motion for a component of velocity can be written as

$$\begin{aligned} \rho \frac{Dv_i}{Dt} &= \rho g_i - \frac{\partial p}{\partial x_i} + \mu \frac{\partial}{\partial x_j} \left(\frac{\partial v_j}{\partial x_i} + \frac{\partial v_i}{\partial x_j} \right) \\ \rho \frac{Dv_i}{Dt} &= \rho g_i - \frac{\partial p}{\partial x_i} + \mu \frac{\partial}{\partial x_i} \left(\frac{\partial v_j}{\partial x_j} \right) + \mu \frac{\partial^2 v_i}{\partial x_j^2} \end{aligned} \tag{4.5}$$

where it is assumed the body force is given by $\mathbf{F} = (g_1, g_2, g_3)$. A repeated j suffix denotes summation over the three dimensions. Thus

$$\frac{\partial^2}{\partial x_j^2} = \frac{\partial^2}{\partial x_1^2} + \frac{\partial^2}{\partial x_2^2} + \frac{\partial^2}{\partial x_3^2} \equiv \nabla^2$$

where ∇^2 is known as the Laplacian operator. Also

[1]Here, the stress tensor is symmetric, that is $\tau_{ij} = \tau_{ji}$.

$$\frac{\partial v_j}{\partial x_j} = \nabla \cdot \mathbf{v}$$

But for an incompressible fluid $\nabla \cdot \mathbf{v} = 0$ so that Equation (4.5) becomes

$$\rho \frac{Dv_i}{Dt} = \rho g_i - \frac{\partial p}{\partial x_i} + \mu \frac{\partial^2 v_i}{\partial x_j^2} \tag{4.6}$$

and the momentum equation for all three dimensions becomes

$$\rho \frac{D\mathbf{v}}{Dt} = \rho \mathbf{F} - \nabla p + \mu \nabla^2 \mathbf{v} \tag{4.7}$$

Equation (4.7) is a form of what are known as the Navier-Stokes equations, this particular form assuming constant viscosity and density. If the only body force comes from a uniform gravitational force, such that $\mathbf{F} = (0, 0, g)$ Equation (4.7) can be simplified by defining a modified pressure $P \equiv p - \rho g z$ such that the equation becomes

$$\frac{D\mathbf{v}}{Dt} = -\frac{1}{\rho} \nabla P + \nu \nabla^2 \mathbf{v} \tag{4.8}$$

where ν is known as the kinematic viscosity and is defined as

$$\nu = \frac{\mu}{\rho} \tag{4.9}$$

4.1.1 Transfer of momentum and shear stresses

If we take the x component of the Navier-Stokes momentum equations we can write it as follows

$$\begin{aligned}
\rho\frac{DV_x}{Dt} &= \rho g_1 - \frac{\partial p}{\partial x} + \mu\left[\frac{\partial^2 V_x}{\partial x^2} + \frac{\partial^2 V_x}{\partial y^2} + \frac{\partial^2 V_x}{\partial z^2}\right] \\
\rho\frac{DV_x}{Dt} &= \rho g_1 - \frac{\partial p}{\partial x} + \frac{\partial}{\partial x}\left(\mu\frac{\partial V_x}{\partial x}\right) + \frac{\partial}{\partial y}\left(\mu\frac{\partial V_x}{\partial y}\right) + \frac{\partial}{\partial z}\left(\mu\frac{\partial V_x}{\partial z}\right) \quad (4.10)
\end{aligned}$$

The quantities $\mu\partial V_x/\partial y$ and $\mu\partial V_x/\partial z$ are known as shear stresses[2] as they generate forces parallel to the direction of flow being considered due to the gradient, or shear, of the velocity in the second dimension. Shear stresses and the resultant shearing of flow fields are important in relation to bottom friction and the vertical gradient in horizontal velocity such friction creates in combination with the viscosity of the fluid. Sheared flow is one mechanism for the dispersion of passive tracers. The forces occur because of the transfer of momentum between planes parallel to the direction of motion, due to molecular diffusion. Shear stresses are denoted using the stress tensor terminology τ_{ij} where the second subscript denotes the direction of the force while the first subscript denotes the direction of the momentum flux. So, for example

$$\tau_{zx} = \mu\frac{\partial V_x}{\partial z} \quad (4.11)$$

4.2 Turbulent flow

In turbulent flow the velocity vector is considered to be comprised of a mean component denoted by an over-score and a fluctuating component denoted by a prime, (Nunn 1989), such that the instantaneous velocity vector is given by

[2] $\mu\partial V_x/\partial x$ is a normal stress.

$$\mathbf{v} = \bar{\mathbf{v}} + \mathbf{v}' \tag{4.12}$$

Importantly, the mean of the fluctuating part of any individual velocity component, (if taken over a sufficiently long time), is zero, but the mean of the product of any two fluctuating velocity components is not zero.

4.2.1 Equations of motion for turbulent flow

To derive these equations the substantive derivative is first cast in a different form as follows

$$\frac{Dv_i}{Dt} = \frac{\partial v_i}{\partial t} + v_j \frac{\partial v_i}{\partial x_j} = \frac{\partial v_i}{\partial t} + \frac{\partial}{\partial x_j}(v_i v_j) - v_i \frac{\partial v_j}{\partial x_j} \tag{4.13}$$

For an incompressible fluid the last term becomes zero such that the substantive derivative becomes

$$\frac{Dv_i}{Dt} = \frac{\partial v_i}{\partial t} + \frac{\partial}{\partial x_j}(v_i v_j) \tag{4.14}$$

Writing the Navier-Stokes equations for the instantaneous velocity components gives

$$\rho \left\{ \frac{\partial}{\partial t}(\bar{v}_i + v_i') + \frac{\partial}{\partial x_j}[(\bar{v}_i + v_i')(\bar{v}_j + v_j')] \right\} = -\frac{\partial}{\partial x_i}(\bar{P} + P') + \mu \nabla^2 (\bar{v}_i + v_i') \tag{4.15}$$

This may be expanded and rearranged to show how the new Navier-Stokes equations incorporate those for the mean motion and those for the fluctuations, as follows

$$\left.\begin{array}{l} \rho \left[\frac{\partial \bar{v}_i}{\partial t} + \frac{\partial}{\partial x_j}(\bar{v}_i \bar{v}_j) \right] \\ +\rho \left[\frac{\partial v_i'}{\partial t} + \frac{\partial}{\partial x_j}(\bar{v}_j v_i' + \bar{v}_i v_j' + v_i' v_j') \right] \end{array}\right\} = \left\{ \begin{array}{l} -\frac{\partial \bar{P}}{\partial x_i} + \mu \nabla^2 \bar{v}_i \\ -\frac{\partial P\prime}{\partial x_i} + \mu \nabla^2 v_i' \end{array} \right. \tag{4.16}$$

The momentum equations are expected to govern the motion of the fluid on an average basis as well as instantaneously (Nunn 1989), and taking a time average of Equation (4.16) leaves only one surviving turbulence quantity, $\overline{v_i' v_j'}$ such that the equation becomes

$$\rho \left[\frac{\partial \bar{v}_i}{\partial t} + \frac{\partial}{\partial x_j}(\bar{v}_i \bar{v}_j + \overline{v_i' v_j'}) \right] = -\frac{\partial \bar{P}}{\partial x_i} + \mu \nabla^2 \bar{v}_i \tag{4.17}$$

As far as the acceleration of the mean flow is concerned the turbulent fluctuation quantities can be considered additional shear and normal stress terms, which is illustrated by an alternative form of the above result

$$\rho \frac{D\bar{v}_i}{Dt} = -\frac{\partial \bar{P}}{\partial x_i} + \mu \nabla^2 \bar{v}_i - \frac{\partial}{\partial x_j}(\overline{v_i' v_j'}) \tag{4.18}$$

Equations (4.18) are known as the Reynolds equations and the last term on the right hand side represents the Reynolds stresses. In all but virtually laminar flows these Reynolds stresses are orders of magnitude greater than those due to molecular diffusion. A strategic simplification to working with turbulent flow can be made by considering the modelling of Reynolds stresses to be analogous to molecular viscosity and then ignoring the latter on the basis of its much smaller effect. To show this the Reynolds equation for the x direction can be considered and written in the following form

$$\rho \frac{D\overline{V_x}}{Dt} = -\frac{\partial \overline{P}}{\partial x} + \frac{\partial}{\partial x}\left(\mu \frac{\partial \overline{V_x}}{\partial x} - \rho \overline{V_x'^2} \right) + \frac{\partial}{\partial y}\left(\mu \frac{\partial \overline{V_x}}{\partial y} - \rho \overline{V_x' V_y'} \right) + \frac{\partial}{\partial z}\left(\mu \frac{\partial \overline{V_x}}{\partial z} - \rho \overline{V_x' V_z'} \right) \tag{4.19}$$

It is now possible to define eddy viscosity such that, for example

$$\rho \overline{V_x' V_y'} = -N \frac{\partial \overline{V_x}}{\partial y} \tag{4.20}$$

and the appropriate shear stress term from Equation (4.19) can be written

$$\frac{\partial}{\partial y}(\tau_{yx}) = \frac{\partial}{\partial y}\left(\mu\frac{\partial\overline{V_x}}{\partial y} - \rho\overline{V_x'V_y'}\right) = \frac{\partial}{\partial y}\left[(\mu+N)\frac{\partial\overline{V_x}}{\partial y}\right] \tag{4.21}$$

If it is then argued that the stresses due to molecular viscosity can be ignored this leads to Equation (4.19) becoming

$$\rho\frac{D\overline{V_x}}{Dt} = -\frac{\partial\overline{P}}{\partial x} + \frac{\partial}{\partial x}\left(N\frac{\partial\overline{V_x}}{\partial x}\right) + \frac{\partial}{\partial y}\left(N\frac{\partial\overline{V_x}}{\partial y}\right) + \frac{\partial}{\partial z}\left(N\frac{\partial\overline{V_x}}{\partial z}\right) \tag{4.22}$$

where N is known as the coefficient of eddy viscosity. In practice N is not a constant but varies with the magnitude of the velocity vector and is not a scalar because the turbulent fluctuations upon which its definition is based are directional and likely to vary throughout the flow. If these two assumptions are made however, then the momentum equations for turbulent flow become exactly equivalent to the Navier-Stokes equations but with N replacing μ. In practise the coefficient is split into three component parts, N_x, N_y and N_z. Numerical schemes, such as the Princeton Ocean Model, (POM), described in chapter 5 do calculate time varying values of these coefficients based on theories involving the gradients of the time averaged velocity components. In subsequent equations dealing with turbulent flows the mean nature of the time averaged terms is considered implicit and the over-line is omitted.

If considering passive tracers within the flow, the description of the concentration of tracer over time and space can be performed by use of an equation analogous to the momentum equation. Diffusive movement of tracers by turbulence has been found from experiment to be similar but not equivalent to the spreading of momentum in flows of near uniform density. Therefore new coefficients are defined, (K_x, K_y and K_z), which are known as the coefficients of eddy diffusion. The ratio of eddy viscosity coefficient to eddy diffusion coefficient is known as the Prandtl number. Its value is often taken to be 1, although the value can move well away from unity in the presence of density stratification, as described below. In the analytical population models and discrete space-time simulations the 'diffusion' coefficients used represent a potential mixture of fluid flow and

organismal induced diffusive movement. They might also be representing dispersion rather than pure diffusion. They are therefore given the separate notation of $\Phi_x,\ \Phi_y,\ \Phi_z$.

In general the Navier-Stokes equations, in laminar or turbulent form, can only be solved analytically for special cases. Otherwise numerical methods must be employed. For initial investigations of persistence in advective environments, however, valuable insights can be gained using analytic flow regimes derived from strategic simplifications to the problem. These are considered after special focus is given to the vertical component of turbulence.

4.3 Vertical turbulent eddy viscosity and diffusion

It will be seen in later sections and chapters that the value of the vertical component of turbulent eddy viscosity is an important consideration in relation to producing Lagrangian residual movements from the analytic treatment of tidal flows presented in section 4.5. If it is considered that an animal has a random movement not very different to that for a passive tracer, that is a movement almost solely determined by water movement, then the value of vertical eddy diffusivity is very significant for analytic population persistence results in two dimensional river flow. Finally, when producing a transition matrix for the discrete time population model from solutions to the fluid dynamic equations and particle tracking, diffusion must be imposed at each tracking timestep to prevent all tracks following the same path. The vertical eddy diffusivity values that would be expected from the type of flow being considered provide an obvious guide to the vertical diffusion coefficient, Φ_z, to be applied in the tracking program.

For a two dimensional flow, referring to Equation (4.20), the vertical eddy viscosity N_z is related to the shear stress τ_{zx} by

$$\tau_{zx} = \rho\overline{V_x' V_z'} = N_z \frac{dV_x}{dz} \tag{4.23}$$

For steady flows, (rivers), values for the vertical component of eddy viscosity can be deduced after establishing a second relationship between the shear stress and velocity profile. In classical hydraulic theory this is done by making use of Prandtl's mixing length concept, which describes the average distance travelled by a block of fluid in turbulent flow before it suddenly acquires the velocity of the flow at a different location, (Smith 1975). This theory suggests the following relationship between the shear stress and the velocity gradient

$$\tau_{zx} = K' \rho l^2 \left| \frac{dV_x}{dz} \right| \frac{dV_x}{dz} \tag{4.24}$$

where l is the mixing length and K' is a constant of proportionality. If it is assumed that

1. Near the bed the shear stress is constant and equal to the stress on the bed itself. That is $\tau_{zx} = \tau_{zxo} = constant$.

2. The scale of the turbulence is proportional to the distance from the bed. That is $(K')^{1/2} l \propto z$ where z represents distance from the bed.

then $(K')^{1/2} l$ can be replaced by κz where κ is a constant known as von Karman's constant. Experimental determinations have concluded that the value of κ is about 0.40 or 0.41. Using these assumptions and a value of von Karman constant of 0.4 Equation (4.24) can be re-cast as

$$dV_x = \sqrt{\frac{\tau_{zxo}}{\rho}} \frac{1}{0.4} \frac{dz}{z} \tag{4.25}$$

The quantity $\sqrt{\tau_{zxo}/\rho}$ has the dimensions of velocity and is known as the friction or shear velocity and is given the symbol U_f or U_*. Solving Equation (4.25) gives

$$V_x = 2.5\sqrt{\frac{\tau_{zxo}}{\rho}}\ln\left(\frac{z}{C}\right) \tag{4.26}$$

The constant of integration, C, depends on the ratio between the height of roughness elements at the bed and the thickness of a laminar sub-layer which is present in all turbulent flows. For natural rivers and estuaries the roughness elements almost always project beyond the sub-layer, (dynamically rough flow), and for such flow C is dependent only on the height of roughness projections, r_p. The relationship is found from experiment to be $C = r_p/30$ such that Equation (4.26) becomes

$$V_x = 2.5U_* \ln\left(\frac{30z}{r_p}\right) \tag{4.27}$$

Some oceanographic calculations, including those represented within the Princeton Ocean Model, (POM), express Equation (4.26) in the form

$$V_x = 2.5U_* \ln\left(\frac{z}{z_o}\right) \tag{4.28}$$

where z_o is known as the roughness parameter. If dynamically rough conditions can be assumed for the flow then z_o is actually related to the size of roughness elements[3] in the bed by $z_o = C = r_p/30$.

Maintaining the assumption that shear stress is constant up the water column, then given that $U_* = \sqrt{\tau_{zxo}/\rho} = 0.4z(dV_x/dz)$ and using Equation (4.23), ($\tau_{zxo} = \Phi_z(dV_x/dz)$), it can be seen that

[3]For the relationships $z_o = C = r_p/30$ and $C = r_p/30$, r_p only represents the actual physical height of roughness projections if those roughness projections are distributed in a uniform manner, (Smith 1975). If the spread of projections is uneven, or the grains vary in size, then an 'equivalent roughness height' is employed. There is, however, no definite correlation between grain size and equivalent roughness height, (Chanson 1999, page 235)

$$N_z = \rho 0.4 U_* z \tag{4.29}$$

if N_z is to represent the turbulent equivalent to dynamic viscosity or

$$n_z = 0.4 U_* z \tag{4.30}$$

if n_z is to represent the turbulent equivalent to kinematic viscosity. In other words eddy viscosity increases linearly with distance above the bed, regardless of velocity profile. For a gradient current, such as rivers, where flow is due to gravity alone, U_* can be calculated from the relation

$$U_* = \sqrt{gHS} \tag{4.31}$$

where g is acceleration due to gravity, H the total depth of the water and S the slope of the water surface. Using this result the vertically averaged value of the eddy viscosity coefficient is found to be

$$\overline{n_z} = \frac{\kappa}{6} U_* H \approx 0.0667 U_* H \tag{4.32}$$

Laboratory studies of steady flow have found that the vertical eddy viscosity does not increase linearly with depth but has a magnitude which is roughly parabolic in shape with a maximum at approximately half depth and values of zero at bed and surface, (McDowell and O'Connor 1977, page 65). An improvement on Equation (4.30) that allows reproduction of this shape is given by

$$n_z = 0.4 U_* z \sqrt{1 - z/H} \tag{4.33}$$

Equation (4.33) is achieved by assuming the distribution of shear stress is linear over the depth of the flow rather than constant, while retaining a logarithmic

velocity profile as described by Equation (4.27) or (4.28).

The additional complication in constant-density tidal flow, (as found when trying to determine longitudinal dispersion), is the unsteady nature of the flow. Turbulence will be caused predominantly by bottom shear stress such that it could be expected possible to utilise Equation (4.30) or (4.33) but U_* will vary from a maximum at maximum flood and ebb to virtually zero at slack tide. Engineering studies have often used the average value of U_* over a tidal cycle, (Fischer, List, Koh, Imberger, and Brooks 1979).

In general, in shear flows the vertically averaged horizontal velocity, $\overline{U}$, is found a distance $0.4H$ from the bed. Equation (4.27) or (4.28) can therefore be used to determine a relation between the shear velocity and the mean velocity for a given flow. As shear velocity is a difficult quantity to measure a formula using the vertical mean velocity in its place was suggested by Bowden (1967), namely

$$n_z = 0.0025H\overline{U} \tag{4.34}$$

at the mid depth of the vertical cross section. If the tidal average value for $\overline{U}$ is used then the tidally averaged value of n_z at a horizontal location has been derived using the vertical average of the Eulerian residual velocity at that point.

The value of the vertical eddy viscosity and diffusivity can be considered equal for a homogeneous estuary. Lewis (1987) considers that in general a value for these quantities in such estuaries is of the order $0.01m^2s^{-1}$. McDowell and O'Connor (1977) quote a range for such coefficients of $0.01 - 0.1m^2s^{-1}$ for maximum instantaneous values and for tidally averaged values of $0.001 - 0.01m^2s^{-1}$.

The picture is complicated further when density stratification is taken into account. A stable vertical density gradient can reduce turbulent exchange, or, if it is sufficiently strong, extinguish turbulence altogether. Any mixing now must be caused by velocity shear at the pycnocline, (Dyer 1973). The Richardson number, Ri, is a comparison of the stabilising forces of the density gradient to the

destabilising influences of velocity shear. It is defined as

$$Ri = -\frac{g}{\rho}\frac{\partial \rho}{\partial z} \Big/ \left(\frac{\partial U}{\partial z}\right)^2 \tag{4.35}$$

For $Ri > 0$ stratification is stable, for $Ri = 0$ it is neutral such that there is no density gradient in the vertical and $Ri < 0$ signals instability, such that denser water over-lies lighter water and gravitational forces will exist to overturn this phenomenon, thereby increasing turbulence. The point at which stratification is sufficient to change turbulent flow to laminar flow is generally taken to occur at $Ri = 0.25$ for uniform flow. Flow is non-uniform in tidal flows, however, and the transition is believed to occur at higher Ri. Field observations in the Mersey Narrows led to an empirical relationship between the vertical eddy viscosity in homogeneous conditions, N_o and that in the presence of density stratification, N, namely

$$\langle N \rangle = \langle N_o \rangle \left(1 + aRi\right)^b \tag{4.36}$$

where the constants a, b were found to be 10 and $-1/2$ respectively, (McDowell and O'Connor 1977). The <> brackets indicate a tidally averaged value. Equation (4.36) indicates a reduction in momentum transfer of 60% for $Ri = 0.5$ and 86% for $Ri = 5$. Different quantities are used to represent the coefficients of eddy viscosity and eddy diffusivity of scalars partly because field work and laboratory experiments have shown that stratification reduces the vertical transfer of salt faster than momentum. Equation (4.36) can be used for eddy diffusivity of salt, K, as well as momentum but the constants a, b change to 3.33 and $-3/2$ respectively. An Ri value of five leads to a 74 fold reduction in salt diffusion.

The value of the Richardson number also changes continuously in an estuary. When tidal currents are at their maximum, conditions might be roughly neutral in their surface and bottom layers while the halocline has stable conditions. The Columbia River has Ri values reaching 5 at mid-depth. At those points in time

when tidal currents are diminished, however, it is possible for the whole water column to be stable, (Dyer 1973).

Fischer, List, Koh, Imberger, and Brooks (1979) suggest that for a stratified estuary the value of K can range between 1/10 and 1/100 the value of K_o during a tidal cycle.

4.4 'Steady' turbulent flow: Rivers

Analytic expressions for river flow are possible if the mean motion of the water is considered. The nature of the fluid flow is characterised by two ratios, the Reynolds number and the Froude number. The Reynolds number, R_e, represents the ratio of inertial forces to viscous forces and is given by

$$R_e = \frac{\hat{V}_R H}{\nu} \tag{4.37}$$

where $\hat{V}_R$ represents the vertically averaged river velocity, H is the depth of the river and ν is kinematic viscosity. As inertial forces dominate viscous forces flow changes from laminar to increasingly turbulent. For wide channels, flow is definitely laminar for $R_e < 500$ and turbulent for $R_e > 2000$, with a transitionary band between, (Smith 1975). The Froude number, F_r, is defined by

$$F_r = \frac{\hat{V}_R}{\sqrt{gH}} \tag{4.38}$$

where g is the acceleration due to gravity. The Froude number represents the ratio of inertial forces to gravitational forces. If $F_r < 1$ flow is designated as sub-critical or tranquil flow. Where $F_r = 1$ flow is critical and when $F_r > 1$ flow is super-critical[4]. Generally, flow in streams and rivers under non-flood conditions

[4]Super-critical flow is also known as shooting or streaming flow, (Davis and Barmuta 1989)

are either sub-critical-turbulent or super-critical-turbulent, (Davis and Barmuta 1989).

4.4.1 1D flow: well mixed river

The most basic representation of a steady flow with a significant mean component in only one direction, the x direction say, is to state that $V_x = constant$. Although it appears a gross over-simplification this representation of fluid flow is reasonable when considering highly energetic shallow streams and rivers.

When the depth of the water body is equal to or less than three times the height of the substrate roughness, or rocks and/or boulders extend all the way through the flow, local flow is very dependent on individual substrate elements and very difficult to determine even numerically. Such flows are often characterised by super-critical 'white water' common in shallow riffles, (Davis and Barmuta 1989). Such flows, however, still possess a mean motion which, because of the vigorous momentum mixing caused by the high turbulence, is more or less uniform over the depth.

4.4.2 2D flow: weakly mixed river

In deeper and more tranquil rivers, (those in the sub-critical regime), turbulence is not enough to cause an approximately uniform vertical profile of horizontal momentum. To approximate the flow of such systems it is therefore important to account for the vertical velocity profile caused by viscous forces preventing movement at the substrate and, (except in a laminar boundary layer), turbulent diffusion mixing momentum between different water depths. A logarithmic profile can be established through the method of solving for V_x from the equation for bottom shear stress as detailed in section 4.3. This, however, requires stipulation of the roughness of the bed in some form. An alternative approach is to consider a simplified form of the momentum equation.

If the horizontal component of a steady two dimensional, (x,z), flow is considered uniform in the x direction and all non-linear terms of the substantive derivative are ignored Equation (4.22) reduces to

$$\frac{1}{\rho}\frac{\partial P}{\partial x} = \frac{N_x}{\rho}\frac{\partial^2 V_x}{\partial z^2} \tag{4.39}$$

For rivers the pressure gradient is a result of the slope of the free surface, η, such that Equation (4.39) becomes

$$g\frac{\partial \eta}{\partial x} = n_x \frac{\partial^2 V_x}{\partial z^2}, \qquad n_x = \frac{N_x}{\rho} \tag{4.40}$$

Appendix B shows that if a no slip condition is applied at the bottom then the horizontal velocity at any depth is given by

$$V_r(z) = V_R\left(1 - \left[\frac{z}{H}\right]^2\right) \tag{4.41}$$

where V_R is the velocity at the river surface, H is the river depth and z the distance below the free surface. Determining the vertically averaged velocity, $\hat{V}_R$, reveals it is exactly two thirds the value at the surface, such that Equation (4.41) can also be written as

$$V_r = \frac{3\hat{V}_R}{2}\left(1 - \left[\frac{z}{H}\right]^2\right) \tag{4.42}$$

Extensive measurement in rivers has shown the mean velocity, $\hat{V}_R$ to reside at a distance approximately $0.4H$ from the bed, (Smith 1975, page 34). To check this representation of the horizontal velocity we can set $V_r = \hat{V}_R$ in Equation (4.42) and solve for z. This gives $z = H\sqrt{1/3}$ such that $\hat{V}_R$ occurs at a distance from the bed of $H(1 - \sqrt{1/3}) \approx 0.4226H$.

4.5 Tidal estuary

In general, the time and space dependent flow-fields which result from flows experiencing tidal forcing can only be determined numerically. However, Chen, Shaw, and Wolcott (1997) developed an analytic solution for a strategically simplified two-dimensional, (x,z), representation of a tidally driven system. This solution was adapted by Speirs and Gurney (2001) to include a river outflow component and was used to model persistence of passive organisms.

4.5.1 Linearised momentum equation

The model is specified by a linearised version of the equation for the conservation of momentum (Equation 4.22), for the x-component of momentum. It assumes turbulent flow, adopting a constant coefficient of eddy viscosity in the place of molecular viscosity. The only factor affecting the pressure gradient is considered to be the horizontal variation in free surface elevation, η, such that

$$\frac{1}{\rho}\nabla P = g\frac{\partial \eta}{\partial x} \tag{4.43}$$

The momentum equation therefore becomes

$$\frac{\partial V_x}{\partial t} = -g\frac{\partial \eta}{\partial x} + n_x\left(\frac{\partial^2 V_x}{\partial z^2} + \frac{\partial^2 V_x}{\partial x^2}\right) \tag{4.44}$$

where n_x is the constant coefficient of turbulent eddy viscosity. It is then further assumed that, because V_x changes much more slowly with x than with z, that the term $\partial^2 V_x/\partial x^2$ can be omitted, giving a final momentum equation of

$$\frac{\partial V_x}{\partial t} = -g\frac{\partial \eta}{\partial x} + n_x\frac{\partial^2 V_x}{\partial z^2} \tag{4.45}$$

The continuity equation is defined as

$$\frac{\partial V_x}{\partial x} + \frac{\partial V_z}{\partial z} = 0 \tag{4.46}$$

The vertical velocity at the benthos is zero at all times, and so the rate of change of the local surface elevation, $\partial\eta/\partial t \equiv V_z(\eta)$ can be gained by integrating $\partial V_z/\partial z$ up the water column. This gives

$$\frac{\partial \eta}{\partial t} = \int_{-H}^{\eta} \frac{\partial V_z}{\partial z} dz \quad = -\int_{-H}^{\eta} \frac{\partial V_x}{\partial x} dz \tag{4.47}$$

where H is the depth below the mean free surface. Equation (4.47) uses a vertical axis with the origin at the mean free surface and defined positive skyward, and a vertical velocity defined positive skyward, as is the convention in hydraulics. Speirs and Gurney (2001) reversed the positive direction in the vertical, (while maintaining the same origin), such that the equation for surface elevation becomes

$$\frac{\partial \eta}{\partial t} = -V_z(-\eta) \quad = -\int_{-\eta}^{H} \frac{\partial V_x}{\partial x} dz \tag{4.48}$$

The analytic solution for the two components of velocity are achieved by assuming the variation in surface elevation is not significant in comparison to the mean depth of the system. Then $\eta << H$, and Equation (4.48) becomes[5]

$$\frac{\partial \eta}{\partial t} = -\int_{0}^{H} \frac{\partial V_x}{\partial x} dz \quad = -H\frac{\partial V_x}{\partial x} \tag{4.49}$$

Boundary conditions for the Speirs and Gurney (2001) version of the model specify that at the landward end of the system, (x=0), the only velocity present is that from the river. The seaward end, (x=L) contains a linear combination of this river flow and a sinusoidal tidal component, so that

$$V_x(0,0,t) = V_R, \qquad V_x(L,0,t) = V_R + V_T \cos 2\pi \frac{t}{T} \qquad \forall t \tag{4.50}$$

[5]This result applies whether the assumption $\eta << H$ is applied to Equation (4.47) or (4.48).

where T is the tidal period.

To allow inclusion of the river flow, a no slip boundary condition was set at the bottom of the domain by Speirs and Gurney (2001)[6] and a zero wind-stress condition applies at the mean free surface such that

$$\left.\frac{\partial V_x}{\partial z}\right|_{z=0} = 0, \qquad V_x(x,H,t) = 0 \qquad \forall t \tag{4.51}$$

Given these boundary conditions solutions to Equations (4.45) and (4.49) are

$$V_x = V_R\left(1-\left[\frac{z}{H}\right]^2\right) + V_T\left(\frac{\sin kx}{\sin kL}\right)\Re\left\{\left(1-\frac{\cos mz}{\cos mH}\right)\exp\left(i2\pi\frac{t}{T}\right)\right\} \tag{4.52}$$

and

$$V_z = V_T\left(\frac{k\cos kx}{\sin kL}\right)\Re\left\{\left[\exp\left(i2\pi\frac{t}{T}\right)\right]\left[H-z+\frac{\sin mz-\sin mH}{m\cos mH}\right]\right\} \tag{4.53}$$

where

$$k = \frac{2\pi}{T}\frac{1}{\sqrt{gH}}, \qquad m = \frac{(1-i)}{\sqrt{2}}\sqrt{\frac{2\pi}{Tn_x}} \tag{4.54}$$

Intermediate working is contained in appendix B.

The work of this thesis makes use of Equations (4.52) and (4.53) in order to provide the velocities for a particle tracking algorithm, as described in section 3.3.1. This in turn allows determination of the Lagrangian residual movement over a tidal cycle. When considering persistence of planktonic organisms, flows of most interest are those that, at depth, generate landward residual movement.

[6] Chen, Shaw, and Wolcott (1997) used a linear drag law for the bottom boundary condition. If river flow was to be included, however, then to maintain a linear momentum equation, a no slip condition must be used.

When tracking was applied to the solutions generated from Equations (4.52) and (4.53) it was found that such landward 'flows' only prove significant for tidal flows that, in turn, generate variations in surface elevation that can not be considered insignificant compared to the mean depth of the system.

When the free surface rises above its mean value, both horizontal and vertical velocities for any point a given distance from the benthos will be calculated as if that point were a greater proportion of the distance toward the free surface than is actually the case. When the free surface falls below its mean value the situation is reversed. For a given volume of flow, the vertically averaged horizontal velocity will decrease for a rising free surface and increase for one which is falling. Near the benthos these effects are expected to be dominated by the bottom drag. Because of the no slip condition at the bottom and the drag, (caused by the eddy viscosity), horizontal velocities near the benthos are small. The bottom drag also causes the velocity gradient, $\partial V_x/\partial z$ to be greatest near the bottom boundary. This gradient becomes small a relatively short distance from the boundary, and the shape of the velocity gradient curve would only be modestly affected by variations in surface elevation. Also, the effective and actual positions of a particle relative to the benthos stay the same. Further up the water column the bottom drag effect reduces and then stops.

The vertical velocity at any depth, Equation (4.53), is obtained by differentiating Equation (4.52) and then integrating up to the required depth. Artificially high landward flows - during periods when the surface elevation should be above its mean level - lead to greater than desired absolute values of $\partial V_x/\partial x$, (as $V_x(0,\eta,t) = V_R \quad \forall t$), and increased values of vertical velocity. When surface elevation is below its mean, seaward flows lower than the true value lead to suppressed vertical velocities.

There is also a discrepancy between a particle tracked from an initial position at or close to the water surface and the value of the free surface as calculated from Equation (4.49). A particle which moves above the mean free surface level

receives a vertical velocity calculated by integrating $\partial V_x/\partial x$ up to its given altitude. The movement of the surface elevation, $\partial\eta/\partial t$, is only calculated using an integration up to $z = 0$. The movement of the particle becomes greater than that of the free surface and if both quantities are rising, the particle will rise above the free surface. In the work of Speirs and Gurney (2001) only deterministic tracks were performed (ignoring the issue of the free boundary) and the resultant residual movements used as the basis for determining parameters for displaced tent distributions, which are described in section 3.3.1. Using a population model with a time step equal to the tidal period, if the free surface was assumed at its mean level at $t = 0$, it was only necessary to ensure particles were beneath the mean free surface at the end of the tracking run. It was anticipated that incorporating animal behaviour into a tidal system could render use of displaced tents impracticable or impossible. The alternative is to incorporate the random motions of animals into the tracking algorithm. Such random movement can place particles over boundaries in a non-physical manner at each tracking timestep. As a consequence checking particle position against the free boundary at each timestep must be performed and it becomes more important to gain a true representation of the variation of the free surface with time.

4.5.2 Sigma co-ordinates

A modification to this analytic approach uses a form of sigma co-ordinate in the vertical, adapting the true sigma co-ordinate system developed for the Princeton Ocean Model, (Blumberg and Mellor 1987). Blumberg and Mellor (1987) define the instantaneous depth by

$$D(x,t) = H(x) + \eta(x,t) \tag{4.55}$$

They then define a new depth variable

$$\sigma = \frac{z - \eta}{D} \tag{4.56}$$

This depth variable always has a value of zero at the free surface ($z = \eta$) and -1 at the bottom ($z = -H$). For the work in this thesis a new depth measure, z_σ is defined as follows

$$z_\sigma = -\sigma H \tag{4.57}$$

This new depth variable always has a value of zero at the free surface ($z = \eta$) and H at the bottom ($z = -H$). To be consistent with the work of Speirs and Gurney (2001), z_σ is defined positive toward the benthos.

The defining equations of the model, (Equations 4.45 and 4.46) become

$$\frac{\partial V_x}{\partial t} = -g\frac{\partial \eta}{\partial x} + \frac{H^2}{D^2} n_x \frac{\partial^2 V_x}{\partial z_\sigma^2} \tag{4.58}$$

and

$$\frac{\partial V_x}{\partial x} + \frac{H}{D}\frac{\partial V_z}{\partial z_\sigma} = 0 \tag{4.59}$$

for the continuity equation. The changes required for boundary condition equations are contained in Appendix C. This appendix also contains details of how this new approach allows a new, and more self consistent, means of calculating the rate of change of surface elevation with time.

Use of Existing Solutions for V_x and V_z

The expression $(H^2/D^2)n_x$ could be considered to represent a coefficient of eddy viscosity that varies as overall water depth varies. In other words a new term $\Phi_E(x,t)$ could be substituted for $(H^2/D^2)n_x$. Attempting to take account of the

new time and space dependence of the eddy viscosity term, however, leads to a second order differential equation in z_σ for the depth dependent part of the horizontal velocity, (as was the case for the altitude version of the model), but which now includes the variation of surface elevation with time, as shown in Appendix C. Rather than attempting to solve this more complicated equation the existing analytic solutions for V_x and V_z were adopted, but with vertical co-ordinate of the particle taken as the value in z_σ. The disadvantage to this approach is outlined below.

In contrast to the case using a conventional altitude measure in the vertical, when the free surface rises or falls from its mean value, a particle a given distance from the benthos maintains the proportions of its distance above the benthos and its distance below the free surface. When use of Equation (4.52) is made however, this has the effect of determining the velocity as if the particle were closer to the benthos than is actually the case for a raised free surface and as if it is further from the benthos for a free surface below the mean level. Because of the steep velocity gradient near the benthos, particles in the shear flow region of the domain gain a higher than desired horizontal velocity as the free surface falls and a lower than desired horizontal velocity as the free surface rises.

Returning to Equation (4.58), this replaces n_x by $\frac{H^2}{D^2}n_x$, which implies that when the free surface rises the eddy viscosity term reduces and vice versa. At the same time when the free surface is above its mean $z_\sigma > z$ in terms of the distance represented by a single unit. For a velocity gradient that in physical terms remains the same this implies $\frac{\partial V_x}{\partial z_\sigma} > \frac{\partial V_x}{\partial z}$ by a factor D/H. The effect is again reversed when the free surface falls below the mean level. The shear stress restricting horizontal velocity at any depth in the model is given by $\frac{H}{D}n_x\frac{\partial V_x}{\partial z_\sigma}$. Thus the two effects of the change of co-ordinate do not affect this force acting on a fluid element. If the factor $\frac{H}{D}$ is not included however, for a free surface above the mean the shear stress will be at an elevated value and given the fact V_x is zero at the benthos this causes the V_x value to be reduced.

4.5.3 Comparison of analytic solutions to those from a fluid dynamics package

To decide whether the 'altitude' or 'sigma' co-ordinate version of the analytic solution following Chen, Shaw, and Wolcott (1997) provided the better approximate flow fields, residual flows produced by each version were compared to output gained from a fluid dynamics package, the Princeton Ocean Model, (POM), which is described in the next chapter. In its full form the POM package incorporates temperature and salinity as additional state variables and the effects of the variation of these quantities on the momentum equations. For the comparisons of this section it was possible to disable these terms within the momentum equations. In addition, the non-linear momentum terms could be eliminated and the coefficient of vertical eddy viscosity could be made a fixed value, rather than one determined by a turbulence closure scheme. Unlike the analytic solution horizontal diffusion had to be retained in order to prevent numerical instability and high frequency waves persisting in the flow fields[7]. The form of the momentum equation in the x direction, in Cartesian co-ordinates, as used by POM for these comparisons was

$$\frac{\partial V_x}{\partial t} = -g\frac{\partial \eta}{\partial x} + n_x\frac{\partial^2 V_x}{\partial z^2} + F_x \tag{4.60}$$

where F_x represents the horizontal diffusion and is given by $F_x = \frac{\partial}{\partial x}[2A_M\frac{\partial V_x}{\partial x}]$ and where A_M is the coefficient of horizontal kinematic eddy viscosity.

To remove as many confounding effects as possible, initial comparison was made for flows with no river component. Fig. 4.1 shows Lagrangian residual "velocities" obtained when $V_T = 0.3$. Plot a) shows the result using flow fields generated by the Chen solution and a Cartesian vertical coordinate while plot b) gives the result from the modified Chen solution with sigma vertical coordinate used when calculating horizontal velocities. Plots c) and d) show residual velocities derived

[7] In the analytic solution it is possible to pick the trial solution such that only the fundamental mode is represented.

using flow fields output from POM. To drive the POM model an open boundary condition has to be specified at the seaward end of the domain. For the purposes of this comparison a velocity 'inflow' condition was used with the velocities for each boundary cell being specified by the analytic solution at that point in space and time. Because POM utilises a time splitting technique,[8] values for vertically averaged velocity must be supplied as well as those for individual depths. For plot c) the vertically averaged velocity was determined by integrating the analytic solution over the latest depth determined by the POM model. Velocities for separate cells were determined after converting the current sigma value at which the cell velocity is defined to an absolute altitude. For plot d) the sigma implementation to the analytic solution was imposed at the boundary. Vertically averaged velocity was determined ignoring variation in sea surface elevation and the locations for defining cell velocities were converted from full sigma coordinates to a scale running between zero at the free surface and H at the bottom.

The resulting residual velocities using POM flows can be seen to be a much closer qualitative match to the results obtained using an analytic solution with simple Cartesian vertical coordinate. This is true for POM flows using either type of boundary condition forcing. Exact agreement was never expected, firstly because of the need to retain horizontal diffusion terms in the POM solution and secondly because the POM model does not use a no slip condition at the bottom boundary but, (as detailed in the following chapter) a version of the 'law of the wall' together with a bottom roughness parameter to determine the velocity profile near the bottom.

Once a domain is determined for a POM simulation velocities outside of that domain are undefined. To ensure the simulations for these comparisons were being driven by the correct velocities at the correct location, the open boundary of the POM simulation was placed at the same location as the absorbing boundary

[8]The model performs calculations to determine the vertically averaged and density independent aspect of the flow separately and then feeds the results of these calculations to code performing the full baroclinic calculations at longer time intervals.

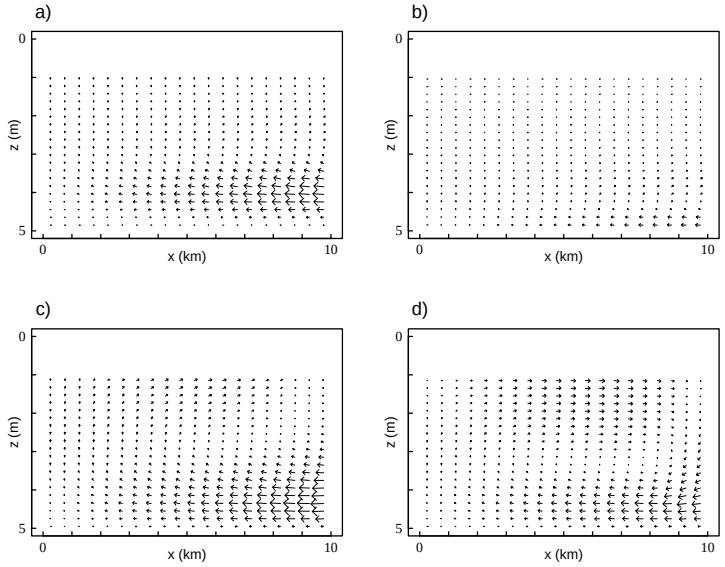

Figure 4.1: *Residual velocity plots derived using flow fields from a) Solution after Chen, Shaw and Wolcott (1997), using Cartesian vertical coordinate; b) Solution after Chen, Shaw and Wolcott (1997), using σ vertical coordinate; c) Princeton Ocean Model, (POM), with boundary condition supplied by 'Chen' velocities; d) POM, with boundary condition supplied by semi-sigma 'Chen' velocities.* $V_T = 0.3$, $V_R = 0.0$.

of the theoretical domain. This meant that residual velocities could only be determined by starting particle tracks from the low tide point in the tidal cycle and consequently residual velocities can only be determined for starting positions up to the approximate low water mark. Particle tracking using the analytic solutions are not subject to these restrictions as velocities remain defined beyond the absorbing boundary. For consistency, residual velocity tracks were defined only to low water mark in all cases. More significantly, it can be argued that a logical inconsistency occurs if the region beyond the seaward boundary of the domain is considered absorbing at instances of completed tidal cycles but not during a tidal cycle.

The true objective in this thesis is to consider the possibilities of persistence when there exists in the domain a net flow in one direction. It was therefore important to be certain the Cartesian form of the analytic solution still represented the better of the analytic flow fields once river flow had been introduced. Fig. 4.2 shows residual velocities obtained when $V_T = 0.3$ and $V_R = 0.005$. The analytic

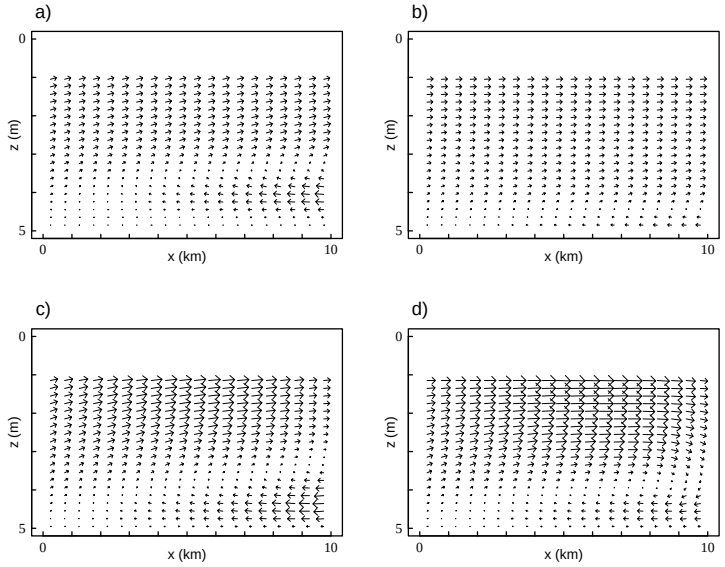

Figure 4.2: *Residual velocity plots derived using flow fields from a) Solution after Chen, Shaw and Wolcott (1997), using Cartesian vertical coordinate; b) Solution after Chen, Shaw and Wolcott (1997), using σ vertical coordinate; c) Princeton Ocean Model, (POM), with boundary condition supplied by 'Chen' velocities; d) POM, with boundary condition supplied by semi-sigma 'Chen' velocities.* $V_T = 0.3$, $V_R = 0.005$.

solution with Cartesian vertical coordinate can still be seen to be the best match to either of the POM implementations.

The river flow open boundary conditions must be imposed at each end of the POM domain. The analytic solution determines a fixed vertical profile of river velocity and assumes no variation in water height whereas the height at each open boundary varies. In these simulations the proportions of velocities assigned to cells remained constant but their absolute value was allowed to change such that a constant volume of water was input and extracted at river and seaward ends respectively.

4.5.4 Comparison with full 'primitive equations' solution

To obtain the analytic flow solutions a number of simplifying assumptions had to be made. As described in the next chapter, the assumption that horizontal

diffusive terms are unimportant can be justified via scaling arguments and are used in simplifying numerical oceanographic flow models such as POM. It was always expected that density variations would significantly alter flows. The main source of density variation, especially in shallow water, is due to salinity variation. Flows derived from the analytic solution could be considered as representing those from tidal rivers, or a very well mixed portion of an estuary in which the vertical profile of salinity is almost constant.

The reduction of the momentum equation to a linear form and the stipulation of a constant vertical eddy viscosity coefficient, however, is only performed because of the difficulty in solving non-linear differential equations. To determine the difference in residual velocity caused by introduction of the non-linear terms residual velocities arising from flow with $V_T = 0.3$ and $V_R = 0.005$ was determined using flows from a POM run incorporating these components. As such the momentum equation, (in the x direction), now being solved by the POM model becomes

$$\frac{\partial V_x}{\partial t} + V_x \frac{\partial V_x}{\partial x} + V_x \frac{\partial V_z}{\partial z} = -g \frac{\partial \eta}{\partial x} + n_x(z) \frac{\partial^2 V_x}{\partial z^2} + F_x \tag{4.61}$$

As detailed in chapter 5 oceanographic packages such as POM still retain a few key simplifying assumptions. The fluid dynamics equations containing these assumptions are known as the 'primitive equations'.

The vertical dependence of the vertical eddy viscosity coefficient is determined by a turbulence closure algorithm within the POM package as outlined in the next chapter. To avoid over prescription of the open boundary condition, a sinusoidal surface elevation is prescribed. The vertically averaged horizontal velocities are then calculated from the continuity equation but the depth dependent horizontal velocities are allowed to be determined from a radiation condition, (given that their average must be consistent with the vertically averaged value). For a given value of V_T and V_R, the parameters specifying the surface elevation in the POM model were taken from the results for surface elevation of the semi-sigma analytic solution. Fig. 4.3 shows the comparison to residual velocities derived from the

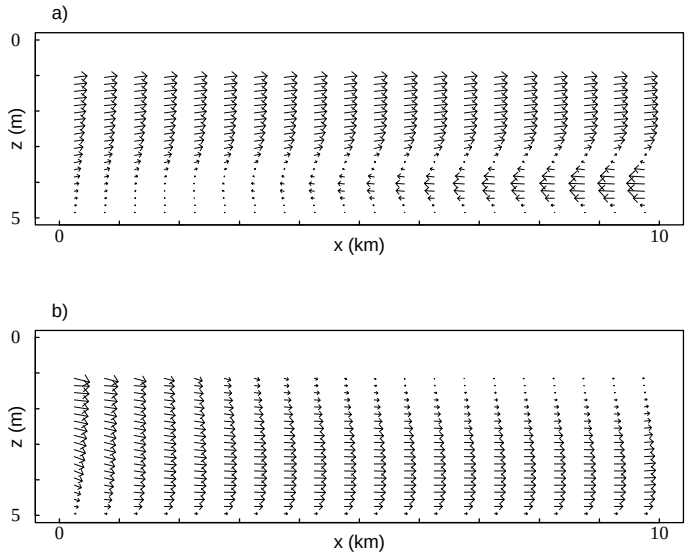

Figure 4.3: *Residual velocity plots derived using flow fields from a) Solution after Chen, Shaw and Wolcott (1997), using Cartesian vertical coordinate,* $V_T = 0.3$, $V_R = 0.005$*; b) POM, with inclusion of non-linear terms in momentum equation and coefficient of vertical eddy viscosity calculated from package's turbulence closure scheme. Boundary conditions supplied by specified river velocities at landward end and surface elevation at seaward end.*

Cartesian analytic solution for $V_T = 0.3$, $V_R = 0.005$, (the same result as displayed in Fig. 4.2, frame a)).

From Fig. 4.3 it can be seen the compensatory flow seen in the 'Chen' solution is absent once the non-linear terms are introduced. After also performing comparisons where only the non-linear components of the advection were introduced, the essential difference appears to be due to the structure and magnitude of the coefficient of vertical eddy viscosity.

Chen, Shaw, and Wolcott (1997) used a drag law condition in the form

$$n_x \frac{\partial V_x}{\partial z} = r V_{x(bot)} = \tau_o \tag{4.62}$$

where r is the friction constant and $V_{x(bot)}$ the velocity at the bottom. A normalised parameter for bottom friction was then defined as $\epsilon \equiv r/(\omega H)$ where $\omega = 2\pi/T$ and T is the tidal period. A value of $\epsilon = 0.5$ implies $r \approx 3 \times 10^{-4} ms^{-1}$

for the depth used in their simulations of $4m$ and a tidal cycle of $12.42hr$. This bottom friction value was combined with a value for n_x of $2.25 \times 10^{-5} m^2 s^{-1}$, chosen chiefly to allow their chosen characteristic depth for diffusion, $z_d \equiv (n_x/\omega)^{1/2}$, to equal $0.4m$. This value falls outside of the range normally associated with a homogeneous tidal system. The linearised equations are based on similar work performed by Prandle (1982). Prandle defined the bottom boundary condition to be

$$\frac{8}{3\pi} k \left|\overline{V_x}\right| V_{x(bot)} = \tau_o \tag{4.63}$$

where $\overline{V_x}$ is the depth averaged velocity. Comparing results from the linearised equations to field data Prandle (1982) derived a relationship between the constant k and n_x as follows

$$n_x = k\overline{V_x}H \tag{4.64}$$

Assuming the value of τ_o to be the same in equations (4.62) and (4.63) this gives a relationship between n_x and r as

$$n_x = \frac{3\pi r H}{8} \tag{4.65}$$

For $r = 3 \times 10^{-4} m s^{-1}$ and $H = 4$ this relationship would give $n_x \approx 1.4 \times 10^{-3} m^2 s^{-1}$, and the scale depth for diffusion becomes $z_d \approx 3.16m$. Combining a lower than expected value of vertical diffusion coefficient with a given friction parameter allows shearing of the longitudinal flow, (due to bottom friction), while reducing the transfer of momentum, (caused by the eddy viscosity), that would work to reduce this shearing.

The value of $n_x \approx 1.4 \times 10^{-3} m^2 s^{-1}$ is more in line with field study estimates of coefficients in real systems. The values of vertical diffusion coefficient determined by the POM package vary with position and point in the tidal cycle. Values

during periods of high tidal flow were in the region of $1 \times 10^{-3} - 2.5 \times 10^{-3} m^2 s^{-1}$. It is unlikely the POM model is over-predicting vertical eddy viscosities (and diffusivities) as in a comparison with laboratory data, Burchard, Petersen, and Rippeth (1998, page 10553) found the model to under represent this quantity at intermediate depths for homogeneous flow.

4.5.5 Significance of buoyancy effects.

The literature on the general circulation of estuaries suggests that buoyancy effects, due to salinity differences between the river inflow and sea water at opposite ends of the system, are very significant. This has proved to be the case in this investigation. Fig. 4.4 shows a run set up as for Fig. 4.3, frame b) with the exception that the river inflow is given a salinity 2psu lower than any water drawn in from the seaward end of the system. The resultant residual velocities are clearly very different to the case when density was homogeneous and although complex, there is also evidence of circulations that could also be expected to enhance persistence. A difference in salinity of 2psu between river and sea water is much lower than the normal difference in salinities between fresh water runoff and sea water, (which can be as much as 35psu). This difference was used to demonstrate the fact that only small variations in salinity can have a dramatic effect. For example, the Mersey Narrows has been observed to show the classic residual velocity patterns of a partially mixed estuary. Salinity differences of 1psu were measured between top and bottom and it was estimated vertical salinity difference would range between 0.5psu and 2.0psu, (Bowden and Sharaf El Din 1966).

The complexity of the patterns seen in Fig. 4.4 is thought to be for two reasons. Firstly the value of bottom friction is considered to be rather high. It was a value that worked well when the objective was to match the residual velocities of the analytic solution. A value two orders of magnitude smaller is felt more appropriate for the shallow systems being modelled and with the high vertical resolution available from the model (especially in comparison to when the same

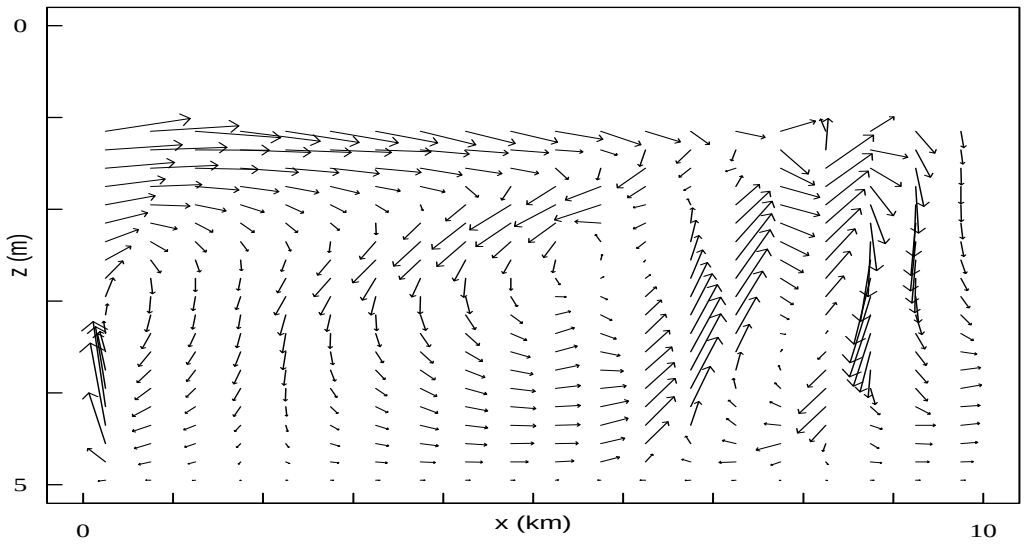

Figure 4.4: *Residual velocity plots derived using flow fields from POM, with inclusion of non-linear terms in momentum equation and coefficient of vertical eddy viscosity calculated from package's turbulence closure scheme. Boundary conditions supplied by specified river velocities at landward end and surface elevation at seaward end. Salinities between inflows at landward and seaward ends differ by 2psu.*

number of depth layers are being used to model the deep ocean). Secondly, lower salinity water is input across the full depth of a rectangular domain. Buoyancy effects are generated all the way down to the maximum $5m$ depth at the landward end of the system. Compensatory flow from denser water is forced to move deeper as it approaches the river end. The characteristic wedge shape of the denser water, caused in large part by systems that become deeper as they move seaward, is not able to form. The greater realism enabled by a sloping bottom was considered important in modelling systems with salinity effects and domains with sloping bathymetry were adopted when using the fluid dynamics package.

Chapter 5

Computational fluid dynamics approach to deriving flow fields: POM

All analytic solutions to fluid dynamic equations require simplifying assumptions in order to solve the differential equations. Hopefully, the assumptions still allow valid solutions to be obtained for a restricted scenario. In some cases, even considering a restricted scenario, the assumptions necessary may produce solutions which lack significant features in the flow. In the last chapter it was seen that the analytic solution, (following Chen, Shaw, and Wolcott (1997)), for a tidally driven estuary including river flow but with constant density differed from the solution obtained from a computational fluid dynamics (CFD) package, (the Princeton Ocean Model or POM), once the restriction of a linearised momentum equation had been removed. More importantly the CFD package was required to investigate persistence in scenarios too complex to obtain analytic solutions. These scenarios can be considered tidal systems involving non-uniform bathymetry, tidal systems involving non-uniform density that then affects body forces, or systems combining both these two aspects.

5.1 Key assumptions made in oceanographic CFD packages

In general, oceanographic CFD packages use as their starting point the full set of Navier-Stokes equations (Nunn 1989, pages 181–183) and apply simplifying assumptions that lead to a set of equations known as the primitive equations. Temperature and salinity are important to oceanographic flows as they both affect density. The variation of density, as applied to the body force term of the momentum equations for fluid elements is an important driver of flows. As a consequence temperature and salinity conservation equations are incorporated into the models. These equations can be considered analogous to the conservation of momentum equation but for scalar quantities. They receive the same simplifying assumptions as applied to the momentum equation.

5.1.1 Boussinesq approximation

In the work deriving analytic flow fields the density of the water was assumed to be constant. For the primitive equations variations in density are ignored when considering conservation of mass, (the continuity equation), and the horizontal components of the momentum equations. The simplification is justified on the grounds that the variations in horizontal accelerations for a given force, due to mass variations with density are too small to be significant (averaging over an entire ocean the discrepancy is at most 3%, (Pond and Pickard 1983)) Within the vertical component of the momentum equation density is again assumed constant for the acceleration terms. This component also contains, however, the gravity body force, ρg. Even though the variation in density over the depth of an ocean is small compared to the average value, its effect through this term is capable of generating significant currents, (Mellor 1996) and so actual in situ values must be used when calculating the pressure field.

In effect this approximation is such that variations in density are neglected when considering the inertia of the fluid but not when considering its weight. This is reflected in the use of a constant density term in the horizontal components of the POM momentum equations (Equations 5.4 and 5.5), but a variable in situ density term in the vertical component of the momentum equations (Equation 5.6). The approximation is known as the Boussinesq approximation after the mathematician who first suggested its use.

5.1.2 Hydrostatic approximation

The hydrostatic approximation uses a scaling argument. For oceans the horizontal scale of the domain is normally orders of magnitude greater than the vertical scale. If H is taken to represent the approximate depth and L to represent the approximate length scale, then the scale of the horizontal variations of quantities (that is terms involving $\partial/\partial x$ or $\partial/\partial y$) are taken to be of the order $O(1/L)$ and the scale of vertical variations is taken as $O(1/H)$. From the continuity equation, $\partial V_x/\partial x + \partial V_y/\partial y + \partial V_z/\partial z = 0$, the scales of the vertical and horizontal velocities can also be related by $w_o = u_o O(H/L)$ where w_o represents the order of the vertical velocity and u_o the order of horizontal velocities. If the z component of the momentum equation has this scaling applied and all terms of order $\approx O(1/L^2)$ or $\approx O(1/t_o L)$, (where t_o is the characteristic time scale), are ignored this component of the momentum equation reduces to (Mellor 1996, pages 31–32)

$$\frac{\partial p}{\partial z} = -g\rho + \rho_o \left[O\left(\frac{u_o^2}{L}\right) + O(u_o f_o) \right] \tag{5.1}$$

where f_o represents the order of magnitude of the Coriolis force. The gravity body force, ρg is left unaltered for the same reason as in the Boussinesq approximation. The pressure gradient term $\partial p/\partial z$ is also left unaltered. This is because otherwise the three components of velocity could be determined independent of the continuity equation, which generally could then not be satisfied(Mellor 1996).

To obtain values of the pressure for insertion into the horizontal components of the equation of momentum Equation (5.1) can be integrated with respect to z and then differentiated with respect to x or y. The last part of the scaling argument then notes that the scaling associated with this integration and differentiation process is such that the quantities in the square bracket of Equation (5.1) are multiplied by H/L and if this ratio is sufficiently small they may be neglected. Thus the z component of the momentum equation finally reduces to

$$\frac{\partial p}{\partial z} = -g\rho \tag{5.2}$$

This is the same as the hydrostatic equation for a fluid at rest, which explains the name given to the approximation. This approximation is not restricted to ocean applications but can be applied to any situation where the vertical distance over which velocities change significantly is much less than the horizontal distances. It effectively states that the acceleration and viscous/turbulent terms that effect the vertical component of velocity are unimportant in a thin layer.

5.1.3 Boundary layer approximations

The scaling arguments that lead to the hydrostatic approximation can also be applied to the horizontal components of the momentum equation. Taken collectively the resulting simplifications are known as the boundary layer approximations as they are only valid if the fluid involved has a vertical depth much less than its horizontal extent[1]. For the horizontal components the scaling effectively simplifies the terms related to the Coriolis accelerations and eliminates terms related to horizontal diffusion. In most applications, however, the horizontal diffusion terms have to be reinstated. This is because the grid spacing required to achieve a reasonable program run length do not allow sufficient horizontal resolution to

[1] Which in atmospheric fluid dynamics is only true of the boundary layer region close to the earth's surface.

fully describe the flow and diffusion has to be used to represent the effects of those unresolved flow patterns.

5.2 Outline of POM package

As its name implies the Princeton Ocean Model, POM, was developed at Princeton University and is described fully by Blumberg and Mellor (1987). The model uses the full set of primitive equations describing conservation of mass, momentum, temperature and salinity using the hydrostatic and Boussinesq approximations. To be consistent with the literature describing POM, notation is altered in this section such that U, V and W replace V_x, V_y and V_z as the three cartesian components of velocity. Following Blumberg and Mellor (1987) the equations are:

the continuity equation

$$\frac{\partial U}{\partial x} + \frac{\partial V}{\partial y} + \frac{\partial W}{\partial z} = 0 \tag{5.3}$$

the Reynolds momentum equations

$$\frac{\partial U}{\partial t} + \frac{\partial U^2}{\partial x} + \frac{\partial UV}{\partial y} + \frac{\partial UW}{\partial z} - fV = -\frac{1}{\rho_0}\frac{\partial P}{\partial x} + \frac{\partial(-\overline{uw})}{\partial z} + F_u \tag{5.4}$$

$$\frac{\partial V}{\partial t} + \frac{\partial UV}{\partial x} + \frac{\partial V^2}{\partial y} + \frac{\partial VW}{\partial z} - fU = -\frac{1}{\rho_0}\frac{\partial P}{\partial y} + \frac{\partial(-\overline{vw})}{\partial z} + F_v \tag{5.5}$$

$$\rho g = -\frac{\partial P}{\partial z} \tag{5.6}$$

the integral of the hydrostatic equation

$$P = P_{atm} + \rho_0 g\eta = g\int_z^0 \rho(x, y, z^{'})dz^{'} \tag{5.7}$$

the conservation equations for temperature and salinity (the mean temperature and salinity equations)

$$\frac{\partial T}{\partial t} + \frac{\partial UT}{\partial x} + \frac{\partial VT}{\partial y} + \frac{\partial WT}{\partial z} = \frac{\partial}{\partial z}(-\overline{w\theta}) + F_T \tag{5.8}$$

$$\frac{\partial S}{\partial t} + \frac{\partial US}{\partial x} + \frac{\partial VS}{\partial y} + \frac{\partial WS}{\partial z} = \frac{\partial}{\partial z}(-\overline{ws}) + F_S \tag{5.9}$$

and an equation of state

$$\rho = \rho(T, S) \tag{5.10}$$

The equation of state is that given by Fofonoff (1962). The terms F_U, F_V, F_T and F_S are related to small scale mixing processes not directly resolved by the model and parameterised as horizontal diffusion. These terms are given by:

$$F_U = \frac{\partial}{\partial x}\left(2A_M \frac{\partial U}{\partial x}\right) + \frac{\partial}{\partial y}\left[A_M\left(\frac{\partial U}{\partial y} + \frac{\partial V}{\partial x}\right)\right] \tag{5.11}$$

$$F_V = \frac{\partial}{\partial y}\left(2A_M \frac{\partial V}{\partial y}\right) + \frac{\partial}{\partial x}\left[A_M\left(\frac{\partial U}{\partial y} + \frac{\partial V}{\partial x}\right)\right] \tag{5.12}$$

$$F_{T,S} = \frac{\partial}{\partial x}\left(A_H \frac{\partial (T,S)}{\partial x}\right) + \frac{\partial}{\partial y}\left[A_H \frac{\partial (T,S)}{\partial y}\right] \tag{5.13}$$

The horizontal kinematic eddy viscosity, A_M, can be given a constant value, or can be calculated according to Smagorinsky (1963)

$$A_M = C\Delta x \Delta y \frac{1}{2}\left|\bigtriangledown \boldsymbol{v} + (\bigtriangledown \boldsymbol{v})^T\right| \tag{5.14}$$

where C is a user specified constant, (the Smagorinsky constant), and

$$\frac{1}{2}\left|\nabla \boldsymbol{v} + (\nabla \boldsymbol{v})^T\right| = \left[\left(\frac{\partial U}{\partial x}\right)^2 + \frac{1}{2}\left(\frac{\partial V}{\partial x} + \frac{\partial U}{\partial y}\right)^2 + \left(\frac{\partial V}{\partial y}\right)^2\right]^{1/2}$$

The eddy viscosity coefficient is therefore related to the spatial variation in velocity values and the cell sizes. The advantage of this form of formulation is that as cell size becomes smaller and/or flows become more homogeneous the value of eddy viscosity is automatically reduced. The coefficient of scalar diffusivity, A_H is regarded to be a fixed ratio to A_M with A_M/A_H known as the turbulent Prandtl number, (Mellor and Yamada 1982). For isotropic turbulence the constant C should be in the region 0.04, Ferziger and Peric (1999). Ferziger and Peric (1999, pages 270-271) cite several problems with the use of the Smagorinsky scheme. The Smagorinsky constant can be a function of Reynolds number and it should be reduced close to solid boundaries. Such effects are probably unimportant in ocean basin scale calculations but the work of this thesis involves flows of higher Reynolds number and it was found that the simpler approach of using a constant value of A_M could provide the same qualitative flow fields while being more likely to ensure numerical stability.

In the vertical, the Reynolds stresses, $\overline{uw}$ and $\overline{vw}$, and the turbulent heat and salt fluxes, $\overline{w\theta}$ and $\overline{ws}$, are evaluated using the level $2\frac{1}{2}$ closure model of Mellor and Yamada (1982) where

$$-(\overline{uw}, \overline{vw}) = K_M \frac{\partial}{\partial z}(U, V) \tag{5.15}$$

$$-(\overline{w\theta}, \overline{ws}) = K_H \frac{\partial}{\partial z}(T, S) \tag{5.16}$$

K_M and K_H represent vertical eddy viscosity and vertical diffusivity of heat and salt respectively. They are given by

$$(K_M, K_H) = lq(S_M, S_H) \tag{5.17}$$

S_M and S_H are stability functions given in Mellor and Yamada (1982), while l represents the turbulence macroscale, (describing the size of the largest turbulent

eddies) and q^2 is twice the turbulence energy[2]. The closure model used adds two more prognostic equations to the model which describe the evolution of q^2 and $q^2 l$.

5.2.1 Boundary conditions

Remaining in the cartesian representation of the model, boundary conditions at the free surface are given by:

$$W = U\frac{\partial \eta}{\partial x} + V\frac{\partial \eta}{\partial y} + \frac{\partial \eta}{\partial t} \tag{5.18}$$

$$\frac{1}{\rho_0}(\tau_{0x}, \tau_{0y}) = K_M \frac{\partial}{\partial z}(U, V) \tag{5.19}$$

$$Q_T = K_H \frac{\partial T}{\partial z} \tag{5.20}$$

$$Q_S = K_H \frac{\partial S}{\partial z} \tag{5.21}$$

$$q^2 = \frac{1}{\rho_0}|\tau_0| B_1^{2/3} \tag{5.22}$$

$$q^2 l = 0 \tag{5.23}$$

Equation 5.18 is the condition for Equation 5.3. Equation 5.19 gives the conditions for the momentum equations 5.4 and 5.5, where $\tau_0 = (\tau_{0x}, \tau_{0y})$ is the wind stress vector and ρ_0 the surface water density. Equations 5.20 and 5.21 relate to

[2]The quantity q can be described as the turbulence intensity, (Burchard, Petersen, and Rippeth 1998).

equations 5.8 and 5.9, where Q_S is the surface salinity flux and Q_T is the surface heat flux. Boundary conditions at the bottom are given by

$$W = -U\frac{\partial H}{\partial x} - V\frac{\partial H}{\partial y} \tag{5.24}$$

where H represents the bottom topography.

$$\frac{1}{\rho_0}(\tau_{Hx}, \tau_{Hy}) = K_M\frac{\partial}{\partial z}(U, V) \tag{5.25}$$

$$q^2 = U_f^2 B_1^{2/3} \tag{5.26}$$

$$q^2 l = 0 \tag{5.27}$$

In addition the normal gradient of temperature and salinity are set to zero at the bottom boundary. The term U_f is a shear velocity term whose value is determined from the bottom shear stresses (τ_{Hx}, τ_{Hy}). The bottom stresses are determined by matching velocities with the logarithmic 'law of the wall'. This means, (assuming horizontal flow in the x direction only for simplicity), that the bottom stress is given by

$$\tau_{Hx} = \rho_0 C_D |U_b| U_b \tag{5.28}$$

with the value of the drag coefficient C_D given by

$$C_D = \left[\frac{1}{\kappa}\ln(z_b/z_0)\right]^{-2} \tag{5.29}$$

Here z_b represents the height of the lowest defined velocity grid point above the bottom and U_b represents the velocity at that point, κ is the von Karman constant

and the term z_0 is known as the 'roughness parameter'. When equations (5.25), (5.28) and (5.29) are used together they produce a vertical velocity profile near the bottom boundary of the form

$$U(z) = \frac{\tau_{Hx}}{\kappa U_f} \ln(z/z_0) \tag{5.30}$$

where here z denotes the distance away from the bottom boundary.

5.2.2 Mode splitting

The dynamics of coastal circulation contain both the propagation of fast moving external gravity waves and slow moving internal gravity waves. Calculations involving external waves, those determining the vertically integrated volume transport between cells and subsequently the free surface elevations, must use a time step sufficiently small that no wave will traverse a whole cell in that time. If calculations affected only by the internal gravity waves, those dealing with the internal vertical structure of the flow, can be calculated separately these calculations can be calculated using longer timesteps. The POM model achieves this by a technique known as mode splitting. The volume transport equations are obtained by integrating the vertically structured equations over the depth, eliminating the vertical structure. These equations are known as the external mode equations, the unintegrated equations the internal mode equations. This technique implies that open boundary conditions must be supplied for both vertically integrated velocities and velocities at individual cell depths.

5.2.3 Sigma coordinates

The POM model makes use of σ-coordinates for the vertical. This coordinate system replaces points in space defined in the vertical according to an altitude on the z cartesian axis by a position defined relative to the positions of the bottom

and free surface. Because the deepest σ coordinate is always defined at the bottom this system is referred to as a bottom following coordinate system. The reason for adopting this coordinate system is that when a model is cast in finite difference form, a smooth representation of the bottom topography is obtained. It is also relatively easy to incorporate a bottom boundary layer as well as a surface boundary layer. By contrast, it is difficult to model bottom boundary layers in a z-level model, (Mellor, Hakkinen, Ezer, and Patchen 1999). The ability to be able to cope with significant topographical variability is important when dealing with estuaries and sea lochs. Resolving bottom boundary layers is also important in modelling such systems, (Oey, Mellor, and Hires 1985a; Oey, Mellor, and Hires 1985b)[3]. The horizontal eddy viscosity (applied to the momentum equations) and diffusion (applied to scalar quantities) in a numeric model in order to ensure computational stability can be considered as a source of error, especially if their values are that much greater than could be considered justified in reality. Use of σ-coordinates has been found to make models capable of operating with smaller prescribed values of horizontal diffusion, and, unlike z-level models, they are capable of accepting diffusion constants calculated dynamically and related to velocity values, such that in areas of low velocity these constants take small values (Mellor, Hakkinen, Ezer, and Patchen 1999).

The set of equations 5.3 to 5.17 is therefore transformed using the relationship

$$\sigma = \frac{z - \eta}{D}, D \equiv H + \eta \tag{5.31}$$

where η is the free surface elevation and H is the depth below mean sea level. At the free surface $\sigma = 0$ ($z = \eta$) and at the bottom $\sigma = -1$ ($z = -H$). The distance between levels at which values are calculated for variables remain in fixed proportion to each other independent of elevation or depth.

[3]When topography is steep and the vertical resolution coarse, errors in the pressure gradients result from the use of sigma coordinates (Mellor, Ezer, and Oey 1994; Mellor, Oey, and Ezer 1998). However, use of a similarly coarse z-level model can lead to errors in the barotropic component of the flow (Bell 1997).

The transformation leaves the U and V components of velocity with the same physical meaning as for cartesian coordinates. However, the cartesian vertical velocity, W is transformed to ω, which physically represents the velocity component normal to sigma surfaces. The transformation from ω to W is

$$W = \omega + U\left(\sigma\frac{\partial D}{\partial x} + \frac{\partial \eta}{\partial x}\right) + V\left(\sigma\frac{\partial D}{\partial y} + \frac{\partial \eta}{\partial y}\right) + \sigma\frac{\partial D}{\partial t} + \frac{\partial \eta}{\partial t} \tag{5.32}$$

The full set of the Equations (5.3) through (5.23), once converted to take account of sigma coordinates can be found in (Blumberg and Mellor 1987).

5.2.4 Open lateral boundary condition

Open lateral boundary conditions are an important and difficult component of a CFD package. In effect they are being used to specify the environment, (in terms of velocities, turbulent energy, salinity and temperature), exterior to the domain. In this work domains were always assumed to run East, West with the North and South boundaries closed. In POM the q^2 and q^2l terms are considered to be calculated with sufficient accuracy at the boundaries even after neglecting advection terms such that specification of exterior values becomes unimportant. Temperature effects were not considered in this work and for the strategic studies undertaken realistic but approximate estimates of salinity were sufficient. These external values are used with an 'upstream advection' boundary condition of the form

$$\frac{\partial S}{\partial t} + U\frac{\partial S}{\partial x} = 0 \tag{5.33}$$

Velocity boundary conditions were more problematic. For the comparison with the analytic solution, after Chen, Shaw, and Wolcott (1997), to a tidally driven flow both the external, vertically integrated, velocity and the internal, vertically structured, velocities could be specified by the solution to the analytic equations

at the boundary. For problems where no kind of analytic solution exists this can not be done. As the studies are strategic it is also not possible to drive the model via field data. In these circumstances the usual approach is to specify the surface elevation, (Blumberg and Mellor 1987). The external mode velocities were then determined from application of the vertically integrated form of the continuity equation. No information is available to determine the profile of the internal velocities so a radiation condition was applied of the form

$$\frac{\partial U}{\partial t} + c_i \frac{\partial U}{\partial x} = 0 \tag{5.34}$$

where c_i represents the phase speed of the fastest internal waves It was calculated using Orlanski's scheme, (Orlanski 1976).

Although radiation conditions require no knowledge of desired boundary velocities, in cases where substantial inflows are required as well as substantial outflows they can cause numerically valid, yet nonphysical baroclinic structures interior to the boundary, (Mellor 1998). To test for this phenomenon, a version of POM with the same simplifications used to provide the comparison to the analytic tidal solution in section 4.5.3 was implemented, but with the open boundary driven in the manner described above, the surface elevation being assumed sinusoidal but with an amplitude provided by output from the analytic solution. Fig. 5.1 shows residual velocities over a tidal cycle resulting from use of flows from this model compared to those from the POM model with analytically defined velocity boundary conditions. The anti-clockwise rotation in residual displacements seen at the seaward end of frame b) is known to be a consequence of the radiation boundary condition because of the general agreement in residual velocity pattern between the result shown in frame a) and that given by using flows from the analytic solution. Comparison of frames a) and b) also suggest that the pattern of residual velocities are possibly not seriously affected away from the open lateral boundary. Fig. 5.2 shows the result of extending the POM domain to double the length of the domain being considered for persistence experiments.

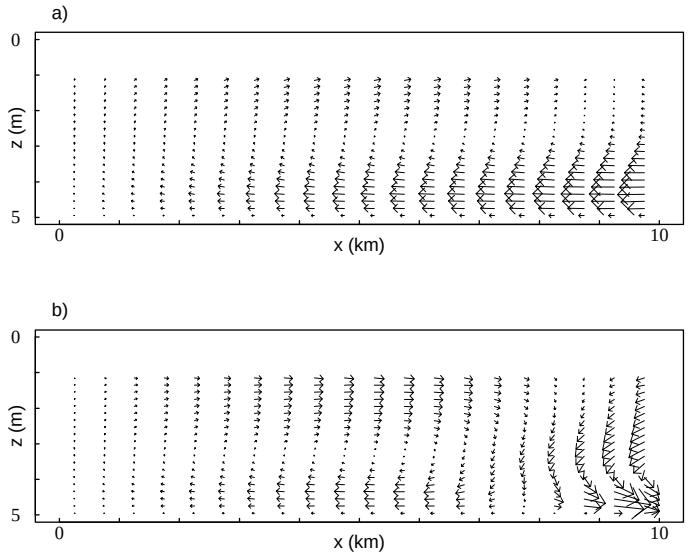

Figure 5.1: *Residual velocity plots derived using flow fields from a) Princeton Ocean Model, (POM), with boundary condition supplied by 'Chen' velocities; b) POM, with boundary condition supplied by sinusoidal surface elevation. Surface elevation set to match those of a surface tidal velocity of* $V_T = 0.3$. *No river flow.*

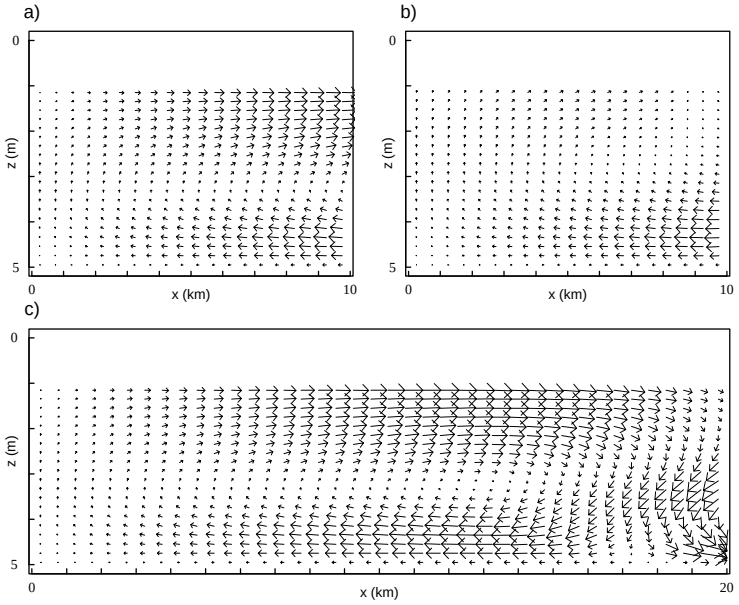

Figure 5.2: *Residual velocity plots derived using flow fields from a) and c) POM, with boundary condition supplied by sinusoidal surface elevation. Surface elevation set to match those of a surface tidal velocity of* $V_T = 0.3$*; b) Princeton Ocean Model, (POM), with boundary condition supplied by 'Chen' velocities. Frame c) displays the whole of the extended domain used to distance open boundary effects from the area for study, frame a) shows the resulting residual velocities supplied to a tracking algorithm if the domain's absorbing boundary is assumed to be at half POM domain length. No river flow.*

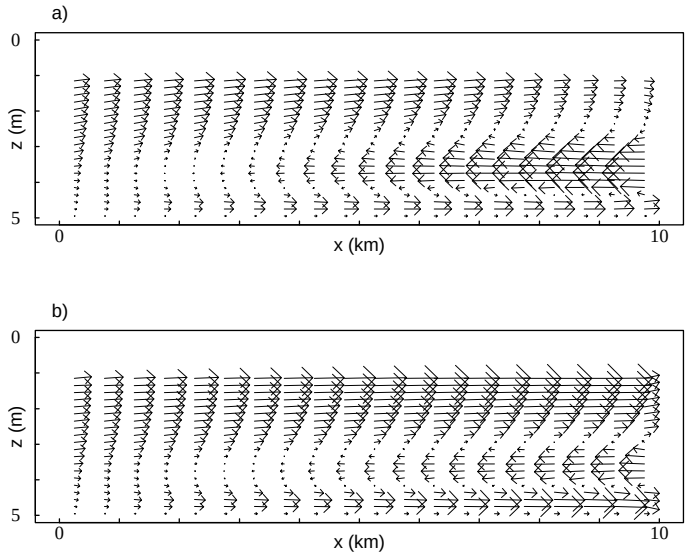

Figure 5.3: *Residual velocity plots derived using flow fields from a) Princeton Ocean Model, (POM), with boundary condition supplied by 'Chen' velocities; b) POM, with boundary condition supplied by sinusoidal surface elevation. Surface elevation set to match those of a surface tidal velocity of* $V_T = 0.3$. *In both cases river flow is given by* $V_R = 0.005$ *and there is inclusion of non-linear terms in the momentum equation.*

Residual velocities over the whole POM domain give an overall pattern much as in frame b) of Fig. 5.1. However, if residual velocities are only considered in the landward half of the domain, (frame a), Fig. 5.2), the resulting set have a pattern sufficiently similar to those generated using the prescribed inflow boundary velocities (frame b), Fig. 5.2), to expect the qualitative nature of any persistence experiments to be unaffected.

The extent of non-physical flow generated by radiation lateral boundary conditions is dependent upon the character of the flow within the domain. Fig. 5.3 shows the comparison between residual velocities generated by the same two types of lateral boundary condition - operating on the same standard domain length - once a river flow, ($V_R = 0.005$), and the non-linear components of the momentum equation are introduced. The only differences that now appear concern the strength of the seaward flowing components of residual movement. In general, the only means of determining whether an open boundary has caused non-physical flow features, and the extent of such features, is by visual inspection of the flow patterns or residual velocities.

5.3 Flow fields solved solely by CFD packages

The POM package is capable of three dimensional modelling. All runs conducted in this study, however, were concerned with two dimensional, (x,z) vertical slices. As such the 'steering' effect of the Coriolis force could not be considered and so this force was disabled.

5.3.1 Eliminating unwanted buoyancy effects

Buoyancy effects are effectively changes to a flow field, (as derived assuming uniform density throughout the fluid), caused by variations in density. These variations can be caused by temperature and salinity. To isolate the effect of salinity variations it was desired to remove any effects due to temperature. The temperature field could be made steady by setting initial values and altering the code to effectively eliminate Equation (5.8). In the absence of outside forces the static stability of a fluid is determined by the buoyancy frequency (or Brunt-Väisälä frequency), N^2. If N^2 is positive a fluid is stable, N is real and has the dimensions of frequency. It can be interpreted as giving the speed with which a packet of water, moved vertically from its resting position, would return to that position. If N^2 is negative the water is unstable and any displacement of a water packet will tend to be amplified by the vertical density variation. With $N^2 = 0$ the fluid can be thought to be neutrally stable. The buoyancy frequency is defined as

$$N^2 = g\alpha\frac{dT}{dz} + C_p^{-1}g^2\alpha^2 T - g\beta\frac{dS}{dz} \tag{5.35}$$

where T is in situ temperature, C_p is the specific heat capacity at constant pressure of the fluid, α the fluid's coefficient of expansion and $\beta = \rho^{-1}(\partial\rho/\partial S)_{p,T}$. Assuming salinity to be constant eliminates the final term. The temperatures used in POM are potential temperatures Θ, defined by

$$\frac{\partial \Theta}{\partial z} = \frac{\partial T}{\partial z} - \frac{dT_a}{dz} \tag{5.36}$$

Here, T_a is the adiabatic temperature, which has a vertical profile assuming changes in hydrostatic pressure change the temperature of the water with no heat transfer. The adiabatic temperature profile is defined as, (Tritton 1988)

$$\frac{dT_a}{dz} = -C_p^{-1} g\alpha T \tag{5.37}$$

If the potential temperature is assumed constant throughout the domain then $\partial T/\partial z = dT_a/dz$ and substituting this back into Equation (5.35) gives (still assuming no salinity variation)

$$N^2 = g\alpha \times -C_p^{-1} g\alpha T + C_p^{-1} g^2 \alpha^2 T = 0 \tag{5.38}$$

Therefore, in the absence of salinity effects a uniform potential temperature field ensures neutral stability and models were run with such.

5.3.2 Buoyancy, turbulence, vertical mixing and POM

One of the important features of buoyancy is the degree to which it can make a domain stratified. As discussed in section 4.3, stratification, which can be represented by the gradient Richardson number, has an important effect on the extent to which turbulence can exchange momentum and scalar quantities. The POM model calculates the stability function values in its turbulence closure routine from a combination of empirically derived constants and a form of Richardson number.

In real systems, when stratification has eliminated turbulent diffusion of salt, vertical transfer of salt across a halocline is still possible. The process is that of entrainment, the one way process whereby salt water is transported from a

low turbulence salt layer into a higher turbulence fresh layer by the breaking of internal waves created at the fresh/saline interface. The POM turbulence closure model is unable to simulate entrainment. For sufficiently high Richardson number the value of the coefficient of vertical diffusivity, K_H falls to zero. As a means to overcome this, the POM model incorporates a constant, 'UMOL', that represents a minimum or 'background' level of diffusion (and eddy viscosity). Alternatively, a minimum value for the turbulent kinetic energy can be specified within the closure scheme algorithm itself, (Burchard, Petersen, and Rippeth 1998). If comparing the model to field data for a stratified system either of these representations of internal wave breaking can be tuned in order to match the thickness and gradients of the stratified region.

In strategic studies, choice of this constant can be an important factor in determining the degree of stratification displayed by the resultant flow regime. In regions where the Richardson number is high the calculated value of vertical diffusivity will fall away to zero leaving the degree of salinity mixing dictated by the background value alone. This in turn influences the speed with which stratification is broken down away from the source of buoyancy, (Garvine 1999, page 1899).

5.3.3 Tidal estuary with salinity driven buoyancy effects

Figures 5.4 and 5.5 illustrate the differences the enhanced diffusion from a higher UMOL value can make. They represent the Lagrangian residual velocity from two POM runs using identical parameter values except for the value of the background diffusivity. In Fig. 5.4 the value of UMOL is set at $2.0 \times 10^{-5} m^2 s^{-1}$. This value of background diffusion is sufficient to enhance the mixing of lower, more saline water with the fresh water inflow but without breaking down the basic stratified nature of the flow. The seaward residual movement in the upper portion of the system and the compensating landward residual movement in the lower region are both considerably enhanced over a salt wedge system experiencing only minimum

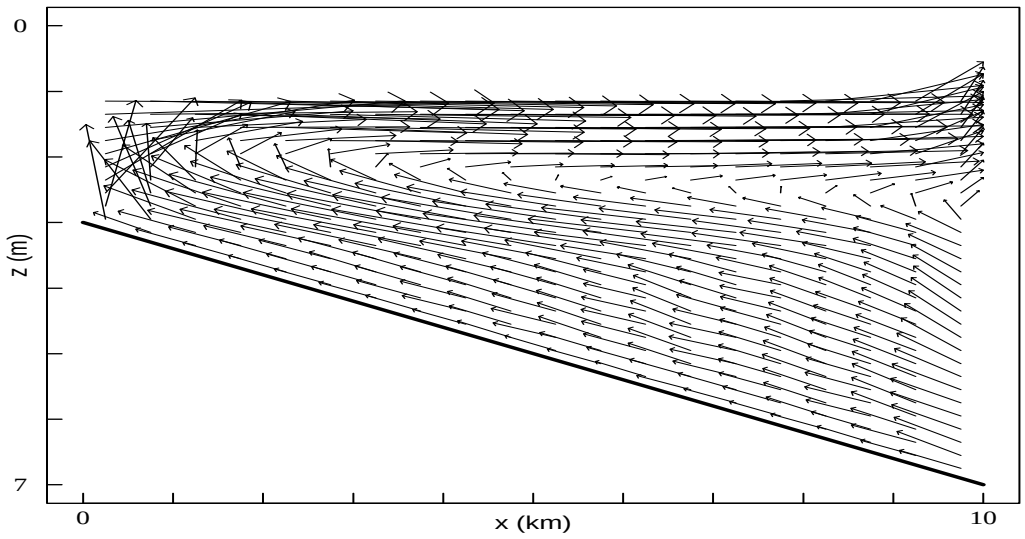

Figure 5.4: *Residual velocity plot derived using flow field from POM, using full primitive equations. Open boundary condition supplied by sinusoidal surface elevation, tidal range* $\pm 1m$. *River flow has per unit width discharge of* $Q_f = 4.17 \times 10^{-3} m^2 s^{-1}$. *Sea water at* $35psu$, *river water at* $0psu$. *Background diffusivity* $2.0 \times 10^{-5} m^2 s^{-1}$.

entrainment, as expected from a partially mixed estuary, (see section 2.1).

In Fig. 5.5 the value of UMOL is set at $2.0 \times 10^{-4} m^2 s^{-1}$. At this value of background diffusivity mixing is sufficiently strong to have broken down stratification completely before the seaward boundary of the system has been reached, such that the seaward end of the system is virtually homogeneous. At the boundary between the stratified and homogeneous sections downwelling takes place as observed in real estuaries, (Dyer 1987). The stratified portion of the estuary still experiences upper seaward and lower landward residual movements but the homogeneous section contains only weak seaward residual movement.

The scaling arguments of the boundary layer approximations apply to the motion of scalars such as salinity as well as to the velocity of the water itself. This in turn implies that horizontal diffusion of salinity can be omitted. Diffusion of horizontal velocity was retained chiefly to ensure numerical stability of the solutions. The same requirement was not necessary with respect to salinity and in fact inclusion of diffusion of salinity had a tendency to undermine stability. Therefore horizontal

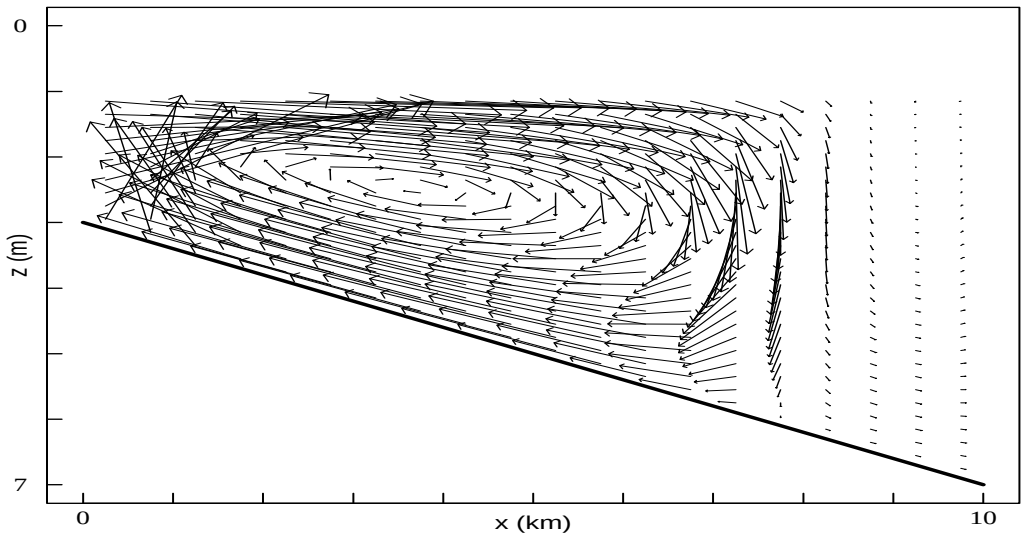

Figure 5.5: *Residual velocity plot derived using flow field from POM, using full primitive equations. Open boundary condition supplied by sinusoidal surface elevation, tidal range* $\pm 1m$. *River flow has per unit width discharge of* $Q_f = 4.17 \times 10^{-3} m^2 s^{-1}$. *Sea water at* $35psu$, *river water at* $0psu$. *Background diffusivity* $2.0 \times 10^{-4} m^2 s^{-1}$.

diffusion of salinity was omitted for this work.

5.3.4 Fjord

Work centred on retention of organisms in fjords were performed using two dimensional, (x,z) vertical slices along a 'strategic' representation of a fjord. In other words, while no attempt was made to reproduce the sub-surface topography, (bathymetry), of a specific fjord, key features common to most fjords were reproduced. The main body of the fjord is $80m$ deep, a value representative of Scottish sea lochs. The seaward end of the fjord rises steeply to a sill of relatively shallow depth, ($30m$). Beyond the sill the depth increases again in a region representing the coastal sea, and this is where the open boundary is situated. At the landward end of the system the bathymetry again rises relatively steeply to a shallow section where fresh water river inflow is injected. It is common for fjords to have their main fresh water inflow at the head of the system. To have a main

body of fjord similar in length to the coastal plane estuary, while accommodating the additional features of sill, coastal sea and river section, the overall length of the domain increases to approximately $25km$.

Spin-up and quasi-steady conditions

Because of steady forcing, (constant river inflow volume and salinity, constant salinity of water beyond the open boundary and tidal elevation as a regular sine wave), a tidally averaged steady state can be expected for both coastal plane estuary and fjord simulation. The nature of this steady state can not be known a priori and it takes a number of tidal cycles for it to be reached. A standard way to determine whether the density structure of the system has been fully formed is to record the domain averaged and tidally averaged salinity over successive tidal cycles. The 'spin-up' of the model is complete when this averaged value ceases to vary, that is when

$$\left\langle \overline{S} \right\rangle = \frac{1}{T} \int_0^T \left\{ \int \int S \; dxdz \times [\int (H + \eta) dx]^{-1} \right\} dt = \text{constant} \tag{5.39}$$

When modelling large and complex real systems achieving a density structure that matches recorded data, by driving the system using forcing parameters from the same data period, can take many cycles. Galperin and Mellor (1990) regarded the density structure of the Delaware Bay and River system to have become fully developed only after 2 months of simulated flows. With the much simpler and smaller, (in terms of physical size represented), strategic estuarine systems under consideration for chapter 8 spin-up periods could be considerably reduced. For the fjord runs, however, spin-up time was much more comparable to those cited for real systems. Enhanced seaward flow near the surface takes time to reach the open boundary. This is especially true of the longer fjord system. Further, the large deep body of the fjord is only weakly connected to the tidal forcing, (the main source of flow). Even after net seaward surface currents have become established across the domain, the full pattern of Lagrangian residuals continues

to evolve.

This second consideration is illustrated by figs. 5.6 and 5.7. Each figure shows residual velocities from flow fields using the same run parameters but taken at different times from the simulation start. In Fig. 5.6 flow fields were taken during tidal cycle 40. The surface residual flow is well established and movements in the body of the loch seem well established. However, Fig. 5.7, with residual flows calculated using flow fields taken during tidal cycle 80 shows the formation, in the body of the fjord, of a distinct landward flow just beneath the surface flow. Comparison of these two figures also shows large differences in flow seaward of the sill. Flows in this region, however, were not included in the determination of when flows were stable enough for persistence calculations. This was because of the uncertainty of the validity of flow patterns near the open boundary and because the focus of this thesis was persistence of organisms within the body of the fjord. To this end the domains of the particle tracking program and final discrete time-space population program only extended a certain distance beyond the sill.

As a minimum requirement, POM was run until $\langle \overline{S} \rangle$ varied by less than 1% of its value, but also a record was kept of horizontal velocities at and adjacent to the open boundary. A model was judged ready when the salinity criteria was met and flows at the boundary appeared to be in a reasonably steady cycle. An illustration of variation in open boundary flows during spin-up of a fjord is given in Fig. 5.8. The model is set up with tidal elevations, river discharge and background vertical diffusivity as employed in Figs. 5.6 and 5.7. Although outputs for three cells are plotted the values are very similar such that only one trace appears evident. The degree to which this remained true was in itself used as an indication of the model remaining numerically stable. Fig. 5.8 also shows clearly the high frequency oscillations present at the start of simulation runs that, to be dampened out, require the use of non-zero horizontal eddy viscosity values.

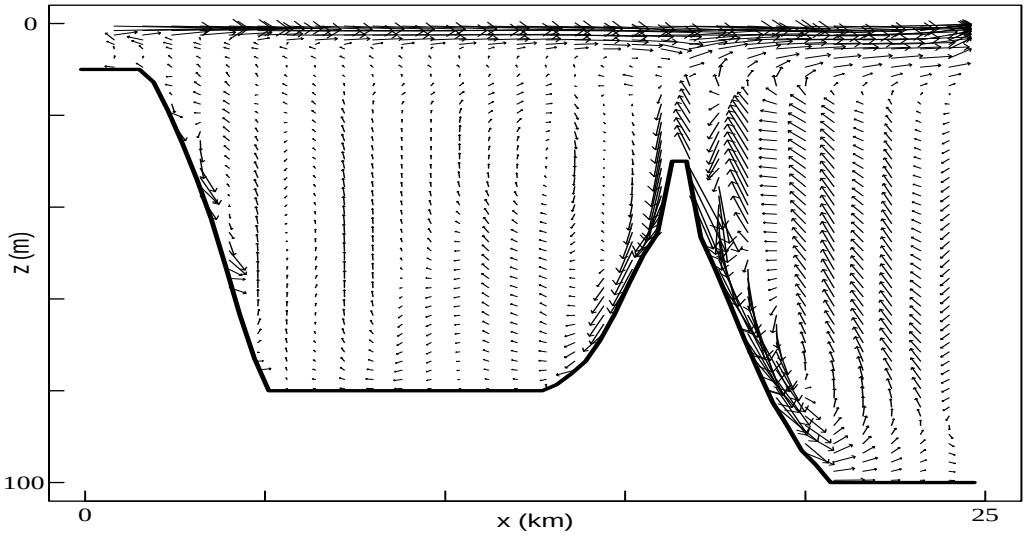

Figure 5.6: *Residual velocity plot derived using flow field from POM, using full primitive equations. Open boundary condition supplied by sinusoidal surface elevation, tidal range* $\pm 1m$. *River flow has per unit width discharge of* $Q_f = 1.67 \times 10^{-2} m^2 s^{-1}$. *Sea water at* $35psu$, *river water at* $0psu$. *Background diffusivity* $2.0 \times 10^{-5} m^2 s^{-1}$. *Velocity fields taken during last tidal cycle of a 20 day run.*

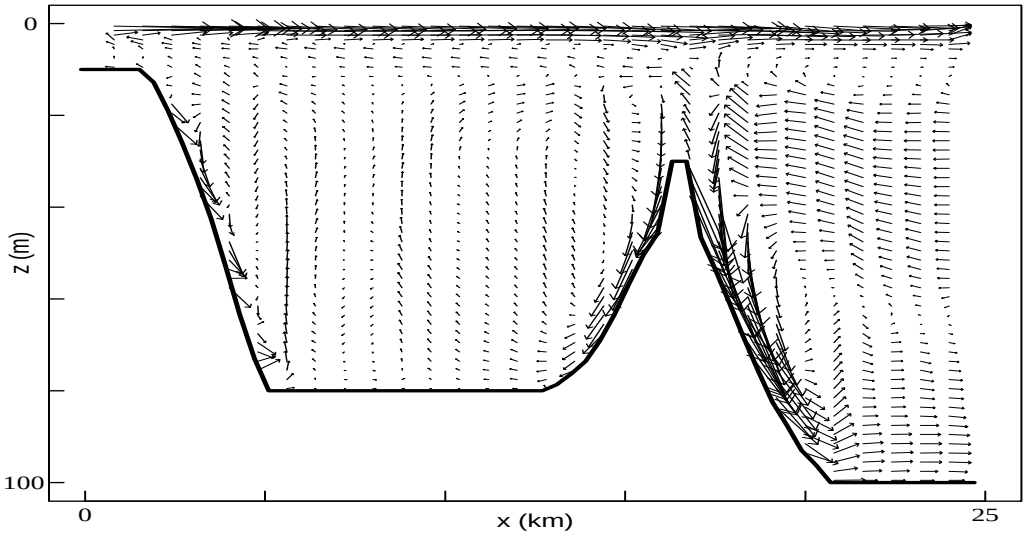

Figure 5.7: *Residual velocity plot derived using flow field from POM, using full primitive equations. Flow parameters as for Fig. 5.6. Velocity fields taken during last tidal cycle of a 40 day run.*

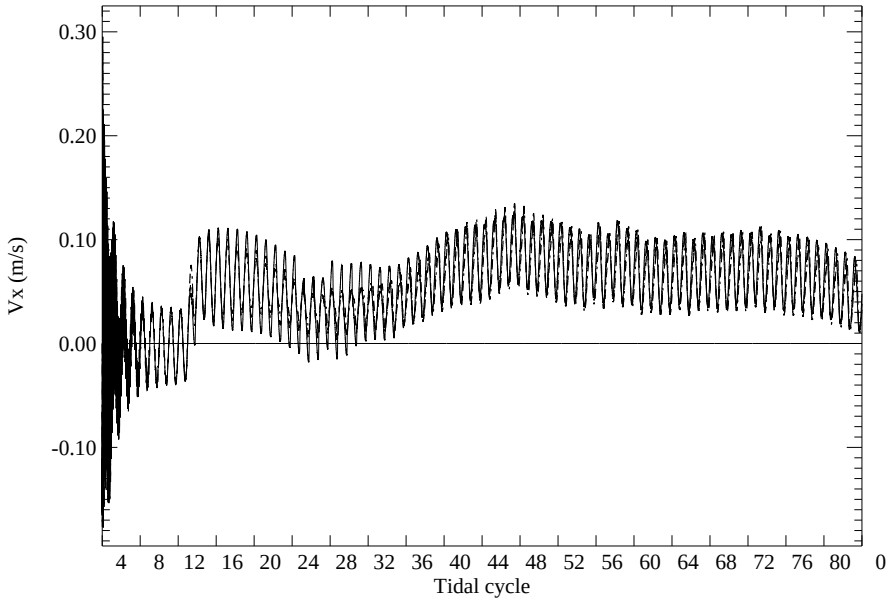

Figure 5.8: *Horizontal velocity at open boundary as a function of time. Traces are for velocity at the open boundary and for two cells adjacent to open boundary.*

There is evidence of low frequency, (wave length of several tidal cycles), variation in flows still present at the point where Lagrangian residuals were derived. This effect becomes more pronounced as river discharge is increased and is presumably due to the greater energy being input to the system. Fig. 5.8 shows it clearly as the run presented had the strongest discharge used with the fjord bathymetry. The two layer residual flow pattern demonstrated in Fig. 5.7 might therefore be quite fragile. Such patterns are cited for real fjords and these runs were intended to give a strategic representation of movements in a fully developed fjordic flow field. Additionally, Dyer (1973) doubts if tidal systems ever establish a true equilibrium. Indeed such an equilibrium is only theoretically possible in this work because of the simplification to both a constant tidal cycle, (ignoring the spring/neap cycle), and river inflow, together with the omission of the transient effects of winds. Residual movements were calculated when further computational effort for flow field spin-up was considered excessive, although a run with river inflow stronger than that used for figures 5.6 to 5.8 was abandoned as it appeared to become increasingly unstable with time.

Part III

Persistence of Passive and Active Organisms

Chapter 6

1D systems: well mixed rivers

6.1 Passive organisms permanently in the drift

As described in Chapter 3, a balance equation for organisms in a one dimensional system, whose population grows with a local per-capita growth rate, $p(n)$, and which is subject to an advection V_x and diffusion with coefficient Φ_x can be written as

$$\frac{\partial n}{\partial t} = p(n)n - V_x \frac{\partial n}{\partial x} + \Phi_x \frac{\partial^2 n}{\partial x^2} \tag{6.1}$$

For passive organisms the quantity V_x can be considered directly related to the mean velocity of the water in the system and Φ_x directly related to the water's coefficient of eddy viscosity. They are not the same however, as even small organisms will possess an inertia that suppresses their movement relative to the water around them.

6.1.1 Linear system

Speirs and Gurney (2001) investigated the possibility for persistence in such a system by considering populations where $p(n)$ always equalled r, the intrinsic growth rate and where the system was bounded by a reflecting boundary at the upstream end and an absorbing boundary at the downstream end. As shown in Appendix A they found that solutions were only possible if the following relation held

$$\tan\left(\kappa\frac{L}{L_d}\right) = -\frac{V_d}{V_x}\kappa \tag{6.2}$$

where

$$L_d \equiv \sqrt{\Phi_x r^{-1}} \quad V_d \equiv 2\sqrt{\Phi_x r} \quad \kappa \equiv \sqrt{1 - \frac{\Lambda}{r} - \left(\frac{V_x}{V_d}\right)^2} \tag{6.3}$$

From Equation (6.3) L_d represents the r.m.s. diffusive dispersal distance organisms can be expected to travel in the time a population with per-capita growth rate r increases in size by a factor $\sqrt{e}$ or $\approx 65\%$, and V_d represents the equivalent velocity of this movement. The term Λ gives the long term growth rate of the overall population. It is obtained by first solving Equation (6.2) numerically to determine κ, and then using the third expression in (6.3) to solve for Λ. This long term growth rate can take positive and negative values, the former indicating population persistence and the latter washout from the system. The boundary between persistence and washout is therefore given when $\Lambda = 0$. By setting $\Lambda = 0$ in Equation (6.3) and back-substituting for κ into a rearranged form of Equation (6.2) Speirs and Gurney (2001) derived an expression for the critical length, L_c, at which, for given values of the other parameters, the population is on the threshold of washout

$$\frac{L_c}{L_d} = \left[\sqrt{\frac{V_d^2}{V_d^2 - V_x^2}}\right] \arctan\left[-\sqrt{\frac{V_d^2 - V_x^2}{V_x^2}}\right] \tag{6.4}$$

As V_x tends to zero L_c/L_d tends to the value $\pi/2$, a result gained for populations experiencing diffusion but no advection (Gurney and Nisbet 1998)[1]. As V_x tends toward the value of V_d the critical length goes to infinity. Therefore, for a given intrinsic growth rate and a given diffusion constant, Φ_x, only systems with advection rates that satisfy

$$V_x < 2\sqrt{\Phi_x r} \tag{6.5}$$

have the potential to sustain a persistent population. A corollary of the results for L_c is that a critical velocity, V_c, for the system can be seen to tend to zero as the ratio L/L_d tends to $\pi/2$, implying no persistence is possible if life time diffusive length becomes sufficiently large compared to overall system length. As L becomes large compared to the value of L_d then the critical velocity tends toward V_d.

For a system of given length and a population with given per-capita growth rate r and advective displacement V_x, all the possible combinations of L/L_d and V_x/V_d that can be obtained from variation in the diffusion coefficient Φ_x lie on the straight line given by

$$\frac{V_x}{V_d} = \frac{1}{2}\left(\frac{V_x}{Lr}\right)\frac{L}{L_d} \tag{6.6}$$

Fig. 6.1 shows contours of constant Λ/r in the L/L_d against V_x/V_d plane. Superimposed are straight lines produced from Equation (6.6) but using different

[1]This critical length was first discovered by Skellam (1951), who considered a reproducing population subject to diffusion in a domain running from $-x_b \leq x \leq x_b$ and with absorbing boundaries at each end. Skellam found that persistence was only possible if $x_b \geq \frac{\pi}{2}\sqrt{\Phi_x r^{-1}}$ (converting to notation used in this text). This result was one of a number concerning reproducing populations experiencing diffusion.

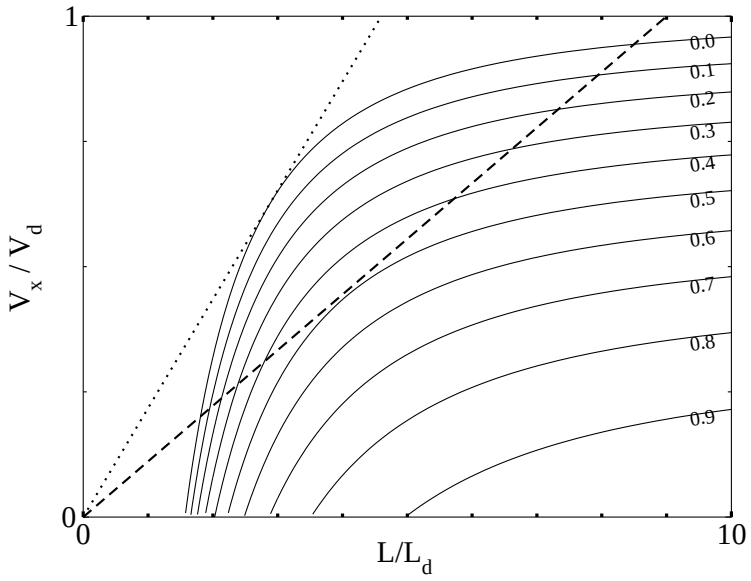

Figure 6.1: *Contours of constant Λ/r defined by Equation (6.2), with the values of Λ/r as marked. Dotted line: set of Λ/r values made accessible by varying the diffusion rate with $V_x/Lr = 0.434$. Dashed line: set of Λ/r values accessible with $V_x/Lr = 0.222$. From Speirs and Gurney (2001), with permission.*

values of V_x/Lr. If this ratio is sufficiently small, Fig. 6.1 shows that there exists a range of diffusion coefficient values over which persistence is possible for the population. As this ratio becomes larger, however, the finite range of possible Φ_x values becomes progressively smaller. Speirs and Gurney (2001) determined to graphical accuracy the marginal case where persistence is just possible, (dotted line), which gives a further inequality required for persistence

$$\frac{V_x}{Lr} < 0.434 \tag{6.7}$$

6.1.2 Non-linear system

Speirs and Gurney (2001) modelled the same system but with a constant local per-capita birth rate replaced by one obeying the logistic equation, that is

$$p(n) = r\left(1 - \frac{n}{k}\right) \tag{6.8}$$

They used the discrete space-time model described in section 3.3.1 with displaced tent distributions providing the redistribution matrix. Because the fixed per-capita growth rate is considered to represent the intrinsic growth rate of a population, the linear analysis developed conditions for the persistence of an invading propagule and it was argued that for populations with $p(n)$ made a decreasing function of density, no system in which an invading propagule could not grow could show a persistent population. Results using the non-linear growth term supported this assumption. Combinations of the ratios L/L_d and V_x/V_d from which the linear analysis predicted washout lead to washout in the non-linear model and equally combinations leading the linear analysis to predict a persistent population did lead to results of persistence.

In cases of persistence a reproducing population, (cited at some point along the domain), would have some proportion of its total spread in the upstream direction fast enough to overcome advection, that is, part of the population is physically moved upstream. A steady increase with time in population density in the region of the river source results until the requirement of zero flux at the boundary, coupled with the eventual effects of density dependence, create a steady state density decreasing toward the river source so that diffusive movement upstream exactly balances advection downstream. Population density also falls away, (toward zero), as the seaward, absorbing boundary is approached. As the boundary is approached ever fewer contributions to population are available from downstream.

6.2 Swimming

In this section the same fluid dynamics as in Section 6.1 are assumed, that is a constant value of advection, V_x, and diffusion coefficient, Φ_x. In order to discuss the effect of swimming it is useful to consider the movement of individuals as a random variable within a statistical distribution. The displacement of a passive particle over a time, τ, is a normally distributed random variable with a mean of

$V_x\tau$ and standard deviation $\sqrt{2\Phi_x\tau}$. Its coefficient of variation is therefore

$$C(\tau) = \frac{\sqrt{2\Phi_x\tau}}{V_x\tau} \tag{6.9}$$

Re-arranging Equation (6.5) we see that

$$V_x r^{-1} < \sqrt{4\Phi_x r^{-1}} \tag{6.10}$$

If one takes $\tau = r^{-1}$ then $C(r^{-1}) \equiv C_g$ becomes the coefficient of variation of the net displacement of the organism over a generation. Substituting the inequality of Equation (6.10) into Equation (6.9) gains a condition on C_g for persistence

$$C_g \equiv C(r^{-1}) > \frac{\sqrt{2\Phi_x r^{-1}}}{\sqrt{4\Phi_x r^{-1}}} = \frac{1}{\sqrt{2}} \tag{6.11}$$

6.2.1 Swimming against the average current

If an organism is assumed to swim upstream at a steady speed V_s, then the random part of its dispersal is unchanged but the average downstream velocity is reduced to $V_x - V_s$. The coefficient of variation of the average organismal displacement over a generation is thus

$$C_o(r^{-1}) = \frac{\sqrt{2\Phi_x r^{-1}}}{(V_x - V_s)r^{-1}} \tag{6.12}$$

From Equation 6.11 we have potential persistence if and only if $C_o(r^{-1}) > 1/\sqrt{2}$. If C_w is defined as the coefficient of variation of fluid elements within the flow then $C_o(r^{-1})/C_w(r^{-1})$ is given by

$$\frac{C_o(r^{-1})}{C_w(r^{-1})} = \frac{V_x}{V_x - V_s} = \frac{1}{1 - V_s/V_x} \tag{6.13}$$

So the persistence condition for the coefficient of variation of the fluid element displacement over the generational time becomes

$$C_w(r^{-1}) > \frac{1}{\sqrt{2}}\left(1 - \frac{V_s}{V_x}\right) \tag{6.14}$$

Equation 6.14 suggests swimming velocities small compared to V_x have essentially no effect on population persistence, while animals that can swim at velocities comparable to the average water velocity require almost no diffusion to persist. From Equation 6.12 it can be seen that modelling swimming against the average current is effectively the same as modelling a passive organism, but for an average water velocity reduced by the amount V_s.

Removing the logistic regulation from the model means long term population growth reverts to being exponentially increasing or decreasing. The influence of the ratio V_s/V_x can then be seen by comparing the long term growth rate, Λ, to V_s/V_x. Fig. 6.2 shows these values of Λ, normalised by dividing by the intrinsic growth rate, for a case in the absence of behaviour of marginal non-persistence, ($V_x = 0.001ms^{-1}$, $\Phi_x = 0.06m^2s^{-1}$ and $r = 0.39day^{-1}$).

To show how this behaviour can effect the distribution of a logistically regulated population and its average population density, Fig. 6.3 takes the same marginally non-persistent scenario, in the absence of behaviour. The initial population and that after 50 days is shown in frame a) while the time history of the average population density is shown in frame b). Lower frames show the effect of introducing V_s values of $0.1V_x$, $0.5V_x$ and $1.0V_x$. Even for a value of $V_s = 0.1V_x$ a considerable effect can be seen on both population distribution and the long term average density.

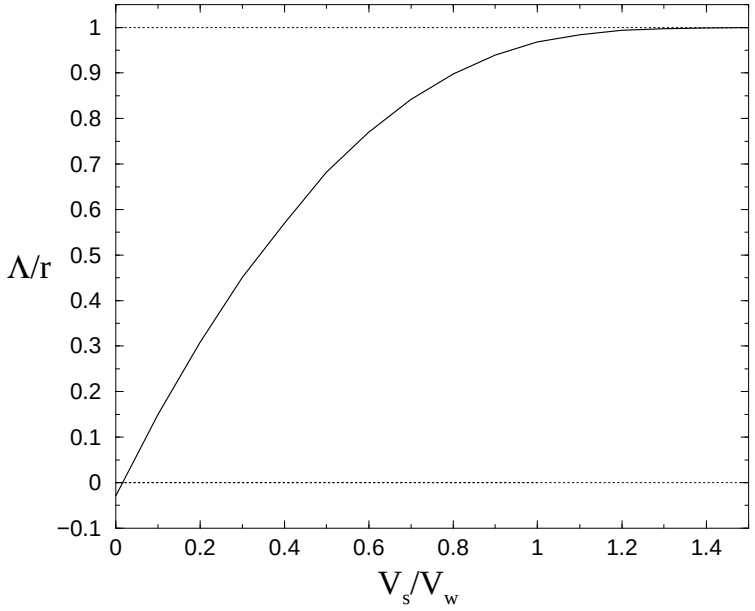

Figure 6.2: *Population with an exponential growth rate, (intrinsic growth rate* $= 0.39day^{-1}$*), swimming in a* $1km$ *river against a current with* $V_x = 0.001ms^{-1}$*,* $\Phi_x = 0.06m^2s^{-1}$*. Graph of ratio of long term growth rate to intrinsic growth rate compared to* V_s/V_x*: swimming against average current.*

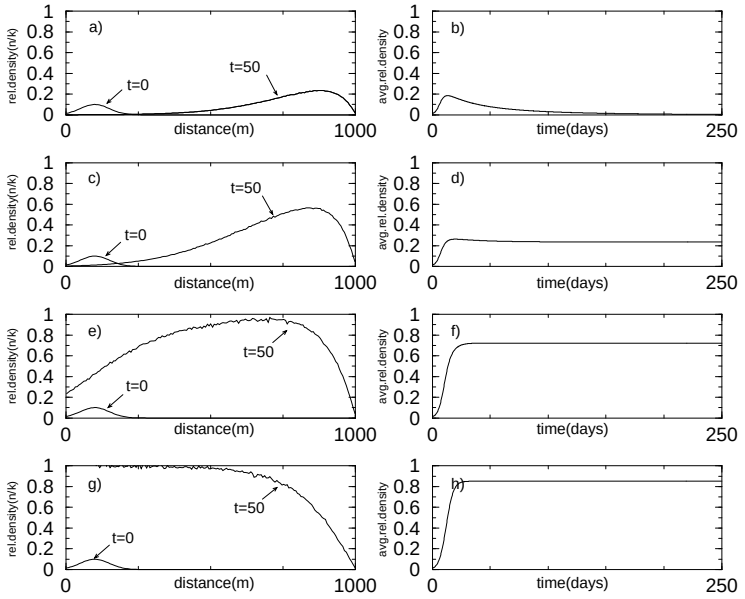

Figure 6.3: *Logistically regulated population with an intrinsic growth rate of* $0.39day^{-1}$*, being advected along a* $1km$ *river with a velocity of* $0.001ms^{-1}$*,* $\Phi_x = 0.06m^2s^{-1}$*.* $\Delta t = 6hrs$*. Organism swims against average current with constant velocity* V_s*. Right hand frames show the time history of average population density. Frames a),b):* $V_s = 0.0$*; Frames c),d):* $V_s = 0.1V_x$*; Frames e),f):* $V_s = 0.5V_x$*; Frames g),h):* $V_s = 1.0V_x$*.*

6.2.2 Swimming against the instantaneous current

The term instantaneous current is actually used to define, in this context, the fluid movement averaged over some time, τ, a time considerably shorter than the time required for the mean motion of the flow to dominate the size and direction of movement. It is assumed that an organism, with a maximum swimming speed of V_s, swims against this instantaneous current, which it matches to within a normally distributed error ε. It is further assumed that ε has a mean of zero and a standard deviation equivalent to a diffusion constant Φ_s. If the passive displacement an organism would experience in the time τ is W, then the conditional probability density function for the organism's facultative displacement, s, relative to the water movement in the same period is given by the Gaussian

$$p(s|W) = G\left(s, \overline{s}(W), \sqrt{2\Phi_s \tau}\right) \tag{6.15}$$

where

$$\overline{s}(W) = -\frac{W}{|W|}\min(|W|, V_s\tau) \tag{6.16}$$

Let W_r be the resultant displacement over the period τ. This is given by

$$W_r = W + s \tag{6.17}$$

Any combination of W and s satisfying the restriction $s = W_r - W$ gives the same value of W_r. Integrating the product of the probabilities of getting s for a given value of W, and W over all possible values of W therefore gives the unconditional probability density function for the resultant displacement. That is

$$p(W_r) = \int_{-\infty}^{\infty} p(W)p((W_r - W)|W)dW \tag{6.18}$$

The value of $p((W_r - W)|W)$ is given by Equation (6.15) with $W_r - W$ substituted for s, while $p(W)$ is given by

$$p(W) = G(W, V_x\tau, \sqrt{2\Phi_x\tau}) \tag{6.19}$$

The values of Φ_s, V_s and τ need to be defined with consideration to each other. If we wish to investigate changes in long term growth rate with changes in V_s, it is reasonable to assume that over any period of averaging, τ, the average error in an organism's swimming speed will be some fixed percentage of it's maximum swimming speed, V_s. This in turn requires Φ_s to vary with V_s, rather than remain a fixed value. The root mean square distance of error in a time τ is $\sqrt{2\Phi_s\tau}$. A pseudo velocity can be obtained from

$$\frac{1}{\tau}\sqrt{2\Phi_s\tau} = \sqrt{\frac{2\Phi_s}{\tau}} \tag{6.20}$$

If a single, fixed value of Φ_s is assumed, this pseudo velocity is unaffected by the value of V_s. As V_s is reduced, a greater proportion of possible errors in the swimming speed become comparable to the notional maximum swimming speed itself. Eventually V_s becomes dominated by the swimming error.

Equation (6.20) shows that the velocity error is affected by the value given to τ. The value to be chosen for τ is a mute point. The large size of even plankton in comparison to water molecules and their individual diffusive movements guarantees some averaging in the response to water movements. A reasonable averaging time, however, is difficult to determine. If the value of τ is changed for any reason, then Φ_s must be changed if one wishes to maintain the same relationship between $\sqrt{\frac{2\Phi_s}{\tau}}$ and any given value of V_s.

Taking the same values of V_x, Φ_x and r that gave marginal non-persistence in the absence of behaviour, (as in section 6.2.1), a τ value of $0.1r^{-1}$ was chosen and values of Φ_s were chosen such that $\sqrt{2\Phi_s\tau} = 0.1 \times V_s\tau \;\forall\; V_s$. Fig. 6.4 shows

numerical solutions to Equation (6.18) for V_s values of 0.0, $0.1V_x$, $0.5V_x$ and $1.0V_x$. The pdf displayed when $V_s = 0.0$ is, of course, the same as that in the absence of behaviour. Fig. 6.4 also shows the result for the pdf obtained from the particle tracking, population model combination. Particles were tracked from one cell, (well away from the boundaries), for the period τ. The population model was then run for a single timestep (again equal to τ) with an initial population of 1 in the same start cell and no population growth. This figure shows the results obtained for the case where $V_s = V_x$, $\Delta x = 1$ and $N = 60000$.

As discussed in relation to Equation (6.20), for a fixed value of diffusion constant, the effective velocity of diffusion increases as the time interval considered decreases. This implies that as the averaging time τ is reduced, an organism is required to have a greater swimming speed in order to neutralise the diffusive water movement. Fig. 6.5 shows the effect of varying τ while maintaining $V_s = V_x$. The x-axis denotes W_r/τ, a measure of velocity of the resultant movement. As expected, as τ reduces, the pdf becomes more spread, showing increasing proportions of water movement that have not been counter-acted by swimming.

6.2.3 Swimming against a moving average

A problem with the model of swimming against the instantaneous current as defined so far is that it requires an organism to instantaneously gauge the net water movement over the forthcoming period τ and swim accordingly; in effect to *predict* the displacement due to water movement. A more realistic model can be considered one in which the organism swims against a moving average built up over previous time. The overall averaging period remains τ, but the moving average is composed of smaller timesteps. It is convenient to make these component timesteps, δt, equal to the individual timesteps of the particle tracking program. If ϑ represents the fraction of maximum swimming distance represented by the root mean squared diffusive distance of swimming error, this fraction needs to hold true over the period τ. This gives the following relationship between Φ_s

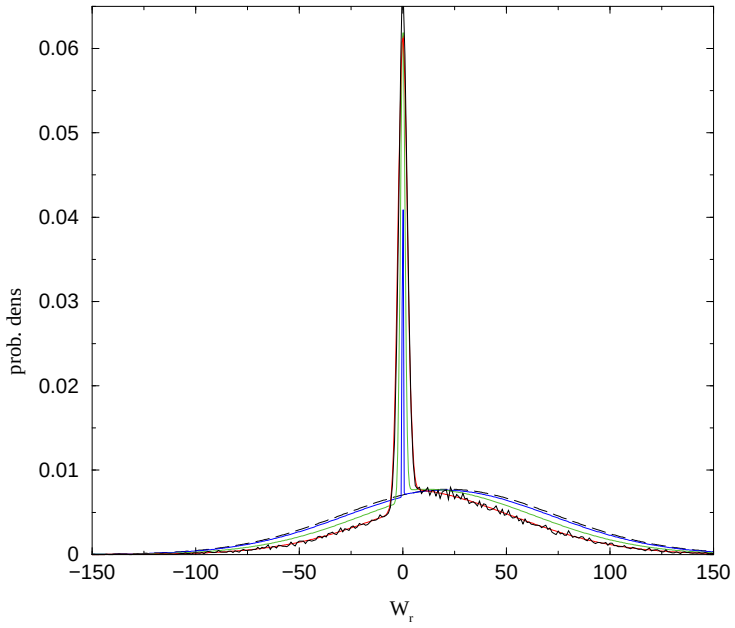

Figure 6.4: *Probability density function for the net displacement of an organism swimming against flow averaged over a period* τ. $V_x = 0.001ms^{-1}$, $\Phi_x = 0.06m^2s^{-1}$, $\tau = 0.1r^{-1}$, $\sqrt{2\Phi_s/\tau} = 0.1V_s$: $V_s = 0.0ms^{-1}$ *(long-dashed),* $V_s = 0.1V_x$ *(blue),* $V_s = 0.5V_x$ *(green) and* $V_s = 1.0V_x$ *(red). Solid line shows approximation to pdf when* $V_s = 1.0V_x$*, given by particle tracking and population model using* $\Delta x = 1m$ *and* $N = 60000$.

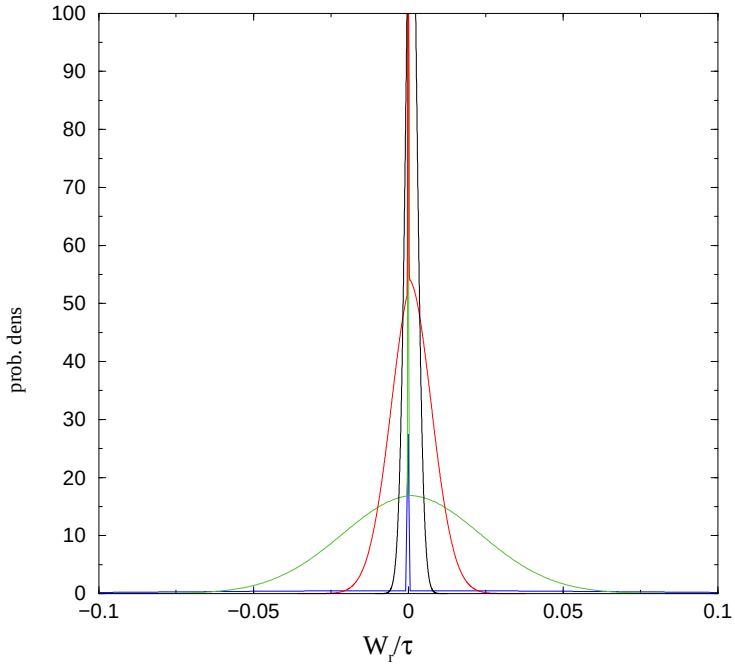

Figure 6.5: *Probability density function for the net displacement velocity of an organism swimming against flow averaged over a period* τ. $V_x = 0.001ms^{-1}$, $\Phi_x = 0.06m^2s^{-1}$, $V_s = 1.0V_x$, $\sqrt{2\Phi_s/\tau} = 0.1V_s$: $\tau = 0.1r^{-1}$ *(black),* $\tau = 0.01r^{-1}$ *(red),* $\tau = 0.001r^{-1}$ *(green) and* $\tau = 0.0001r^{-1}$ *(blue).*

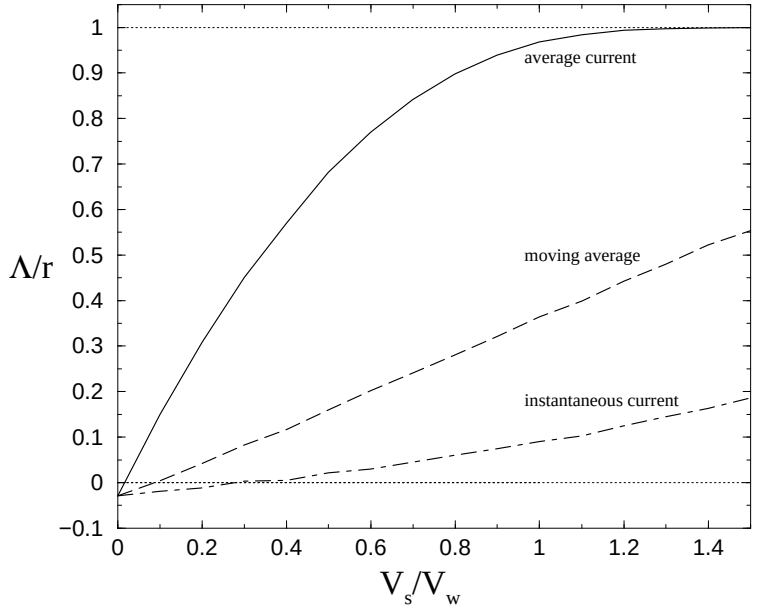

Figure 6.6: *Population with an exponential growth rate, (intrinsic growth rate* $= 0.39day^{-1}$*), swimming in a* $1km$ *river against a current with* $V_x = 0.001ms^{-1}$*,* $\Phi_x = 0.06m^2s^{-1}$*. Graphs of ratio of long term growth rate to intrinsic growth rate compared to* V_s/V_x*: swimming against average current, (solid line); swimming against a moving average, (dashed line); swimming against a predicted current averaged over a period* τ*, (dot-dashed line).* $\tau = 6hrs$*.*

and V_s

$$\begin{aligned} \sqrt{2\Phi_s\tau} &= \vartheta V_s\tau \\ 2\Phi_s\tau &= \vartheta^2 V_s^2\tau^2 \\ \Phi_s &= \frac{\vartheta^2\tau}{2}V_s^2 \end{aligned} \tag{6.21}$$

For the much smaller time periods δt the ratio of diffusive to advective swimming distance will be much greater. The tracking timesteps, however, are not intended as part of the biological model and the choice of δt should be such that smaller values have little or no effect on the final result.

Fig. 6.6 shows graphs of λ/r against V_s/V_x produced from the particle tracking and population model combination for the case where $\vartheta = 0.1$. Values for V_x, Φ_x and r are as in section 6.2.1. The dashed line represents the result obtained using a moving average. The dot-dashed line represents the earlier case of a prediction

of the water movement by the organism. For comparison the solid line shows the result obtained by swimming against the average current, (as seen in Fig. 6.2). Both models of swimming against an instantaneous current show significantly less improvement in Λ/r values as swimming speed increases relative to water advective velocity.

The relatively poor performance of swimming against the instantaneous, predicted, current is underlined by re-considering Fig. 6.4. This shows how the upstream region of the pdf, (negative values of W_r), is more effectively reduced than the downstream region. The animal swims against both downstream and upstream currents. Upstream currents are on average smaller (because of the net downstream advection) and so the animal is better at resisting them. Interestingly, by comparison, swimming against a moving average appears not only a more realistic model of behaviour, but also to achieve greater improvements in persistence.

6.3 Clinging to the benthos: No facultative movement in benthos or water column

6.3.1 Extension of analytical solution to a $1\frac{1}{2}$D problem

Section 3.2.1 and Appendix A describes the method for a semi-analytic determination of the long term growth rate of a population in a one dimensional advection, diffusion system. It was found possible to extend this technique to solve for a system as before but with the addition of a benthic state and constant rates of transfer between benthos and water column.

To attain an analytic solution organisms are assumed to be static while in their benthic 'state'. A further simplification is to assume that the times spent in the drift or in the benthos are independent of the river velocity, or more accurately

the organismal advection and diffusion coefficient used for organisms when they are in the drift. If, in addition, organisms are assumed to have exponential decay distributions for the benthic and water column residence times then the rate of transfer between states are simple constants. With these assumptions the single continuity equation, (Equation 3.2), becomes a coupled pair

$$\begin{aligned} \frac{\partial n}{\partial t} &= p(n)n - \beta n + \alpha m - V_x \frac{\partial n}{\partial x} + \Phi_x \frac{\partial^2 n}{\partial x^2} \\ \frac{\partial m}{\partial t} &= p(m)m + \beta n - \alpha m \end{aligned} \tag{6.22}$$

where m(t,x) represents population density in the benthos at time t and point x, α is the rate of transfer from benthos to drift and β is the rate of transfer from drift to benthos. As in the previous theory, it is only possible to derive analytic solutions if the per capita growth rates are constants. In the following solution it is assumed $p(n) = p(m) = r$.

If the population in the benthos assumes the same long term spatial pattern as that in the drift, then the population density in the benthos at all points is a constant multiple of the population in the drift at the same location. That is $m = \theta n$ where θ is the constant of proportionality. With no movement in the benthos the boundary conditions for this problem remain as in Equations (3.3) and (3.4).

To simplify the problem the following scaled terms are introduced

$T \equiv t/t_0$ where $t_0 = r^{-1}$

$X \equiv x/x_0$ where $x_0 = L_d \equiv \sqrt{\Phi_x r^{-1}}$

$\omega \equiv \alpha/\alpha_0$ where $\alpha_0 = r$

$\sigma \equiv \beta/\beta_0$ where $\beta_0 = r$

$\nu \equiv V_x/V_0$ where $V_0 = V_d \equiv 2\sqrt{\Phi_x r}$

Substituting these scaled terms into Equation (6.22) yields a simplified set of equations

$$\frac{\partial n}{\partial T} = n - \sigma n + \omega m - 2\nu \frac{\partial n}{\partial X} + \frac{\partial^2 n}{\partial X^2} \tag{6.23}$$

$$\frac{\partial m}{\partial T} = m - \omega m + \sigma n \tag{6.24}$$

with boundary conditions

$$2\nu n(0,T) - \left.\frac{\partial n}{\partial X}\right|_{X=0} = 0 \tag{6.25}$$

$$n(l,T) = 0 \tag{6.26}$$

where $l \equiv L/L_d$. Using the assumption $m = \theta n$ solutions were sought of the form

$$\begin{aligned} n &= e^{\lambda T} f(X) \\ m &= \theta n \end{aligned} \tag{6.27}$$

where $\lambda = \Lambda/r$ is the scaled long term growth rate. Back-substituting into Equations (6.23) and (6.24) and dropping the (X) notation gives

$$\lambda f = f - \sigma f + \omega\theta f - 2\nu \frac{df}{dX} + \frac{d^2 f}{dX^2} \tag{6.28}$$

and

$$\theta\lambda = \theta + \sigma - \omega\theta \tag{6.29}$$

Using the relationship $-\sigma + \omega\theta = \theta(1-\lambda)$ from equation (6.29) in equation (6.28) gives

$$0 = (1-\lambda)(1+\theta)f - 2\nu\frac{df}{dX} + \frac{d^2f}{dX^2} \tag{6.30}$$

Appendix D shows that the general solution to this problem should be in the form

$$f(X) = Ae^{\xi X}\cos kX + Be^{\xi X}\sin kX \tag{6.31}$$

where $\xi \equiv \nu$ and solutions are only possible if

$$\tan kl = -\frac{k}{\nu} \tag{6.32}$$

where

$$k = \sqrt{(1-\lambda)\left(1 - \frac{\sigma}{1-\lambda-\omega}\right) - \nu^2} \tag{6.33}$$

Converting equation (6.32) back to dimensional form gives

$$\tan\left(\kappa\frac{L}{L_d}\right) = -\frac{V_d}{V_x}\kappa \tag{6.34}$$

where κ is given by

$$\kappa = \sqrt{\left(1-\frac{\Lambda}{r}\right)\left(1 + \frac{\beta}{\alpha+\Lambda-r}\right) - \left(\frac{V_x}{V_d}\right)^2} \tag{6.35}$$

or

$$\kappa = \sqrt{\left(1-\frac{\Lambda}{r}\right)\left(1 + \frac{\frac{\beta}{r}}{\frac{\alpha}{r}+\frac{\Lambda}{r}-1}\right) - \left(\frac{V_x}{V_d}\right)^2} \tag{6.36}$$

Obtaining values of the scaled long term growth rate λ

With parameters l and ν fixed, equation (6.32) can be satisfied by an infinite series of values for k. From equation (6.33), however, it can be seen that negative values of k will always have a positive equivalent of the same magnitude. Because all other parameters, (including σ and ω), are held fixed this must be derived using the same value of λ.

Concentrating on positive values of k, we investigate the relationship between k and λ. Squaring k, to remove the square root, and differentiating with respect to λ we obtain

$$\begin{aligned}\frac{dk^2}{d\lambda} &= \left(-1 - \frac{\sigma}{\omega+\lambda-1}\right) - \left(\frac{\sigma(1-\lambda)}{(\omega+\lambda-1)^2}\right) \\ &= -1 - \frac{\sigma}{\omega+\lambda-1}\left(1 + \frac{1-\lambda}{\omega+\lambda-1}\right) \\ &= -1 - \frac{\sigma\omega}{(\omega+\lambda-1)^2} \end{aligned} \tag{6.37}$$

The product $\sigma\omega$ is always positive, as is any term squared. Therefore $dk^2/d\lambda$ is negative for any value of λ showing that the maximum possible value of λ is obtained from the smallest permissible value of k^2 and, given the relationship between positive and negative k values, the smallest positive value of k.

The above suggests $k = 0$ provides the maximum possible λ value. However, substituting $k = 0$ back into the general solution given by equation (6.31) means that the right hand boundary of the system requires that

$$Ae^{\nu l} = 0 \tag{6.38}$$

This can only be satisfied if $A = 0$, which in turn implies $f(X) = 0\ \forall X$ and we are not interested in systems containing zero population density.

With $k = 0$ excluded, the next value for positive k in which the straight line

$-k/\nu$ cuts the curves for $\tan kl$ is in the region $\pi/2 < kl < \pi$.

Because determining k involves a quadratic in λ, it is possible for two values of λ to satisfy equation (6.32) for the single value of k of interest. As we are interested in the largest possible long term growth rate we simply need to consider the larger of the two roots. If we substitute $\varpi \equiv (1-\lambda)$ into Equation 6.33 then the quadratic for obtaining the roots of λ becomes

$$-\varpi^2 + \varpi(\omega + \sigma + \nu^2 + k^2) - \omega(\nu^2 + k^2) = 0 \tag{6.39}$$

Which has roots given by

$$\begin{aligned} \varpi &= (1-\lambda) = \frac{1}{2}(\omega + \sigma + \nu^2 + k^2) \pm \frac{1}{2}\sqrt{(\omega + \sigma + \nu^2 + k^2)^2 - 4\omega(\nu^2 + k^2)} \\ \lambda &= 1 - \frac{1}{2}(\omega + \sigma + \nu^2 + k^2) \pm \frac{1}{2}\sqrt{(\omega + \sigma + \nu^2 + k^2)^2 - 4\omega(\nu^2 + k^2)} \end{aligned} \tag{6.40}$$

6.3.2 Effect of exchange rates on proportions of population in drift and benthos

Significant relationships between the scaled long term growth rate λ, the scaled sinking and re-suspension rates σ and ω, and the constant of proportionality between benthic and drifting population density at any point, θ, can be seen from consideration of Equation (6.29). Gathering all terms involving θ to one side gives

$$\sigma = \theta(\omega + \lambda - 1) \tag{6.41}$$

As $\sigma \geq 0$ this implies

$$\theta(\omega + \lambda - 1) \geq 0 \tag{6.42}$$

As $\theta \geq 0$, two cases must be considered. If $\theta > 0$ then the following relation holds

$$\begin{aligned} \omega + \lambda &\geq 1 \\ \lambda &\geq 1 - \omega \end{aligned} \tag{6.43}$$

If $\omega > 1$, λ can become negative and therefore the dimensional long term growth rate Λ can become negative. If $\omega = 1$ then from Equation (6.43) $\lambda \geq 0$ and if $\omega < 1$ then $\lambda > 0$.

If $\theta = 0$ then nothing can be inferred about the relationship between ω and λ from Equation(6.42). However, the trial solution of Equation (6.27) and the O.D.E. of Equation (6.30) can be seen to collapse down to the case when all organisms are permanently in the drift and the long term growth rate can be determined as in section 6.1

If ω is set to zero then Equation (6.41) becomes

$$\sigma = \theta(\lambda - 1) \tag{6.44}$$

As $\sigma \geq 0$ and $\theta \geq 0$ and the maximum possible value for λ is one, this implies that $\sigma = 0$ also. Further $\lambda = 1$, that is the long term growth rate equals the intrinsic growth rate and/or $\theta = 0$. These results are reasonable if it is remembered that population in the benthos grows exponentially with no density dependence and without being subjected to any form of dispersal. With the rate of recruitment to the drift equal to zero any population in the benthos at a point x will grow at the intrinsic growth rate. To obtain a value of λ less than one there can be no population in the benthos, that is θ must be zero.

The value of θ for any given combination of ν, l, σ, and ω is again found from Equation (6.29), that is

$$\theta = \frac{\sigma}{\omega + \lambda - 1} \tag{6.45}$$

If we define $N = n + m$ then using Equation (6.45), N can be expressed as

$$\begin{aligned} N &= n\left(1 + \frac{\sigma}{\omega + \lambda - 1}\right) \\ N &= n\left(\frac{\omega + \lambda - 1 + \sigma}{\omega + \lambda - 1}\right) \end{aligned} \tag{6.46}$$

and the proportions of total population made up of individuals from the drift and the benthos becomes

$$\begin{aligned} \frac{n}{N} &= \frac{\omega + \lambda - 1}{\omega + \lambda - 1 + \sigma} \\ \frac{m}{N} &= \frac{\sigma}{\omega + \lambda - 1 + \sigma} \end{aligned} \tag{6.47}$$

If $\lambda = 1$ then $\theta = \sigma/\omega$ such that $m = (\sigma/\omega)n$, $n = (\omega/\sigma)m$ and

$$\begin{aligned} \frac{n}{N} &= \frac{\omega}{\omega + \sigma} \\ \frac{m}{N} &= \frac{\sigma}{\omega + \sigma} \end{aligned} \tag{6.48}$$

It is shown in section 6.3.3 that the proportions of Equation 6.48 can be predicted from a non-spatial Markov process with two discrete states (Cox and Miller 1990).

More generally, θ can be found by solving for λ first, or by substituting for λ from Equation (6.40), giving

$$\begin{aligned} \theta &= \frac{\sigma}{(\omega - 1) + 1 - \frac{1}{2}(\omega + \sigma + \nu^2 + k^2) + \frac{1}{2}\sqrt{(\omega + \sigma + \nu^2 + k^2)^2 - 4\omega(\nu^2 + k^2)}} \\ \theta &= \frac{\sigma}{\frac{\omega}{2} - \frac{1}{2}(\sigma + \nu^2 + k^2) + \frac{1}{2}\sqrt{(\omega + \sigma + \nu^2 + k^2)^2 - 4\omega(\nu^2 + k^2)}} \end{aligned} \tag{6.49}$$

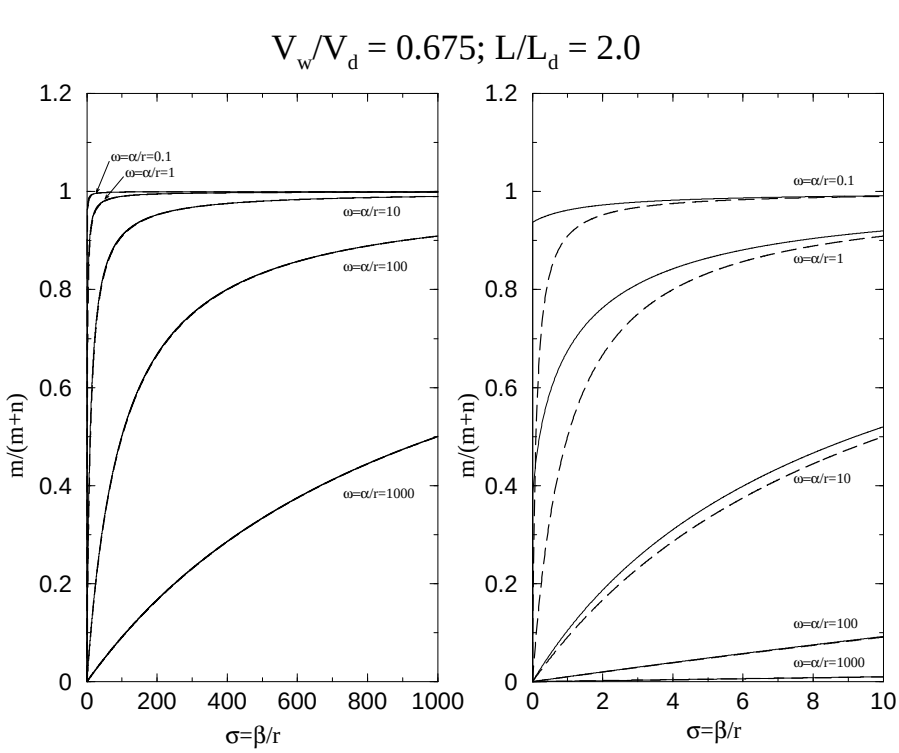

Figure 6.7: *Graphs of proportion of population in benthos against scaled sinking rate for various values of scaled re-suspension rate. Right hand frame repeats the data of left hand frame over a small range of σ. Results are for fixed values of V_x/V_d and L/L_d. Dashed lines represent proportion of population that would be found in benthos if there were no horizontal movement.*

Fig. 6.7 shows graphs of the proportion of population in the benthos against scaled sinking rate for various values of scaled re-suspension rate. The right hand panel is identical to the left hand panel except in only showing results over a small range in σ. As these proportions depend not only on ω and σ but also on λ, they therefore depend on the scaled quantities ν and l. To produce Fig. 6.7 specific values were chosen for ν and l. The dashed lines represent the proportion of the population that would be found in the benthos if there were no horizontal movement, (that is, they are determined by Equation 6.53 of section 6.3.3). The right hand panel shows that this approximate result for the proportion in the benthos is very close to the true result for all values of σ if ω is sufficiently high and only differs significantly from the true result when both ω and σ values are low.

Re-considering Equation (6.47) for m/N, it can be seen that as σ tends to zero

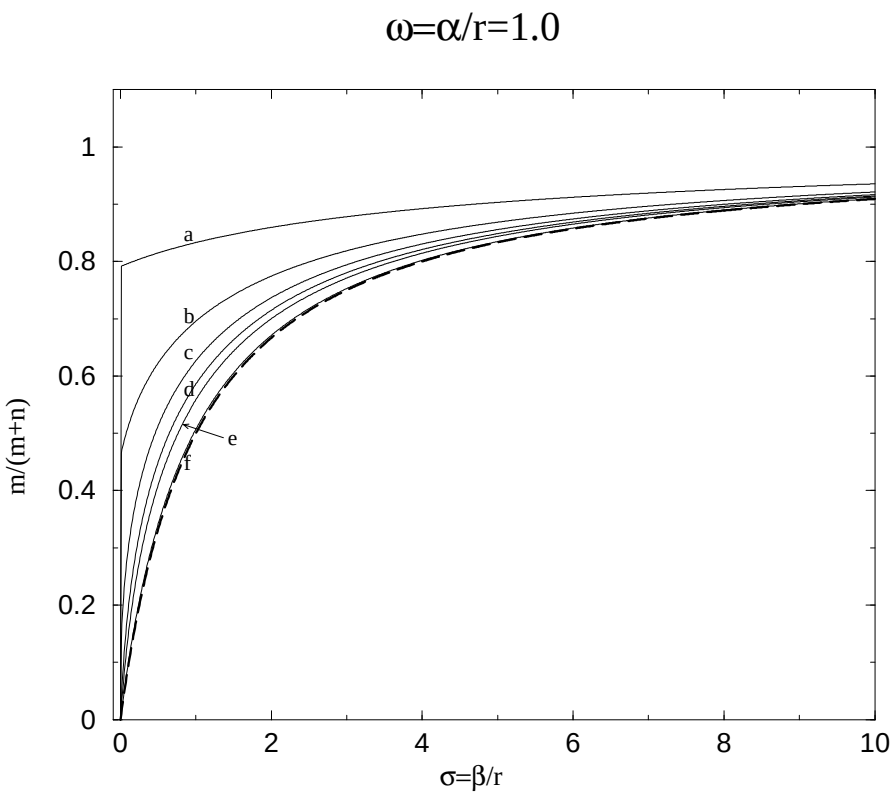

Figure 6.8: *Graphs of proportion of population in benthos against scaled sinking rate for scaled re-suspension rate of* $\omega = 1.0$. *Solid lines represent different combinations of* V_x/V_d *and* L/L_d. *a)* $V_x/V_d = 0.9,\ L/L_d = 1.0$*; b)* $V_x/V_d = 0.8,\ L/L_d = 2.0$*; c)* $V_x/V_d = 0.7,\ L/L_d = 3.0$*; d)* $V_x/V_d = 0.6,\ L/L_d = 4.0$*; e)* $V_x/V_d = 0.5,\ L/L_d = 5.0$*; f)* $V_x/V_d = 0.1,\ L/L_d = 9.0$. *Dashed line represents proportion of population that would be found in benthos if there were no horizontal movement.*

the denominator is dominated by the expression $\omega + \lambda - 1$. Small values of ω in turn make the expression more critically dependent on the value of λ. The difference between systems with and without horizontal movement is that horizontal movement can generate equilibrium solutions with $\lambda < 1$.

The value of λ for given values of ω and σ depends on values chosen for ν and l. Thus, as combinations of ν and l move the value of λ to the lowest permissible for a given value of ω, values of m/N will diverge from the approximation assuming no movement as σ values decrease. This effect can be seen in Fig. (6.8) which shows graphs of m/N against σ for the single value $\omega = 1.0$ but for different combinations of ν and l. The case equating to no horizontal movement in the system is also represented via a dashed curve. The values for $\nu \equiv V_x/V_d$ and

$l \equiv L/L_d$ represent points on a straight line taken through Fig 6.1, (not drawn). As ν increases and l decreases we move to progressively lower values of Λ/r and, as expected, the curves of Fig. (6.8) diverge from that equating to no horizontal movement in the system. Thinking in physical terms, low values of ω and low values of λ equate to a population allowed a greater chance to grow in the benthos without entering the drift, but with a higher chance of being washed out of the system if entrained.

6.3.3 Comparison to a two discrete state Markov process

The assumptions about residence times and movements between the drift and benthic states that allow an analytic solution to the problem of benthic clinging can also be used as the basis of a statistical approach for assessing the proportion of population in each state.

Assuming exponential decay distributions for the benthic and water column residence times allows these distributions to have no 'memory'. If in addition the movement of the population in the drift is ignored and the population in drift and benthos is considered uniformly spread then the problem has ceased to be spatial. It can now be dealt with as a Markov process with two discrete states (Cox and Miller 1990).

The two states are that of being in the benthos (labelled state 0) and being in the water column (state 1). Let the mutually independent and random residence times in the benthos, $\{T_{b1}, T_{b2}, ...\}$, and those in the water column $\{T_{w1}, T_{w2}, ...\}$ be exponentially distributed with mean values of $\overline{T_b}$ and $\overline{T_w}$ respectively. The rates of transition between states are $1/\overline{T_b} = \alpha$ and $1/\overline{T_w} = \beta$. Given that an organism is in state 0 at time t the probability of a transition to state 1 in the interval $(t, t + \delta t)$ is given by

$$p(S(t+\delta t)=1|S(t)=0)=\alpha\delta t+O(\delta t^2) \tag{6.50}$$

where S is the record of the state of the organism.

Now let $p_b(t)$ be the probability of being in the benthos at time t and $p_w(t)$ the probability of being in the water column at the same point in time. The rates of change of these two probabilities are given by

$$\begin{aligned} p_b'(t) &= -\alpha p_b(t)+\beta p_w(t), \\ p_w'(t) &= -\beta p_w(t)+\alpha p_b(t) \end{aligned} \tag{6.51}$$

If the initial probabilities $p_b(0)$ and $p_w(0)=1-p_b(0)$ are specified, then the solution to Equations 6.51 are given by

$$\begin{aligned} p_b(t) &= \frac{\beta}{\alpha+\beta}+\left\{p_b(0)-\frac{\beta}{\alpha+\beta}\right\}e^{-(\alpha+\beta)t}, \\ p_w(t) &= \frac{\alpha}{\alpha+\beta}+\left\{p_w(0)-\frac{\alpha}{\alpha+\beta}\right\}e^{-(\alpha+\beta)t} \end{aligned} \tag{6.52}$$

From Equation 6.52 it is clear that as $t\to\infty$, then independently of the initial conditions, the probability distribution tends to

$$p_b=\frac{\beta}{\alpha+\beta},\quad p_w=\frac{\alpha}{\alpha+\beta} \tag{6.53}$$

Therefore, for a population in the one dimensional domain, regardless of what proportion are considered to start in the water column, after a time large compared with $1/(\alpha+\beta)$, all organisms will have the same probability, $\alpha/(\alpha+\beta)$ of being in the water column. With respect to investigating persistence through simulation, Equation 6.52 shows that the time-dependent terms vanish if $p_b(0)=p_b,\ p_w(0)=p_w$. Thus, if each particle tracked to form the redistribution matrix

starts in the water column with probability p_w and in the benthos with probability $p_b = 1 - p_w$ then – if exchange rates are sufficiently high in comparison to intrinsic growth – we can effectively assume the proportion of time spent in the water column to equal p_w during the simulation.

6.3.4 Effect of retention in the benthos on critical velocity

The previous sections show that with transition rates, α and β, sufficiently high, the proportions of population found in the drift and benthos closely approximate those predicted by Equation (6.53). This equation suggests that with V_x and Φ_x constant throughout the domain, and with organisms non-moving in the benthos and acting as passive particles in the water column, the effect of transitions between the benthos and water column is analogous to considering passive particles permanently resident in the water column but subject to advective water velocity of $\alpha/(\alpha+\beta) \times V_x$ and diffusion constant of $\alpha/(\alpha+\beta) \times \Phi_x$. With this assumption the coefficient of variation of the average organismal displacement over a generation becomes

$$C_o(r^{-1}) = \frac{\sqrt{2\Phi_x p_w r^{-1}}}{p_w V_x r^{-1}}, \quad p_w \equiv \frac{\alpha}{\alpha+\beta} \tag{6.54}$$

As in the case for swimming against the average current potential persistence is possible iff $C_o(r^{-1}) > 1/\sqrt{2}$. In this case $C_o(r^{-1})/C_w(r^{-1})$ is given by

$$\frac{C_o(r^{-1})}{C_w(r^{-1})} = \frac{1}{\sqrt{p_w}} \tag{6.55}$$

so for persistence we have the inequality

$$C_w(r^{-1}) > \frac{\sqrt{p_w}}{\sqrt{2}} \tag{6.56}$$

Using the same assumption a prediction can be made regarding how the amount

of time spent in the benthos affects the critical water velocity, V_c, at which persistence becomes impossible. For passive organisms permanently in the water column the relationship was found to be

$$V_c = 2\sqrt{\Phi_x r} \tag{6.57}$$

If the organism spends the fraction, p_w, of time in the water column this relationship becomes

$$\begin{aligned} p_w V_c(p_w) &= 2\sqrt{p_w \Phi_x r} \\ V_c(p_w) &= 2\sqrt{p_w^{-1} \Phi_x r} \end{aligned} \tag{6.58}$$

The relationship between V_c and $V_c(p_w)$ is therefore

$$\frac{V_c(p_w)}{V_c} = \frac{1}{\sqrt{p_w}} \; ; \quad V_c(p_w) = \frac{V_c}{\sqrt{p_w}} \tag{6.59}$$

Plotting $\log(V_c(p_w)/V_c)$ against $\log(1/\sqrt{p_w})$ gives a straight line with slope -0.5.

This predicted relationship is shown as the black line of Fig. (6.9). The other lines show the calculated results for different values of $l \equiv L/L_d$. As the length of the system increases relative to the diffusion length the results more closely approximate the predicted relationship. With $L/L_d = 10$ this agreement becomes very close except for high values of p_w.

For any given value of L/L_d the same line in Fig. (6.9) is obtained by choosing any value of σ or ω and then varying the other scaled rate of state change in order to achieve the desired value of p_w via use of Equation (6.47) with λ set to zero. This assumes $p_w = n/N$, that is the proportion of time an individual spends in the drift is equivalent to the proportion of population found in the drift at any one time.

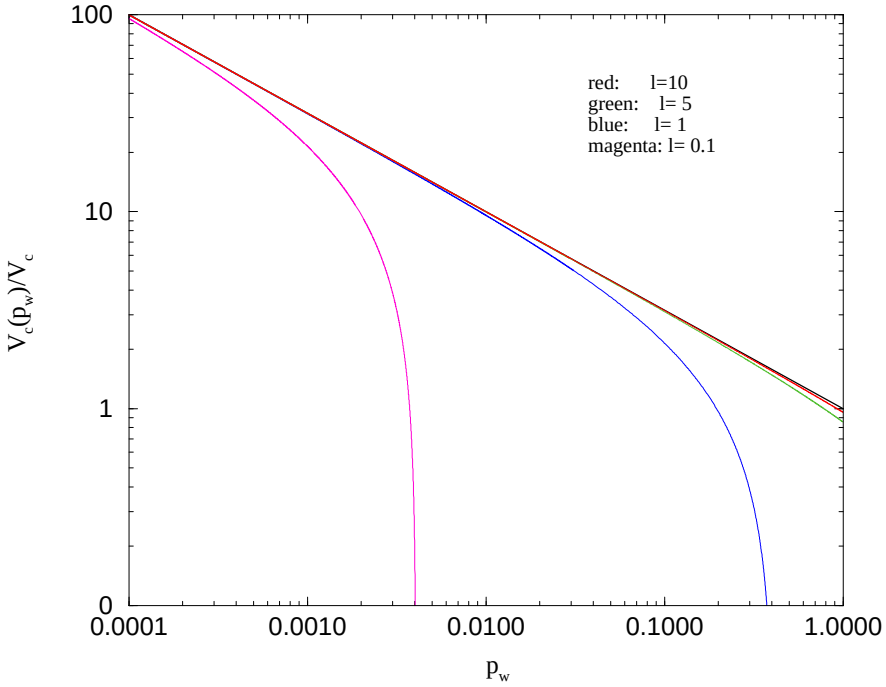

Figure 6.9: *Graph of the ratio of critical velocities (that for individuals spending time in the benthos against the maximum possible for passive particles found permanently in the drift), against the proportion of the long term population found in the drift. Black line is the relationship predicted by Equation (6.59). Coloured lines are results for systems with different values of* $l \equiv L/L_d$ *and* $V_c(p_w)$ *determined from Equations 6.47 and 6.40.*

The advantage in terms of persistence gained from time spent in the benthos is illustrated by the fact that even for a value of $L/L_d = 0.1$ non zero values of V_x are possible. By contrast Speirs and Gurney (2001) found that for passive particles permanently in the drift, it was not possible to achieve persistence for an L/L_d value less than $\pi/2$.

6.3.5 Appropriateness of exponential residence times

The above theory is based on exponential residence times for both the drift and benthic states of individuals. The literature is very unclear as to the timing and reasons for benthic animals to enter the water column. Exponential residence times in the water column, however, is supported by theory and observations.

With regard to benthic residence times, there has been considerable debate on

whether drift entry is passive, (as the result of hydrological displacement), or active, (Wilzbach 1990). Poff and Ward (1991) compared between day differences in drift density and drift rate of indigenous benthic insects for three riffles, (reference, experimentally increased flow, experimentally decreased flow), in the upper Colorado River. They found increased drift rates following flow reduction for several taxa including *Baetis* (mayflies), *Simuliidae*, (blackflies) and *Brachycentrus americanus*, (caddisfly). This was considered indication of active drift joining as reduction in flow rate and velocity would be enough to reduce the mean shear stress acting on the stream bed. For *Baetis spp.* several authors have reported active entry into the drift under conditions of low velocity, (Minshall and Winger 1968; Corkum, Pointing, and Ciborowski 1977; Corkum 1978; Ciborowski 1983; Allan and Feifarek 1989). Drift density and rate results for other species - the mayflies *Paraleptophlebia heteronea* and *Ephemerella infrequens* and the caddisfly *Lepidostoma ormea* - seemed to suggest passive recruitment to be at least a significant component to these species' rate of entry to the drift. Statzner, Gore, and Resh (1988) cite results of laboratory experiments, performed on various macro-invertebrates, to determine the maximum velocity that could be withstood before individuals were swept into the drift. For caddisflies, mayflies and stoneflies the velocities were well beyond what would normally be encountered in natural streams, lending support to active drift entry.

Such results do not provide the means to determine a rate of entry to the water column and the situation is complicated further by the fact that conflicting results, concerning benthic (and drift) activity, have been reported, even within species, (Wilzbach 1990). Statzner, Gore, and Resh (1988) conclude that most field experiments, and indeed many laboratory experiments, are un-repeatable and not comparable because too few hydraulic characteristics are measured. To fully characterise the hydraulic conditions acting on benthic invertebrates measurements are required of mean velocity, depth, substratum roughness and temperature, the last used to determine the kinematic viscosity of the water. Most field studies by contrast provide only mean velocity and/or mean discharge and

stream order. These last two measures are not so useful. Those hydraulic parameters that seem to most significantly correlate to benthic population distributions can vary considerably for the same discharge or stream order.

With regard to residence times in the water column, Smith (1982) considered particles/individuals of negative buoyancy introduced to a column of completely static quiescent water column of depth H. It is then assumed that the terminal sinking velocity V_s of each particle is achieved instantaneously and that particles will continue to sink at speed V_s until they hit the bottom. The settling time for a particle initially at the top of the water column, t', is therefore H/V_s.

If a large number of particles are spread homogeneously through the water column, at a concentration n_0, these particles will then settle in times in the range $0 - t'$. At any intermediate time t less than t' the proportion of the original suspension that has settled is given by $n_0 V_s t/H$, and the proportion left in the water column is therefore $n_0 - n_0 V_s t/H$.

It is now assumed that at time t the column is instantaneously and homogeneously mixed, such that particles still in suspension are evenly mixed throughout the water column. Particles already on the bottom are considered protected from mixing, a not unreasonable assumption given that turbulent flows have a laminar sub-layer. If the new concentration over the water column is labelled n_t then its value is given by

$$n_t = n_0(1 - V_s t/H) \tag{6.60}$$

If there are many instantaneous mixings – m say – in the time t' rather than one, the periods of quiescence become t'/m and the population remaining after the first and second mixings become

$$n_{t'/m} = n_0(1 - V_s t'/mH), \qquad n_{2t'/m} = n_0(1 - V_s t'/mH)(1 - V_s t'/mH) \tag{6.61}$$

The population density after the mth mixing (at time t') becomes

$$n_{t'} = n_0(1 - V_s t'/mH)^m \tag{6.62}$$

Since $t' = H/V_s$ Equation (6.62) simplifies to

$$n_{t'} = n_0(1 - 1/m)^m \tag{6.63}$$

As m becomes large, Equation (6.63) tends towards

$$n_{t'} = n_0(1/e) \tag{6.64}$$

where e is the natural logarithmic base.

The above theory then, suggests exponential residence times with β being given by $\beta = 1/t'$. In turn this gives β in terms of the sinking speed and overall depth as follows

$$\beta = \frac{V_s}{H} \tag{6.65}$$

This result does not need a large number of mixing events within the time t' to hold true, (Reynolds 1984), and fully developed turbulent flow in rivers can be considered to have a very large number of mixing events within the timeframe needed for planktonic settling. Even in flows where the water column might pass between periods of turbulent and laminar flow, such as in tidal bodies at periods of slack tidal flow, settling rates are likely to resemble the pattern for a turbulent water column rather than one which is quiescent. Experiments on three species of killed phytoplankton gave results that matched the time for 95% elimination from the water column predicted from Equation (6.64) to a good degree, (Reynolds 1984, page 76). Elimination time was however influenced by the 'form resistance'

of each species. Those with higher form resistance achieved longer times in the water column. Form resistance is a non-dimensional measure of the degree to which an organism's shape increases its drag. It is therefore also a measure of how readily an organism can be entrained by random water movements.

The theory of Smith was developed with a view to explaining phytoplankton concentrations. In the shallow and turbulent streams considered capable of being represented by the one dimensional modelling approach of this chapter benthic dwelling microphytes[2] do occur but phytoplankton are absent, (Horne and Goldman 1994). Of considerable interest in upland streams, however, are invertebrates. In drift samples of swift flowing temperate streams, the insect taxa *Ephemeroptera*, *Simuliidae*, *Plecoptera*, and *Trichoptera* are usually of most quantitative importance, (Brittain and Eikeland 1988). Applying the above theory to these larger and more dense organisms requires considerably more faith in the idea of instantaneous mixing. Perhaps remarkably then, most studies of invertebrate drifting times and distances have demonstrated fixed proportions of animals remaining in the water column settle to the bottom for each unit of time (or distance) that passes. Higher stream advections, as well as moving individuals further per unit time, increase drift distances by reducing the rate of settlement, but the general pattern remains the same, (Madsen 1968; McLay 1970; Elliott 1971a; Ciborowski and Corkum 1980; Lancaster, Hildrew, and Gjerlov 1996). Elliott (1971a) also observed that live animals were able to settle more quickly than dead individuals, and that there were differences in settling rates between live specimens from different species. This suggested behavioural differences as settling rates did not vary amongst dead animals. However, the exponential rate of return to the benthos over time still held true. It seems that for settling at least exponential residence time in the water column is not only convenient mathematically but also the truest representation of reality.

[2]Interestingly, one study at least has shown that benthic diatoms have selectively emigrated from experimentally darkened flumes by altering their buoyancy or form resistance to increase their likelihood of entrainment into the flow, (Bothwell, Suzuki, Bolin, and J. 1989).

Chapter 7

2D river systems

This chapter considers persistence in a model formulation that sets out to describe the circumstances in a deep river with modest flow rates. As shown in Appendix B, the horizontal velocity, V_r, in a uniform channel of depth H at a depth z below the surface is given by

$$V_r(z) = V_R\left(1 - \left[\frac{z}{D}\right]^2\right) = \frac{3}{2}\hat{V}_R\left(1 - \left[\frac{z}{D}\right]^2\right) \tag{7.1}$$

where V_R represents the velocity of the water at the free surface, ($z = 0$), and $\hat{V}_R$ the depth averaged or mean velocity. The horizontal advection of any organism at any depth, $V_x(z)$, can be considered a fraction, ε, of the water velocity at that depth. In a river system the long-term average water movement can be considered parallel to the bottom of the channel as can the advective dispersal of planktonic organisms. Diffusive dispersal on the other hand can act both in the horizontal and the vertical although rates of hydrodynamic mixing can be several orders of magnitude lower in the vertical than in the horizontal, (Reynolds 1994b).

7.1 Passive organisms permanently in the drift

To understand how the vertical gradient in advection and vertical diffusion influence the story of persistence, (as determined from the one dimensional analysis), Speirs and Gurney (2001) initially considered the limiting case when vertical diffusion is set to zero. Apart from enabling analysis this representation can be supported by the difference in mixing rates cited above and – leaving aside the premise of passive organisms for a moment – from the argument that any behaviour is likely to be more successful in decoupling vertical water movement from individual motion. The effect of the assumption is to dictate that any members of a population starting at a depth, z will live out their lives at the same depth, as will their descendants. The problem therefore becomes a set of uncoupled one dimensional systems as considered in the previous chapter. The advection velocity of the population in a layer is given by

$$V_x(z) = \varepsilon \frac{3}{2} \hat{V}_R \left(1 - \left[\frac{z}{D} \right]^2 \right) \tag{7.2}$$

From the one dimensional analysis inequality (6.7) implied that for a system of length L and a population with intrinsic growth rate r, washout will occur if

$$\frac{V_x}{Lr} > 0.434 \tag{7.3}$$

Back-substituting for V_x into Equation (7.2) gives a critical depth above which washout is assured, that is washout occurs if

$$z < z_c \equiv H \sqrt{1 - 0.289 \frac{Lr}{\varepsilon \hat{V}_R}} \tag{7.4}$$

Speirs and Gurney (2001) found that if the average value of V_x in the water column was set at the critical level specified by inequality (6.7), $z_c = 0.58H$ such that persistent population is restricted to the bottom 42% of the water column.

This is consistent with the vertically averaged value of the velocity profile residing $0.4H$ from the bottom, as discussed in section 4.4. The persistent zone diminishes rapidly as the average value of V_x, the effective discharge rate of the organisms, increases.

7.1.1 Critical vertical diffusion coefficient

Speirs and Gurney (2001) used populations with exponential growth rates to consider the effect of non-zero vertical mixing, the coefficient for vertical diffusion being represented by Φ_z. The effect of such mixing was different between systems allowing persistence at all depths when $\Phi_z = 0$ and systems where washout occurs nearer the free surface. If the rate of organismal advection at the surface still allows persistence, vertical mixing exports population from the faster growing (and more densely populated) lower layers to the upper layers where greater advection removes individuals more quickly and causes slower overall population growth. The average per-capita loss rate over the depth of the water column as a whole is increased and overall system population growth is reduced, but it is impossible for the system to obtain a negative long term growth rate.

In systems where the advection in upper layers is sufficient to cause washout in the absence of vertical diffusion, it was found sufficiently high values of Φ_z would cause the overall growth rate to become negative, leading to washout of the entire population. Thus, in such systems there exists a critical vertical diffusion coefficient Φ_{zc} that represents the limiting amount of diffusion for population to persist in the system as a whole.

To form an analytic estimate for this diffusion coefficient the deeper region of water allowing persistence in the absence of vertical diffusion was effectively treated like a one dimensional system as in the previous chapter, with the layer at the critical depth z_c acting as the absorbing boundary. The intrinsic growth rate was taken to be the per-capita growth rate over the whole of this deeper region. From the one dimensional analysis, it was found that when only diffusion is present,

the ratio of the system length (represented here by $H - z_c$) to the diffusion length must exceed $\pi/2$ for persistence, that is

$$\frac{H - z_c}{\sqrt{\Phi_z r^{-1}}} > \frac{\pi}{2} \tag{7.5}$$

Rearranging for Φ_z and back substituting for z_c from Equation (7.4) gives an upper bound for Φ_z

$$\Phi_z < \Phi_{zc} \equiv \frac{4rH^2}{\pi^2}\left(1 - \sqrt{1 - 0.289\frac{Lr}{\varepsilon \hat{V}_R}}\right)^2 \tag{7.6}$$

The length of a system that provides the threshold between population persistence and washout for a given value of diffusion or, in cases with advection present, a given combination of advection and diffusion values, can be called the critical system length, L_c. If investigating the critical value of diffusion coefficient for given values of system length and advection, the system length can still be thought of as the critical length for the point at which the diffusion equals its critical value.

7.2 Effect of sinking

Phytoplankton that have a density greater than water and no means of actively swimming will sink. This is true of a whole class of phytoplankton, the diatoms. This form of movement is not behaviour in itself although there is considerable evidence to indicate such non-buoyant algae use various means to control the rate of sinking, for example through alteration of their own density, (Reynolds 1984). The sinking velocity, V_s, is also known as the terminal velocity because if the algae were to fall through still water it would initially accelerate before reaching a steady (terminal) velocity at the point where the force causing the motion (the density difference between the algae and the surrounding water) is balanced by the drag force resisting motion. The drag force depends on a dimensionless quantity called the drag coefficient, C_D which in turn is dependent

on the particle Reynolds Number $R_{ep} \equiv V_s d/\nu$ where d represents the diameter of the particle and ν is kinematic viscosity. This Reynolds number is the ratio between the inertial forces being exerted on the fluid by the falling particle to the viscosity of the fluid. For $R_{ep} < 0.1$ the flow around the particle is entirely laminar and for $R_{ep} < 0.5$ it can be assumed laminar to an error within 10%, (Reynolds 1984). Most phytoplankton generate particle Reynolds numbers less than 0.1 and the laminar nature of the flow around them means their sinking velocity can be estimated using a modified version of the Stokes equation for the terminal velocity of a sphere, namely

$$V_s = \frac{1}{18} g d^2 (\rho_s - \rho) \frac{1}{\mu \phi} \tag{7.7}$$

where ρ_s is the density of the algae, ρ that of the surrounding fluid, g is acceleration due to gravity and μ the dynamic viscosity. The term ϕ is known as the coefficient of form resistance which takes account of the shape of the algae (for a sphere $\phi = 1$), which means the term d represents the diameter of a sphere having the same volume as the actual shape in question. Any adaptive mechanisms adopted by phytoplankton to alter their sinking speed compared to that of an inert particle of the same density and shape can be accounted for, if the magnitude of their effect is known, by adjusting the value of ϕ. Importantly the value V_s, in water bodies with homogeneous density, remains constant and is a relatively simple addition to the the previous theory while potentially having a significant effect on persistence.

7.2.1 Incorporating sinking into estimation of critical vertical diffusion coefficient

The estimation of critical vertical diffusion coefficient employed by Speirs and Gurney (2001) made use of the fact that in a one dimensional system in the absence of advection the ratio of the critical length of that system to the population

diffusion length will be $L_c/L_d = \pi/2$. Once a settling velocity is introduced this ratio is no longer known a-priori. From their work on the linear 1D problem with advection toward the absorbing boundary Speirs and Gurney (2001) derived an equation for determining this ratio, namely

$$\frac{L_c}{L_d} = \left[\sqrt{\frac{V_d^2}{V_d^2 - V_x^2}}\right] \arctan\left[-\sqrt{\frac{V_d^2 - V_x^2}{V_x^2}}\right] \tag{7.8}$$

When estimating critical vertical diffusion, the domain of interest is that found below the critical depth and the sinking velocity is a velocity *away* from the absorbing boundary. The effect of this on the results of the one dimensional analysis must be considered, especially as there is now the prospect that solutions for advection velocities sufficient to allow the general solution to the population equation to have real roots may be obtainable.

If the analysis of the one dimensional linear system is re-worked with Φ_z replacing Φ_x and V_z replacing V_x such that $V_z = -V_s$ then the working of Appendix A can effectively be left unchanged.

Case where $V_s^2 < 4\Phi r(1 - \Lambda/r) = 4\Phi(r - \Lambda)$

With $V_z = -V_s$ the equation to be satisfied for valid solutions of long term population growth rate is

$$\tan\left(\kappa\frac{L}{L_d}\right) = -\frac{V_d}{(-V_s)}\kappa \quad = \quad +\frac{V_d}{V_s}\kappa \tag{7.9}$$

with κ, L_d and V_d defined as before. As for the case with advection toward the absorbing boundary, with the parameters of the problem fixed, Equation (7.9) can be satisfied by an infinite series of values for κ, but the smallest non zero value provides the solution with the maximum long term growth rate. Potential solutions for $\kappa L/L_d$, however, now lie between 0 and $\pi/2$. Since $\tan\left(\kappa\frac{L}{L_d}\right) \to \infty$ as $\kappa \to \pi L_d/2L$ a solution to Equation (7.9) for $0 < \kappa < \pi L_d/2L$ is assured if

$$\left.\frac{d}{d\kappa}\left(\frac{V_d}{V_s}\kappa\right)\right|_{\kappa=0} > \left.\frac{d}{d\kappa}\left(\tan\left(\kappa\frac{L}{L_d}\right)\right)\right|_{\kappa=0} \tag{7.10}$$

Differentiating the left hand side gives

$$\left.\frac{d}{d\kappa}\left(\frac{V_d}{V_s}\kappa\right)\right|_{\kappa=0} = \frac{V_d}{V_s} \tag{7.11}$$

and the right hand side

$$\left.\frac{d}{d\kappa}\left(\tan\left(\kappa\frac{L}{L_d}\right)\right)\right|_{\kappa=0} = \frac{L}{L_d}\sec^2\left(\kappa\frac{L}{L_d}\right)\Big|_{\kappa=0} = \frac{L}{L_d} \tag{7.12}$$

therefore a solution is assured if

$$\frac{V_d}{V_s} > \frac{L}{L_d} \tag{7.13}$$

The equation for the critical length of the system, when $\Lambda = 0$, becomes

$$\frac{L_c}{L_d} = \left[\sqrt{\frac{V_d^2}{V_d^2 - V_s^2}}\right] \arctan\left[+\sqrt{\frac{V_d^2 - V_s^2}{V_s^2}}\right] \tag{7.14}$$

This equation is defined for $0 < |V_s| < V_d$ and as expected has a maximum value of $\pi/2$ when $V_s = 0$. As $|V_s| \to V_d$ then $L_c/L_d \to 1$. Therefore, with $|V_s| < 2\sqrt{\Phi r}$ critical system length values are such that

$$1 < L_c/L_d < \pi/2 \tag{7.15}$$

The inequality for persistence in the deeper region of the river, previously given by Equation (7.5) is now given by

$$\frac{H - z_c}{\sqrt{\Phi_z r^{-1}}} > \left[\sqrt{\frac{V_d^2}{V_d^2 - V_s^2}}\right] \arctan\left[+\sqrt{\frac{V_d^2 - V_s^2}{V_s^2}}\right]$$

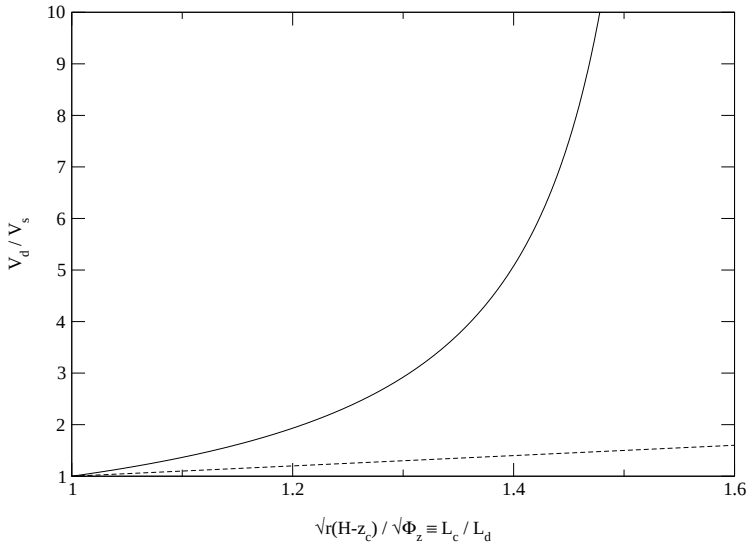

Figure 7.1: *Characteristic curve for V_d/V_s against $(H - z_c)/\sqrt{\Phi_z r^{-1}} \equiv L_c/L_d$. Dashed line shows line of equality between the two ratios.*

$$\frac{H - z_c}{\sqrt{\Phi_z r^{-1}}} \quad > \quad \left[\sqrt{\frac{1}{1 - \left(\frac{V_s}{V_d}\right)^2}}\right] \arctan \left[+\sqrt{\frac{1 - \left(\frac{V_s}{V_d}\right)^2}{\left(\frac{V_s}{V_d}\right)^2}}\right] \tag{7.16}$$

Values of the right hand side of inequality (7.16) are known for when $V_s = 0$ and $V_s = V_d$, but for intermediate values it is necessary to treat the inequality as an equation and solve numerically. Fig. 7.1 shows the characteristic curve for V_d/V_s against $H - z_c/\sqrt{\Phi_z r^{-1}} \equiv L/L_d$, with a dashed line showing the line of equality between the two ratios. As expected, it shows that solutions to Equation (7.9) are found when $V_d/V_s > L/L_d$.

Case where $V_s^2 > 4\Phi(r - \Lambda)$

The inequality $V_s^2 > 2\sqrt{\Phi r}(1 - \Lambda/r)$ defines when the general solution to the population balance equation has real roots. Appendix A gives the boundary conditions, written in terms of scaled variables, to be satisfied under these conditions, namely

$$-\frac{A}{B} = \frac{\nu - \psi}{\nu + \psi} \tag{7.17}$$

and

$$-\frac{A}{B} = \exp[2\psi l] \tag{7.18}$$

where ν here represents V_z/V_d, $l \equiv L/L_d$, $\psi \equiv \sqrt{\nu^2 - (1-\lambda)}$ and A and B are arbitrary constants. If the scaled velocity term ν_s is defined such that $\nu_s = V_s/V_d$, given the relationship between V_s and V_z then $\nu = -\nu_s$. Substituting for ν_s in Equation (7.17) gives

$$-\frac{A}{B} = \frac{(-\nu_s) - \psi}{(-\nu_s) + \psi} = \frac{\nu_s + \psi}{\nu_s - \psi} \tag{7.19}$$

With $\psi > 0$ Equation (7.19) requires $-A/B > 1$ as does Equation (7.18). With $\psi < 0$ Equations (7.19) and (7.18) are again consistent. Therefore, unlike in the case where advection is toward the absorbing boundary, there is no inconsistency between the boundary conditions at either end of the system.

Equating boundary conditions and substituting back in dimensional terms gives

$$\begin{aligned} \frac{\frac{V_s}{V_d} + \sqrt{\left(\frac{V_s}{V_d}\right)^2 + \frac{\Lambda}{r} - 1}}{\frac{V_s}{V_d} - \sqrt{\left(\frac{V_s}{V_d}\right)^2 + \frac{\Lambda}{r} - 1}} &= \exp\left[2\frac{L}{L_d}\sqrt{\left(\frac{V_s}{V_d}\right)^2 + \frac{\Lambda}{r} - 1}\right] \\ \frac{\frac{V_s}{V_d} + \Psi}{\frac{V_s}{V_d} - \Psi} &= \exp\left[\frac{L}{L_d}2\Psi\right] \end{aligned} \tag{7.20}$$

As $|V_s|$ is such that $V_s^2 > 2\sqrt{\Phi r}(1 - \Lambda/r)$ and $\Lambda \leq r$, Ψ is restricted to the range $0 < |\Psi| \leq V_s/V_d$. The left hand side of Equation (7.20) goes to infinity when $\Psi = +V_s/V_d$ and to zero when $\Psi = -V_s/V_d$, while the right hand side remains finite between these limits. Therefore, Equation (7.20) is always satisfied when $\Psi = 0$ but also both a positive and negative value of Ψ must satisfy Equation (7.20) if

$$\left.\frac{d}{d\Psi}\left(\frac{\frac{V_s}{V_d}+\Psi}{\frac{V_s}{V_d}-\Psi}\right)\right|_{\Psi=0} < \left.\frac{d}{d\Psi}\left(\exp\left[\frac{L}{L_d}2\Psi\right]\right)\right|_{\Psi=0} \tag{7.21}$$

.

When $\Psi = 0$ so too is ψ and the absorbing boundary condition dictates that $e^{\lambda T} f(l) = 0$ where $f(l) \equiv A\exp[(\nu-\psi)l + B\exp[(\nu+\psi)l]$. This implies that $A = -B$ and in turn that $f(X) = A\exp[\nu l] - A\exp[\nu l] = 0 \quad \forall X$, that is $\Psi = 0$ is a solution only possible for zero population in the system.

Differentiating the left hand side of inequality (7.21) and evaluating at $\Psi = 0$ gives

$$\left.\frac{2V_s}{V_d\left(\frac{V_s}{V_d}-\Psi\right)^2}\right|_{\Psi=0} = \frac{2V_s}{V_d\left(\frac{V_s}{V_d}\right)^2} = \frac{2V_d}{V_s} \tag{7.22}$$

and performing the same to the right hand side gives

$$\left.\frac{2L}{L_d}\exp\left[\frac{L}{L_d}2\Psi\right]\right|_{\Psi=0} = \frac{2L}{L_d} \tag{7.23}$$

Therefore solutions are assured if

$$\frac{V_d}{V_s} < \frac{L}{L_d} \tag{7.24}$$

which is the exact reverse of the condition for the low sinking velocity case. Looking at Equation (7.20) it can be seen that on setting Ψ to a negative value, the expressions on both sides are the reciprocal of when Ψ is positive and of equal magnitude. Thus, for a positive value of Ψ satisfying Equation (7.20), the negative value of equal absolute value will also satisfy the equation and both roots are given by the same value of long term growth rate.

An expression for the critical length can be obtained, as before, by setting $\Lambda = 0$ and rearranging Equation (7.20) as follows

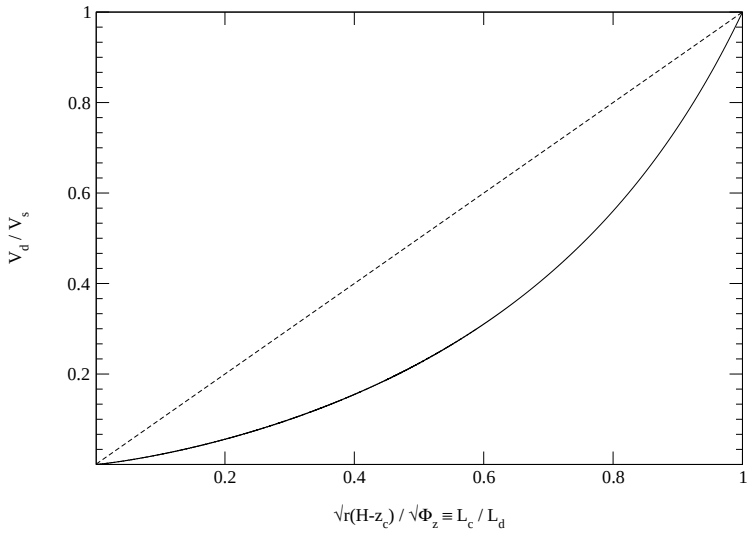

Figure 7.2: *Characteristic curve for* V_d/V_s *against* $(H - z_c)/\sqrt{\Phi_z r^{-1}} \equiv L_c/L_d$. *Dashed line shows line of equality between the two ratios.*

$$\frac{L_c}{L_d} = \frac{1}{2\sqrt{\left(\frac{V_s}{V_d}\right)^2 - 1}} \ln \left[\frac{\frac{V_s}{V_d} + \sqrt{\left(\frac{V_s}{V_d}\right)^2 - 1}}{\frac{V_s}{V_d} - \sqrt{\left(\frac{V_s}{V_d}\right)^2 - 1}} \right] \tag{7.25}$$

The new inequality for persistence in the weakly mixed river is given by requiring that the left hand side of Equation (7.25) exceed the right hand side and replacing L_c by $H - z_c$.

Characteristic curve for critical diffusion coefficient

As has already been seen, the term $H - z_c$, which is determined by the horizontal flow parameters of the river and intrinsic growth rate of the population under consideration, represents a boundary layer adjacent to the bed of the river within which persistence is possible in the absence of vertical diffusion. When investigating values of vertical diffusion coefficient that will remove sufficient individuals from this layer to make overall population persistence marginal, it is convenient for simplifying notation to regard $H - z_c \equiv L_c$, even though strictly $H - z_c$ is only a critical length once $\Phi_z = \Phi_{zc}$. For any given value of L_c and V_s it is possible to determine the critical value of the vertical diffusion constant, Φ_z, by first realising

that $V_s/V_d \propto 1/\sqrt{\Phi_z} \propto L_c/L_d$. Therefore, holding V_s and L_c fixed while varying Φ_z produces a straight line. If ς is the slope of the line its value is given by

$$\begin{aligned} \varsigma &= \frac{V_s}{2\sqrt{r}\sqrt{\Phi_{z2}}} - \frac{V_s}{2\sqrt{r}\sqrt{\Phi_{z1}}} \Big/ \frac{L_c}{\sqrt{r^{-1}}\sqrt{\Phi_{z2}}} - \frac{L_c}{\sqrt{r^{-1}}\sqrt{\Phi_{z1}}} \\ \varsigma &= \frac{V_s}{2rL_c} \end{aligned} \tag{7.26}$$

where Φ_{z1} and Φ_{z2} are two arbitrarily chosen values of Φ_z. The critical vertical diffusion coefficient, Φ_{zc}, is that value which causes Equation (7.14) or (7.25) to be satisfied for the given values of V_s and L_c. If the value of L_c/L_d at which this occurs is named $\Lambda_{\Phi z}$ then

$$\begin{aligned} \frac{V_s}{2\sqrt{\Phi_{zc}r}} &= \varsigma\Lambda_{\Phi z} = \frac{V_s}{2rL_c}\Lambda_{\Phi z} \\ \sqrt{\Phi_{zc}} &= \frac{2rL_c}{2\sqrt{r}\Lambda_{\Phi z}} \\ \Phi_{zc} &= \frac{rL_c^2}{\Lambda_{\Phi z}^2} \end{aligned} \tag{7.27}$$

The expression Φ_{zc}/rL_c^2 is a dimensionless expression involving Φ_{zc}. This expression equals $1/\Lambda_{\Phi z}^2$ which is itself a function of the dimensionless term ς. A characteristic curve for the system involving Φ_{zc} can therefore be obtained from plotting Φ_{zc}/rL_c^2 against $\varsigma \equiv V_s/2rL_c$.

Fig. 7.3 shows this characteristic curve. The region represented by V_s values giving critical diffusion values derived from Equation (7.14) is a very small fraction of the total curve. When $V_s/V_d \to 1$ so too does L_c/L_d which in turn means the slope variable ς also tends to one. The minimum value of Φ_{zc} is given when $V_s = 0$. It is known that when $V_s/V_d = 0$ then $L_c/L_d = L_c/L_d = \pi/2$ such that

$$\frac{L_c\sqrt{r}}{\sqrt{\Phi_{zc}}} = \frac{\pi}{2} \;\Rightarrow\; \Phi_{zc} = \frac{4rL_c^2}{\pi^2} \tag{7.28}$$

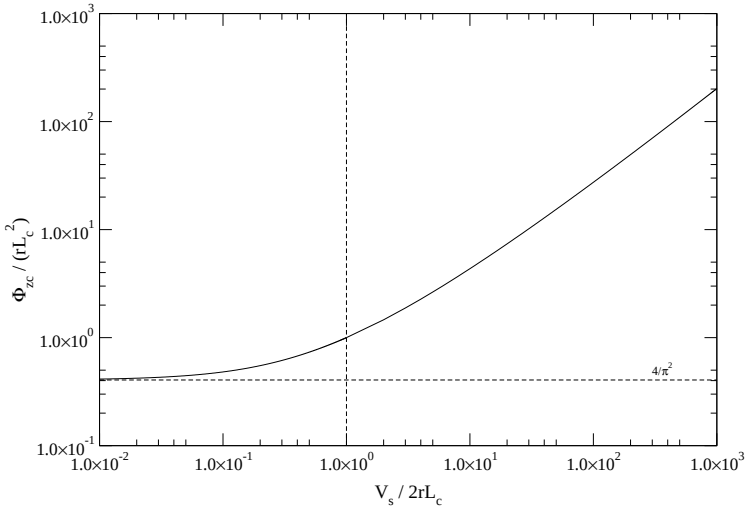

Figure 7.3: *Characteristic curve relating critical vertical diffusion coefficient to sinking velocity.*

Fig. 7.4 shows curves of long term growth rate against vertical diffusion coefficient for a population growing exponentially. Domain dimensions, advection rate and horizontal diffusion coefficient and population intrinsic growth rate were made the same as those used by Speirs and Gurney (2001) to test the estimate of critical vertical diffusion coefficient for neutrally buoyant particles. The comparison is not exactly the same as Speirs and Gurney (2001) used a logistic growth rate and compared equilibrium mean densities to Φ_z, but they found non-linear effects to be small. The figure shows the good prediction of Φ_{zc} when sinking speed is zero. The additional two curves correspond to values of the dimensionless variable $V_s/2rL_c$ of 1.0 and 10.0 for this system and it can be seen that as sinking speed increases the prediction of the critical vertical diffusion coefficient becomes less accurate. This is believed to be because the assumption made that the end of the vertical system represented by the critical depth is an absorbing boundary beyond which no population returns is progressively violated as sinking speed increases. An improved, but more complicated estimate of Φ_{zc} is presented below.

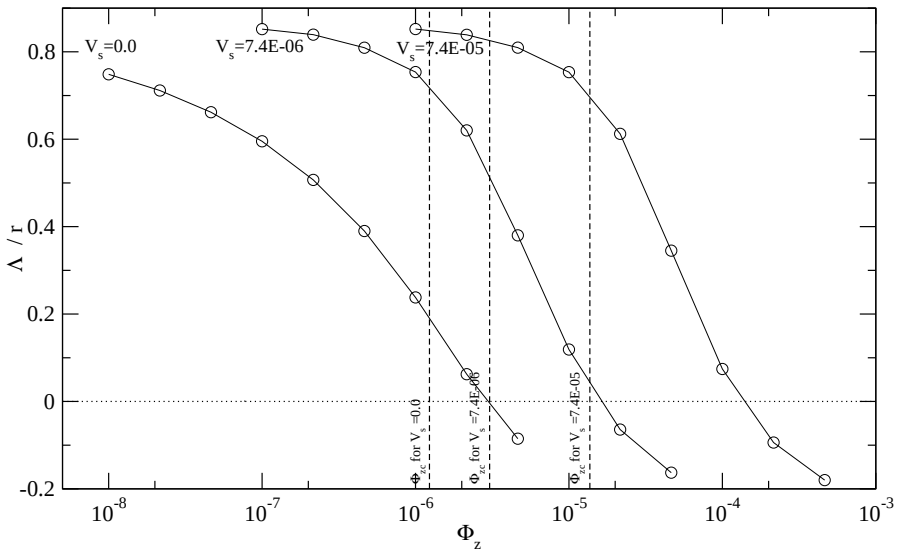

Figure 7.4: *Curves of long term growth rate against vertical diffusion coefficient for a population growing exponentially with* $r = 0.39day^{-1}$*, in a* $1km$ *long and* $2m$ *deep river with* $\hat{V}_R = 0.002ms^{-1}$*. Individuals are advected at the water velocity and diffuse horizontally with constant* $\Phi_x = 0.25m^2s^{-1}$*. Curves are for sinking speeds of* $V_s = 0ms^{-1}$ *(neutrally buoyant organisms),* $V_s = 7.4 \times 10^{-6}ms^{-1}$ *and* $V_s = 7.4 \times 10^{-5}ms^{-1}$*. Dashed lines indicate estimated values of critical vertical diffusion coefficient for these sinking speeds.*

7.2.2 Revised estimation of critical vertical diffusion coefficient

The preceding estimation of the critical vertical diffusion coefficient, by assuming an absorbing boundary at the critical depth, effectively assumed the long term growth rate, Λ, above the critical depth to equal $-\infty$. In reality, in the absence of vertical diffusion the long term growth rate will be a smooth function, reducing with increasing altitude to a negative but finite value at the water surface. Unfortunately, assuming Λ to be a linear function of depth, and applying the method of Appendix A, leads to an ordinary differential equation but with non-constant coefficients and the form of the solution could not be found. A less optimal but

more tractable approach was to consider the regions above and below the critical depth to each have a separate and constant value of per-capita growth rate.

The domain being considered now runs the length of the water column with a reflecting boundary at either end. It is still possible to have an overall growth rate of zero as the region above the critical depth receives a negative per-capita growth rate. If the long term growth rate in the boundary region between the bed and the critical depth is labelled Λ_{br}, and that in the surface region Λ_{sr}, then the problem becomes one of two advection-diffusion equations which are independent, except that they share a common boundary condition at $Z_+ = H - z_c$, where Z_+ is defined positive upwards from the bed and with origin at the bed. The two equations are given by

$$\frac{\partial n}{\partial T} = \Lambda_{br} n - V_z \frac{\partial n}{\partial Z_+} + \Phi_z \frac{\partial^2 n}{\partial Z_+^2} \tag{7.29}$$

and

$$\frac{\partial n}{\partial T} = \Lambda_{sr} n - V_z \frac{\partial n}{\partial Z_+} + \Phi_z \frac{\partial^2 n}{\partial Z_+^2} \tag{7.30}$$

As before scaling is used to help simplify the problem. In this instance it is as follows

$\mathbf{t} \equiv \mathbf{T}/\mathbf{t_0}$ where $t_0 = \Lambda_{br}^{-1}$.

$\mathbf{z_+} \equiv \mathbf{Z_+}/\mathbf{z_0}$ where $z_0 = L_{bd} = \sqrt{\Phi_z \Lambda_{br}^{-1}}$.

$\mathbf{v_z} \equiv \mathbf{V_z}/\mathbf{v_0}$ where $v_0 = V_{bd} = 2\sqrt{\Phi_z \Lambda_{br}}$.

This leads to the scaled equations

$$\frac{\partial n}{\partial t} = n - 2v_z \frac{\partial n}{\partial z_+} + \frac{\partial^2 n}{\partial z_+^2} \tag{7.31}$$

and

$$\frac{\partial n}{\partial t} = \frac{\Lambda_{sr}}{\Lambda_{br}} n - 2v_z \frac{\partial n}{\partial z_+} + \frac{\partial^2 n}{\partial z_+^2} \tag{7.32}$$

Trial solutions are assumed of the form

$$\begin{aligned} n &= e^{\lambda_z t} f(z_+) \quad \text{for } z_+ \text{ below the critical depth} \\ n &= e^{\lambda_z t} g(z_+) \quad \text{for } z_+ \text{ above the critical depth} \end{aligned} \tag{7.33}$$

where λ_z represents the scaled long term growth rate for this vertical problem. Back-substituting these trial solutions into Equations (7.31) and (7.32) leads to

$$0 = (1 - \lambda_z) f - 2v_z \frac{df}{dz_+} + \frac{d^2 f}{dz_+^2} \tag{7.34}$$

and

$$0 = (\frac{\Lambda_{sr}}{\Lambda_{br}} - \lambda_z) g - 2v_z \frac{dg}{dz_+} + \frac{d^2 g}{dz_+^2} \tag{7.35}$$

We now have two ordinary differential equations with constant coefficients. These O.D.E.s will have solutions of the form

$$\begin{aligned} f(z_+) &= A e^{\gamma_1 z_+} + B e^{\gamma_2 z_+} \\ g(z_+) &= C e^{\gamma_3 z_+} + E e^{\gamma_4 z_+} \end{aligned} \tag{7.36}$$

where A, B, C, D are arbitrary constants and the γs are given by the roots of the auxiliary equations

$$\gamma^2 - 2v_z \gamma + (1 - \lambda_z) = 0 \quad for \quad f(z_+)$$

$$\gamma^2 - 2v_z\gamma + (\frac{\Lambda_{sr}}{\Lambda_{br}} - \lambda_z) \;\; = \;\; 0 \;\; for \;\; g(z_+) \tag{7.37}$$

For $f(z_+)$, γ_1 and γ_2 are given by

$$\begin{aligned} \gamma_1 &= v_z - \psi \\ \gamma_2 &= v_z + \psi \end{aligned} \tag{7.38}$$

where $\psi \equiv \sqrt{v_z^2 + \lambda_z - 1}$. For $g(z_+)$, γ_3 and γ_4 are given by

$$\begin{aligned} \gamma_3 &= v_z - \psi_2 \\ \gamma_4 &= v_z + \psi_2 \end{aligned} \tag{7.39}$$

where $\psi_2 \equiv \sqrt{v_z^2 + \lambda_z - \frac{\Lambda_{sr}}{\Lambda_{br}}}$.

Boundary conditions

At the river bed, $(z_+ = 0)$, there is a reflecting boundary requiring no flux at the boundary. That is

$$2v_z f(0) - \left.\frac{df}{dz_+}\right|_{z_+=0} = 0 \tag{7.40}$$

At the top of the water column, $z_+ = h$ where $h \equiv H/\sqrt{\Phi_z \Lambda_{br}^{-1}}$, is another reflecting boundary requiring

$$2v_z g(h) - \left.\frac{dg}{dz_+}\right|_{z_+=h} = 0 \tag{7.41}$$

At the intersection of the split domain, $z_+ = l_c \equiv (H - z_c)/\sqrt{\Phi_z \Lambda_{br}^{-1}}$, the curve defining population density along the domain must be continuous. That is, we require a single value for the population density. This requires

$$\begin{aligned} e^{\lambda_z t} f(l_c) &= e^{\lambda_z t} g(l_c) \\ f(l_c) &= g(l_c) \end{aligned} \tag{7.42}$$

A continuous population flux is also required, implying

$$2v_z f(l_c) - \left.\frac{df}{dz_+}\right|_{z_+=l_c} = 2v_z g(l_c) - \left.\frac{dg}{dz_+}\right|_{z_+=l_c} \tag{7.43}$$

The term $2v_z$ is constant throughout the domain and given the requirement expressed in Equation (7.42) this implies $2v_z f(l_c) = 2v_z g(l_c)$. This in turn implies that

$$\left.\frac{df}{dz_+}\right|_{z_+=l_c} = \left.\frac{dg}{dz_+}\right|_{z_+=l_c} \tag{7.44}$$

Solutions satisfying the boundary conditions

Appendix E shows how, on substituting in the general form of the solutions to $f(z_+)$ and $g(z_+)$ into the boundary condition equations, it is possible to eliminate two of the arbitrary constants (A, B, C, D), using the fact that all boundary conditions must be satisfied simultaneously. It is then shown that a solution exists satisfying all boundary conditions if a value of λ_z can be found that satisfies one of the following two equations.

$$\begin{aligned} \frac{v_z - \psi}{v_z + \psi} &= e^{2\psi l_c} + \frac{1}{v_z + \psi} \times \\ &\quad \frac{\left[(v_z + \psi)^2 e^{2\psi l_c} - (v_z - \psi)^2\right]}{\left[(v_z + \psi_2)^2 - e^{2\psi_2(d-l_c)}(v_z - \psi_2)^2\right]} \times \left[e^{2\psi_2(d-l_c)}(v_z - \psi_2) - (v_z + \psi_2)\right] \end{aligned} \tag{7.45}$$

$$-\frac{k}{v_z} = \tan k l_c + \tag{7.46}$$

$$\frac{\left[2k + \frac{v_z^2 - k^2}{v_z} \tan kl_c\right]}{\left[(v_z + \psi_2)^2 - e^{2\psi_2(d-l_c)}(v_z - \psi_2)^2\right]} \left[(v_z - \psi_2)e^{2\psi_2(d-l_c)} - (v_z + \psi_2)\right]$$

where $k \equiv \sqrt{1 - \lambda_z - v_z^2}$.

Equation (7.45) is for sinking speeds that satisfy $V_s^2 > 4\Phi_z(\Lambda_{br} - \Lambda_z)$, while Equation (7.46) is that which needs to be satisfied when $V_s^2 < 4\Phi_z\Lambda_{br}(1 - \Lambda_z/\Lambda_{br}) = 4\Phi_z(\Lambda_{br} - \Lambda_z)$. The second equation comes about because for these lower sinking speeds the roots to the auxiliary equation are complex. The two regions of sinking speed value are equivalent to those for the case where the continuity equation was solved with one constant value of intrinsic growth rate, the value Λ_{br} simply replacing r in the inequalities. In each case the term on the left hand side of the equation and the first term on the right hand side form the equivalent to the equations to be satisfied for the single growth rate case.

The term λ_z is contained within the terms ψ and ψ_2. If the length and depth of the system are known, along with the horizontal advection and diffusion coefficient then it is possible to determine the critical depth. If the constant boundary region and surface region per-capita growth rates, Λ_{br} and Λ_{sr}, are also defined then on setting $\lambda_z = 0$ the only variable that can be used to satisfy either of the above equations is l_c which in turn provides an estimate for the critical diffusion coefficient through the relationship $l_c \equiv (H - z_c)/\sqrt{\Phi_z\Lambda_{br}^{-1}}$. Determination of Φ_{zc} values is performed via a NAG penalty function minimisation algorithm.

Values for Λ_{br} and Λ_{sr}

The values of the boundary region and surface region per-capita growth rates, Λ_{br} and Λ_{sr}, must be related to the values of long term growth rate at each vertical depth in the system assuming no vertical diffusion. The best relationship, however, was unclear. To consider this problem an algorithm was produced to determine the long term growth rates at finely spaced vertical intervals for any given combination of system length and depth, intrinsic growth rate, r and hor-

izontal diffusion coefficient Φ_x, using the value of horizontal advection derived from Equation (7.2), (with $\varepsilon = 1$), and the analytic result for the one dimensional advection-diffusion equation outlined in Appendix A. Three possibilities were considered

1. Making Λ_{br} and Λ_{sr} the means of the Λ values determined below and above the critical depth respectively.

2. Considering that the long term growth rate at the critical depth is zero, setting $\Lambda_{br} = \Lambda(Z_+ = 0)/2$ and $\Lambda_{sr} = \Lambda(Z_+ = H)/2$.

3. Setting Λ_{br} and Λ_{sr} equal to the Λ values at the bed and water surface respectively.

Fig. 7.5 shows the value of Φ_{zc} predicted using these three methods to provide values for the per-capita growth constants. The domain and horizontal diffusion coefficient are as used in the previous section, sinking speed is zero, and there are two flow regimes. The left hand panel has $\hat{V}_R = 0.002$ while the right shows results using double the mean flow speed. Predictions as given by Speirs and Gurney (2001) are also shown. The figure shows that using Λ values from the extreme ends of the water column gives the highest predicted critical vertical diffusion value. With other parameters held constant, as the horizontal advection is increased the negative long term growth rate at the water surface becomes a greater magnitude while the positive value at the bed is unaffected. Critical vertical diffusion coefficient predictions therefore become more pessimistic compared to results from numerical runs. Depending on flow conditions, predictions using either of the averaging approaches for the growth rate parameters can produce results more inaccurate than the prediction from the much simpler method of Speirs and Gurney (2001). Using Λ values from the extremes of the water column can cause an over-estimate in critical vertical diffusion coefficient. This is the situation for neutrally buoyant particles, however, and this method is only sought to improve predictions for non-zero sinking speeds, where (as shown below) there

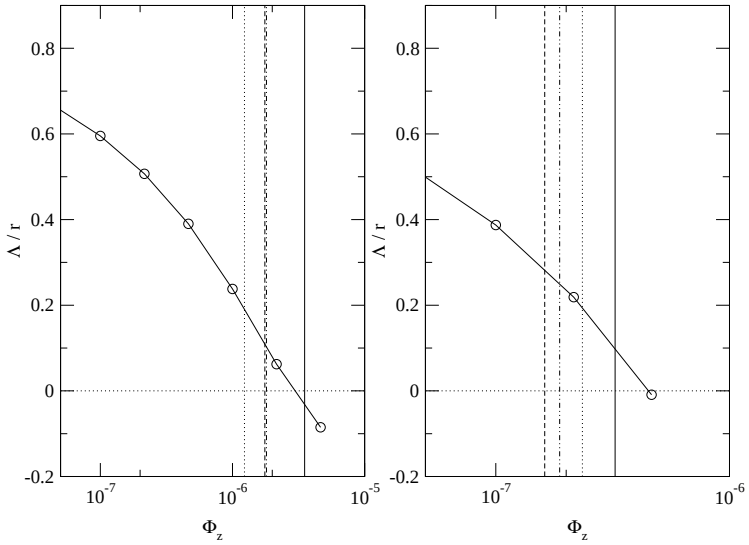

Figure 7.5: *Estimates of critical vertical diffusion coefficient, (vertical lines). In both frames* $L = 10km$, $H = 2m$ *and* $\Phi_x = 0.25$. *In the left hand frame* $\hat{V}_R = 0.002$ *and in the right hand frame* $\hat{V}_R = 0.004$. *Solid lines: estimates using* Λ *values at extreme ends of water column for* Λ_{br} *and* Λ_{sr}*; dashed lines: estimates using (endvalues)/2; dot-dashed lines: estimates using calculated means of* Λ *values below and above critical depth; dotted lines: estimates derived from formula of Speirs and Gurney (2001).*

is still a modest degree of more pessimistic prediction as sinking speed increases. Therefore, this option was the one chosen for subsequent investigations.

Critical depth revisited

The determination of the critical depth in the previous theory relied on turning inequality (7.3) into an equation and substituting for V_x. As demonstrated in Fig. 6.1 this value of V_x providing the critical depth is the absolute maximum value possible, derived when the relationship between system length, intrinsic growth rate and horizontal diffusion coefficient is at an optimum for persistence. If the relationship between these values departs from the optimum the value of V_x/Lr that gives the critical depth will reduce. This in turn requires the constant found in Equation (7.4), (0.289), to be reduced. If the constant is not altered then calculation of the critical depth can become impossible as the term inside the square root of Equation (7.4) becomes negative. It is not known how to adjust

the constant found in inequality (7.3) by analytic means. To investigate the issue of boundary region and surface region growth rates, (as described above), a simple numerical routine to determine long term growth rates at finely spaced heights up the water column was employed. This program has very low computational overhead and can be used to make an accurate determination of the true critical depth.

Old and new estimates of critical vertical diffusion coefficient

Fig. 7.6 shows the new predictions for critical diffusion coefficient compared to the estimates of the previous section. The numerical results are the same as those shown in fig. 7.4. It can be seen that the new estimates still become more pessimistic as sinking speeds increase but not to the same extent as the earlier estimates. Therefore, the advantage of employing the modified method increases as expected sinking speed increases. The values of sinking speed represented with Fig. 7.6 are well within the range expected for water living plankton. Reynolds (1984) states the sinking speed of *Stephanodiscus astraea*, a large freshwater diatom, to be approximately $2.5 \times 10^{-5} ms^{-1}$. Benthic living invertebrates can be expected to have greater sinking speeds.

7.2.3 Characteristic curves for critical diffusion coefficient

When the critical vertical diffusion coefficient was estimated by only considering the region of water column up to the critical depth, it was seen that the relationship between Φ_{zc} and the sinking velocity V_s could be described by a single characteristic curve. To make the diffusion and velocity terms non-dimensional required use of the intrinsic growth rate r and the length of the water column up to the critical depth, $L_c \equiv H - z_c$. The value of the critical depth, and therefore of L_c, was derived by using a fixed relationship between the intrinsic growth rate, horizontal advection and horizontal system length at which persistence becomes

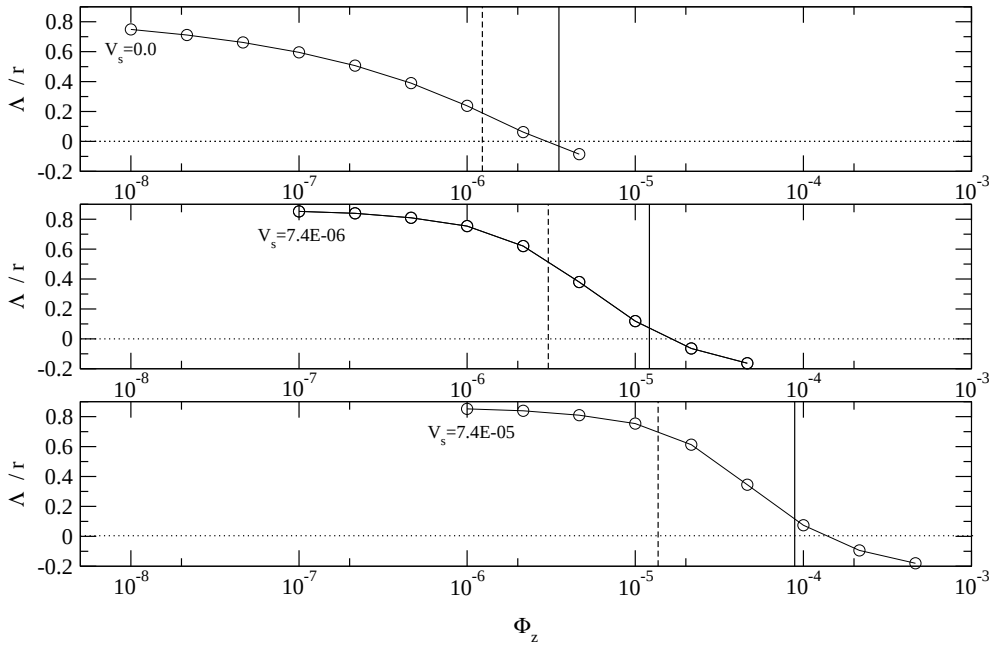

Figure 7.6: *Estimates of critical vertical diffusion coefficient for a system with* $L = 10km$, $H = 2m$, $\Phi_x = 0.25$ *and* $\hat{V}_R = 0.002$. *Sinking speed* $V_s = 0.0ms^{-1}$ *(top frame);* $V_s = 7.4 \times 10^{-6}ms^{-1}$ *(middle frame);* $V_s = 7.4 \times 10^{-5}ms^{-1}$ *(bottom frame). Solid vertical lines: estimates using two segment vertical 'domain' and* Λ *values at extreme ends of water column for* Λ_{br} *and* Λ_{sr}*; dashed vertical lines: estimates derived assuming single segment vertical domain up to critical depth, (as described in section 7.2.1).*

marginal. In other words, L_c is fixed by those parameters of the system that might need to be altered to match different horizontal flow characteristics and/or different domains. Altering these independent parameters alters the location along the characteristic curve for a given value of V_s.

Re-considering Equations (7.45) and (7.46) they are functions of

- $\psi \equiv \sqrt{v_s + \lambda_z - 1} = f(v_s)$ or $k \equiv \sqrt{1 - (v_s + \lambda_z)} = f(v_s)$ – given that determining Φ_{zc} requires $\lambda_z = 0$.
- $\psi_2 \equiv \sqrt{v_s + \lambda_z - \Lambda_{sr}/\Lambda_{br}} = f(v_s, \Lambda_{sr}/\Lambda_{br})$.
- $l_c \equiv (H - z_c)/\sqrt{\Phi_{zc}\Lambda_{br}^{-1}}$.
- $h - l_c \equiv H/\sqrt{\Phi_{zc}\Lambda_{br}^{-1}} - (H - z_c)/\sqrt{\Phi_{zc}\Lambda_{br}^{-1}} = z_c/\sqrt{\Phi_{zc}\Lambda_{br}^{-1}}$.

It is still true that $v_s \equiv V_s/V_d \propto 1/\sqrt{\Phi_z} \propto l_c \equiv L_c/L_d$, but the relationship between Φ_{zc} and V_s will now also depend upon the ratio between the per-capita growth rates chosen for the boundary region and surface region and, through the term $h - l_c$, the ratio of the distance up to the critical depth to the overall depth of the system. Fig 7.7 shows families of curves of $\Phi_{zc}/\Lambda_{br}L_c^2$ against $V_s/2\Lambda_{br}L_c$. These non-dimensional terms are the same as used in the previous characteristic curve except that Λ_{br} has replaced r. This is not a significant difference. It is the ratio of surface region to boundary region growth rate that determines the curve to be used rather than the actual value used to scale the diagnostic variables. The different frames show curves for different values of $|\Lambda_{sr}|/\Lambda_{br}$ while each curve of a given frame is that established on using a different ratio of $(H - L_c)/H \equiv z_c/H$. The use of $|\Lambda_{sr}|$ is simply to allow the ratio of growth rates to be expressed as a positive number, given that all systems of interest have a negative value of Λ_{sr}.

For a given ratio of $|\Lambda_{sr}|/\Lambda_{br}$ there exists a minimum ratio z_c/H beyond which solutions can not be found with $\Lambda_z = 0$, implying persistence is possible for any value of Φ_z at ratios smaller than this minimum. Above a certain value of z_c/H the curves become very close and the relationship between Φ_{zc} and V_s can effectively be considered as represented by a single curve. It can be seen, however, that the value of z_c/H at which this effect is seen to happen varies considerably as the value of $|\Lambda_{sr}|/\Lambda_{br}$ is altered.

One characteristic which does seem robust from inspection of Fig. 7.7 is the fact that the scaled critical diffusion value does not increase appreciably until the scaled sinking velocity reaches unity.

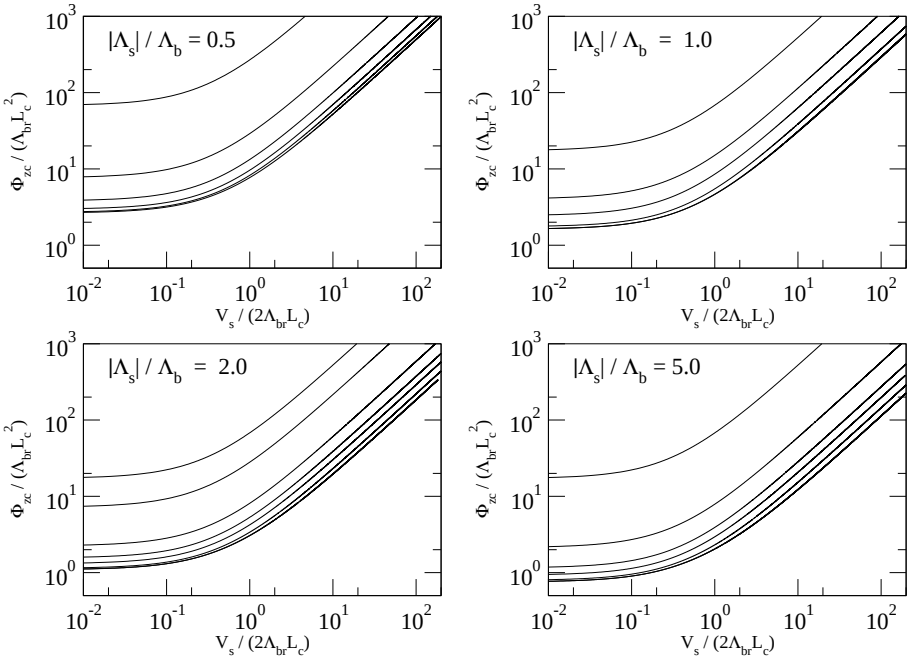

Figure 7.7: *Curves of* $\Phi_{zc}/\Lambda_{br}L_c^2$ *against* $V_s/2\Lambda_{br}L_c$ *for different ratios of* $|\Lambda_{sr}|/\Lambda_{br}$. *In each frame curves are for different values of* z_c/H. *Going from top to bottom* z_c/H *are: For* $|\Lambda_{sr}|/\Lambda_{br} = 0.5$*; 0.67,0.7,0.75,0.08,0.85,0.95 and above; for* $|\Lambda_{sr}|/\Lambda_{br} = 1.0$*; 0.51,0.55,0.6,0.7,0.85 and above; for* $|\Lambda_{sr}|/\Lambda_{br} = 2.0$*; 0.34,0.35,0.4,0.45,0.5,0.6,0.8 and above; for* $|\Lambda_{sr}|/\Lambda_{br} = 2.0$*; 0.17,0.2,0.25,0.3,0.4,0.7 and above. Top most curves in each frame are for the smallest ratio of* z_c/H *for which solutions could be obtained.*

7.2.4 Attempted application to real river system

Data on river phytoplankton, (potamoplankton) populations has been collected for a number of years for the river Meuse. This river has its source in France and then runs through Belgium and the Netherlands before entering the North Sea. The total length of the river is 885 km. Data on phytoplankton growth and biomass is mainly available at a distance 530 km from the source, with some other measurements between 480 km and 620 km, the Belgian sector of the river, (Everbecq, Gosselain, Viroux, and Descy 2001).

The one dimensional advection-diffusion equation assumes no recruitment of individuals at the upstream end of the system. Descy, Gosselain, and Evrard (1994) predict no significant phytoplankton biomass closer than 200 km to the source. The downstream absorbing boundary has been taken as the location 620 km from source as beyond this point no data is available. Although this choice of downstream boundary is somewhat arbitrary, the solution becomes increasingly insensitive to the length of the system as the ratio L/Φ_x increases. A system length of 420 km should make calculations very insensitive to changes in the system length value.

The discharge and morphology of the river Meuse changes in the 420 km stretch being considered. The river receives inflows from several significant tributaries. The analytic solutions, however, require uniform values of advection velocity and diffusion coefficient. Forcing a single value of discharge, depth, and therefore mean velocity, for the whole domain length is an obvious source of error. The method here, however, is only intended as a rough order of magnitude predictor, so the whole domain is assumed to have the discharge as measured 570 km from the source, as well as the river morphology at that location. It is true that along the Belgian section, the river is regulated for navigation. Also fortunate is the fact the tributaries to the river Meuse carry little or no phytoplankton, such that input of phytoplankton from the tributaries need not be considered, (Everbecq et al. 2001).

Descy, Servais, Smitz, Billen, and Everbecq (1987) calculated the growth rate of the phytoplankton community in the river and found it to peak a little above $0.7d^{-1}$. They concluded that growth in this eutrophicated river was never nutrient limited. The phytoplankton is dominated in the spring and early summer (before the impact of zooplankton grazing) by the diatom *Stephanodiscus hantzschii*. A study of growth rate in culture also found the intrinsic growth rate for *S. hantzschii* to be $r = 0.7d^{-1}$, (Swale 1963).

Estimation of Φ_x

No measured values for the longitudinal dispersion coefficient, Φ_x are available. Two formulas are available to estimate this value however. One is by Fischer[1], (Fischer, List, Koh, Imberger, and Brooks 1979)

$$\Phi_x = 0.011 \frac{\hat{V}_r^2 B^2}{H U_*} \tag{7.47}$$

where $\hat{V}_r$ is the mean river velocity, B is the width of the river at its surface, H is the mean depth and U_* is the friction velocity given by $U_* = \sqrt{gHS}$ where g is the acceleration due to gravity and S is the slope (gradient) of the water surface. This slope can normally be taken as equivalent to the gradient of the river bed.

The second is by McQuivey and Keefer (McQuivey and Keefer 1974)

$$\Phi_x = 0.05937 \frac{Q}{SB} \tag{7.48}$$

where Q is the discharge of the river. Both equations require the slope of the river to be provided. If a slope is not provided it can be calculated from the Manning equation (Chapra 1997)

[1]Equation (7.47) is a simplified version of Equation (2.12), using assumptions about the values of certain parameters from typical rivers.

$$\hat{V}_r = \frac{1}{n_{man}} R^{2/3} S_e^{1/2} \tag{7.49}$$

where R is the hydraulic radius of the river, given by A_c/P_w where A_c is the cross sectional area and P_w the wetted perimeter, S_e is the slope of the energy grade line[2] and n_{man} is the Manning roughness coefficient. Manning roughness coefficients have been determined experimentally for various open channel surfaces. For the river Meuse comparison the most appropriate values are those of 0.030 for clean and straight natural stream channels or 0.040 for clean but winding natural stream channels, (Chow 1959). The Manning formula can be substituted into the continuity equation and re-arranged to provide a relationship between river slope and discharge

$$S = \left[\frac{Q n_{man}}{A_c R^{2/3}} \right]^2 \tag{7.50}$$

Thus a reasonable relationship between discharge, width, depth and slope can be maintained even when slope is not given and only single, mean values of width and depth are provided.

The discharge of the river Meuse can be broadly split into a period of summer discharge, with values of $30 - 80 m^3 s^{-1}$ and winter values of $200 - 800 m^3 s^{-1}$. Significant phytoplankton counts only occur for the lower range of discharge. Table (7.1) shows values of river slope, and Φ_x provided by Equations (7.47) and (7.48) for values of discharge between 30 and 80 $m^3 s^{-1}$ and for width and depth values given at the recording site ($120m$ and $6m$ respectively). A Manning roughness coefficient of 0.030 was assumed due to the regulation of the river.

It can be seen that the estimates of Φ_x from Equations (7.47) and (7.48) differ by three orders of magnitude or more. Generally, each method is expected to predict recorded values to within a factor of five (Chapra 1997). The problem

[2]By assuming that the flow is steady and the cross section constant, the energy slope is made equal to the channel slope.

Table 7.1:

Q	$\hat{V}_R$	S	U_*	Φ_x Eqn (7.47)	Φ_x Eqn (7.48)
30.0	0.042	1.627×10^{-7}	3.09×10^{-3}	15.055	91226.2
40.0	0.056	2.893×10^{-7}	4.12×10^{-3}	20.095	68406.5
50.0	0.069	4.520×10^{-7}	5.16×10^{-3}	24.380	54724.7
60.0	0.083	6.509×10^{-7}	6.19×10^{-3}	29.397	45603.9
70.0	0.097	8.860×10^{-7}	7.22×10^{-3}	34.397	39088.6
80.0	0.111	1.157×10^{-6}	8.25×10^{-3}	39.433	34209.2

stems from the fact the estimation of McQuivey and Keefer is sensitive to the flow's Froude number, F_r, given by $\hat{V}_R/\sqrt{gH}$. A more general form of Equation (7.48) is

$$\Phi_x = 0.66 \frac{\hat{U}_{tt}^3}{\hat{C}^3} \frac{Q}{2SB} \tag{7.51}$$

where $\hat{U}_{tt}^3$ represents the mean travel time velocity of a tracer and $\hat{C}^3$ the advective velocity. Equation (7.48) assumes $\hat{C}/\hat{U}_{tt} = 1.79$ which is true for $F_r = 0.2$ and does not vary much for higher Froude numbers up to a limit of $F_r = 0.5$. For smaller Froude numbers, however, the ratio varies rapidly, greatly affecting the prediction of Φ_x. McQuivey and Keefer (1974) provide a curve for reading more accurate values of $\hat{C}/\hat{U}_{tt}$, down to a value of $F_r = 0.1$. For the discharges and channel dimensions used here, however, the Froude number varies from 0.0055 to 0.0145 and as such estimation of the correct ratio of $\hat{C}$ and $\hat{U}_{tt}$ is very uncertain. Equation (7.47) appears much less sensitive to changes in channel dimensions and river slope. Equation (7.47) was therefore considered the preferred method for obtaining Φ_x estimates.

Table 7.2 shows the results calculated using Φ_x estimates from this equation for $|\Lambda_s|/r$, z_c/H, the value of Φ_{zc} calculated when $V_s = 0$ and when $V_s = 2.5 \times 10^{-5} ms^{-1}$, the value obtained from use of Equation 7.6 and an estimate of the vertically averaged vertical diffusion coefficient that would be found in the river.

Table 7.2:

Q	Φ_x	$\lvert\Lambda_s\rvert/r$	z_c/H	Φ_{zc} $V_s = 0$	Φ_{zc} $V_s = 2.5 \times 10^{-5}$	Φ_{zc} Eqn 7.53	Φ_z $U_*H/15$
30.0	15.055	7.135	0.8058	7.49×10^{-6}	2.37×10^{-5}	4.46×10^{-6}	1.24×10^{-3}
40.0	20.095	9.835	0.8344	5.03×10^{-6}	1.73×10^{-5}	3.24×10^{-6}	1.65×10^{-3}
50.0	24.380	12.558	0.8534	3.74×10^{-6}	1.38×10^{-5}	2.54×10^{-6}	2.06×10^{-3}
60.0	29.397	15.270	0.8672	2.96×10^{-6}	1.16×10^{-5}	2.08×10^{-6}	2.48×10^{-3}
70.0	34.397	17.992	0.8778	2.43×10^{-6}	1.00×10^{-5}	1.77×10^{-6}	2.89×10^{-3}
80.0	39.433	20.694	0.8862	2.06×10^{-6}	8.85×10^{-6}	1.53×10^{-6}	3.30×10^{-3}

This last value is an approximation used by hydraulic engineers of

$$\Phi_z = \frac{U_* H}{15} \tag{7.52}$$

The term Λ_b/r was taken to equal one in all cases. Equation 7.6 was not used directly because of the difficulty highlighted in section 7.2.2. Instead the critical depth was determined from the numerical scheme used to calculate the value of Λ for many slices within a river and Equation 7.6 was substituted by the following

$$\Phi_{zc} = \frac{4r(H - z_c)^2}{\pi^2} \tag{7.53}$$

These results are shown in graphical form in Fig. 7.8

From Fig. 7.8 and table 7.2 it can be seen that none of the estimates of Φ_{zc} come close to matching or exceeding the estimate of the value to be found in the river given by Equation 7.52. Section 4.3 however described how measurements of vertical diffusion have shown its magnitude to be roughly parabolic such that the diffusion coefficient can be represented by the equation

$$\Phi_z = 0.4 U_* Z_+ \sqrt{1 - Z_+/H} \tag{7.54}$$

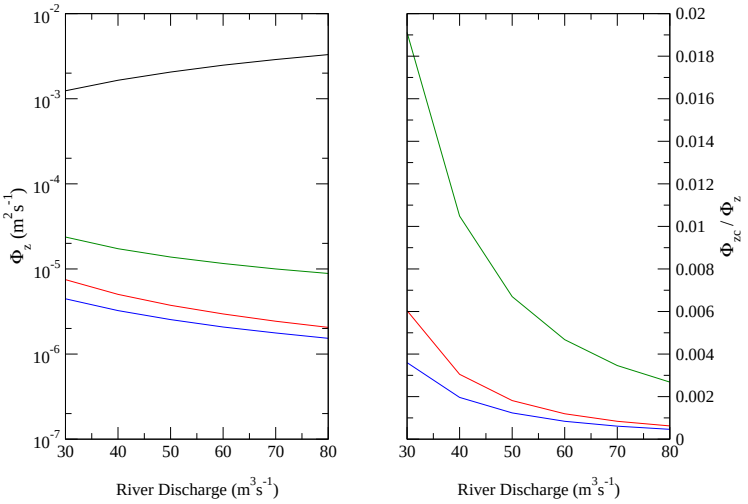

Figure 7.8: *Curves of Φ_{zc} against river discharge as estimated for the river Meuse, Belgium, compared to estimate of vertically averaged vertical diffusion coefficient. Left hand frame; estimates of Φ_{zc} when $V_s = 0$, (red line), $V_s = 2.5 \times 10^{-5} ms^{-1}$, (green line) and estimate from Equation 7.53, (blue line). Estimate of the vertically averaged vertical diffusion coefficients, (from Equation 7.52) given by the black line. Right hand frame; ratio of Φ_{zc} values to Φ_z value from Equation (7.52).*

This means the vertical diffusion in the river must be smaller than the estimates of Φ_{zc} for at least some distance from the river bed. Fig. 7.9 shows plots of depth for this new measure of flow refuge region, labelled L_*, against river discharge for the three estimations of Φ_{zc} performed. The left hand frame gives actual distances in metres while the right hand frame shows the ratio of L_* to the assumed overall depth of the river.

Fig. 7.9 gives a poor indication of potamoplankton persistence in the river Meuse. Even with a sinking speed likely to be slightly greater than that for the primary species being considered in this instance the right hand frame suggests that persistence is only guaranteed for organisms that spend their time in a region near the bottom that represents less than 0.5% of the overall water depth.

Fig. 7.10 shows how the two non-dimensional quantities, $(V_s/(2\Lambda_{br}L_c)$ and $\Phi_{zc}/(\Lambda_{br}L_c^2))$, used to form the graphs of Fig. 7.7 vary with river discharge. The conclusion from Fig. 7.7 was that sinking could start to have a significant effect on the critical vertical diffusion determined if its scaled value became greater than one.

The values shown in Fig. 7.10 are just beyond this level, and indeed figures 7.8 and 7.9 do indicate sinking has made some difference. Figures 7.8 and 7.9 also indicate the relative benefit of sinking to become less as river discharge increases whereas the scaled values for sinking speed and tolerable diffusion both increase with discharge in Fig. 7.10. This is because the greater discharges lead to smaller values of L_c, sufficiently so that Φ_{zc} values actually decrease as discharge increases. When comparing Φ_{zc} values to values of Φ_z from Equation (7.52) it must also be remembered that values of Φ_z increase with discharge.

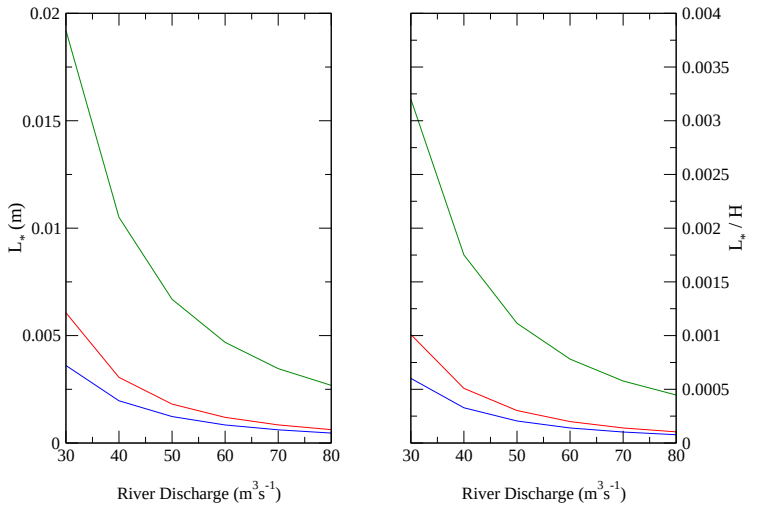

Figure 7.9: *Depth over which estimation of river vertical diffusion coefficient, from Equation (7.54), is smaller than estimation of Φ_{zc} for the river Meuse, Belgium. Estimate when $V_s = 0$, (red line); $V_s = 2.5 \times 10^{-5} ms^{-1}$ (green line); estimate from Equation 7.53, (blue line). Left hand frame shows actual distances, right hand frame these distances as a proportion of overall river depth.*

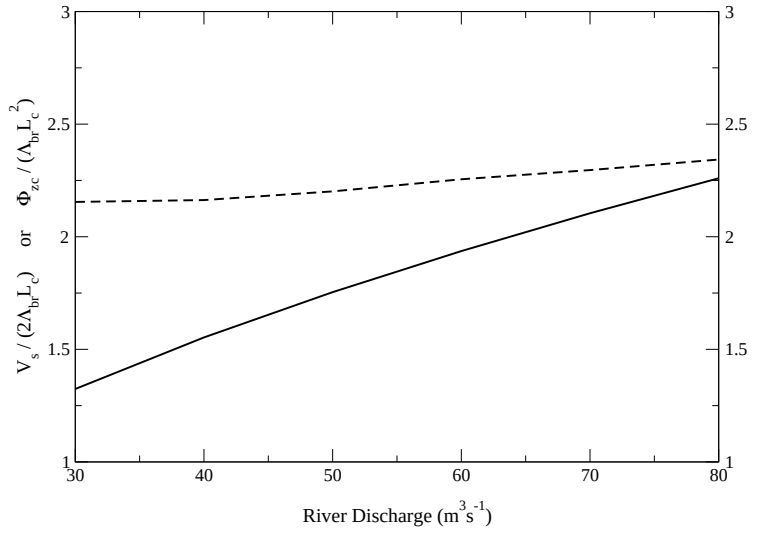

Figure 7.10: *Values of scaled sinking speed, $V_s/(2\Lambda_{br}L_c)$ (solid line) and scaled critical vertical diffusion coefficient, $\Phi_{zc}/(\Lambda_{br}L_c^2)$, (dashed line) against river discharge for the case when sinking speed is assumed to be $V_s = 2.5 \times 10^{-5} ms^{-1}$.*

Chapter 8

Tidal estuaries

8.1 Passive organisms permanently in the drift

8.1.1 Results using analytically derived flow fields

Speirs and Gurney (2001) investigated a population that grows logistically in the absence of advection and diffusion, using the two dimensional population model outlined in section 3.3.1 and flow fields provided by the adaptation to the analytic solution of Chen, Shaw, and Wolcott (1997) described in section 4.5 and appendix B. The domain had a constant depth below mean sea surface of $5m$. A typical example of the Lagrangian residual velocities for this system is as shown in Figs. 4.1 through 4.3 and is reproduced here in Fig. 8.1

Speirs and Gurney (2001) found that compared to a system with the same river flow and no tidal motion a small amount of tidal motion led to an increase in domain average population density. Contour plots of the steady state population distributions showed that landward residual flow, as seen in fig. 8.1 moved the centre of population landward in the deeper water of the domain.

It was found, however, that if tidal velocities were increased further average pop-

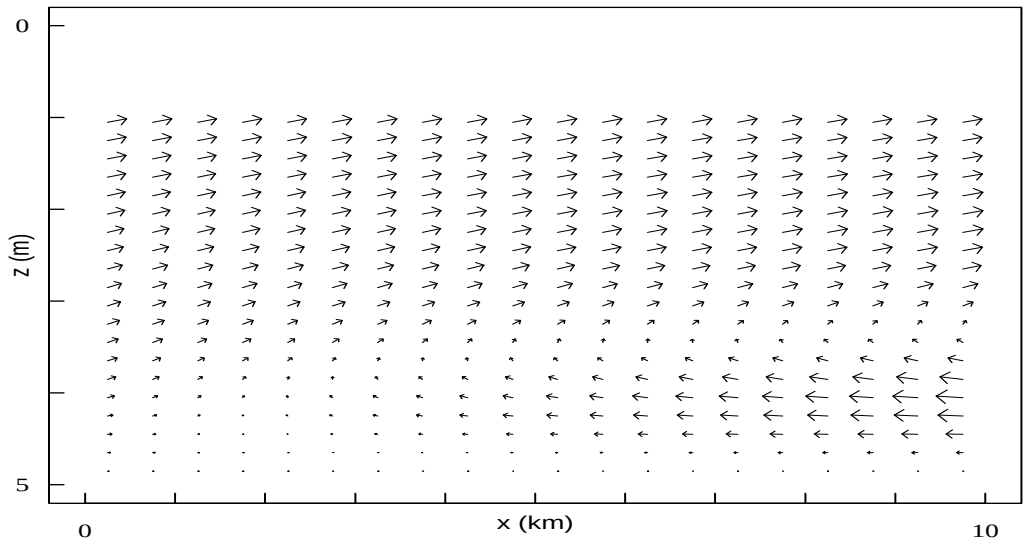

Figure 8.1: *Residual velocity plots derived using flow fields from solution after Chen, Shaw and Wolcott (1997), as modified by Speirs and Gurney (2001).*

ulation was reduced until it fell to well below the value obtained without tidal motion. Again, the reason could be found from investigation of the residual velocities. As can be seen from Fig. 8.1 there is is an upward component to the residual movement toward the landward end of the domain which takes population into the region of high seaward residual motion. As tidal velocity increases both this upward movement and the magnitude of the seaward 'flow' in the upper layers increases. Above a certain level of tidal motion, although the centre of deeper population is moved further landward, an increasing proportion is being advected into the surface layers and transported across the seaward boundary. At a tidal velocity representative of a real system, (the Ythan estuary in N.E. Scotland), this effect was enough to cause the population to wash out of the system.

Speirs and Gurney (2001) concluded that for tidal systems with constant density, near bottom residual flows had little effect on the break-point between persistence and washout for passive particles. As supporting evidence to this conclusion all parameters were fixed with the exception of the intrinsic growth rate, r. The critical growth rate at which the population is at the point of suffering washout

was determined and found to be very similar to the value estimated for a non-tidal system with the same river flow. Equation (7.6) was used to determine the value for the non-tidal system. As a further check the intrinsic growth rate was set at a fixed value, (sufficient for persistence at small organismal vertical dispersion) and the vertical diffusion value Φ_z altered until its critical value was established. Again Equation (7.6) was used to compare this value to that obtained in the non-tidal situation and again the values obtained were similar.

8.1.2 Effect of adopting CFD derived flow fields

Section 4.5.3 discussed concerns over the validity of the analytic flow results – at least in shallow systems – and therefore the Lagrangian residual movements generated by these solutions. Since the ability to generate these residual velocities using the Princeton Ocean Model, (POM), had been developed it was considered further investigations should be conducted using this technique. The conclusion from section 4.5.3 that in shallow systems with homogeneous density, Lagrangian residual landward flow is not generated led to concentration on systems with salinity differences. Finally, as use of a fluid dynamics package no longer restricts investigation to domains of constant depth, and as virtually all estuaries deepen as they approach the sea, a sloping bottom was included. To give a degree of continuity with the work using analytic flow fields the same length of domain was retained and the average depth over the length remains at $5m$.

Two flow regimes were considered. One can be regarded as having a net circulation typical of partially mixed estuaries. The second regime starts as partially mixed at the head of the domain but incorporation of more intense eddy diffusion leads to the system gaining the character of a well mixed estuary by the time it reaches the seaward boundary. Locations of different points along the domain on the Hansen and Rattray stratification-circulation diagram are shown in Fig. 8.2.

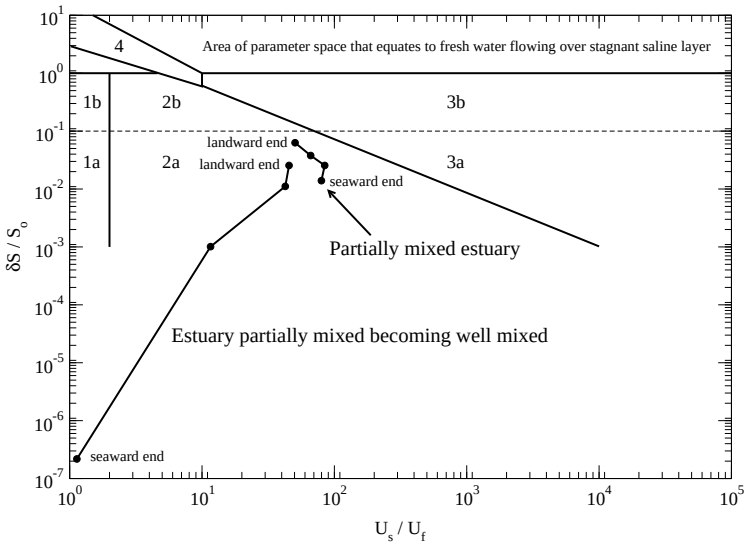

Figure 8.2: *Stratification-circulation diagram, after Hansen and Rattray (1966), with results marked for the two flow regimes used. Results were taken for four locations from the head of the domain to the seaward boundary as indicated.*

Problem of longitudinal dispersion in tidal estuaries

If the random movement of animals is to be represented as analogous to Fickian diffusion then random diffusion and multiple repetitions must be built into the particle tracking algorithm that creates the redistribution matrix, $R_{p',p}$, for the discrete time population model. The timesteps of the tracking model are much greater than the timescales of turbulent water movement, but much less than the final timestep of the population model of one tidal cycle (assumed to equal 12 hours in this work). In the horizontal this poses a problem because the longitudinal spread, (and landward movement), of a cohort of individuals can depend much more on diffusion carrying different individuals onto divergent advective paths than on the distance of diffusive travel itself. As discussed in the introduction, this requires a coefficient of dispersion different to, and usually much larger than, the coefficient representing turbulent diffusion.

Previously, one-dimensional longitudinal dispersion coefficients have been obtained by trial and error adjustment when fitting a model to a set of field data, (West and Mangat 1986). Obviously, this is not possible using strategic models and section 2.1.5 outlined the uncertainty in determining longitudinal dispersion

coefficients from anything other than field measurements. When considering two dimensional vertical slices along a domain, longitudinal dispersion is chiefly the result of interaction between the advective flow field and vertical diffusion. Section 4.3 discussed how for estuaries, and especially for stratified estuaries, the estimation of the coefficient of vertical diffusivity, K_z can also be uncertain. This is partly because the value of K_z is expected to vary throughout the tidal cycle as the dominant form of advection, (the tidal flow) varies from maximum flood and ebb values to nothing at slack water. The particle tracking code was constructed in such a way that it is possible to adopt the values determined for the coefficient of vertical diffusivity from POM, (K_H), for the same times and locations as the velocity data, as the value required for the particle tracking vertical diffusivity, Φ_z. It was felt that for computational speed, and conceptual simplicity, adoption of a single, constant value of Φ_z was preferable. It is not clear however, what value Φ_z should take.

To explore these ideas, the POM velocity data to be used for population runs was used to track large ensembles of particles from selected start locations using a wide spread of values of Φ_z. The range of values for vertical diffusivity of a tracer, K_z is considered to be in the range $0.0001 - 0.01 m^2 s^{-1}$ for a stratified estuary, with the value in a neutrally buoyant estuary capable of reaching $0.1 m^2 s^{-1}$, (see section 4.3). The upper limits of these ranges were used as the upper limits of investigation for Φ_z for homogeneous and stratified estuary flow. Lower values were also investigated in consideration of the fact that even small phytoplankton have a size, and inertia, much greater than a true tracer. If their random movement is passive, it is likely to be that much less than that for a true tracer. Initially the value of the tracking program horizontal diffusion coefficient, Φ_x was kept at zero.

Fig. 8.3 shows the results from four locations selected from the run demonstrating a front in the Lagrangian residual movement. These start positions are shown in Fig. 8.4, the letters corresponding to those above the frames in Figs.8.3, 8.5 and 8.6. It can be seen from Fig. 8.3 that use of only a vertical diffusion coef-

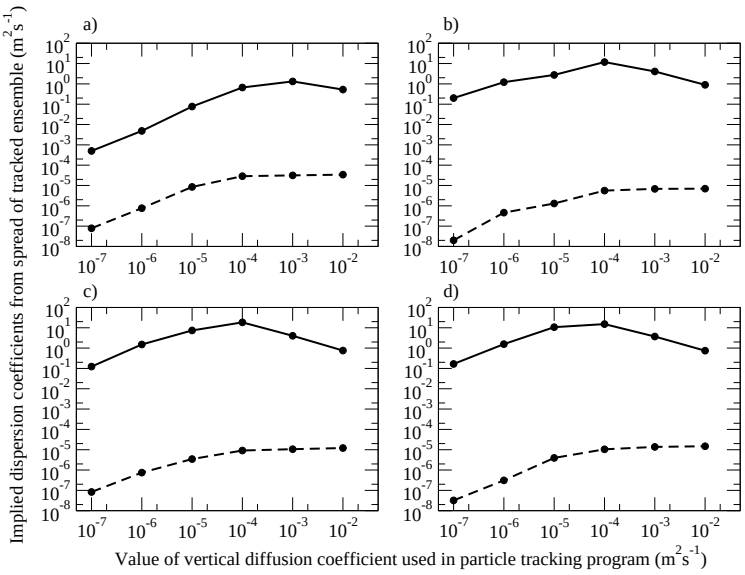

Figure 8.3: *Dispersion coefficients implied from the spread of an ensemble of particles tracked using POM generated flow field against vertical diffusion coefficient imposed in the tracking algorithm. Solid curve represents horizontal dispersion coefficient; dashed curve represents vertical dispersion coefficient.*

ficient produces spread of the ensemble in the horizontal, implying a dispersion coefficient, (as would be used in a one dimensional advection diffusion equation), orders of magnitude greater than the vertical diffusion coefficient used. This demonstrates the presence of dispersive mechanisms within the flow. The values of implied dispersion coefficient increase in line with the increase in Φ_z value used until the latter becomes sufficient for the ensemble to become well mixed over the depth of the system over the period of a tidal cycle. The consequences resulting from rapid diffusion over the depth of the water column at high values of vertical diffusion coefficient can be seen in section 8.1.3.

For a system varying in depth from 7 to 3 metres, as in Fig. 8.4, the longitudinal dispersion peaks for an imposed vertical diffusion in the range 1×10^{-4} to $1 \times 10^{-3} m^2 s^{-1}$. The lower value in this range corresponds to the lower value quoted for vertical turbulent diffusion coefficients in stratified estuaries. Taking this value as a fixed value for the vertical diffusion coefficient in the tracking program an investigation was then made of the effect of using different values of horizontal

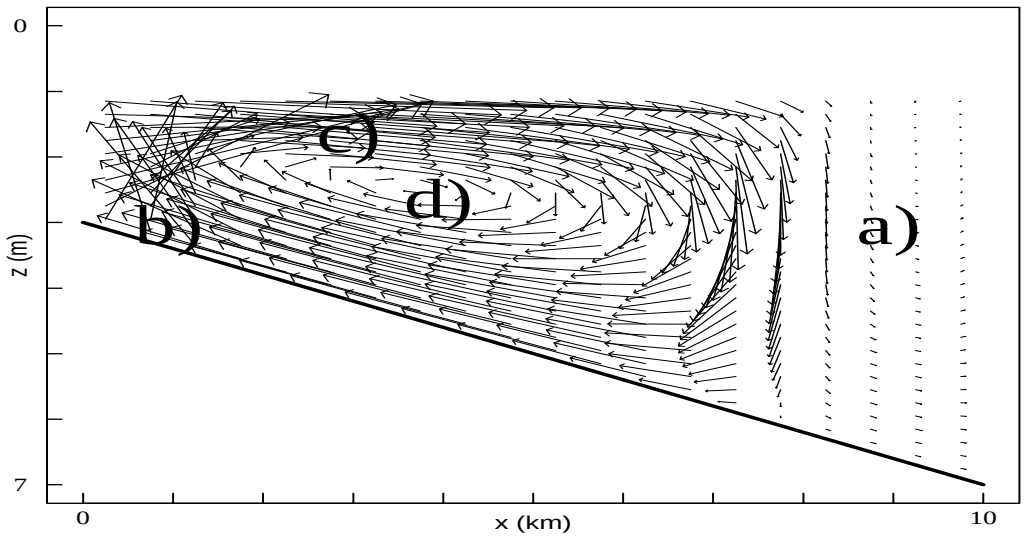

Figure 8.4: *Lagrangian residual movements over a tidal cycle calculated from POM derived flow. Tidal range* $\pm 1m$*;* $V_R = 0.003125ms^{-1}$*,* $(Q_f = 4.167 \times 10^{-3}m^2s^{-1})$*;* $UMOL = 2.0 \times 10^{-4}m^2s^{-1}$*. Letters indicate starting positions for ensemble tracking experiments.*

dispersion coefficient, Φ_x. The results are presented in Fig. 8.5, using the same selection of starting positions as before. The dotted horizontal line in each frame represents the value of longitudinal dispersion coefficient implied from the run using the same value of vertical diffusion coefficient and zero horizontal coefficient. If the horizontal coefficient value for the particle tracking program is set to less than the value implied by the dispersive mechanisms of the advective flow the final implied value remains much the same. As Φ_x is made larger than the implied value obtained from dispersive mechanisms the coefficient implied by the final spread of the ensemble rises to match Φ_x. It is now the case that the coefficient imposed on the tracking program has caused diffusion to dominate dispersion in terms of the final spread of particles. If a smaller value of vertical diffusion coefficient is used, sufficiently small to cause smaller horizontal spreading from dispersion, then the point at which imposed diffusion takes over from dispersion as the main spreading mechanism in the horizontal also reduces. The vertical dispersion coefficient implied by the final spread of particles is essentially unaffected by any variation

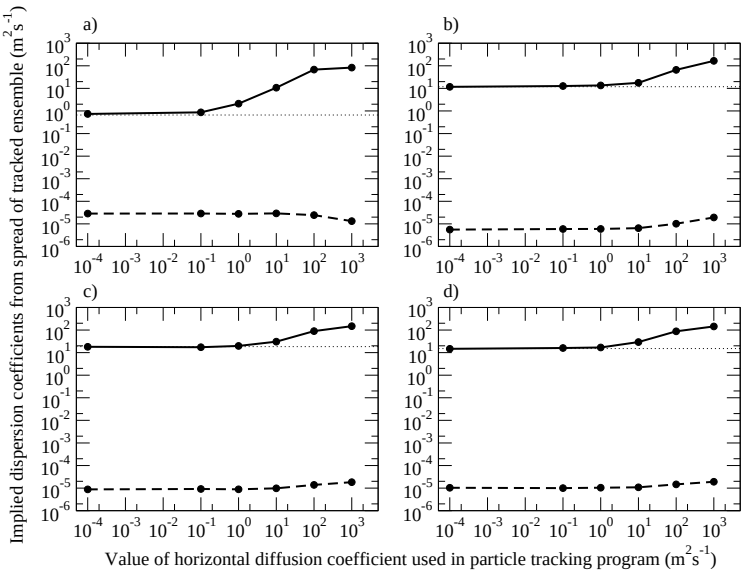

Figure 8.5: *Dispersion coefficients implied from the spread of an ensemble of particles tracked using POM generated flow field and a tracking algorithm vertical diffusion coefficient of* 1.0×10^{-4}*, against horizontal diffusion coefficient imposed in the tracking algorithm. Solid curve represents horizontal dispersion coefficient; dashed curve represents vertical dispersion coefficient.*

in imposed horizontal diffusion.

In light of the relationship between vertical diffusion rate and horizontal dispersion rate in stratified tidal bodies the persistence of organisms was investigated over a range of values for the population model vertical coefficient Φ_z, leaving the horizontal coefficient Φ_x set at zero. Although these investigations are non-organism specific it was hard to imagine a planktonic organism that could create horizontal random movements with a diffusion coefficient greater than the dispersion coefficients indicated by Fig. 8.3. The implied horizontal diffusion is also beyond expected horizontal turbulent diffusion values, (McDowell and O'Connor 1977, page 65), especially during periods of slower tidal flow. This approach conveys the advantage of reducing the number of independent variables by one. Further, vertical diffusion and dispersion in estuaries are considered virtually equivalent such that Φ_z can be regarded as the result of short duration, random movements alone.

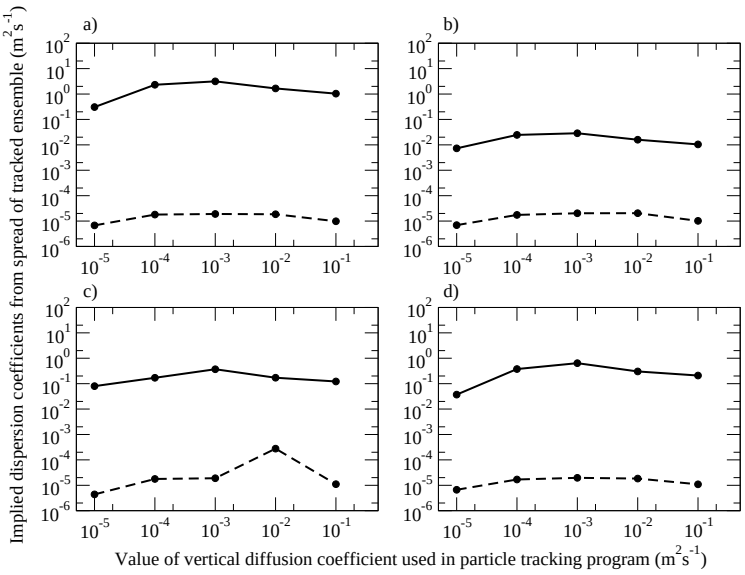

Figure 8.6: *Dispersion coefficients implied from the spread of an ensemble of particles tracked using POM generated flow field against vertical diffusion coefficient imposed in the tracking algorithm. Solid curve represents horizontal dispersion coefficient; dashed curve represents vertical dispersion coefficient. Case of tidal flow in neutrally buoyant system.*

To show that the stratified system being used for Figs. 8.3 and 8.5 produces greater dispersion than a system without salinity, (or temperature), variation – a homogeneous or neutrally buoyant system – the same experiment using only a vertical diffusion coefficient in the tracking program was applied to flow fields taken from a system with uniform temperature and salinity. The results are shown in Fig. 8.6. It can be seen that the implied horizontal dispersion coefficients are an order of magnitude or more less than those obtained with the stratified system. The flow field for Fig. 8.6 is the same as that which provided the residual velocity plot of Fig. 5.5. Starting positions were at the same depths and longitudinal locations as in the stratified system.

Diffusion coefficient correction

The correction factor for the diffusion coefficient used in a particle tracking program given by Equation (3.23) was not used. The ratio of cell width in the

vertical to vertical diffusion length, $\Delta z/\sqrt{2\Phi_z \Delta t}$, where Δt is the timestep of the population model, (12 hrs), remains less than 0.1 down to values of Φ_z of approximately $1 \times 10^{-5} m^2 s^{-1}$. At the minimum value used for full population runs, $(1 \times 10^{-6} m^2 s^{-1})$, the ratio is approximately 0.3. At this ratio the difference in resultant diffusion between corrected and uncorrected tracking is moderate. The effect of use of Equation (3.23) in a two dimensional flow field with time varying advection is uncertain while use of uncorrected coefficients is considered not to have made a significant difference to the results presented in the next sections.

8.1.3 Estuary with sloping bathymetry and salinity gradients

Taking the system with residual flows as represented by Fig. 8.4 it might be expected that persistence is possible regardless of vertical diffusion/dispersion due to the circular pattern of the residual flows behind the front. This expectation was tested for two intrinsic growth rates. The first $r = 0.39 day^{-1} \equiv 4.5 \times 10^{-6} s^{-1}$ is the same growth rate used in chapters 6 and 7 and is representative of phytoplankton. The second, $r = 0.026 day^{-1} \equiv 3.0 \times 10^{-7} s^{-1}$ is the same growth rate as that used by Speirs and Gurney (2001) in their work on a tidal estuary and is loosely based on the growth rates for a mysid shrimp. The results are shown in Fig. 8.7 which displays normalised domain mean density as a function of Φ_z.

For smaller values of vertical dispersion coefficient results are as anticipated. Increases in Φ_z cause little difference to the overall long term population density achieved. However, as vertical mixing increases further, population mean density decreases rapidly and eventually conditions of washout occur.

The explanation for this surprising result requires re-consideration of the theory of shear dispersion introduced in section 2.1.5. Taylor's theory of shear flow dispersion is only applicable if the flow regime remains constant for a time 'much longer'

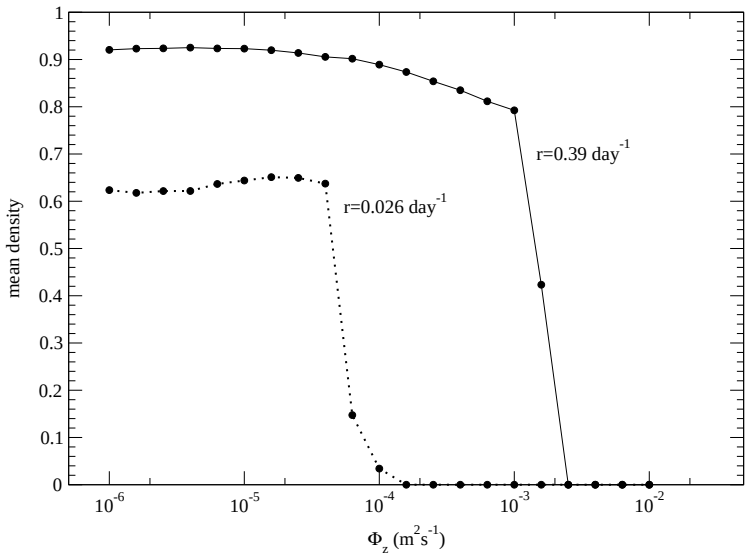

Figure 8.7: *Mean population density in a tidal estuary, (with residual velocities as shown in Fig. 8.3), as a function of the population vertical mixing rate* Φ_z. *Curves are for population intrinsic growth rates of* $0.39day^{-1}$ $(4.5 \times 10^{-6}s^{-1})$ *and* $0.026day^{-1}$ $(3.0 \times 10^{-7}s^{-1})$ *as indicated.*

than the 'forgetting time'. This forgetting time is the time required for random motions to have enabled a particle to sample all locations in a cross section sufficiently for its location to have become independent of its initial location, and its mean velocity to have become independent of its initial velocity. The horizontal dispersions experienced by particles in the stratified tidal regimes of this chapter are not caused solely by shear dispersion for values of Φ_z that allow persistence. Instead, particles experience both the upper net seaward and compensating net landward flows for extended periods through each flood and ebb half tidal cycle. If Φ_z becomes sufficiently large, however, particles can experience flow at all depths sufficiently quickly in contrast to the temporal change in flow regime that an approximation to shear flow dispersion results. When this occurs the mean movement of particles becomes equal to the depth averaged advection of the flow over the flood and again over the ebb. This mean movement over a tidal cycle becomes the depth averaged river flow. Fig. 8.8 shows this effect taking place. The three frames display contour plots of the long term population within the domain. With very low vertical mixing, frame a), population density is high everywhere[1].

[1]Interestingly, the front in the residual flow is reflected by a slight decrease in population

At a value of Φ_z where domain averaged density starts to decline, frame b), population density starts to reduce toward the landward (and more shallow) end of the domain. This is expected to be due to the shallower depths allowing complete sampling of all depths for smaller vertical mixing. With a further slight increase in vertical diffusion coefficient, frame c), population mean density falls sharply. The reduction in population density has progressed to greater depths and regions near the landward boundary now contain no population at all.

density.

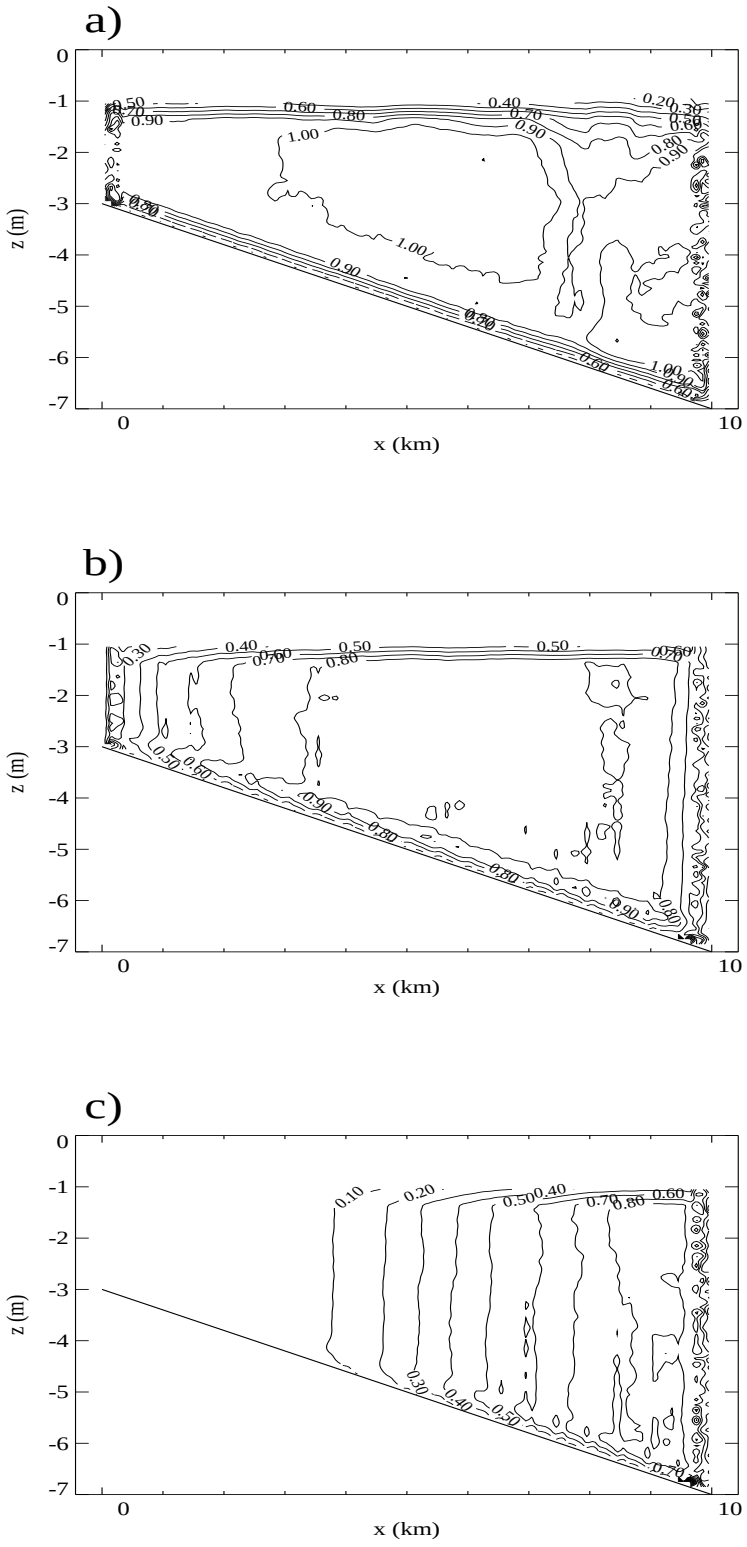

Figure 8.8: *Contours of population density in a tidal estuary, with residual velocities as shown in Fig. 8.3) and population intrinsic growth rate of* $0.39day^{-1}$ *(*$4.5 \times 10^{-6}s^{-1}$*). Frame a), vertical mixing rate* $\Phi_z = 1.0 \times 10^{-6}m^2s^{-1}$*; Frame b), vertical mixing rate* $\Phi_z = 1.0 \times 10^{-3}m^2s^{-1}$*; Frame c), vertical mixing rate* $\Phi_z = 1.0 \times 10^{-2.8}m^2s^{-1}$.

To investigate a system where the residual movements over a tidal cycle do not seem to represent such a closed system, the persistence of populations subject to the residual flows represented by Fig. 8.9 was investigated. These Lagrangian movements were obtained with the same tidal elevation and river flow parameters, but with a smaller degree of background vertical eddy viscosity. The resultant flows can be considered a classic example of those from a partially mixed estuary, with residual movements much greater than the actual flow of the river water.

Again, mean long term population density was considered for a range of vertical diffusion coefficient values while the horizontal dispersion coefficient was retained at zero. The results are shown in Fig. 8.10. As might be expected in this flow regime, very small values of vertical diffusion coefficient lead to population washout. Over successive tidal cycles, individuals starting in the lower water regions are carried toward the landward boundary and then out through the seaward boundary, while washout for individuals starting higher up the water column occurs sooner. Greater values of Φ_z allow particles resident in the upper layers (experiencing net seaward movement) to be diffused to lower regions experiencing net landward movement. This overall delay in net seaward movement is only sufficient for sufficiently high intrinsic growth rates. For the lower of the two intrinsic growth rates considered, washout occurs over the whole range of vertical diffusion.

The 'phytoplankton' growth rate is sufficiently high, however. The long term population distribution for one of the first viable Φ_z values is shown in frame a) of Fig. 8.11. Mean population density increases as this phenomenon increases, frame b). As for the initial flow regime, however, there exists a threshold in Φ_z values after which persistence becomes rapidly more difficult and then impossible; frame c).

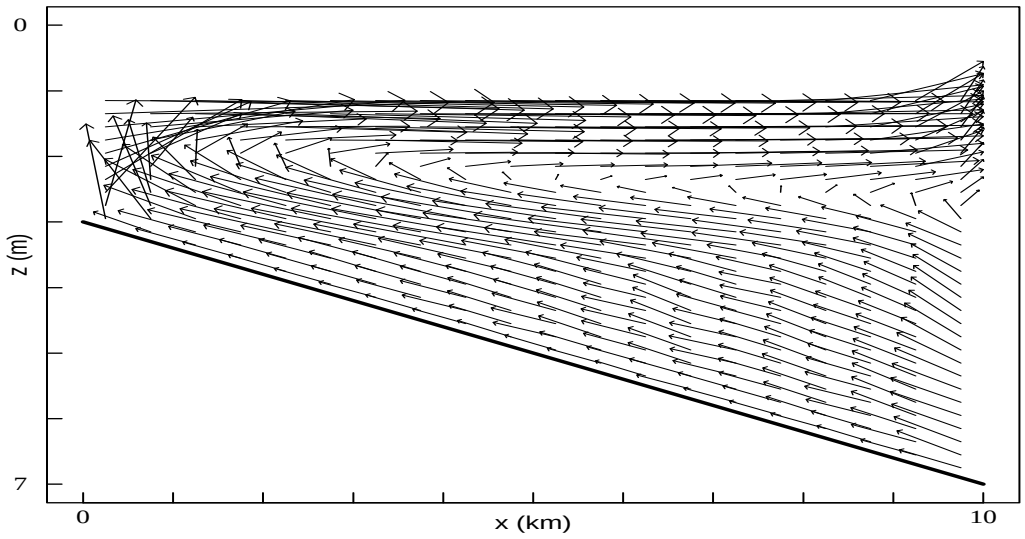

Figure 8.9: *Lagrangian residual movements over a tidal cycle calculated from POM derived flow. Tidal range* $\pm 1m$*;* $V_R = 0.003125ms^{-1}$*,* $(Q_f = 4.167 \times 10^{-3}m^2s^{-1})$*;* $UMOL = 2.0 \times 10^{-5}m^2s^{-1}$*.*

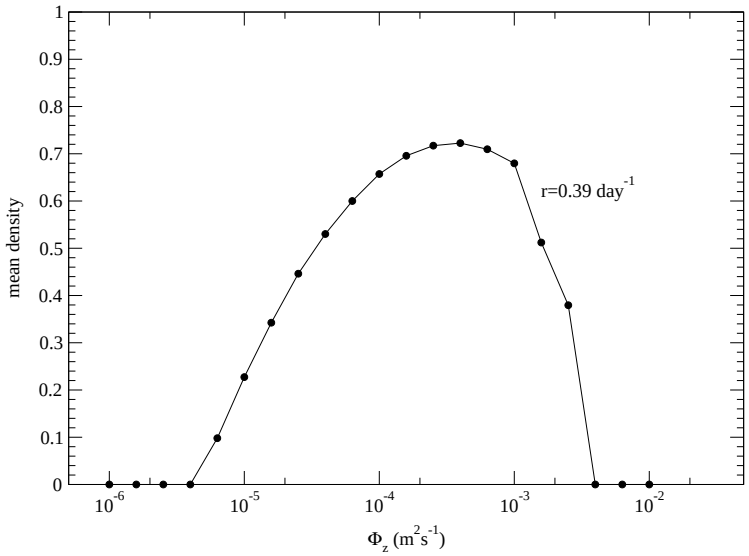

Figure 8.10: *Mean population density in a tidal estuary, (with residual velocities as shown in Fig. 8.8), as a function of the population vertical mixing rate* Φ_z*. Curve is for population intrinsic growth rates of* $0.39day^{-1}$ $(4.5 \times 10^{-6}s^{-1})$*.*

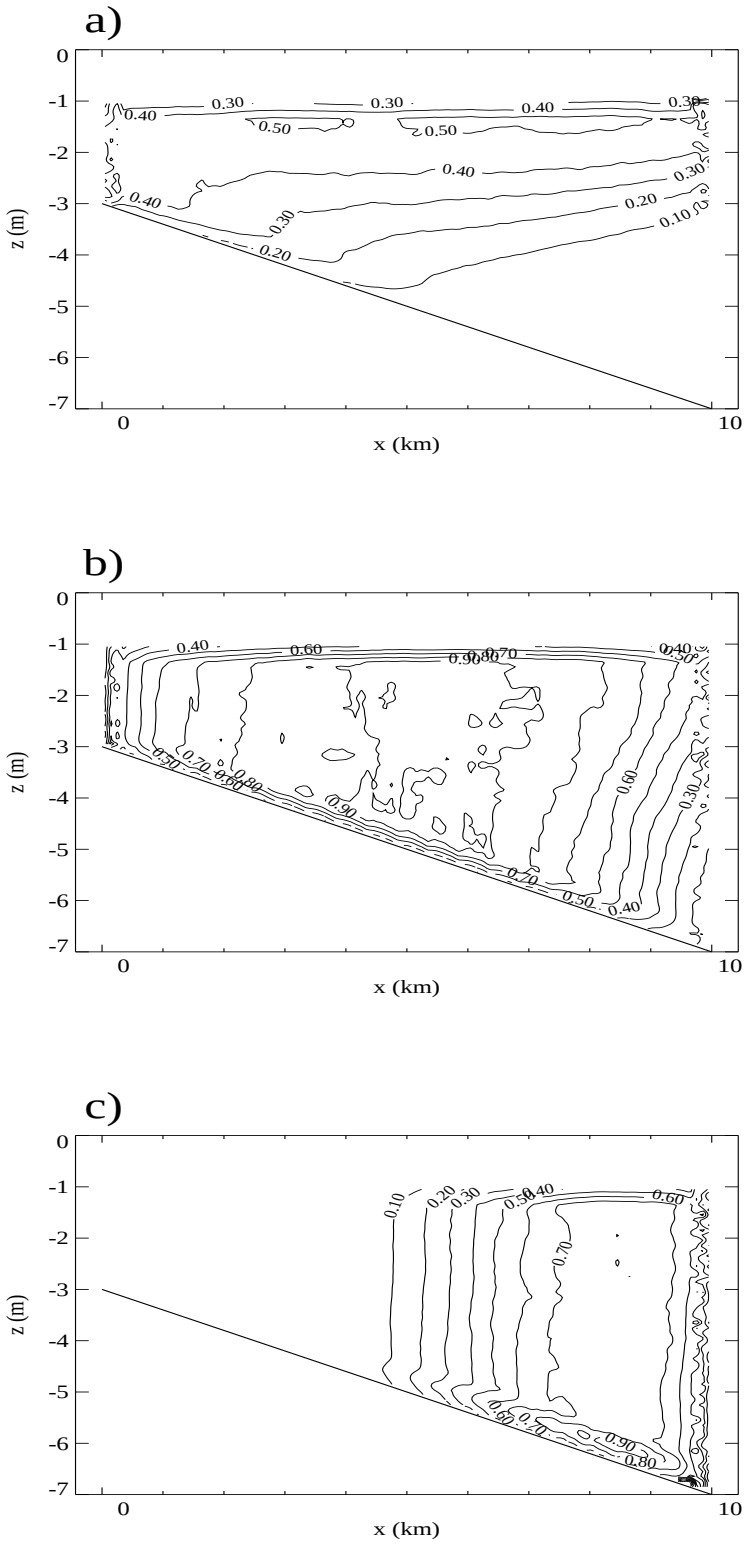

Figure 8.11: *Contours of population density in a tidal estuary, with residual velocities as shown in Fig. 8.8) and population intrinsic growth rate of* $0.39day^{-1}$ $(4.5 \times 10^{-6}s^{-1})$*. Frame a), vertical mixing rate* $\Phi_z = 1.0 \times 10^{-5}m^2s^{-1}$*; Frame b), vertical mixing rate* $\Phi_z = 1.0 \times 10^{-3.6}m^2s^{-1}$*; Frame c), vertical mixing rate* $\Phi_z = 1.0 \times 10^{-2.6}m^2s^{-1}$.

8.1.4 Depth dependent growth rates

If the population being considered is supposed to be that of phytoplankton, then the assumption of uniform growth rate could be a significant source of error. The dependence of phytoplankton on incident light for photosynthesis and reduction of light levels with depth is well documented, eg (Sverdrup 1953).

Considering the distribution of light in the water column first, field studies have shown light intensities to reduce exponentially with depth. The rate of this exponential decay is given by an attenuation (or extinction) coefficient ε. That is

$$I(z) = I_o \exp(-\varepsilon z) \tag{8.1}$$

where I_o is the light incident on the surface and $I(z)$ is the amount of light left at depth z below the surface. If the light intensity values I are expressed as a percentages, (that is $I_o = 100\%$), then ε gives the reduction in $\ln I(z)$ over a depth increment of one metre. The attenuation coefficient varies for different spectral wavelength blocks but an overall coefficient can be defined for the range of wavelengths used in photosynthesis (photosynthetically active radiation or PhAR). The overall attenuation coefficient is made up of the components ε_w, the effect of the water, ε_p, that attributable to inert suspended particulate matter and ε_a, shading produced by the algal biomass itself, (Reynolds 1984).

To retain the logistic growth rate equation and incorporate light dependency, relationships must be determined between light attenuation and the intrinsic growth rate, r, and carrying capacity k. This can be done by re-formulating the logistic growth equation in terms of gross 'growth' rates and loss or 'death' rates. The intrinsic growth rate is the net per-capita growth of a population in the absence of density dependence. As such it can be formulated as

$$r = \beta_o - \delta_o \tag{8.2}$$

where β_o and δ_o are density independent growth and death rates. In a system with no advection or diffusion the rate of change of population density n with time can be written as

$$\frac{dn}{dt} = \beta n - \delta n \tag{8.3}$$

where $\beta = \beta_o - \beta_1 n$, $\delta = \delta_o + \delta_1 n$ and β_1 and δ_1 are density dependent terms. Substituting for β and δ in Equation (8.3) gives

$$\begin{aligned} \frac{dn}{dt} &= (\beta_o - \delta_o)n - (\beta_1 + \delta_1)n^2 \\ \frac{dn}{dt} &= (\beta_o - \delta_o)n\left(1 - \frac{n}{\frac{(\beta_o - \delta_o)}{(\beta_1 + \delta_1)}}\right) \end{aligned} \tag{8.4}$$

Equation (8.4) can be seen to be the logistic equation with $r = \beta_o - \delta_o$ as expected and the carrying capacity $k = r/(\beta_1 + \delta_1)$.

For plants, this form of the logistic equation can be satisfied by regarding $\beta_o = \alpha N$, where α is the slope of a linear functional response and N is the total amount of bound and unbound nutrient in the system, (Gurney and Nisbet 1998). The term α can be regarded as proportional to the light intensity, while the amount of nutrient remains constant. Therefore, an equation for a depth dependent value of β_o can be formed analogous to Equation (8.1)

$$\beta_o(z) = \beta_o|_{z=0} \exp(-\varepsilon z) \tag{8.5}$$

In turn, this gives a relationship between the intrinsic growth rate and the light intensity of

$$r(z) = \beta_o|_{z=0} \exp(-\varepsilon z) - \delta_o \tag{8.6}$$

The carrying capacity is related to the intrinsic growth rate and therefore must change as r changes. If the value of r at the surface is labelled r_o and the value of k at the surface is set equal to one, then $(\beta_1 + \delta_1) = r_o$. Thus the depth dependent values of carrying capacity, $k(z)$ are given by

$$k(z) = r(z)/r_o \tag{8.7}$$

Because density dependence is built into the logistic equation, self shading should not be included in the attenuation coefficient. The value of ε in this work is therefore a combination of ε_w and ε_p only.

The term δ_o can be considered attributable to various factors including predation. It is therefore perfectly possible for r to become negative at greater depths. The relationship between r and k shows that k will become negative whenever r is negative and zero when r is zero. The case when $r = k = 0$ produces $0/0$ in the logistic equation so it is necessary to replace the exact solution with an approximation and determine behaviour in the limit. Sensible behaviour from the discrete time solution to the logistic equation should also be checked for the situation when r and k are negative.

As stated in section 3.3.1 the discrete time solution to the logistic equation is given by

$$B_{x,t} = \frac{k n_{x,t}}{n_{x,t} + \xi(k - n_{x,t})}, \quad \xi \equiv e^{-r\Delta t} \tag{8.8}$$

With $r = k = 0$ this gives $0/0$. When $|r|$ is very small $|r\Delta t| \ll 1$ and $e^{-r\Delta t}$ can be represented by the first two terms of its Maclaurin series without significant error. Therefore $e^{-r\Delta t}$ can be represented by $1 - r\Delta t$. Substituting this new expression into Equation (8.8), along with r/r_o in place of k gives

$$
\begin{aligned}
B_{x,t} &= \frac{(r/r_o)n_{x,t}}{n_{x,t} + (1 - r\Delta t)((r/r_o) - n_{x,t})} \\
B_{x,t} &= \frac{rn_{x,t}}{r_o n_{x,t} + r - r_o n_{x,t} - r^2\Delta t + r\Delta t r_o n_{x,t}} \\
B_{x,t} &= \frac{n_{x,t}}{(1 + \Delta t r_o n_{x,t}) - r\Delta t}
\end{aligned} \tag{8.9}
$$

As $r \to 0$ Equation (8.9) tends to

$$
B_{x,t} = \frac{n_{x,t}}{1 + \Delta t r_o n_{x,t}} \tag{8.10}
$$

To be biologically sensible $B_{x,t}$ can not be negative. This is assured as all terms on the right hand side are positive. So long as $\Delta t r_o n_{x,t} \geq 0$, however, then $B_{x,t} \leq n_{x,t}$ with the two terms becoming equal when the population density becomes zero.

When r and k are negative, $-R$ and $-K$ say, Equation (8.8) becomes

$$
\begin{aligned}
B_{x,t} &= \frac{-Kn_{x,t}}{n_{x,t} + e^{R\Delta t}(-K - n_{x,t})} \\
B_{x,t} &= \frac{Kn_{x,t}}{n_{x,t}\left(e^{R\Delta t} - 1\right) + Ke^{R\Delta t}} \\
B_{x,t} &= \frac{K}{n_{x,t}\left(e^{R\Delta t} - 1\right) + Ke^{R\Delta t}} \times n_{x,t}
\end{aligned} \tag{8.11}
$$

Again all terms on the right hand side are positive ensuring $B_{x,t}$ remains positive. As $e^{R\Delta t} > 1$ for $|R| > 0$ the term $K/[n_{x,t}\left(e^{R\Delta t} - 1\right) + Ke^{R\Delta t}] < 1$ and $B_{x,t} \leq n_{x,t}$, as would be expected for a negative intrinsic growth rate.

Gurney and Nisbet (1998) list background light attenuation coefficients $(\varepsilon_w + \varepsilon_p)$ for four different sea lochs. Three lochs have the same value of $0.22m^{-1}$, while one is more turbid with a coefficient of $0.48m^{-1}$. In comparing results obtained using depth dependent growth rate, ε can be taken as one of these two values, r_o needs to be equal to the constant intrinsic growth rate used before and the value for k is determined for all depths from Equation (8.7). If a depth z_{rc} is chosen

for the point at which $r(z) = 0$ then the remaining parameters, δ_o and β_o can be determined as follows. Substituting for β_o from Equation (8.2) into Equation (8.6) gives

$$r(z) = (r_o + \delta_o)\exp(-\varepsilon z) - \delta_o \tag{8.12}$$

$r(z) = 0$ at $z = z_{rc}$ giving

$$\delta_o = \frac{r_o \exp(-\varepsilon z_{rc})}{1 - \exp(-\varepsilon z_{rc})} \tag{8.13}$$

β_o can then be found from Equation (8.2).

Gross photosynthetic rate in phytoplankton generally falls to zero when the incident light falls in the range $0.5 - 3\%I_o$ and a 'euphotic depth' z_{eu} is defined as $1\%I_o$, (Reynolds 1984). Using this definition, from Equation (8.1), z_{eu} can be given as

$$z_{eu} = \ln(I_o)/\varepsilon \tag{8.14}$$

The values of z_{eu} obtained for given values of ε are the maximum sensible values of z_{rc} that can be chosen for that value of attenuation coefficient. This critical depth value can be assumed to be one obtained in the absence of predation. Decreasing values of z_{rc} can be interpreted as representing increasing rates of predation.

Fig. 8.12 repeats the same graph of mean population density against vertical diffusion coefficient for a population with intrinsic growth rate of $0.39day^{-1}$, ($4.5\times 10^{-6}s^{-1}$) as shown in Fig. 8.10 but with additional curves showing the effect of depth dependent growth rate. The left hand frame shows curves for $\varepsilon = 0.22$ and the right hand frame those where $\varepsilon = 0.48$. In each frame z_{rc} has been set to equal z_{eu}, $7m$, (the depth of the deepest part of the system) and $3.5m$, (the mid depth). It can be seen that even with $\varepsilon = 0.22$ and z_{rc} set to its maximum sensible

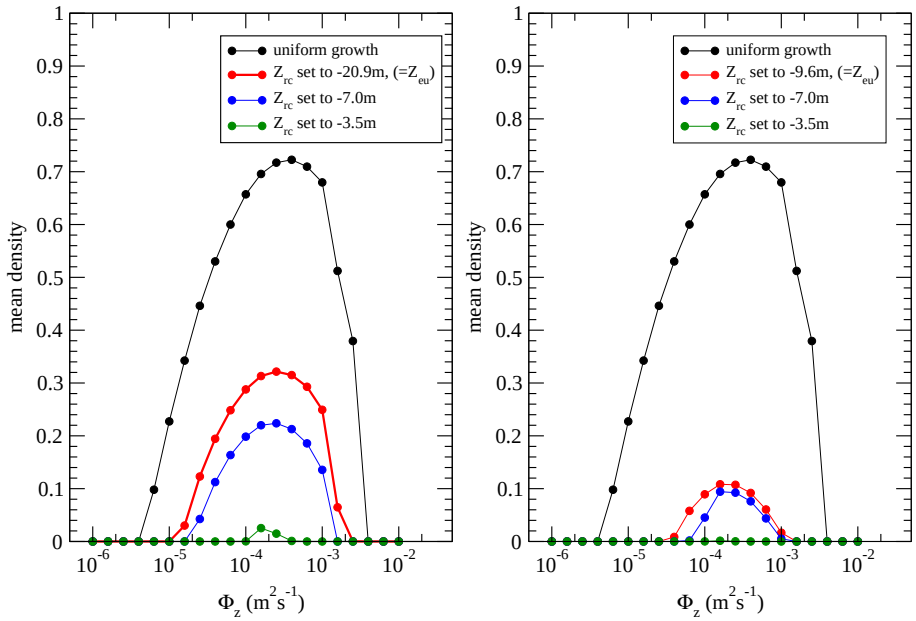

Figure 8.12: *Mean population density in a tidal estuary, (with residual velocities as shown in Fig. 8.8), as a function of the population vertical mixing rate* Φ_z. *Curves are for constant population intrinsic growth rates of* $0.39day^{-1}$ $(4.5 \times 10^{-6}s^{-1})$ *(black line);* $r = 0.39day^{-1}$ *at the surface with* $r(z) = \beta_o|_{z=0} \exp(-\varepsilon z) - \delta_o$ *and* $z_{rc} = z_{eu}$ *(red line);* $z_{rc} = 7m$ *(blue line) and* $z_{rc} = 3.5m$ *(green line). Left hand frame: Light attenuation coefficient,* ε *equals* $0.22m^{-1}$*; right hand frame:* $\varepsilon = 0.48m^{-1}$.

value the reduction in mean population density is marked. The reductions when $\varepsilon = 0.48$ could be described as dramatic.

Although the reduction in mean population density brought about by the introduction of depth dependent growth rate is large, the overall pattern remains consistent. If an organism allows itself to be moved in a diffusive manner to a certain extent, then persistence becomes possible, whereas near total avoidance of random motions leads to washout. Too great a degree of random vertical motion, however, is sub-optimal and there is an increasing risk that washout will again occur.

This is at least true when z_{rc} is set greater than $3.5m$. At this value, even though the transition from net seaward to net landward flow occurs at a depth of around $2m$, persistence has been made impossible in the case of higher attenuation coefficient and is only very marginal in the case for clearer waters. This suggests

persistence relies on population surviving, and quite probably growing, in the deeper regions closer to the seaward boundary. Fig. 8.13 shows how the pattern of distribution of population density is not altered by transition to depth dependent growth rates. Rather, concentrations are simply reduced. Frames a), b) and c) all show distributions for a vertical diffusion of $\Phi_z = 1.0 \times 10^{-4} m^2 s^{-1}$ but frame a) is that for uniform growth, frame b) that for growth when $\varepsilon = 0.2 m^{-1}$, $z_{rc} = 20.9 m$ and frame c) that for $\varepsilon = 0.48 m^{-1}$, $z_{rc} = 7 m$. It should be noted that to make the frames of this figure more readable, the minimum contour and the contour step size has been altered for each frame.

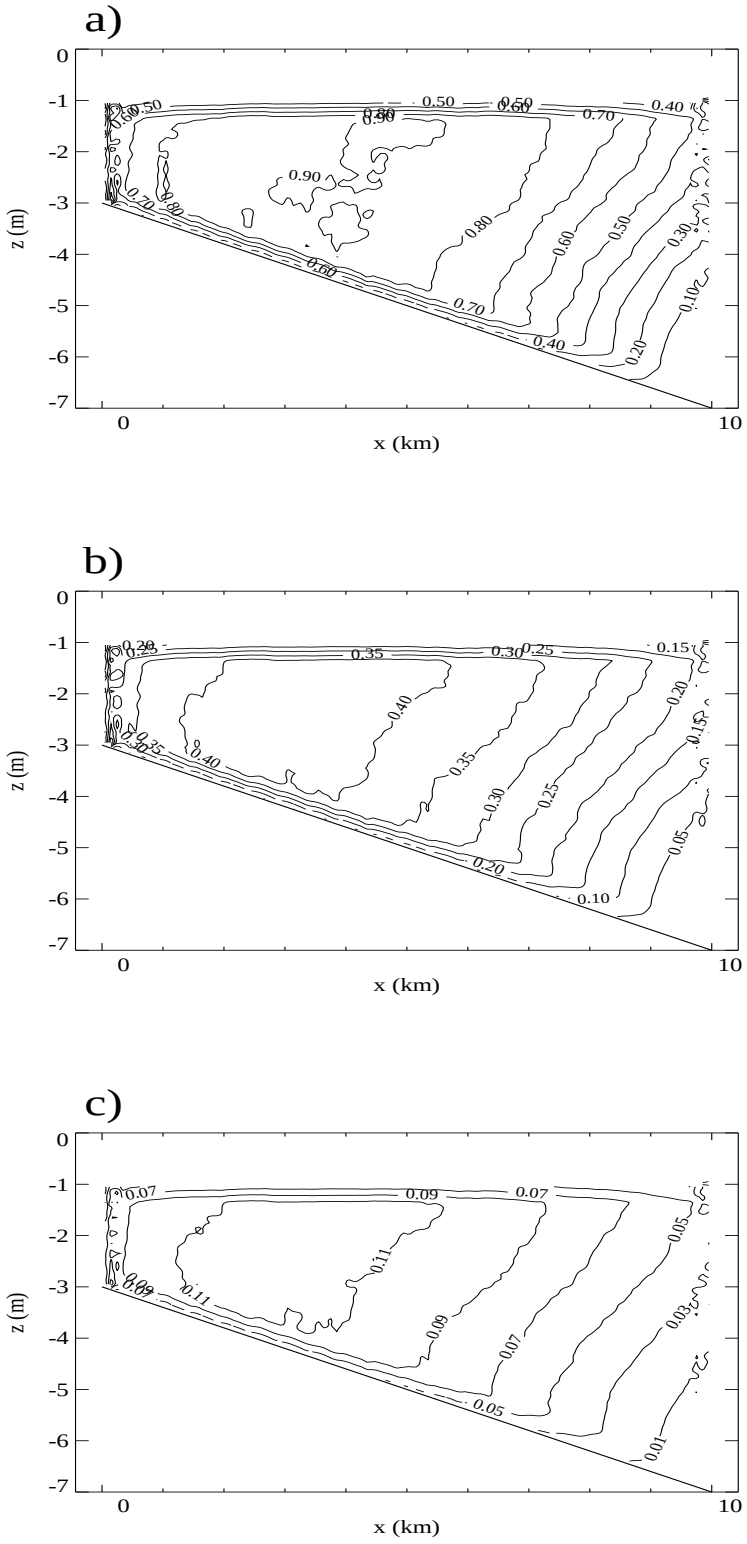

Figure 8.13: *Contours of population density in a tidal estuary, with residual velocities as shown in Fig. 8.8), population intrinsic growth rate of* $0.39day^{-1}$ $(4.5 \times 10^{-6}s^{-1})$ *and vertical mixing rate of* $\Phi_z = 1.0 \times 10^{-4}m^2s^{-1}$. *Frame a), uniform growth. Frame b), attenuation coefficient* $\varepsilon = 0.22m^{-1}$ *and* $z_{rc} = 20.9m$. *Frame c), attenuation coefficient* $\varepsilon = 0.48m^{-1}$ *and* $z_{rc} = 7.0m$.

8.2 Vertical motion toward the benthos

8.2.1 Uniform in situ growth rate

As in the consideration of a vertically heterogeneous river the effect of a constant rate of sinking is investigated. As mentioned in chapter 7 a number of species of phytoplankton are known to be negatively buoyant and have no means of swimming. Such phytoplankton are an important component of many estuaries and fjords. To link with chapter 7, the same sinking velocity, V_s, is used as in section 7.2.4. This represents a maximum recorded value for freshwater phytoplankton species but there are marine species with higher values, (Reynolds 1984).

Using the constant intrinsic growth rate of $0.39day^{-1}$ ($4.5 \times 10^{-6}s^{-1}$) the graph of normalised, (and domain averaged), long term population density against vertical diffusion coefficient, (as shown in Fig. 8.10), is compared to the result when sinking is present in Fig. 8.14. The former is given by a solid line and the latter a dotted line. The overall pattern could be regarded as remarkably similar. The only region where results are qualitatively different is that for which Φ_z values are smallest. There has been a shift from washout to moderate persistence. Given the pattern of the residual flows, it seems surprising that organisms with a sinking velocity should persist less well for any values of Φ_z, especially as in situ growth rates are constant throughout the domain.

A more significant result of sinking is that persistence is now possible with the lower of the considered intrinsic growth rates, $0.026day^{-1}$. The curve of population density is shown by the dashed line. The lower growth rate is intended to be representative of organisms as large as small shrimp. Zooplankton are likely to have either significantly greater sinking speeds, or swimming ability. Even amongst motile phytoplankton swimming speeds are estimated to reach $1.0 \times 10^{-3}ms^{-1}$, (Reynolds 1994b, page 153).

If organisms possess a quiescent settling velocity the theory of settling in the

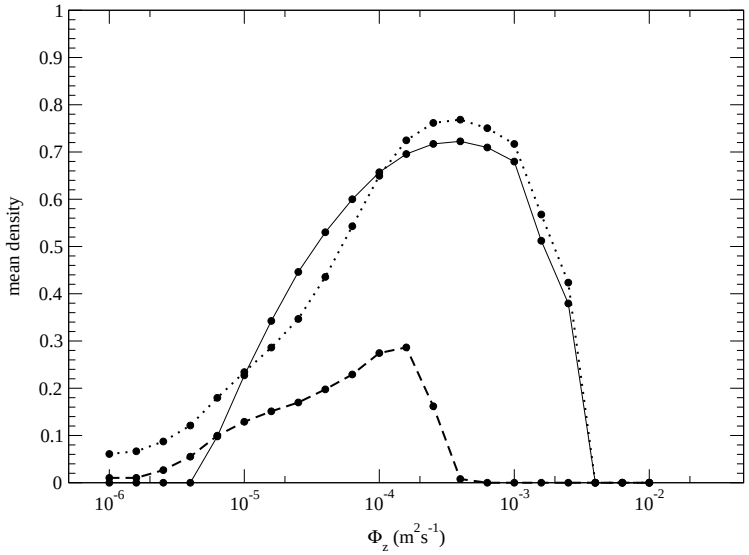

Figure 8.14: *Mean population density in a tidal estuary, (with residual velocities as shown in Fig. 8.8), as a function of the population vertical mixing rate* Φ_z. *Curves are for population intrinsic growth rates of* $0.39day^{-1}$ *(*$4.5 \times 10^{-6}s^{-1}$*) with organisms neutrally buoyant (solid line); sinking with a velocity of* $V_s = 2.5 \times 10^{-5}ms^{-1}$ *(dotted line). The same sinking velocity and intrinsic growth rate of* $0.026day^{-1}$ *(*$3.0 \times 10^{-7}s^{-1}$*).*

presence of turbulence implies that turbulence will delay the settling of individuals in the water column, (by a factor directly related to their settling velocity), but if only random motion is present in the vertical eventual settling is inevitable, (Reynolds 1984, page 50). As a consequence one might expect contour plots of the long term distribution of population density to show strong concentration toward the benthic boundary. Fig. 8.15 shows this to be only partially true. This figure shows frames of population distribution when the intrinsic growth rate is $0.39day^{-1}$.

The strong landward bias to flow nearer the benthos conveys population toward the head of the estuary. Close to the reflecting boundary net flow tends to be vertically upwards, but this advection is counter balanced by the downward advection of sinking. Strong concentrations therefore form at the head of the estuary. It is thought the fact only modest domain mean populations are achieved in the region of Φ_z values where there was no persistence previously is due to this focusing of individuals and density dependence. The result when $\Phi_z =$

$1.0 \times 10^{-6} m^2 s^{-1}$ is shown in frame a). The same explanation seems to account for the small range of values of Φ_z for which the domain mean population density is reduced in the presence of sinking. Frame b) shows a contour plot from this range, when $\Phi_z = 1.0 \times 10^{-4.4} m^2 s^{-1}$. The advective component to organismal vertical movement does seem to delay the onset of complete mixing and resultant washout. Frame c) of Fig. 8.15 takes the same Φ_z value of $1.0 \times 10^{-3.6} m^2 s^{-1}$ as used in frame b) of Fig. 8.11. In the case of vertical sinking, the density of population can be seen to be more concentrated both toward the benthos, (to a modest degree), and toward the landward end of the domain.

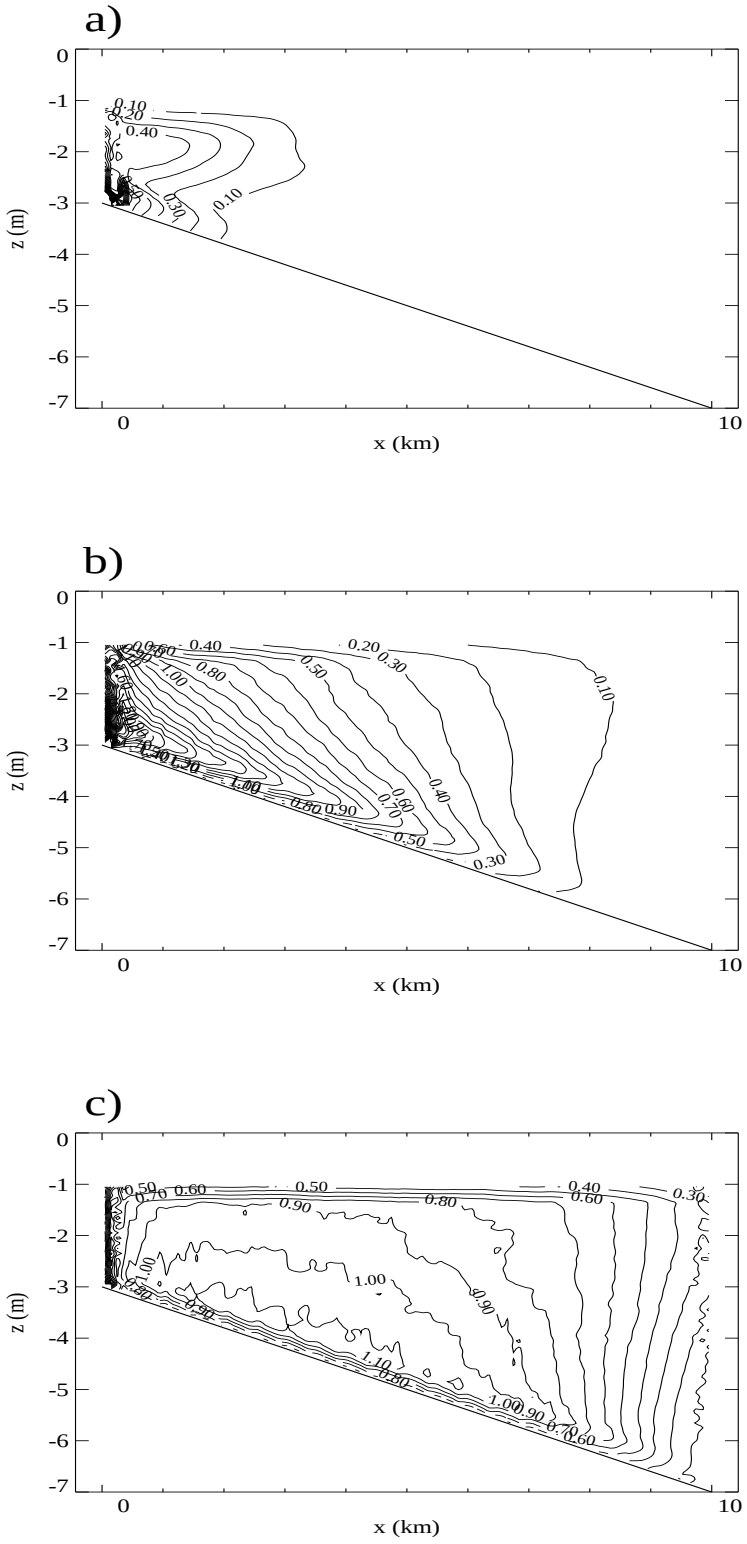

Figure 8.15: *Contours of population density in a tidal estuary, with residual velocities as shown in Fig. 8.8), population intrinsic growth rate of* $0.39day^{-1}$ *(*$4.5 \times 10^{-6}s^{-1}$*), sinking speed of* $V_s = 2.5 \times 10^{-5}ms^{-1}$*. Frame a), vertical mixing rate* $\Phi_z = 1.0 \times 10^{-6}m^2s^{-1}$*; Frame b), vertical mixing rate* $\Phi_z = 1.0 \times 10^{-4.4}m^2s^{-1}$*; Frame c), vertical mixing rate* $\Phi_z = 1.0 \times 10^{-3.6}m^2s^{-1}$*.*

8.2.2 Sinking and depth dependent growth rate

Given the results from section 8.1.4 and those for organisms with sinking velocity but uniform growth, it is intriguing as to the effect of sinking and light dependent growth combined. Light restrictions on growth led to sharp reductions in overall population density. Sinking, however, did lead to gains in persistence, but for the higher intrinsic growth rate only to small gains, and then for only some values of vertical diffusion coefficient. Perhaps most interesting is whether the ability to persist at very low values of Φ_z provided by sinking can be maintained.

The left hand frame of Fig. 8.16 repeats the left hand frame of Fig. 8.12 that shows results for the case of neutral buoyancy given uniform growth and three values of z_{rc} when the attenuation coefficient $\varepsilon = 0.22m^{-1}$. The right hand frame gives the results when sinking is included. With sinking present, the pattern of persistence against vertical diffusion again remains much the same whether growth is considered uniform or light dependent. In turn this leads to gains in persistence at low diffusion rates. The effect is most marked when the growth reduction with depth is most severe.

Fig. 8.17 makes a similar comparison to that of Fig. 8.16 but for the case where the attenuation coefficient equals $0.48m^{-1}$. Again, the same form of relationship can be seen between mean density curves when comparing between depth dependent growth and uniform growth and when comparing between sinking and neutrally buoyant organisms subject to the same growth regimes. The greatest difference when sinking is present again occurs for the smallest value of z_{rc}. Indeed, the situation has been changed from one of extinction at all values of vertical diffusion to a finite region of diffusion coefficients where persistence is secured.

It is believed the increasing advantage of organisms possessing sinking as reduction in r with depth becomes more severe is due to the same mechanism that allows persistence with uniform but much lower intrinsic growth rate. A greater proportion of population becomes part of a gyre like pattern of motion that is

restricted to the upper, and more shallow, part of the domain. If growth is sufficient for density dependence to take effect this can become a disadvantage, as seen in Fig. 8.14. Here, however, growth rates are being suppressed by other factors.

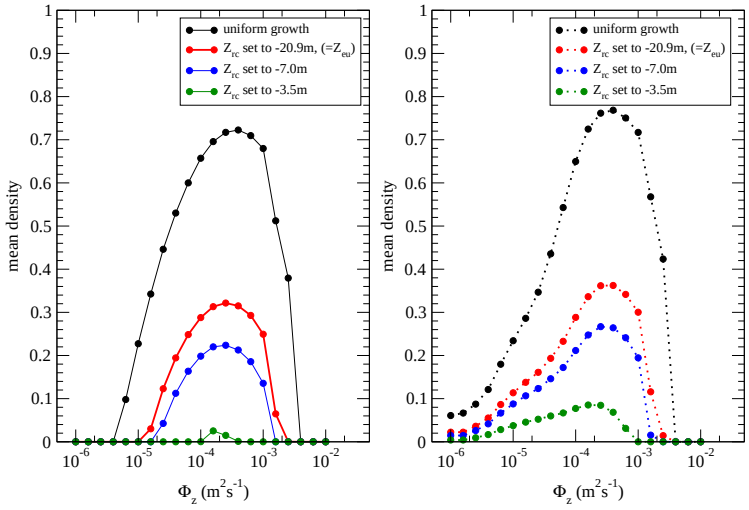

Figure 8.16: *Mean population density in a tidal estuary, (with residual velocities as shown in Fig. 8.8), as a function of the population vertical mixing rate* Φ_z. *Curves are for population intrinsic growth rates of* $0.39day^{-1}$ $(4.5 \times 10^{-6}s^{-1})$. *Results for uniform growth rates and for values of* z_{rc} *as indicated. Attenuation coefficient* $\varepsilon = 0.22m^{-1}$ *in all cases. Left hand frame, (solid lines) for neutrally buoyant organisms; Right hand frame, (dotted lines), for organisms with sinking velocity of* $V_s = 2.5 \times 10^{-5}ms^{-1}$.

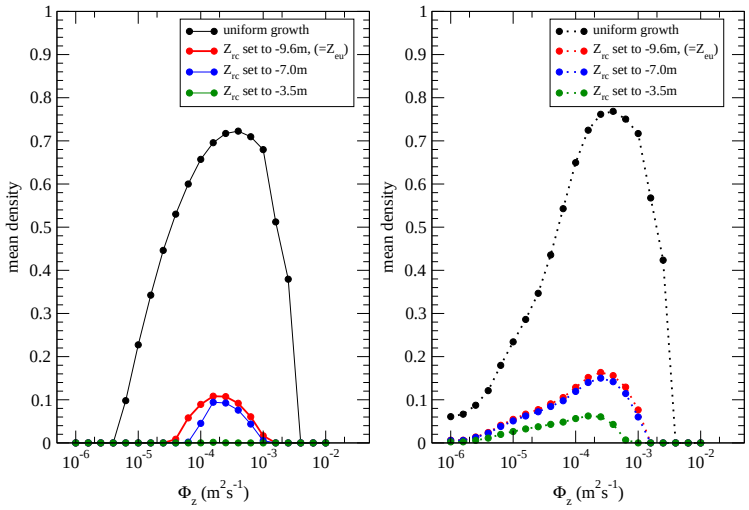

Figure 8.17: *Mean population density in a tidal estuary, (with residual velocities as shown in Fig. 8.8), as a function of the population vertical mixing rate* Φ_z. *Curves are for population intrinsic growth rates of* $0.39day^{-1}$ $(4.5 \times 10^{-6}s^{-1})$. *Results for uniform growth rates and for values of* z_{rc} *as indicated. Attenuation coefficient* $\varepsilon = 0.48m^{-1}$ *in all cases. Left hand frame, (solid lines) for neutrally buoyant organisms; Right hand frame, (dotted lines), for organisms with sinking velocity of* $V_s = 2.5 \times 10^{-5}ms^{-1}$.

Chapter 9

Strategic fjord

9.1 Ratios of tidal inflow to river discharge

In chapter 8 the river discharge into the system was chosen as much to allow the comparison of two very different residual flow patterns as any other reason. For the work on fjords it was possible to consider the appropriateness of the ratio of river discharge to tidal inflow thanks to a comprehensive survey of Scottish sea lochs performed by Edwards and Sharples (1986). Edwards and Sharples recorded physical dimensions and other statistics pertinent to oceanographic work, including figures for annual fresh water discharge and total annual tidal inflow. The latter value, (with units of $m^3 year^{-1}$), was determined from the following formula

$$inflow = 490 \times tiderange \times (hwarea + lwarea)/2 \tag{9.1}$$

where the constant is derived from the fact that there are approximately 700 semidiurnal tides per year and study of tidal tables for North West Scotland showed the mean tidal range in a year to be about 70% of the spring tidal range, (the term 'tiderange' represents spring tidal range). In the strategic simulations performed in this work the tidal range is considered constant and only a two

dimensional slice is considered such that the term $(hwarea + lwarea)/2$ can be replaced by the length of the fjord. This length was taken as the distance from the inner edge of the sill region to the point at which the river flow is injected. A per unit width inflow value ,(in $m^2 s^{-1}$), can then be obtained from

$$inflow = \frac{tiderange \times length}{T} \tag{9.2}$$

where T is the tidal period. Edwards and Sharples ranked 109 sea lochs according to this 'freshtideratio'. With the tidal range of these strategic simulations retained as, $2m \equiv \pm 1m$, the river discharge used in chapter 8 gives a ratio of ≈ 0.0055. This equates to values obtained for sea lochs ranking 76th to 87th in the league table and is similar in value to lochs ranking as high as 69 and as low as 98. With the discharge value used by Speirs and Gurney (2001) in their investigation of tidal regimes the ratio becomes ≈ 0.022, equal to sea lochs ranked 16th and 17th and similar to those from rank 15 to 19. The river discharge to tidal flow ratios represented by these two inflows cover the majority of the range found in Scottish sea lochs.

Two additional runs were conducted. One increased the river discharge to tidal inflow ratio to 0.1, greater than all but one sea loch, and the other reduced the ratio to 0.002, lower than all but two lochs. The run with higher discharge showed no sign of settling to a quasi steady state. A more steady cycle could probably have been forced through adjustment of parameters such as imposed horizontal diffusion or bottom friction but this would compromise the ability to make comparisons between systems where the only difference is supposed to be one of river inflow. Fig. 9.1 shows the Lagrangian residual movement obtained using the river discharge as in Speirs and Gurney (2001), while Fig. 9.2 shows residual flows when river flow was reduced to give the freshtideratio of 0.002. These residual movements are used in the remainder of this chapter.

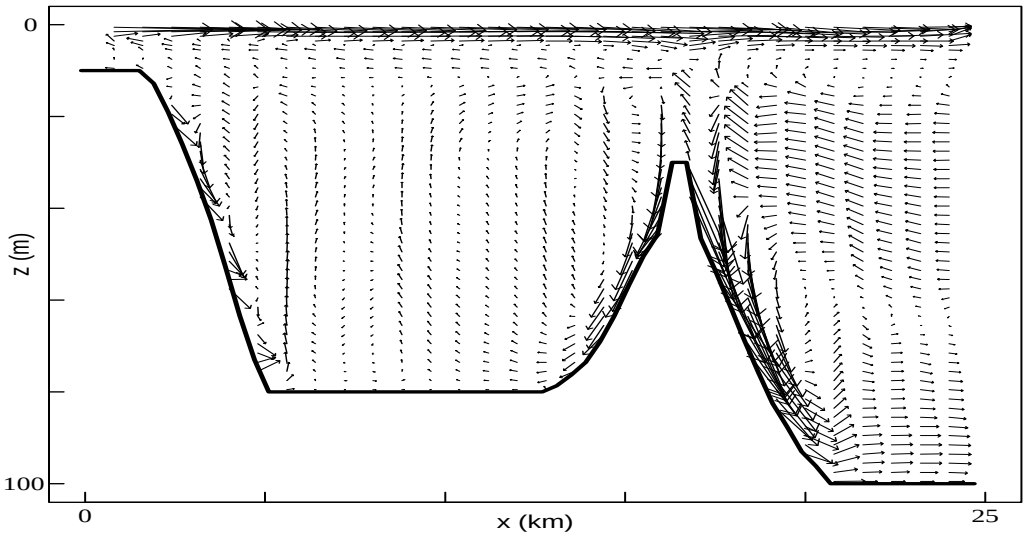

Figure 9.1: *Lagrangian residual movements over a tidal cycle calculated from POM derived flow. Tidal range* $\pm 1m$*;* $V_R = 0.003125ms^{-1}$*,* $(Q_f = 4.167 \times 10^{-3}m^2s^{-1})$*;* $UMOL = 2.0 \times 10^{-5}m^2s^{-1}$.

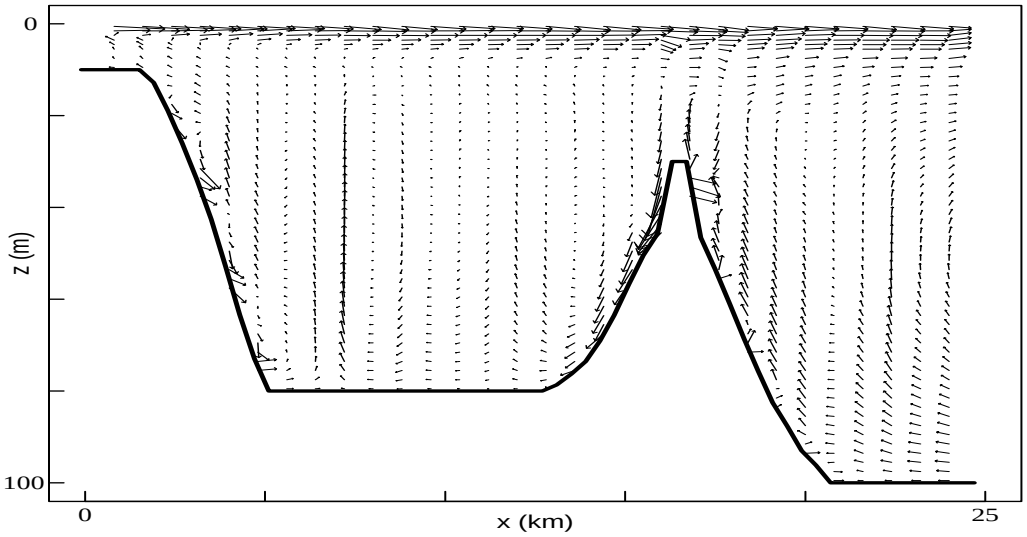

Figure 9.2: *Lagrangian residual movements over a tidal cycle calculated from POM derived flow. Tidal range* $\pm 1m$*;* $V_R = 0.001125ms^{-1}$*,* $(Q_f = 1.5 \times 10^{-3}m^2s^{-1})$*;* $UMOL = 2.0 \times 10^{-5}m^2s^{-1}$.

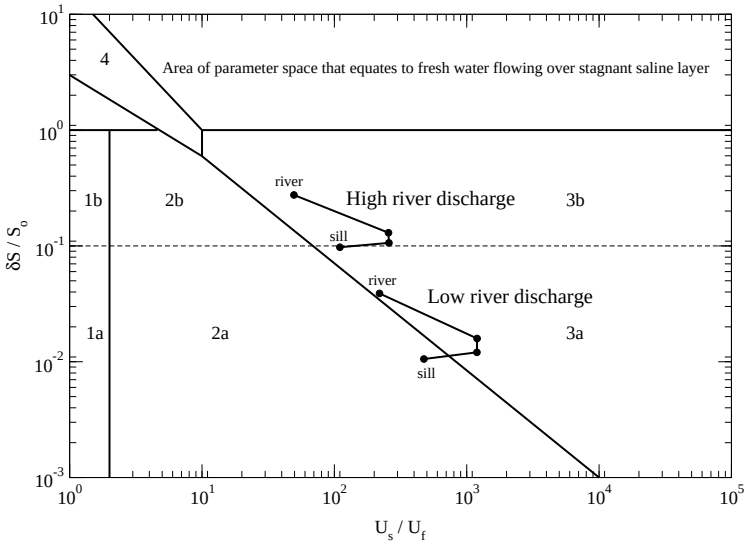

Figure 9.3: *Stratification-circulation diagram, after Hansen and Rattray (1966), with results marked for the two flow regimes used. Results were taken for four locations; the point at which the riverine section feeds into the body of the fjord, the upstream and downstream locations at which the fjord basin is at its deepest and the location of the sill.*

The overall pattern of residual movement was found to alter subtly between the extremes of river discharge considered. With higher river discharge there is a clear indication of a two layer flow regime in the near surface region of the fjord, (Fig. 9.1). This seems absent in the case of low river flow, (Fig. 9.2). Fig. 9.3 shows the location of these two flow regimes on the Hansen and Rattray stratification-circulation diagram. Both results show the regimes to be of type 3 as would be expected of fjords. As mentioned in section 2.1.2 a typical fjord is expected to be of type 3b. The system with the higher river flow conforms to this expectation very well. The lower stratification indicated for the case of lower river discharge is because the river flow was insufficient to form a well defined near surface brackish layer. The diagram clearly shows how the difference between surface and vertically averaged net velocity is greatly reduced in the region of the sill, indicating the breaking down of buoyancy driven near surface flows in this region by greater levels of turbulent mixing.

9.2 Passive organisms permanently in the drift

9.2.1 Persistence relative to vertical diffusion

Diffusion coefficient correction

To track particles over the much deeper domain represented by the fjord but keep within the memory constraints of available computers it was necessary to increase vertical cell height from $0.1m$ to $1m$. The criterion for accurate representation of intended diffusion established by Gurney et al. (2001), namely that $\Delta z/\sqrt{2\Phi_z \Delta t} \leq 0.1$ is only satisfied down to values of $\Phi_z \approx 1.0 \times 10^{-2.8} m^2 s{-}1$. At the lowest value used to investigate persistence, $1.0 \times 10^{-6} m^2 s{-}1$, this ratio becomes roughly 3.4. Between these values, if this non-steady flow regime behaves in a similar manner to the case with no advection, uncorrected parameter values used in the particle tracking program are likely to lead to over-representation of vertical diffusion. An algorithm developed by Gurney et al. (2001) was used to produce corrected coefficient values. This only corrects exactly for the case with no advection. Individually tuned corrections for regimes with constant advection are possible but in this case the advections change with time and space and are not known a priori. As stated in section 3.3.1 confidence in the correction to within a 10% error are possible up to a cell to diffusive distance ratio of 2. Vertical diffusion was still likely to be represented with error $> 10\%$ for target values of $1.0 \times 10^{-5.8}$ and $1.0 \times 10^{-6} m^2 s{-}1$. These values were omitted for the fjord work.

Domain averaged population densities

Phytoplankton and zooplankton that could be regarded as passive are important trophic levels within fjords. Such plankton are unlikely to exhibit intrinsic growth rates of as low as $0.026 day^{-1}$ however, (O'Doherty 1985), so only the higher of the two growth rates considered previously, $(0.39 day^{-1})$, is considered in this

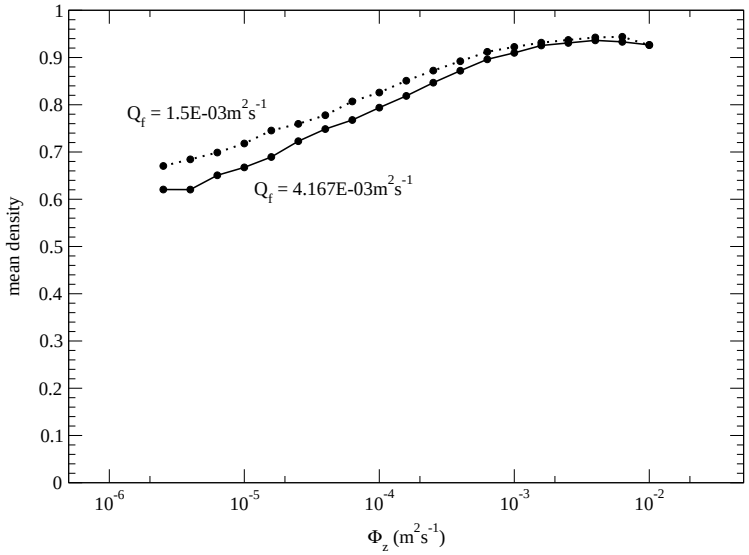

Figure 9.4: *Mean population density in a tidal fjord, (with residual velocities as shown in Figs. 9.1 and 9.2), as a function of the population vertical mixing rate* Φ_z. *Curves are for population intrinsic growth rate of* $0.39day^{-1}$ $(4.5 \times 10^{-6}s^{-1})$.

section. Fig. 9.4 shows a plot of domain averaged population density against vertical diffusion rate for residual movements over a tidal cycle as shown in Figs. 9.1 and 9.2. Most planktonic life that can live in saline fjords can also survive in the coastal sea. It is also considered legitimate for planktonic organisms to be carried into such bodies from outside of the sill region. Therefore, when tracking organisms to generate the redistribution matrix, tracks were started between the sill region and open boundary to allow for organisms to be washed into the fjord region. Also, the boundary at which organisms were considered washed out during tracking was set between sill and open boundary. The extent of this extended tracking region can be seen from the population contour plots used in this section. In determining the results for domain averaged population density, however, only the domain found inside of the fjord sill was included.

It can be seen from Fig. 9.4 that persistence is strong for all values of diffusion coefficient considered and for both river discharges. At higher diffusion rates population is virtually at the carrying capacity throughout the domain and the difference between river discharges has become irrelevant. At lower levels of diffusion there is a modest difference in persistence between the regimes. What differences

do exist in long term population pattern between results for low and high vertical diffusion and river discharge are shown by Figs. 9.5, 9.6 and 9.7 which show contours of long term population density for the cases of $\Phi_z = 1.0 \times 10^{-5} m^2 s^{-1}$ and $\Phi_z = 1.0 \times 10^{-2} m^2 s^{-1}$. It should be remembered that cells between the sill and seaward open boundary were not included in the determination of domain averaged population densities.

Fig. 9.5 confirms the idea that population is almost uniformly at the carrying capacity. There is clear indication, however of a large gyre or eddy formation at the seaward end of the fjord behind the sill. This feature extends to the deepest part of the fjord. The figure shown represents the result for the higher river discharge but plots for the case of lower river discharge showed no significant differences for those values of vertical diffusion where the domain averaged population densities were convergent.

In Fig. 9.6, which shows the case for high river discharge but low vertical diffusion, densities can be seen to reduce in the surface layers – as might be expected – and in the regions close to where the bathymetry drops toward the middle basin. In the case of the same low value of diffusion and also low river discharge, Fig. 9.7, reductions in population density can be seen to be slightly less in the upper regions of the water column. There is, however, a sizeable region with a near absence of population at the landward end of the fjord basin.

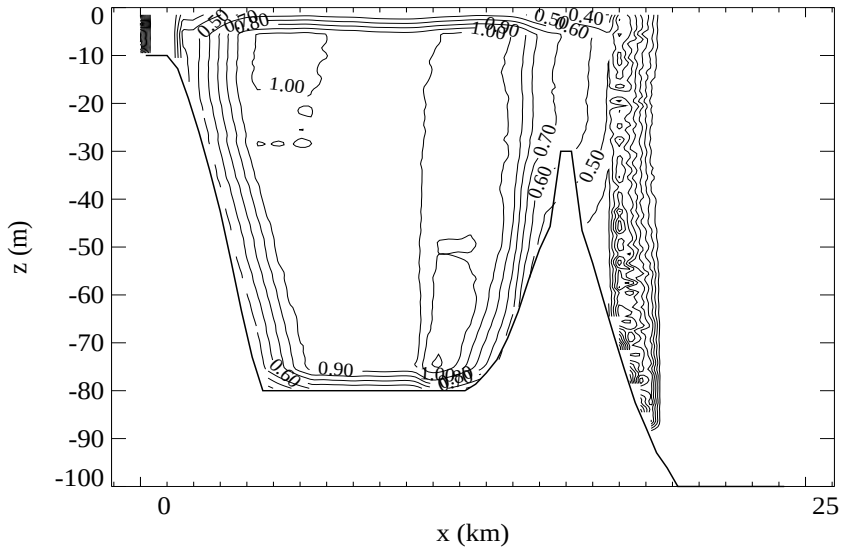

Figure 9.5: *Contours of population density in a tidal fjord, with residual velocities as shown in Fig. 9.1), population intrinsic growth rate of* $0.39day^{-1}$ *(*$4.5 \times 10^{-6}s^{-1}$*) and vertical mixing rate of* $\Phi_z = 1.0 \times 10^{-2}m^2s^{-1}$*. Contour intervals 0.1.*

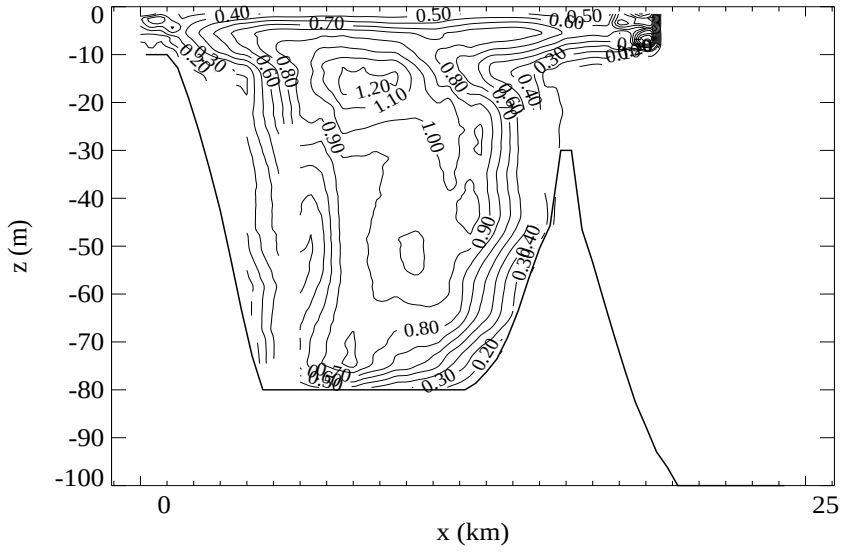

Figure 9.6: *Contours of population density in a tidal fjord, with residual velocities as shown in Fig. 9.1), population intrinsic growth rate of* $0.39day^{-1}$ *(*$4.5 \times 10^{-6}s^{-1}$*) and vertical mixing rate of* $\Phi_z = 1.0 \times 10^{-5}m^2s^{-1}$*. Contour intervals 0.1.*

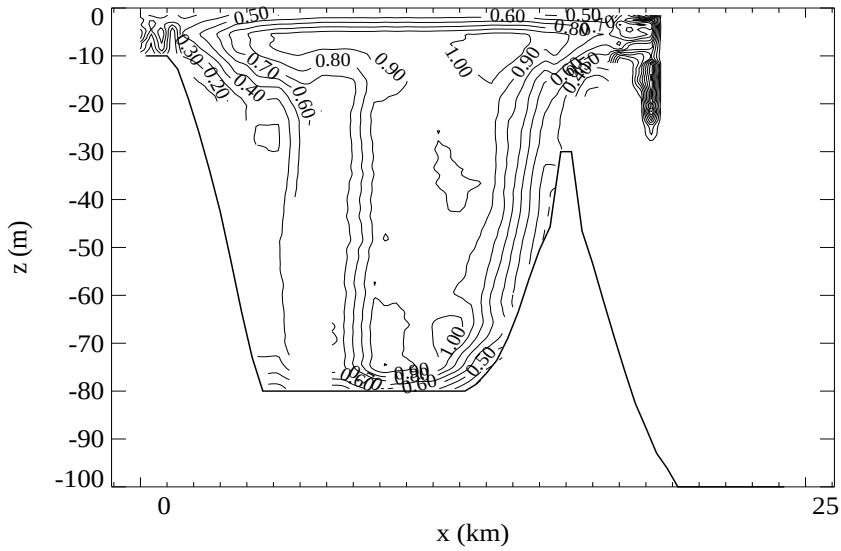

Figure 9.7: *Contours of population density in a tidal fjord, with residual velocities as shown in Fig. 9.2), population intrinsic growth rate of* $0.39day^{-1}$ *(*$4.5 \times 10^{-6}s^{-1}$*) and vertical mixing rate of* $\Phi_z = 1.0 \times 10^{-5}m^2s^{-1}$*. Contour intervals 0.1.*

9.2.2 Depth dependent growth rate

The very high domain averaged population concentrations shown in Fig. 9.4 would suggest in themselves that depth dependent growth rates are likely to have a big impact on the results for persistence. The deepest part of the fjord region is over ten times as deep as the deepest part of the estuary domain considered in the previous chapter. The degree of reduction, however, depends on the extent to which population in the upper regions depends on supply from deeper regions.

Fig. 9.8 shows the domain averaged population densities obtained using depth dependent growth rate and light attenuation coefficient, $\varepsilon = 0.22m^{-1}$. For the depth dependent growth rate, the depth for zero intrinsic growth rate, z_{rc} was set equal to the 'euphotic depth' z_{eu}, such that predation can essentially be considered absent. Even so effects on persistence are so dramatic a logarithmic scaling has been employed for the normalised population density and for only a fraction of the full range. For higher river flow persistence is only possible for vertical diffusion coefficients above $1.0 \times 10^{-3}m^2s^{-1}$ and then it is only marginal. Washout and extinction of population was slow in the other cases. After a population model run representing one year very small finite population densities were still present, but they were subject to a steady decrease in all cases. This was confirmed by running the simulations for two years. A dotted line is included in Fig. 9.8 to distinguish between results that indicated persistence and those where the population was still slowly decaying.

The case for low river flow is very similar with the exception of a persistent population in one narrow window of lower vertical diffusion. Fig. 9.9 shows the long term population distribution for a vertical diffusion from this region, ($\Phi_z = 1.0 \times 10^{-3.4}m^2s^{-1}$). Non-zero population is found throughout the fjord but there is a small concentration found in the near surface region just inside of the sill. A concentration can also be seen, however, at the upstream end of the domain used to introduce the river flow. It should be noted that contours in Fig. 9.9 are at values an order of magnitude smaller than those of previous contour

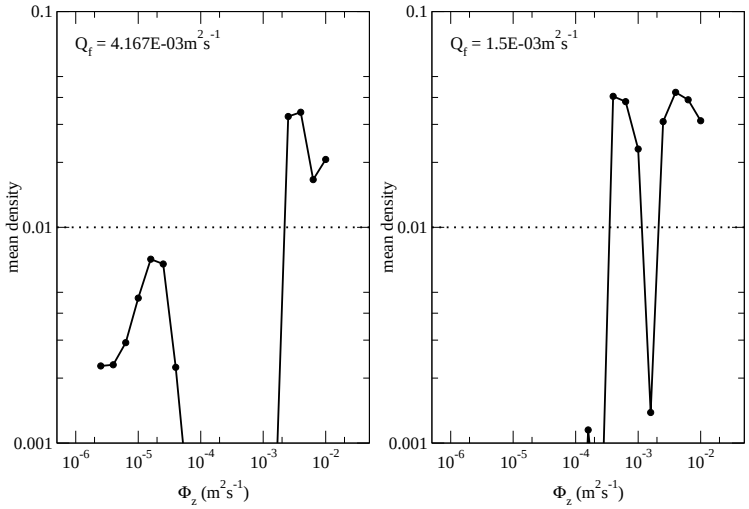

Figure 9.8: *Mean population density in a tidal fjord as a function of the population vertical mixing rate* Φ_z*. Results are for population intrinsic growth rate of* $0.39day^{-1}$ *(*$4.5 \times 10^{-6}s^{-1}$*), light attenuation coefficient,* ε *equals* $0.22m^{-1}$ *and* $z_{rc} = z_{eu} = 20.9m$*, (intrinsic growth rate critical depth equalling euphotic depth). Left hand frame; residual movements as in Fig. 9.1, right hand frame; residual movements as in Fig. 9.2. Dotted lines indicate split between results for persistence and results where population was still declining after two years.*

plots.

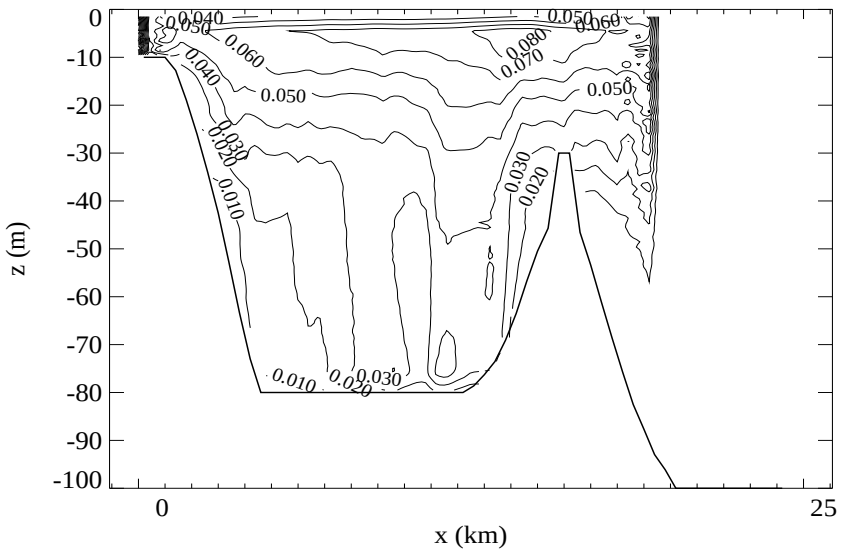

Figure 9.9: *Contours of population density in a tidal fjord, with residual velocities as shown in Fig. 9.2, and depth dependent intrinsic growth rate of* $0.39day^{-1}$ *(*$4.5 \times 10^{-6}s^{-1}$*) at the surface. Light attenuation coefficient,* $\varepsilon = 0.22m^{-1}$*, depth of zero intrinsic growth* $z_{rc} = 20.9m$ *and vertical mixing rate of* $\Phi_z = 1.0 \times 10^{-3.4}m^2s^{-1}$*. Contour intervals 0.01.*

The small levels of persistence seen for higher vertical diffusion coefficients seems due to the fact the random movement of individuals manages to repeatedly transfer sufficient numbers between the large scale eddies – both at the head of the fjord and toward the sill region – and the upper layers. Fig. 9.10 illustrates the effect for when the Φ_z value equals $1.0 \times 10^{-2.6} m^2 s^{-1}$. Contour plots were very similar between high and low river flow. This latter result suggests that in the presence of only small values of vertical diffusion, the near surface and and deeper waters are weakly linked. Population in regions suitable for growth are subject to washout while that in the deeper gyres dies out. If connection between the two is increased, (by increasing vertical diffusion), then each region can re-supply the other, so long as the reduction (and transition to negative) intrinsic growth rate is not too rapid. This was confirmed by setting $z_{rc} = 10m$. This led to extremely low values of persistent population at high values of vertical diffusion, (approximately an order of magnitude smaller than the values for persistent population in Fig. 9.8). For the case of higher river flow extinction occurred for all other values of Φ_z. For the smaller values of Φ_z allowing persistence under conditions of lower river flow the situation was the same. In all cases the reason for persistence clearly becomes one of retention in the shallow riverine section of the domain. Fig. 9.11 is used to illustrate this situation. It could be argued that this no longer represents persistence in the fjord itself. The light attenuation coefficient used, ($\varepsilon = 0.22 m^{-1}$), is the lower of the two values cited by Gurney and Nisbet (1998) for Scottish sea lochs. The higher value has associated with it a euphotic depth of $z_{eu} = 9.6m$.

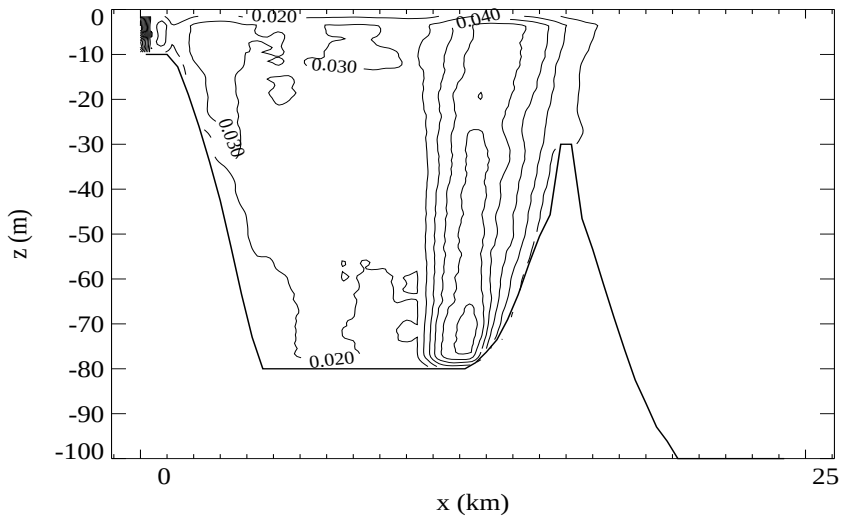

Figure 9.10: *Contours of population density in a tidal fjord, with residual velocities as shown in Fig. 9.1, and depth dependent intrinsic growth rate of* $0.39day^{-1}$ *(*$4.5 \times 10^{-6}s^{-1}$*) at the surface. Light attenuation coefficient,* $\varepsilon = 0.22m^{-1}$*, depth of zero intrinsic growth* $z_{rc} = 20.9m$ *and vertical mixing rate of* $\Phi_z = 1.0 \times 10^{-2.6}m^2s^{-1}$*. Contour intervals 0.01.*

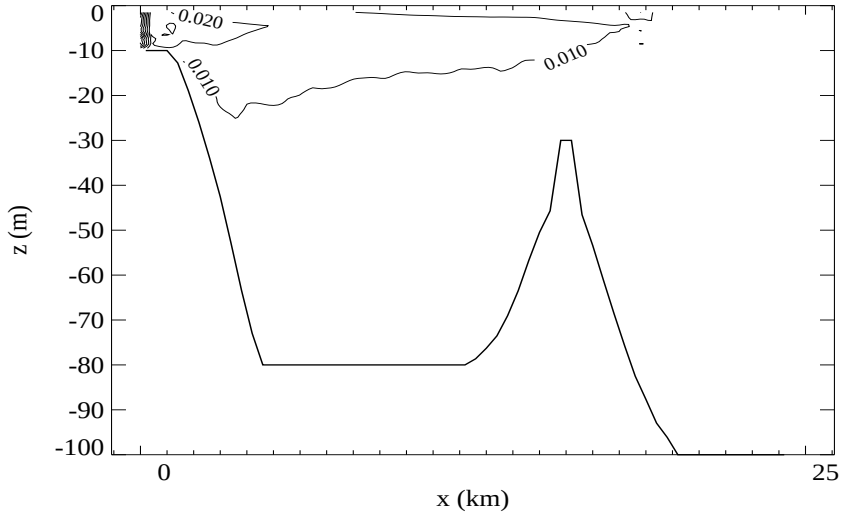

Figure 9.11: *Contours of population density in a tidal fjord, with residual velocities as shown in Fig. 9.2, and depth dependent intrinsic growth rate of* $0.39day^{-1}$ *(*$4.5 \times 10^{-6}s^{-1}$*) at the surface. Light attenuation coefficient,* $\varepsilon = 0.22m^{-1}$*, depth of zero intrinsic growth* $z_{rc} = 10.0m$ *and vertical mixing rate of* $\Phi_z = 1.0 \times 10^{-3.4}m^2s^{-1}$*. Contour intervals 0.01.*

9.3 Vertical motion toward the benthos

9.3.1 Uniform in situ growth rate

In the setting of a coastal plain estuary, a constant sinking speed proved advantageous combined with very small vertical diffusion. In that case, however, there was a clear two layer residual movement that extended the whole depth of the system. In the case of the fjord domain, sinking that is not much modified by turbulent diffusion can be expected to take near surface organisms below the region of two layer flow. Given the circular, or gyre like residual movements in the body of the fjord, (for both flow regimes considered), it is unclear how overall persistence will be affected, at least in the absence of depth dependent growth rates.

Fig. 9.12 contrasts the results for neutrally buoyant organisms with those subject to the constant downward vertical velocity used previously of $V_s = 2.5 \times 10^{-5} ms^{-1}$, in terms of domain mean population density against vertical diffusion. At high diffusion rates the long term populations are virtually identical. At lower values sinking proves detrimental.

The reason is shown clearly in Figs. 9.13 and 9.14 which display population contours for the case of $\Phi_z = 1.0 \times 10^{-5.4} m^2 s^{-1}$. Neither random diffusion or advective currents have prevented the downward velocity from removing individuals from the surface region of the fjord. The greater differences displayed for the case of lower river flow seem due to population becoming absent in the middle of the fjord basin. It is not obvious from inspection of Fig. 9.2 why this should be the case. Increasing vertical diffusion steadily reduces the significance of the downward advective component. Contour plots, (not shown), for organisms with sinking but in the presence of high vertical diffusion appeared very similar to that shown in Fig. 9.5.

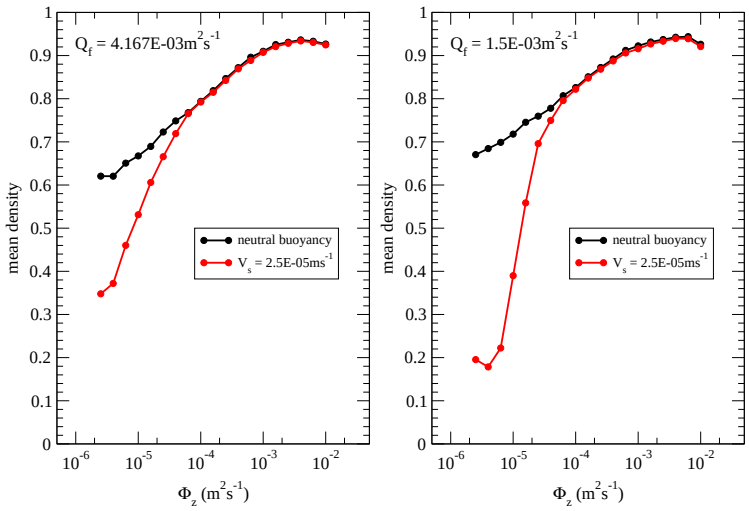

Figure 9.12: *Mean population density in a tidal fjord as a function of the population vertical mixing rate Φ_z. Curves are for a uniform population intrinsic growth rate of $0.39day^{-1}$ $(4.5 \times 10^{-6}s^{-1})$. Black lines show case for neutral buoyancy. Red lines show case for sinking velocity of $V_s = 2.5 \times 10^{-5}ms^{-1}$. Left hand frame; residual movements as in Fig. 9.1, right hand frame; residual movements as in Fig. 9.2.*

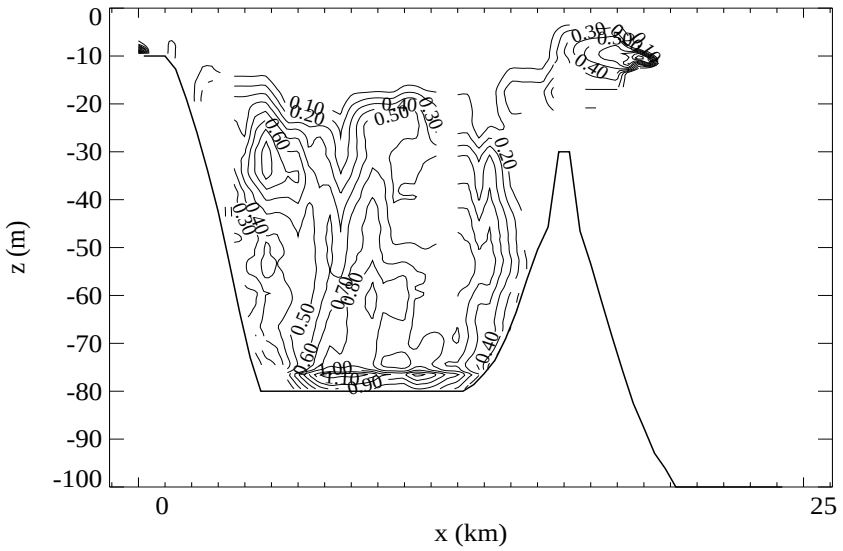

Figure 9.13: *Contours of population density in a tidal fjord, with residual velocities as shown in Fig. 9.1, population intrinsic growth rate of $0.39day^{-1}$ $(4.5 \times 10^{-6}s^{-1})$, sinking velocity of $V_s = 2.5 \times 10^{-5}ms^{-1}$ and vertical mixing rate of $\Phi_z = 1.0 \times 10^{-5.4}m^2s^{-1}$.*

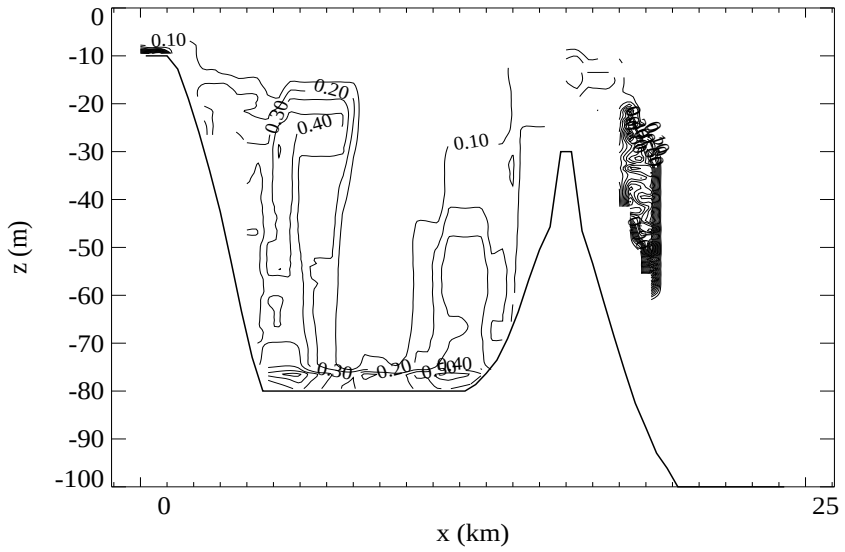

Figure 9.14: *Contours of population density in a tidal fjord, with residual velocities as shown in Fig. 9.2, population intrinsic growth rate of* $0.39day^{-1}$ *(*$4.5 \times 10^{-6}s^{-1}$*), sinking velocity of* $V_s = 2.5 \times 10^{-5}ms^{-1}$ *and vertical mixing rate of* $\Phi_z = 1.0 \times 10^{-5.4}m^2s^{-1}$*.*

9.3.2 Depth dependent growth rate

Given the results for depth dependent growth from section 9.2.2 and that the only significant difference introduced by a sinking velocity was removal of population from the near surface regions in section 9.3 the prospects for persistence when these two attributes are combined is not encouraging. If a light attenuation coefficient of $\varepsilon = 0.22m^{-1}$ is employed and z_{rc} made equal to z_{eu} as before, then persistence at high values of vertical diffusion coefficient is again possible for the same reasons as in the case for neutrally buoyant particles. Surprisingly, in the case of higher river discharge, persistence also just becomes possible for smaller diffusion values. The results for long term population densities when depth dependent growth is used – contrasting the cases with and without sinking – is shown in Fig. 9.15.

For all cases of persistence at vertical diffusion values $\leq 1.0 \times 10^{-3}m^2s^{-1}$, the same pattern of long term population emerges. Population is sustained in the riverine part of the domain and in the gyre like residual flow toward the landward end

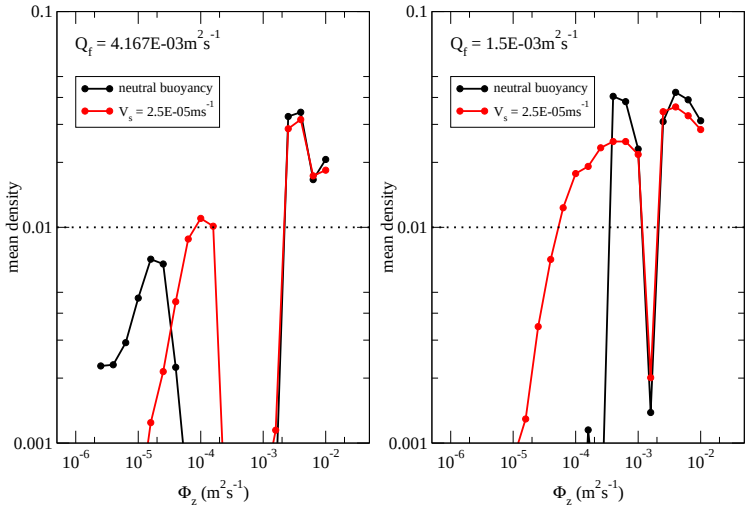

Figure 9.15: *Mean population density in a tidal fjord, (with residual velocities as shown in Fig. 9.1), as a function of the population vertical mixing rate* Φ_z. *Curve for population intrinsic growth rate of* $0.39day^{-1}$ $(4.5 \times 10^{-6}s^{-1})$, *sinking velocity* $V_s = 2.5 \times 10^{-5}ms^{-1}$, *light attenuation coefficient,* ε *equals* $0.22m^{-1}$ *and* $z_{rc} = z_{eu} = 20.9m$, *(intrinsic growth rate critical depth equalling euphotic depth).*

of the fjord basin. Diffusive movement is probably enabling population exchange between the two regions. An example of the population distributions observed is given in Fig. 9.16.

The pattern and scale of persistence is not much changed between the neutrally buoyant case and the case for sinking. It was anticipated that introduction of a critical depth for intrinsic growth of $10m$ might produce results as for section 9.2.2 with the only source of persistence being retention of population in the riverine section of the domain. This did indeed prove to be the case. The conclusion drawn is that with the exception of retention of organisms in that part of the domain representing a river, no mechanism was detected that allowed persistence and did not involve circulation in the deeper part of the fjord.

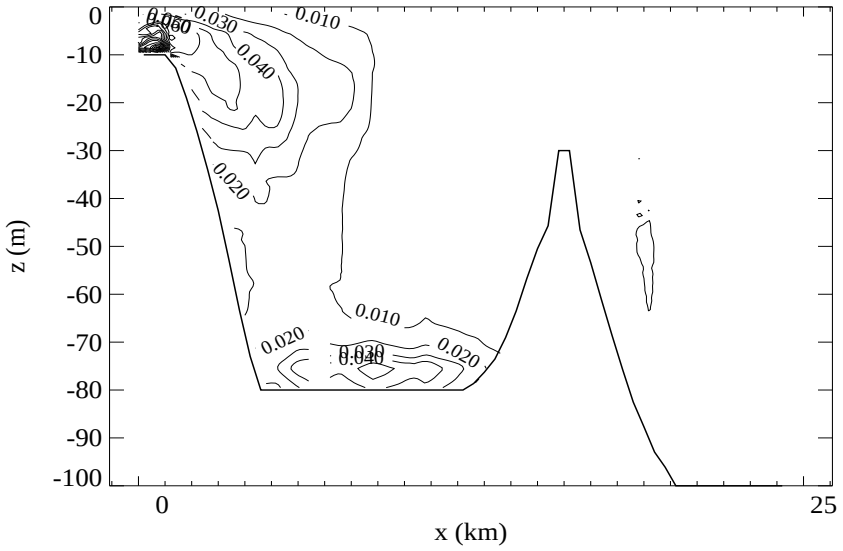

Figure 9.16: *Contours of population density in a tidal estuary, with residual velocities as shown in Fig. 9.2, sinking velocity of* $V_s = 2.5 \times 10^{-5} ms^{-1}$ *and depth dependent intrinsic growth rate of* $0.39 day^{-1}$ $(4.5 \times 10^{-6} s^{-1})$ *at the surface. Light attenuation coefficient,* $\varepsilon = 0.22 m^{-1}$*, depth of zero intrinsic growth* $z_{rc} = 20.9m$ *and vertical mixing rate of* $\Phi_z = 1.0 \times 10^{-4} m^2 s^{-1}$*. Contour intervals 0.01.*

Chapter 10

Overview and Discussion

This thesis has dealt with flow regimes split into four basic categories and considered one or more basic persistence issues for each. The approach, on the whole, has been very strategic. An obvious way forward is to apply the methods developed to comprehensive data sets for given species or groups of species in given hydrodynamic systems. Finding such data is non-trivial in that both reliable hydrodynamic and biological data must be obtained and the two data sets need to be recorded at the same time, or at least at times when abiotic conditions are very similar. Even retaining a more strategic approach, there are many additional issues that can be addressed. The remainder of this chapter discusses the results obtained from chapters 6, 7, 8 and 9 in turn and considers a few of the possibilities for future work.

10.1 1D systems

It was found that if a constant swimming velocity was introduced against the deterministic advection the results regarding key inequalities to be satisfied for persistence, as derived by Speirs and Gurney (2001), can still be applied with a very minor adjustment, namely the subtraction of the swimming velocity from

the advection term. Swimming against a time averaged history of previous net flow, as considered in section 6.2.3, was shown to be less successful. The reason is because net fluid element movements, (conforming to a Gaussian distribution with downstream mean), can be upstream as well as downstream. Upstream movements are smaller on average, however, and the swimming velocity required to completely compensate for them is more often within the maximum attributed to the organisms of the population.

From a hydraulic point of view the one dimensional population models developed seem most applicable to low order shallow streams. The shallow water depth and the size of substrate elements relative to water depth means the effects of turbulence are likely to overwhelm vertical gradients in advection. Traditionally, pelagic plankton have been thought to be virtually absent from headwaters and midreaches of streams, eg (Vannote et al. 1980). Most studies of stream plankton have been lake outlet studies which recorded rapid downstream declines in plankton numbers, (Brown, Limbeck, and Schram 1989). This would point to limited applicability of the initial semi-analytic treatment of organisms permanently in the drift. Brussock, Brown, and Dixon (1985) however, suggested that zooplankton could persist in some abundance in free flowing streams if they possessed a distinct riffle-pool geomorphology. Brown, Limbeck, and Schram (1989) studied the first five orders of a gravel bed stream, (the Illinois River, Arkansas), and found an 'abundant, diverse zooplankton community comparable to that of local reservoirs'. This river was of pool-riffle form and population was concentrated in the pools, with density and abundance especially high when flow through the pools was $< 0.02 ms^{-1}$. As would be expected from the one dimensional analysis the study found an inverse relationship between plankton density and observed flow rate in the pools.

If the pools of such a system were not sufficiently deep to suggest use of the two dimensional model the one dimensional model could be used for each individually. One adjustment necessary might be the alteration of the upstream boundary to account for import of individuals from further upstream. The same could be

done for individual riffle sections. If the horizontal dispersion coefficient, Φ_x was treated as a fitting parameter, the model of section 6.1 could be made to match the overall population density of planktonic species over the system length for a given system averaged flow rate. If used in this way, however, the model is no longer attempting to determine whether representations of turbulent or random motion can predict persistence in any realistic fashion. Population distribution would also not be correct. Brown, Limbeck, and Schram (1989) found densities in the riffles to be much less than in the immediately preceding pool such that a succession of population peaks can be expected for the overall system. This suggests the need for a series of 1D domains linked by common boundaries. The possibility of analytic solutions to such a system has not been investigated. It is also possible that more than just a slow down in overall flow rate is responsible for strong persistence in the pools. Vertically non-uniform advective flow patterns caused by the deepening of the pool and its rise to a lip at the downstream end could be significant. If so, 2D numerical flow simulations would probably be the only way to model the situation.

The variant of one dimensional model including 'clinging' to the benthos is potentially more widely applicable. Many invertebrates live on or amongst the substrate. Their persistence does not seem dependent on a pool-riffle structure and indeed some species are cited as preferring regions of higher velocity and turbulence. Section 6.3.5 showed that although there is no firm evidence for exponential residence times in the benthic state, the existence of exponential residence times in the water column are supported by both theory and field data. What this model can not represent are species which have a nekton developmental stage such as stream insects. Here it seems some form of model of the colonisation cycle still needs to be applied. In turn this requires use of a stage structured model. The $1\frac{1}{2}D$ model could still be useful however, in that it provides a semi-analytic solution to the aquatic stages of the life cycle, while taking into account the intermittent nature of drift events. A problem that would need to be resolved is that both analytic models use the intrinsic growth rate, r, to

non-dimensionalise the problems. For a stage structured model the growth rate during the aquatic phase is zero. It is feasible to use a nominal non-zero growth rate considered sufficiently small not to overly influence the population distribution at the end of aquatic stages. Otherwise an alternative form of scaling must be sought. In either case, the proportion of individuals in the water column could be considered as represented by Equation (6.53) (using the Markov theory). The Markov theory takes no account of population growth and closely approximates the result from the $1\frac{1}{2}D$ solution if exchange rates are high compared to the intrinsic growth rate. An estimate of the proportions of species found in drift and benthos is more likely to be available from field data than rates of drift entry and exit. Equation (6.53) allows determination of these latter parameters.

Non-insect lotic and benthic dwelling stream invertebrates seem less well studied than stream insect larvae. There is evidence of their occurrence in the drift, however, directly from net sampling studies, (Allan et al. 1988; Bergey and Ward 1989).

The analytic tractability of the $1\frac{1}{2}D$ model depends on the assumption of no movement in the benthic 'state'. This assumption is probably valid if considering very small animals such as harpacticoid copepods. Other species, such as *Gammarus* species of amphipod have had significant upstream movements measured , (Elliott 1971b; Marchant and Hynes 1981). Such upstream movements have also been measured for insect larvae, (Elliott 1971b; Hayden and Clifford 1974), although other studies have concluded movements to be random, (Hart and Resh 1980). These upstream movements were not considered enough to compensate for downstream drift but raise the issue of whether results obtained from the semi-analytic treatment are robust enough to be able to ignore the magnitude of upstream movement reported. Performing this test requires use of a form of the discrete space-time simulation. This could be non-trivial because the problem can become 'stiff' as the mean residence time in the water column is made shorter. A simulation model of this problem was developed to test simulation results against the analytic results for the change in critical velocity with clinging

but no benthic movement. As the rate of return from the water column was increased, it was found only very small timesteps, coupled with long periods of simulated time could reproduce the analytic results.

10.2 2D river systems

The longitudinal advection in larger rivers has a vertical profile as discussed in sections 4.3 and 4.4. For organisms with no directed movement, Speirs and Gurney (2001) found the inequalities required for persistence gained from the one dimensional model to be little affected by explicit consideration of depth. After modification to the determination of critical vertical diffusion coefficient, this conclusion remained the same for neutrally buoyant organisms. When a steady sinking speed, V_s, was introduced the value of critical vertical diffusion only increased significantly once $V_s > 2\Lambda_{br}L_c$, that is greater than twice the product of the growth rate at the benthos and the depth of water below the critical depth, (the depth from the surface at which persistence becomes impossible in the absence of vertical diffusion).

For a given stretch of river, the vertical gradient in downstream advection is likely to be much greater than any longitudinal gradient. In the assumption downward movement would be the chief means by which planktonic organisms might show enhanced persistence relative to results from the one dimensional analysis, horizontal swimming was not considered. If a constant horizontal swimming speed is assumed, however, the results of chapter 7 can still be applied, with the proviso that in doing so advections near the benthos becoming upstream must be ignored. If this is considered acceptable then a swimming speed will have the effect of raising the critical depth toward the surface and produce a less negative growth rate at the surface layer. It should be remembered that Λ_{br} was taken as the long term growth rate at the benthos and that this growth rate was used for all depths up to the critical depth. The value of Λ_{br} then is the value obtained when advection is zero. With a constant swimming speed the net horizontal ad-

vection will be rendered zero at some point between the benthos and the new critical depth. Using the long term growth rate at this point for Λ_{br} would seem to remain as reasonable an assumption as in the absence of swimming.

One issue with respect to this work is whether the value of Φ_x associated with each vertical slice of the domain should represent horizontal diffusion or the overall horizontal dispersion of tracers associated with the river. The fact that the original theory of shear flow dispersion is based on movements of particles between different vertical layers, as represented by Equation (2.11) of section 2.1.5 suggests the Φ_x value should simply represent horizontal diffusion. On the other hand, the equation derived by Fischer for dispersion caused by the transverse variations in flow, Equation (2.12), makes no use of the vertical gradient in the horizontal advection, V_x. If Fischer's conclusion, (assuming a large width to depth ratio for the river), that dispersion caused by transverse shear dominates that caused by vertical shear is accepted, this suggests use of dispersion coefficient values for Φ_x is most appropriate. Such dispersion coefficients in this work were derived using Equation (7.47), which can be derived from Equation (2.12) after making some assumptions about parameter values for typical rivers, (Fischer et al. 1979).

The attempt to apply the derivation of critical vertical diffusion coefficient to a real river system, the river Meuse, gave predictions orders of magnitude smaller than an estimate of the expected vertically averaged value, Φ_z, given the same values of shear velocity. If a parabolic vertical profile is assumed for the intensity of vertical diffusion the heights of 'flow refuge' within which the value of Φ_z remains less than the estimated value of Φ_{zc} was found to be very small for all river discharges considered. This was both in absolute terms and as a proportion of the total river depth. It is true that a single depth and width was used for all discharge values. Various studies, (empirical and theoretical), have concluded that river width and depth change with river discharge according to power functions of discharge. A table of different studies and the coefficients and exponents derived are given by Knighton (1984, page 100). Deriving width and depth relationships from such equations allows the possibility for higher horizon-

tal dispersion coefficients from Equation (7.47). Although the general pattern of depth and width alteration with discharge are consistent between studies, the coefficients and exponents used are not. Further, they are highly dependent on the sediment characteristics of the river and these were not known. Unless the values of Φ_x were to rise considerably the basic pessimistic nature of Φ_{zc} forecast is unaltered. Results for Φ_{zc} were derived with the Φ_x values taken as five times their calculated value[1]. Except for the case of lowest river discharge, (where results indicated no limit on Φ_z value), results were still nearly an order of magnitude smaller than the vertically averaged Φ_z value. Additionally, the river slope values calculated are small in comparison to those generally associated with rivers, (Morisawa 1985; Chapra 1997). Smaller slope values lead to higher Φ_x estimates if other variables remain the same.

There does seem growing evidence for potamoplankton populations that are resident in rivers rather than the result of importation from lentic sources. Reynolds and Glaister (1993) found populations of pelagic phytoplankton in the middle reaches of the river Severn, Shropshire including *Stephanodiscus* species. Although nutrient levels were only considered enough for 'moderate' phytoplankton development, recorded downstream increases in population density were greater than could be predicted from assumption of the population at the river head being advected at the mean river flow rate and growing exponentially at its intrinsic growth rate. Moreover, Reynolds (1994a) argues that field data suggests phytoplankton can not be flushed from a river as fast as Fickian models predict, (including use of dispersion coefficients). Other authors have concluded that such models consistently underestimate, sometimes substantially, the actual clearance times of tracers from particular river reaches, (Bencala and Walters 1983). The work of chapter 7 is based on a Fickian model, or at least a series of such models taking their horizontal advection value from the appropriate point on the vertical velocity profile.

An alternative type of model for determining longitudinal transport and disper-

[1]Equation (7.47) is expected to predict Φ_x to within a factor of five.

sion is the 'aggregated dead zone' model, (Wallis, Young, and Beven 1989), which attempts to take the aggregate effect of areas of non-flowing water (dead or storage zones) that exist within what can be considered part of the main channel itself. Such zones have been identified in the field, with enhanced concentrations of planktonic algae, (Reynolds, Carling, and Beven 1991). Beer and Young (1983) suggested that dead zone dispersion dominated turbulent shear flow dispersion. No study is known of, however, that attempts to combine the theory of aggregated dead zones with the mechanism of turbulent diffusion for upstream movements. It is, therefore, a possibility for future study.

A modification to the current approach that could be adopted to see if it improved predictive ability would be to effectively turn the simulation on its side. Instead of depth, the transverse dimension of the river is considered along with domain length. Many 1D domains differentiated vertically are replaced by 1D domains arranged across the transverse direction of the river. Mean advections at given points along the velocity profile are then replaced by estimates of depth averaged advection given a transverse profile of river velocities. It is well known that velocities vary across the transect of rivers and techniques have been established to map these values. Fischer (1967) used such methods to establish his equation for determining longitudinal dispersion coefficients from transverse differences in flow. The study by Reynolds, Carling, and Beven (1991) found persistently higher concentrations of planktonic algae very close to the bottom of a stretch of the river Severn but bigger and more important concentrations toward one bank. Near shore regions with slow flushing rates were also considered to be of vital importance in a study of river zooplankton, (Reckendorfer, Keckeis, Winkler, and Schiemer 1999).

10.3 Tidal estuaries

The investigation of tidal estuaries used two sets of flow conditions that produced very different residual flow characteristics. In the first, all stratification in the system was broken down by internal turbulence part way toward the seaward boundary. This produced a frontal structure in Lagrangian residual movements. In the second the residual flow patterns are very much what can be expected from a partially mixed estuary. It was found that for neutrally buoyant and passive organisms persistence was possible in both systems up to a maximum limit of vertical diffusion. This was true for two cases thought to bracket the bulk of planktonic intrinsic growth rates. For the system with frontal structure there seemed no lower bound to magnitude of vertical diffusion that allowed persistence. This was not true for the partially mixed estuary which required some degree of vertical diffusion to allow persistence.

Beyond a certain limit of vertical diffusion coefficient, population was progressively removed from the shallow end of the system. This is believed to be due to particles becoming sufficiently evenly distributed over the shallower depths of the system as the tidal cycle evolves, that they attain the depth averaged net flow in the system which is always seaward in the presence of river flow. The same phenomenon was recorded for particles given a constant sinking speed and neutrally buoyant particles. It is, however, thought unlikely to be an issue in real systems. Firstly, in the system investigated the effect only became apparent for organismal vertical dispersion coefficients above $1 \times 10^{-3} m^2 s^{-1}$. This value is at the top end of tidally averaged values of vertical diffusion coefficient observed in estuaries with stratification and, depending on the degree of stratification, potentially still high for instantaneous values, (see section 4.3).

It is also probable that even organisms as small as phytoplankton will have an inertia that prevents their random changes in velocity being as rapid or high magnitude as for the surrounding water[2]. Both factors suggest the values of Φ_z

[2]Indeed, this non-complete entrainment is believed beneficial in that it enhances nutrient

causing losses in mean population density are unlikely to occur. Additionally, the phenomenon results from a combination of vertical mixing and water column height. The system investigated here is relatively shallow for an estuary. It is believed deeper systems would not demonstrate the same behaviour unless the value of Φ_z were increased to less realistic values. Finally, simulations were performed with no specification of horizontal diffusion coefficient as it was considered this would normally be dominated by dispersion due to non-uniform advective flows. If rapid vertical mixing eliminates such dispersion, there is still scope for turbulent diffusion to restore some upstream movement.

Introduction of a sinking velocity to organisms had an interesting effect. In the partially mixed estuary, concentration of organisms in upstream regions where net flow is chiefly vertically upwards could actually lead to density dependence reducing overall population levels compared to the case for a neutrally buoyant population. Where sinking did demonstrate an advantage is at very low values of vertical diffusion coefficient. Here sinking could replace diffusive motion as the means to break out of the upper, and seaward bound, deterministic residual flow pattern.

Incorporation of depth dependent intrinsic growth rate produced a surprisingly large difference in overall population densities. If the appropriate abiotic light attenuation coefficients for a system are similar to those for west coast of Scotland sea lochs, it seems results for phytoplankton population levels in systems with an average depth as little as $5m$ must take account of this phenomenon.

An obvious and interesting extension to work in both fjord and coastal plain estuary domains is the incorporation of vertical migration. Selective tidal stream transport, STST, is the easiest to incorporate into the discrete space-time simulation methodology. It is probably only applicable to estuaries. If modelling the larval phase of animals it is appropriate to use a growth rate of zero. In this case the approximation for the discrete time solution of the logistic equation

uptake by allowing fresh medium to pass over the cell surface, (Reynolds 1984, page 18).

developed in section 8.1.4 can be employed. The current 'sinking velocity' constant can be caused to change sign according to the phase of the tidal cycle. A more sophisticated approach would be to change the direction of this movement for each individual track dependent on whether the horizontal velocity being experienced was currently landward or seaward. This allows for phase differences in different parts of an estuary, but also raises the possibility of organisms near the bottom moving upwards during the ebb phase in highly stratified systems. It would be relatively straitforward to develop the tracking program to include data on salinity and or temperature if changes in these quantities were considered more appropriate cues.

One would expect STST behaviour to lead to all population being concentrated at the head of the system. Larvae documented to possibly show such behaviour are only pelagic for a finite period before reverting to a benthic lifestyle. They also tend to enter the estuarine habitat from spawning grounds in the coastal sea. A test of the appropriateness of this behavioural theory would be to initiate a cohort of individuals near the seaward end of a domain, (matched in length, depth, slope and tidal characteristics to a documented system), and to record the final longitudinal positions of individuals after a time thought to represent their pelagic phase.

The incorporation of a 'background' diffusivity in POM to overcome the effective shutting down of the turbulence closure scheme in regions of high Richardson number is not ideal. This number is added everywhere in the domain, regardless of the stratification. Too high a value for this constant may lead to artificially high values of turbulence in regions where the turbulence closure scheme has otherwise made an accurate estimate. One possibility is to incorporate more specialised code within the turbulence closure scheme to parameterise mixing in the pycnocline, (Kantha and Clayson 1994). It is not known, however, whether this would make much difference to the persistence results, qualitatively or quantitatively.

10.4 Fjords

A single strategic characterisation of a fjord was used to investigate persistence for such systems. The same tidal range used for investigation of coastal plain estuaries was employed. Two river inflows were used to give as wide a range of inflow as possible within limits defined by consideration of the ratio of fresh water discharge to tidal inflow in real systems. Given the depth of this system attention was focused on the higher of the planktonic intrinsic growth rates used in this work, considered representative of organisms with the least swimming ability. It was found that if in situ growth was allowed to be uniform very strong persistence was possible for both flow regimes over all values of imposed vertical diffusion considered.

If depth dependent growth rates were introduced, however, long term population densities were cut dramatically. Using the same light attenuation coefficients as used in the case for a plain estuary, persistence in the body of the fjord was only possible for the lower coefficient and if predation was assumed very low or absent. Even then, this was only true for certain values of vertical diffusion. The Lagrangian residuals for the case with higher river discharge had indicated the presence of a two layer residual flow in the surface region of the fjord. It was surprising therefore that use of a critical depth for intrinsic growth rate set just below this feature did not indicate it to have any effect on retention. Instead, with the exception of retention of organisms in that part of the domain representing the river at the head of the system, no mechanism was detected that allowed persistence and did not involve circulation in the deeper part of the fjord.

Introduction of a constant sinking velocity did not show any signs of obvious benefit. In the case of uniform growth long term domain averaged population densities were either unaltered or sinking led to a reduction. Sinking caused no qualitative difference to the effect of depth dependent growth rate on persistence.

Although the present investigation found a lack of a mechanism, (based on resid-

ual fluid motion), acting in the near surface to aid retention, it is too early to conclude they do not exist within fjords. Two parameters whose variation has yet to be considered are sill depth and tidal range. Although of the same basic format, the bathymetry of fjords varies considerably. It is possible, (for Scottish sea lochs at least), for sills to be less than half the depth used in this study, while others are deeper. Turbulent mixing of water relies on kinetic energy. The kinetic energy transported into a fjord basin by the tide is dependent on the combination of the tidal range and the cross sectional area of the outer sill, (Edwards and Sharples 1986). It is therefore possible for the kinetic energy supply for turbulent mixing to be varied independently of the ratio of freshwater runoff to tidal inflow.

This study used a two dimensional vertical slice along what was taken to be the centerline of the fjord. One possibility is that retention of photo-autotrophic organisms relies to some degree on horizontal flow patterns. Fjords often become more narrow in the region of their sills. The head of a fjord is often that much wider than the main river feeding it. These features offer the possibility of horizontal gyres.

It is possible, however, that more complex 'behaviour' than constant sinking (or no behaviour) is required for phytoplankton retention, although it could still be that organisms do not need to be active. The effects of depth and salinity differences ensure the density of water in such systems increases with depth. Organisms negatively buoyant in the 'fresh' surface flow will see their relative density to the surrounding flow reduce with depth. This effect would be especially marked for flows which develop a marked pycnocline. Indeed, studies have indicated that subsurface biomass maxima tend to occur within the pycnocline and at density discontinuities, (Syvitski, Burrell, and Skei 1987, page 214).

To represent correctly the full extent of stratification and the steepness of the density gradient at the pycnocline it may be necessary to include the effects of surface heating. Temperature effects were excluded from this work in order to remove the possibility of confounding joint effects. Dyer (1973) considered that

for estuaries and fjords as a whole temperature would have a relatively small influence on densities. In fjords warming of surface waters during summer can help to stabilise the brackish layer[3], (Syvitski et al. 1987). When using POM, however, once buoyancy frequency has become sufficient to reduce values for eddy diffusion from the turbulence closure scheme to below the specified background level, it is this latter parameter that determines the stability of stratification.

The effect of diurnal migration on persistence in deeper systems is intriguing. This would require slightly greater modification to the present discrete time modelling approach than STST migration mentioned above. The particle tracking program could be run over two tidal cycles including a sinking speed during the first and a rising speed during the second. However, the time step of the resultant population model, one whole day, may well be too long not to influence results. If this were the case, two redistribution matrices would be required from the particle tracking program, one for sinking and one for rising. The population model would then need to alternate between transition matrices.

A more fundamental problem is that the above approach assumes a constant phase between the migration cycle and the tidal cycle. Any longitudinal bias in net tidal cycle movement would then be assumed to continue for the duration of the population model run. The phase differences between these two cycles are known to change throughout the year. The work of Hill (1995) using simple sine waves for tidal velocity and square waves for migration showed sinusoidal patterns of horizontal displacement with no net displacement over seasonal time scales.

This complication does not prevent the tidal cycle being regarded as of constant duration, (and indeed the dominant M2 tide has a steady period of 12.42 hours). If the varying tidal magnitudes of the spring-neap cycle are still ignored use of a single set of flow fields is still possible. The issue then seems to become one of how many transition matrices are required, each representing different phase

[3]Surface cooling in winter has the opposite effect. It mixes surface water downwards through convection.

differences between migration and tide.

10.5 Modelling in three dimensions

When considering 'behaviours' potentially significant to planktonic retention in systems, it is remarkable how much can be investigated at the strategic level without the need to consider a domain in three dimensions. If variation of the advective and/or diffusive components of flow are of primary concern in only one of the axes perpendicular to net flow, modelling in three dimensions can probably be avoided. As considered in section 10.2, in large rivers flow refugia may be more significant in terms of shallow areas at the sides rather than near the benthos. If variation in depth averaged advection across the transverse of the domain is considered to dominate effects from the vertical velocity profile, the problem can be investigated by a two dimensional model.

In the case of fjords, a two dimensional model can again be used to see if features such as horizontal gyres in the lee of areas of rapid flow, (such as the sill or point of river inflow), are important near surface mechanisms for the retention of organisms. Results become potentially less robust in this case however. Significant features of the residual flows created in a horizontal domain may not be retained on inclusion of the third dimension, especially if depths are non-uniform.

A move to three dimensional modelling would allow incorporation of transverse mixing and shear effects into the longitudinal dispersion of populations over a tidal cycle within estuaries and fjords. Also these bodies can become sufficiently wide for the Coriolis force to become significant. The Coriolis force tends to deflect currents to the right in the Northern hemisphere and left in the Southern hemisphere. As mentioned in chapter 2, in wide estuaries this can lead to a transverse residual circulation, which in the Northern hemisphere is a counter-clockwise rotation when looking seawards. The conclusion that very well mixed, (near homogeneous), estuaries lack retentive mechanisms could change if the cir-

culation induced by the Coriolis force, coupled with realistic transverse mixing coefficients, led to enhanced persistence. The Coriolis force is also likely to be important in wide fjords. The onset of such effects is a combination of domain width, latitude and the velocity of water in the system, as determined by the Rossby radius of deformation.

In the POM model it is a simple task to incorporate and specify the magnitude of the Coriolis force. POM also incorporates a representation of friction at lateral boundaries such that transverse velocity shear effects will automatically be present, although this representation, described as 'half slip' is relatively crude. The effect of bottom friction and the resulting vertical profiles of turbulence and velocity, however, are represented as accurately as possible, (within the limits imposed by reasonable computational cost). The reduced momentum of near shore flows therefore, should be represented well if the domain cross section is made more shallow moving away from the centre line. This should introduce a more realistic element of transverse shear as well as allowing the possibility of representing tidal pumping.

Appendix A

Exponential growth in a well-mixed river

Solutions are sought to the balance equation

$$\frac{\partial n}{\partial t} = rn - V_x \frac{\partial n}{\partial x} + \Phi_x \frac{\partial^2 n}{\partial x^2} \tag{A.1}$$

with boundary conditions at the left and right ends of the domain of

$$V_x n(0,t) - \Phi_x \left(\frac{\partial n}{\partial x}\right)_{x=0} = 0 \tag{A.2}$$

and

$$n(L,t) = 0 \tag{A.3}$$

To simplify the problem the following scaled terms are introduced

$T \equiv t/t_0 \quad$ where $t_0 = r^{-1}$

$X \equiv x/x_0 \quad$ where $x_0 = L_d \equiv \sqrt{\Phi_w r^{-1}}$

$\omega \equiv \alpha/\alpha_0$ where $\alpha_0 = r$

$\sigma \equiv \beta/\beta_0$ where $\beta_0 = r$

$\nu \equiv V_w/V_0$ where $V_0 = V_d \equiv 2\sqrt{\Phi_w r}$

Substituting these scaled terms into Equations (A.1) to (A.3) yields

$$\frac{\partial n}{\partial T} = n - 2\nu\frac{\partial n}{\partial X} + \frac{\partial^2 n}{\partial X^2} \tag{A.4}$$

with boundary conditions

$$\begin{aligned} 2\nu n(0,T) - \left.\frac{\partial n}{\partial X}\right|_{X=0} &= 0 && \text{(A.5)} \\ n(l,T) &= 0 && \text{(A.6)} \end{aligned}$$

where $l \equiv L/L_d$.

Solutions are sought in the form

$$n(x,t) = e^{\lambda T} f(X) \tag{A.7}$$

where λ is the scaled long term growth rate. Back-substituting into Equation (A.4) gives

$$\begin{aligned} \lambda f &= f - 2\nu\frac{\partial f}{\partial X} + \frac{\partial^2 f}{\partial X^2} \\ 0 &= (1-\lambda)f - 2\nu\frac{df}{dX} + \frac{d^2 f}{dX^2} && \text{(A.8)} \end{aligned}$$

This is a second-order ordinary differential equation with constant coefficients, which has the general solution

$$f(X) = Ae^{\gamma_1 X} + Be^{\gamma_2 X} \tag{A.9}$$

where A, B are arbitrary constants and γ_1 and γ_2 are given by the roots of the auxiliary equation

$$\gamma^2 - 2\nu\gamma + (1 - \lambda) = 0 \tag{A.10}$$

such that

$$\gamma_1 = \nu - \psi, \quad \gamma_2 = \nu + \psi, \quad \psi \equiv \sqrt{\nu^2 - (1 - \lambda)} \tag{A.11}$$

A.1 High velocity case: γ_1, γ_2 and ψ real

If the scaled velocity is high enough to ensure that

$$\nu^2 > (1 - \lambda) \tag{A.12}$$

then γ_1, γ_2 and ψ are real. To satisfy the left hand boundary condition requires

$$-\frac{A}{B} = \frac{2\nu - \gamma_2}{2\nu - \gamma_1} = \frac{\nu - \psi}{\nu + \psi} \tag{A.13}$$

while matching the right hand boundary condition requires

$$-\frac{A}{B} = \exp[(\gamma_2 - \gamma_1)l] = \exp(2\psi l) \tag{A.14}$$

If $\psi > 0$ then Equation (A.14) requires $(-A/B) > 1$ while Equation (A.13) requires $(-A/B) < 1$. If $\psi < 0$ the inequalities are reversed. The incompatibility of requirements (A.13) and (A.14) means that when the velocity satisfies inequality

(A.12) there is no solution of the form (A.7) which can satisfy both boundary conditions.

A.2 Low velocity case: ψ imaginary; γ_1 and γ_2 complex conjugates

If inequality (A.12) is violated ψ is imaginary and γ_1 and γ_2 are complex conjugates such that they can be expressed as a combination of real and imaginary parts

$$\gamma_1 = \nu - ki, \qquad \gamma_2 = \nu + ki, \qquad k \equiv \sqrt{(1-\lambda) - \nu^2} \tag{A.15}$$

The general solution of Equation (A.8) can be rewritten as

$$f(X) = Ae^{\xi X}\cos kX + Be^{\xi X}\sin kX \tag{A.16}$$

where $\xi \equiv \nu$.

Matching the left hand boundary condition now requires

$$A(2\nu - \nu) - kB = 0 \rightarrow \frac{A}{B} = \frac{k}{\nu} \tag{A.17}$$

while matching the right hand boundary requires

$$-\frac{A}{B} = \tan kl \tag{A.18}$$

A solution matching both boundary conditions is therefore one for which

$$\tan kl = -\frac{k}{\nu} \tag{A.19}$$

Converting Equation (A.19) back into dimensional form gives

$$\tan\left(\kappa\frac{L}{L_d}\right) = -\frac{V_d}{V_x}\kappa \tag{A.20}$$

where κ is the dimensional form of k such that

$$\kappa \equiv \sqrt{\left(1-\frac{\Lambda}{r}\right) - \left(\frac{V_x}{V_d}\right)^2} \tag{A.21}$$

A.3 Obtaining values of the long term growth rate λ

If parameters l and ν are fixed, Equation (A.19) can be satisfied by an infinite series of values for k, any for which the straight line $-k/\nu$ cuts the curves for $\tan kl$. From Equation (A.15), however, it can be seen that negative values of k will always have a positive equivalent of the same magnitude and with ν fixed this must be derived using the same value of λ. Also from Equation (A.15) it can be seen that the maximum possible value for λ is obtained from the smallest possible value for k. This suggests that $k = 0$ provides the maximum scaled long term growth rate. Substituting $k = 0$ back into the general solution given by Equation (A.16), however, means that the right hand boundary of the system requires

$$Ae^{\nu l} = 0 \tag{A.22}$$

This can only be satisfied if $A = 0$, which in turn implies $\forall X,\ f(X) = 0$, that is a system containing zero population. The smallest non-zero value for k therefore gives the maximum possible value for λ and will be found in the region $\pi/2 < kl < \pi$. The actual intersection is easily found by a bisection algorithm.

Appendix B

Analytic Solution for flow in a Tidal River

A solution is sought for a two dimensional fluid flow, with horizontal velocity, V_x and sea surface elevation, η, described by the following equations.

$$\frac{\partial V_x}{\partial t} = -g\frac{\partial \eta}{\partial x} + \Phi_e \frac{\partial^2 V_x}{\partial z^2}, \qquad \frac{\partial \eta}{\partial t} = -\int_0^H \frac{\partial V_x}{\partial x} dz \tag{B.1}$$

The solution must satisfy the following flow boundary conditions at the landward ($x = 0$) and seaward ($x = L$) ends of the system

$$V_x(0, 0, t) = V_R, \qquad V_x(L, 0, t) = V_R + V_T \cos 2\pi \frac{t}{T} \qquad \forall t \tag{B.2}$$

where T is the tidal period, and conditions of zero wind stress at the mean free surface and zero slip at the bottom

$$\left.\frac{\partial V_x}{\partial z}\right|_{z=0} = 0, \qquad V_x(x, H, t) = 0 \qquad \forall t \tag{B.3}$$

This problem is completely linear. As such the solution can be a superposition of

the flow generated by the river, (V_r), and that generated by the tide, (V_t). The river input is constant, such that the flow generated is steady (independent of time) and uniform (independent of x). A solution is therefore sought of the form

$$V_x = V_s(z) + V_t(x, z, t) \tag{B.4}$$

The surface elevation can also be split into that associated with the river flow, (η_r), and that associated with the tidal flow, (η_t). From Equations (B.1), the assumption that the river generated flow is steady and uniform implies that $\partial\eta_r/\partial t = 0$. Such flow also implies that $\partial\eta_r/\partial x = -H'$, where H' is a constant. This is consistent with Equations (B.1) if

$$\frac{\partial^2 V_r}{\partial z^2} = \frac{g}{\Phi_e}\frac{\partial V_r}{\partial x} = -\frac{gH'}{\Phi_e} \tag{B.5}$$

The general solution of Equation (B.5) is $V_r = A + Bz - (gH'/2\Phi_e)z^2$, where A and B are arbitrary constants. To satisfy the top boundary condition on V_x, (Equation B.3), $B = 0$. To ensure $V_r(0) = V_R$, A is set equal to V_R. To satisfy the second element of Equation (B.3), H' must be set such that $H' = 2\Phi_e V_R/(gH^2)$. This gives a final solution for V_r of

$$V_r = V_R\left(1 - \left[\frac{z}{H}\right]^2\right) \tag{B.6}$$

The equations for V_t and η_t become

$$\frac{\partial V_t}{\partial t} = -g\frac{\partial \eta_t}{\partial x} + \Phi_e\frac{\partial^2 V_t}{\partial z^2} \tag{B.7}$$

and

$$\frac{\partial \eta_t}{\partial t} = -\int_0^H \frac{\partial V_t}{\partial x}dz \tag{B.8}$$

To solve this equation it is assumed that the solution is the sum of a term which is independent of z, (V_{t0}), and a z dependent term, (V_{t1}). If the z-dependence of V_{t1} is separable and the x and t dependence of V_{t1} and V_{t0} is the same, then $V_{t1} = V_{t0}\phi(z)$, and the general form of the solution for V_t is given by

$$V_t = V_{t0}\phi(z) \tag{B.9}$$

Substituting this form of the general solution into Equations (B.7) and (B.8) yields

$$\phi\frac{\partial V_{t0}}{\partial t} = -g\frac{\partial \eta_t}{\partial x} + \Phi_e V_{t0}\frac{\partial^2 \phi}{\partial z^2} \tag{B.10}$$

$$\frac{\partial \eta_t}{\partial t} = -H\bar{\phi}\frac{\partial V_{t0}}{\partial x} \tag{B.11}$$

where $\bar{\phi}$ represents the average value of ϕ over the water column. Differentiating Equation (B.10) with respect to time and back substituting for $\partial\eta_t/\partial t$ leads to

$$\phi\frac{\partial^2 V_{t0}}{\partial t^2} = gH\bar{\phi}\frac{\partial^2 V_{t0}}{\partial x^2} + \Phi_e\frac{\partial V_{t0}}{\partial t}\frac{\partial^2 \phi}{\partial z^2} \tag{B.12}$$

Now, a trial solution is assumed of the form

$$V_{t0} = e^{i\omega t}e^{ikx} \quad where \quad k^2 = \frac{\omega^2}{gH} \tag{B.13}$$

This allows Equation (B.12) to be written in the form

$$\omega^2(\phi - \bar{\phi}) = -i\omega\Phi_e\frac{\partial^2 \phi}{\partial z^2} \tag{B.14}$$

Defining $\phi' \equiv \phi - \bar{\phi}$, this becomes

$$\frac{\partial^2 \phi'}{\partial z^2} = i\frac{\omega}{\Phi_e}\phi' \tag{B.15}$$

whose generic solutions are of the form $\phi' = e^{imz}$ where

$$m^2 = -i\frac{\omega}{\Phi_e} \quad \rightarrow \quad m = \overset{+}{-}\left(\frac{1-i}{\sqrt{2}}\right)\sqrt{\frac{\omega}{\Phi_e}} \tag{B.16}$$

There is now a full generic solution to the tidal velocity component, V_t, namely

$$V_t = \Psi_1 e^{\overset{+}{-}i\omega t} e^{\overset{+}{-}ikx}(1 + \Psi_2 e^{\overset{+}{-}mz}) \tag{B.17}$$

where Ψ_1 and Ψ_2 are arbitrary constants and m and k are defined as above.

Appendix C

Analytic Solution for flow in a Tidal River: Semi-sigma Coordinates

With the introduction of semi-sigma coordinates into the fluid flow equations presented in Appendix B, the momentum equation becomes

$$\frac{\partial V_x}{\partial t} = -g\frac{\partial \eta}{\partial x} + \frac{H^2}{D^2}\Phi_e \frac{\partial^2 V_x}{\partial z_\sigma^2} \tag{C.1}$$

and the continuity equation takes the form

$$\frac{\partial V_x}{\partial x} + \frac{H}{D}\frac{\partial V_z}{\partial z_\sigma} = 0 \tag{C.2}$$

Boundary conditions

The landward and seaward boundary conditions on $V_{x\sigma}$ can simply be stated as

$$V_{x\sigma}(0, z_\sigma = 0, t) = V_R, \qquad V_{x\sigma}(L, z_\sigma = 0, t) = V_R + V_T \cos 2\pi \frac{t}{T} \qquad \forall t \tag{C.3}$$

and that at the bottom as

$$V_{x\sigma}(x, z_\sigma = H, t) = 0 \qquad \forall t \tag{C.4}$$

For the free surface condition we note that (with both z_σ and z defined positive towards the benthos)

$$\begin{aligned} z_\sigma &= -\sigma H = -\left(\frac{-z-\eta}{D}\right) H = \frac{zH + \eta H}{D} \\ \frac{\partial z_\sigma}{\partial z} &= \frac{H}{D} \end{aligned} \tag{C.5}$$

so

$$\begin{aligned} \frac{H}{D} \frac{\partial V_{x\sigma}}{\partial z_\sigma}\bigg|_{z_\sigma = 0} &= 0 \\ \frac{\partial V_{x\sigma}}{\partial z_\sigma}\bigg|_{z_\sigma = 0} &= 0 \end{aligned} \tag{C.6}$$

This new free surface condition has the bonus that it applies to wherever the free surface sits at any point in time rather than simply to the mean free surface level.

To implement the new version of the model, new top and bottom boundary conditions on V_z are required. At the bottom flow is forced to become parallel to the bottom, while at the free surface the boundary condition implies that the surface rises and falls in response to flow which is not parallel to the free surface, so that

$$V_z(x, -H, t) = -V_x(x, -H, t) \frac{\partial H}{\partial x} \tag{C.7}$$

$$V_z(x,\eta,t) = V_x(x,\eta,t)\frac{\partial \eta}{\partial x} + \frac{\partial \eta}{\partial t} \tag{C.8}$$

The new bottom boundary condition, (Equation C.7), is consistent with the requirement from the initial version of the model that the vertical velocity is zero at all times because $V_{x\sigma}$ is required to be zero at the bottom.

The new top boundary condition for V_z, (Equation C.8) is also consistent with the non-sigma version for the same reason. With $V_x(x,-H,t) = 0$ the equation for $\partial\eta/\partial t$, Equation (C.13) below, can be written as

$$\frac{\partial \eta}{\partial t} = -V_x(x,\eta,t)\frac{\partial \eta}{\partial x} - \int_{-H}^{\eta} \frac{\partial V_x}{\partial x} dz \tag{C.9}$$

Back substituting for $\partial\eta/\partial t$ into Equation (C.8) gives

$$V_z(x,\eta,t) = -\int_{-H}^{\eta} \frac{\partial V_x}{\partial x} dz \tag{C.10}$$

which is the exact equivalent of Equation (4.47) given that $\partial\eta/\partial t \equiv V_z(\eta)$ in the non-sigma version.

One discrepancy between the two versions of the model is that $\partial\eta/\partial t \equiv V_z(\eta)$ does not hold in the sigma version. In the non-sigma version $\partial\eta/\partial t$ can become zero when $\partial\eta/\partial x \neq 0$. This is only possible however when there is steady river flow but no tidal flow. The gradient $\partial\eta/\partial x$ caused by steady river flow (see Appendix B) is very small for the river velocities of interest in this work and the difference is not considered significant.

New continuity equation

The utility of this new depth measure can be seen once the continuity equation is re-defined in terms of the surface elevation and a vertically averaged horizontal velocity as described below.

Starting with the continuity equation as defined in Equation (4.46), this implies that

$$V_z(x,z,t) = V_z(x,-H,t) - \int_{-H}^{z} \frac{\partial V_x}{\partial x} dz \tag{C.11}$$

Following Blumberg and Mellor (1987) the top and bottom boundary conditions of Equations (C.7) and (C.8) are imposed on V_z. Back substituting Equation (C.7) into Equation (C.11) gives

$$V_z(x,z,t) = -V_x(x,-H,t)\frac{\partial H}{\partial x} - \int_{-H}^{z} \frac{\partial V_x}{\partial x} dz \tag{C.12}$$

and back substituting Equation (C.12) into Equation (C.8) in turn gives

$$\frac{\partial \eta}{\partial t} + V_x(x,\eta,t)\frac{\partial \eta}{\partial x} + V_x(x,-H,t)\frac{\partial H}{\partial x} + \int_{-H}^{\eta} \frac{\partial V_x}{\partial x} dz = 0 \tag{C.13}$$

To simplify Equation (C.13), a vertically averaged horizontal velocity is defined

$$\hat{U} \equiv \frac{1}{D(x,t)} \int_{-H(x)}^{\eta(x,t)} V_x dz \tag{C.14}$$

from which it is noted that

$$\frac{\partial}{\partial x}(D\hat{U}) = V_x(x,\eta,t)\frac{\partial \eta}{\partial x} + V_x(x,-H,t)\frac{\partial H}{\partial x} + \int_{-H}^{\eta} \frac{\partial V_x}{\partial x} dz \tag{C.15}$$

Comparing Equations (C.15) and (C.13) shows that

$$\frac{\partial \eta}{\partial t} = -\frac{\partial}{\partial x}(D\hat{U}) \tag{C.16}$$

Comparing the relationship between horizontal velocities defined using the three vertical co-ordinate systems of z, σ and z_σ, namely

$$U(x,\sigma,t) \equiv V_x(x, D\sigma + \eta, t) \equiv V_{x\sigma}(x, -\sigma H, t) \tag{C.17}$$

and noting that

$$\begin{aligned} \sigma &= \frac{z-\eta}{D} \rightarrow \frac{d\sigma}{dz} = \frac{1}{D} \\ z_\sigma &= -\sigma H \rightarrow \frac{dz_\sigma}{d\sigma} = -H \end{aligned} \tag{C.18}$$

from this comparison it can be seen that $\hat{U}$ can be written as

$$\hat{U} \equiv \int_{-1}^{0} U(x,\sigma,t)d\sigma \equiv -\frac{1}{H(x)} \int_{H(x)}^{0} V_{x\sigma} dz_\sigma \equiv \frac{1}{H(x)} \int_{0}^{H(x)} V_{x\sigma} dz_\sigma \tag{C.19}$$

Expanding Equation (C.16) according to those elements dependent on x gives

$$\frac{\partial \eta}{\partial t} = -\left\{ H\frac{\partial \hat{U}}{\partial x} + \eta\frac{\partial \hat{U}}{\partial x} + \hat{U}\frac{\partial \eta}{\partial x} \right\} \tag{C.20}$$

The $\hat{U}$ term can be found by integrating the right hand side of Equation (4.52) between zero and H and dividing by H. The $\partial\hat{U}/\partial x$ terms are given by the right hand side of Equation (4.53) evaluated at $z = 0$ and divided by H. If initial values of η are assumed at $t = 0$, calculation of η for any point in time or space becomes possible. In this work the $\partial\eta/\partial x$ term was found by central differencing. A look-up table was constructed of surface elevations at each of the cell centres from which particles were tracked, with values for each tracking timestep within the tidal period.

This form of the equation for the rate of change of surface elevation with time, (unlike Equation 4.49), does not break continuity for non-zero η values in as much as the rate of change of surface elevation with time is always internally consistent with the velocities being calculated within the water column and the depth of

water, D, over which these velocities are allowed to exist. It is still true, however, that the velocities are calculated making the assumption that η remains zero. Given the new form of the continuity equation this is equivalent to assuming that $\partial\eta/\partial t = -\partial(H\hat{U})/\partial x$.

Unsolved equation for V_t using z_σ co-ordinates

In solving for V_t we wish to follow the same procedure as in Appendix B and therefore differentiate the equivalent of Equation (B.10) with respect to time. The momentum equation for V_t is now in the form

$$\frac{\partial V_t}{\partial t} = -g\frac{\partial \eta_t}{\partial x} + \frac{H^2}{D^2}\Phi_e\frac{\partial^2 V_t}{\partial z_\sigma^2} \tag{C.21}$$

and this leads to

$$\begin{aligned}
\phi\frac{\partial^2 V_{t0}}{\partial t^2} &= gH\bar{\phi}\frac{\partial^2 V_{t0}}{\partial x^2} + H^2\Phi_e\frac{\partial^2\phi}{\partial z_\sigma^2}\left[\frac{\partial}{\partial D}\left(\frac{V_{t0}}{D^2}\right)\cdot\frac{\partial D}{\partial t} + \frac{\partial}{\partial V_{t0}}\left(\frac{V_{t0}}{D^2}\right)\cdot\frac{\partial V_{t0}}{\partial t}\right] \\
\phi\frac{\partial^2 V_{t0}}{\partial t^2} &= gH\bar{\phi}\frac{\partial^2 V_{t0}}{\partial x^2} + H^2\Phi_e\frac{\partial^2\phi}{\partial z_\sigma^2}\left[\frac{-2V_{t0}}{D^3}\frac{\partial\eta}{\partial t} + \frac{1}{D^2}\frac{\partial V_{t0}}{\partial t}\right] \\
\phi\frac{\partial^2 V_{t0}}{\partial t^2} &= gH\bar{\phi}\frac{\partial^2 V_{t0}}{\partial x^2} + \frac{H^2}{D^2}\Phi_e\frac{\partial^2\phi}{\partial z_\sigma^2}\left[\frac{-2V_{t0}}{D}\frac{\partial\eta}{\partial t} + \frac{\partial V_{t0}}{\partial t}\right]
\end{aligned} \tag{C.22}$$

Substituting from the trial solution of Equation (B.13), namely $V_{t0} = e^{i\omega t}e^{ikx}$ with $k^2 = \omega^2/gH$, gives

$$\begin{aligned}
(i\omega)^2 V_{t0}\phi &= gH\bar{\phi}(ik)^2 V_{t0} + V_{t0}\frac{H^2}{D^2}\Phi_e\frac{\partial^2\phi}{\partial z_\sigma^2}\left[i\omega - \frac{2}{D}\frac{\partial\eta}{\partial t}\right] \\
-\omega^2\phi &= -\omega^2\bar{\phi} + \frac{H^2}{D^2}\Phi_e\frac{\partial^2\phi}{\partial z_\sigma^2}\left[i\omega - \frac{2}{D}\frac{\partial\eta}{\partial t}\right] \\
\omega^2(\phi - \bar{\phi}) &= \frac{H^2}{D^2}\Phi_e\frac{\partial^2\phi}{\partial z_\sigma^2}\left[\frac{2}{D}\frac{\partial\eta}{\partial t} - i\omega\right]
\end{aligned} \tag{C.23}$$

and defining $\phi' \equiv \phi - \bar{\phi}$, and re-arranging leads to

$$\frac{\partial^2 \phi'}{\partial z_\sigma^2} = \left[\frac{\frac{D^2 \omega^2}{H^2 \Phi_e}}{\left(\frac{2}{D} \frac{\partial \eta}{\partial t} - i\omega \right)} \right] \phi' \tag{C.24}$$

Appendix D

Exponential growth in a well-mixed river: Transfer between drift and benthos

It should be remembered it is assumed organisms stay in the drift and benthos with exponentially distributed residence times and that they are motionless while in the benthos.

This problem can be defined as a coupled set of partial differential equations

$$\frac{\partial n}{\partial t} = rn - \beta n + \alpha m - V_w \frac{\partial n}{\partial x} + \Phi_w \frac{\partial^2 n}{\partial x^2} \tag{D.1}$$

$$\frac{\partial m}{\partial t} = rm - \alpha m + \beta n \tag{D.2}$$

Boundary conditions are, (as for the case of particles permanently in the drift), that of zero flux at the left hand boundary

$$V_w n(0,t) - \Phi_w \frac{\partial n}{\partial x}\bigg|_{x=0} = 0 \tag{D.3}$$

and an absorbing boundary at the right hand end of the system

$$n(L,t) = 0 \tag{D.4}$$

To simplify the problem the following scaled terms are introduced

$T \equiv t/t_0$ where $t_0 = r^{-1}$

$X \equiv x/x_0$ where $x_0 = L_d \equiv \sqrt{\Phi_w r^{-1}}$

$\omega \equiv \alpha/\alpha_0$ where $\alpha_0 = r$

$\sigma \equiv \beta/\beta_0$ where $\beta_0 = r$

$\nu \equiv V_w/V_0$ where $V_0 = V_d \equiv 2\sqrt{\Phi_w r}$

Substituting these scaled terms into Equations (D.1) and (D.2) yields a simplified set of equations

$$\frac{\partial n}{\partial T} = n - \sigma n + \omega m - 2\nu \frac{\partial n}{\partial X} + \frac{\partial^2 n}{\partial X^2} \tag{D.5}$$

$$\frac{\partial m}{\partial T} = m - \omega m + \sigma n \tag{D.6}$$

with boundary conditions

$$2\nu n(0,T) - \left.\frac{\partial n}{\partial X}\right|_{X=0} = 0 \tag{D.7}$$

$$n(l,T) = 0 \tag{D.8}$$

where $l \equiv L/L_d$.

In seeking a trial solution it is assumed that the solution, after initial transients have died away, will take the form of a static spatial pattern which scales exponentially with time and that the population in the benthos will be a time independent proportion of the population in the drift. That is we seek solutions of the form

$$\begin{aligned} n &= e^{\lambda T} f(X) \\ m &= \theta n \end{aligned} \tag{D.9}$$

where θ is the constant of proportionality between m and n and λ is the scaled long term growth rate. Back-substituting into Equations (D.5) and (D.6) gives

$$\lambda f(X) = f(X) - \sigma f(X) + \omega\theta f(X) - 2\nu\frac{df}{dX} + \frac{d^2 f}{dX^2} \tag{D.10}$$

and

$$\theta\lambda = \theta + \sigma - \omega\theta \tag{D.11}$$

Using the relationship between $-\sigma + \omega\theta = \theta(1 - \lambda)$ from equation (D.11) in equation (D.10) we obtain

$$0 = (1 - \lambda)(1 + \theta)f - 2\nu\frac{df}{dX} + \frac{d^2 f}{dX^2} \tag{D.12}$$

With this trial solution boundary conditions become

$$2\nu f(0) - \left.\frac{df}{dx}\right|_{x=0} = 0 \tag{D.13}$$

$$f(l) = 0 \tag{D.14}$$

In a similar manner to the case for a permanently water borne particle we are left with a second order linear O.D.E. with constant coefficients. This has solutions of the form

$$f(X) = Ae^{\gamma_1 X} + Be^{\gamma_2 X} \tag{D.15}$$

where γ_1 and γ_2 are given by the roots of the auxiliary equation

$$\gamma^2 - 2\nu\gamma + (1-\lambda)(1+\theta) = 0$$

Therefore

$$\begin{aligned}
\gamma_1 &= \frac{2\nu - \sqrt{4\nu^2 - 4(1-\lambda)(1+\theta)}}{2} \\
&= \nu - \sqrt{\nu^2 - (1-\lambda)(1+\theta)} \\
&= \nu - \psi
\end{aligned}$$

$$\begin{aligned}
\gamma_2 &= \frac{2\nu + \sqrt{4\nu^2 - 4(1-\lambda)(1+\theta)}}{2} \\
&= \nu + \sqrt{\nu^2 - (1-\lambda)(1+\theta)} \\
&= \nu + \psi
\end{aligned}$$

where $\psi \equiv \sqrt{\nu^2 - (1-\lambda)(1+\theta)}$.

D.1 High velocity case: γ_1, γ_2 and ψ real

For γ_1, γ_2 and ψ to be real we require

$$\nu^2 > (1-\lambda)(1+\theta) \tag{D.16}$$

To satisfy the left hand boundary condition we require

$$\begin{aligned} 2\nu(Ae^{\gamma_1 0} + Be^{\gamma_2 0}) - (A\gamma_1 e^{\gamma_1 0} + B\gamma_2 e^{\gamma_2 0}) &= 0 \\ 2\nu(A+B) - (A\gamma_1 + B\gamma_2) &= 0 \\ \frac{-A}{B} &= \frac{2\nu-\gamma_2}{2\nu-\gamma_1} \\ \frac{-A}{B} &= \frac{\nu-\psi}{\nu+\psi} \end{aligned} \tag{D.17}$$

To satisfy the right hand boundary condition requires

$$\begin{aligned} Ae^{\gamma_1 l} + Be^{\gamma_2 l} &= 0 \\ \frac{-A}{B} &= e^{(\gamma_2-\gamma_1)l} \\ \frac{-A}{B} &= e^{2\psi l} \end{aligned} \tag{D.18}$$

If $\psi > 0$ the left hand boundary condition requires $-A/B < 1$; the right hand boundary condition requires $-A/B > 1$.
If $\psi < 0$ the left hand boundary condition requires $-A/B > 1$; the right hand boundary condition requires $-A/B < 1$.

Thus, when the scaled velocity satisfies inequality (D.16) there is no solution of the form (D.9) which satisfies both boundary conditions.

D.2 Low velocity case: ψ imaginary; γ_1 and γ_2 complex conjugates

With γ_1 and γ_2 as complex conjugates they can be expressed as a combination of real and imaginary parts

$$\begin{aligned} \gamma_1 &= \nu - ki \\ \gamma_2 &= \nu + ki \end{aligned}$$

where $k \equiv \sqrt{(1-\lambda)(1+\theta) - \nu^2}$, and the general solution of equation (D.12) can be written as

$$f(x) = Ae^{\xi x}\cos kx + Be^{\xi x}\sin kx \tag{D.19}$$

where $\xi \equiv \nu$.

The left hand boundary condition therefore requires that

$$\begin{aligned} 0 &= 2\nu e^{\nu 0}(A\cos k0 + B\sin k0) \\ &\quad -[e^{\nu 0}(-kA\sin k0 + kB\cos k0) + \nu e^{\nu 0}(A\cos k0 + B\sin k0)] \\ 0 &= 2\nu A - kB - \nu A \\ \frac{A}{B} &= \frac{k}{\nu} \end{aligned} \tag{D.20}$$

The right hand boundary requires that

$$\begin{aligned} 0 &= e^{\nu l}(A\cos kl + B\sin kl) \\ 0 &= 1 + \frac{B}{A}\tan kl \\ \frac{A}{B} &= -\tan kl \end{aligned} \tag{D.21}$$

A solution matching both boundary conditions is one for which

$$\tan kl = -\frac{k}{\nu} \tag{D.22}$$

where

$$k = \sqrt{(1-\lambda)\left(1 - \frac{\sigma}{1-\lambda-\omega}\right) - \nu^2} \tag{D.23}$$

Converting equation (D.22) back to dimensional form gives

$$\tan(\kappa \frac{L}{L_d}) = -\frac{V_d}{V_w}\kappa \tag{D.24}$$

where κ is the dimensional form of k such that

$$\kappa = \sqrt{(1-\frac{\Lambda}{r})\left(1 + \frac{\beta}{\alpha+\Lambda-r}\right) - \left(\frac{V_w}{V_d}\right)^2} \tag{D.25}$$

or

$$\kappa = \sqrt{(1-\frac{\Lambda}{r})\left(1 + \frac{\frac{\beta}{r}}{\frac{\alpha}{r}+\frac{\Lambda}{r}-1}\right) - \left(\frac{V_w}{\nu_d}\right)^2} \tag{D.26}$$

Appendix E

Exponential growth in a vertical water column split at the critical depth

Expressed in terms of scaled variables this problem consists of two advection-diffusion equations, one for the region below the critical depth of the system

$$\frac{\partial n}{\partial t} = n - 2v_z \frac{\partial n}{\partial z_+} + \frac{\partial^2 n}{\partial z_+^2} \tag{E.1}$$

and one for the surface region between the critical depth and the water surface

$$\frac{\partial n}{\partial t} = \frac{\Lambda_{sr}}{\Lambda_{br}} n - 2v_z \frac{\partial n}{\partial z_+} + \frac{\partial^2 n}{\partial z_+^2} \tag{E.2}$$

On substituting trial solutions of the form

$$\begin{aligned} n &= e^{\lambda_z t} f(z_+) \quad \text{for } z_+ \text{ below the critical depth} \\ n &= e^{\lambda_z t} g(z_+) \quad \text{for } z_+ \text{ above the critical depth} \end{aligned} \tag{E.3}$$

these equations become the following O.D.E.s

$$0 = (1 - \lambda_z)f - 2v_z\frac{df}{dz_+} + \frac{d^2f}{dz_+^2} \tag{E.4}$$

and

$$0 = (\frac{\Lambda_{sr}}{\Lambda_{br}} - \lambda_z)g - 2v_z\frac{dg}{dz_+} + \frac{d^2g}{dz_+^2} \tag{E.5}$$

These are both second-order ordinary differential equations with constant coefficients, which have the general solution

$$\begin{aligned} f(z_+) &= Ae^{\gamma_1 z_+} + Be^{\gamma_2 z_+} \\ g(z_+) &= Ce^{\gamma_3 z_+} + Ee^{\gamma_4 z_+} \end{aligned} \tag{E.6}$$

where A, B, C, D are arbitrary constants and the γs are given by the roots of the auxiliary equations

$$\begin{aligned} \gamma^2 - 2v_z\gamma + (1 - \lambda_z) &= 0 \quad for \quad f(z_+) \\ \gamma^2 - 2v_z\gamma + (\frac{\Lambda_{sr}}{\Lambda_{br}} - \lambda_z) &= 0 \quad for \quad g(z_+) \end{aligned} \tag{E.7}$$

that is

$$\gamma_1 = v_z - \psi, \quad \gamma_2 = v_z + \psi \tag{E.8}$$

where $\psi \equiv \sqrt{v_z^2 + \lambda_z - 1}$ and

$$\gamma_3 = v_z - \psi_2, \quad \gamma_4 = v_z + \psi_2 \tag{E.9}$$

where $\psi_2 \equiv \sqrt{v_z^2 + \lambda_z - \frac{\Lambda_{sr}}{\Lambda_{br}}}$.

As outlined in the main text boundary conditions are two for zero flux, one at the river bed

$$2v_z f(0) - \left.\frac{df}{dz_+}\right|_{z_+=0} = 0 \tag{E.10}$$

where z_+ is a scaled distance defined positive upwards from the bed and with origin at the bed, and zero flux at the water surface

$$2v_z g(h) - \left.\frac{dg}{dz_+}\right|_{z_+=h} = 0 \tag{E.11}$$

where h is the scaled total water depth. At the critical depth, $z_+ = l_c \equiv (H - z_c)/\sqrt{\Phi_z \Lambda_{br}^{-1}}$, are two conditions. Firstly a requirement that the curve defining population density along the domain be continuous

$$\begin{aligned} e^{\lambda_z t} f(l_c) &= e^{\lambda_z t} g(l_c) \\ f(l_c) &= g(l_c) \end{aligned} \tag{E.12}$$

Secondly that there is a continuous population flux

$$2v_z f(l_c) - \left.\frac{df}{dz_+}\right|_{z_+=l_c} = 2v_z g(l_c) - \left.\frac{dg}{dz_+}\right|_{z_+=l_c} \tag{E.13}$$

which, because of the requirement of Equation (E.12) and the fact $2v_z$ is constant leads to

$$\left.\frac{df}{dz_+}\right|_{z_+=l_c} = \left.\frac{dg}{dz_+}\right|_{z_+=l_c} \tag{E.14}$$

E.1 High velocity case

If $v_z \equiv V_z/2\sqrt{\Phi_z \Lambda_{br}}$ is sufficiently large that $v_z^2 > 1 - \lambda_z$ and $v_z^2 > \Lambda_{sr}/\Lambda_{br} - \lambda_z$ then the γs and ψs are real. Substituting the general form of solution for $f(z_+)$ and $g(z_+)$ into the boundary conditions gives

$$\frac{-A}{B} = \frac{v_z - \psi}{v_z + \psi} \tag{E.15}$$

$$\frac{-Ce^{\gamma_3 h}}{Ee^{\gamma_4 h}} = \frac{v_z - \psi_2}{v_z + \psi_2} \tag{E.16}$$

$$Ae^{\gamma_1 l_c} + Be^{\gamma_2 l_c} = Ce^{\gamma_3 l_c} + Ee^{\gamma_4 l_c} \tag{E.17}$$

and

$$A\gamma_1 e^{\gamma_1 l_c} + B\gamma_2 e^{\gamma_2 l_c} = C\gamma_3 e^{\gamma_3 l_c} + E\gamma_4 e^{\gamma_4 l_c} \tag{E.18}$$

Relating the three boundary conditions

Re-arranging Equation (E.15) we obtain

$$A = -B\frac{\gamma_1}{\gamma_2} \tag{E.19}$$

Re-arranging Equation (E.16) we obtain

$$C = -E\frac{e^{\gamma_4 h}}{e^{\gamma_3 h}}\frac{\gamma_3}{\gamma_4} \tag{E.20}$$

Substituting the results from Equations (E.19) and (E.20) into Equation (E.18) we obtain

$$\begin{aligned} -B\frac{\gamma_1}{\gamma_2}\gamma_1 e^{\gamma_1 l_c} + B\gamma_2 e^{\gamma_2 l_c} &= -E\frac{e^{\gamma_4 h}}{e^{\gamma_3 h}}\frac{\gamma_3}{\gamma_4}\gamma_3 e^{\gamma_3 l_c} + E\gamma_4 e^{\gamma_4 l_c} \\ \frac{B}{\gamma_2}[\gamma_2^2 e^{\gamma_2 l_c} - \gamma_1^2 e^{\gamma_1 l_c}] &= \frac{E}{\gamma_4}\left[\gamma_4^2 e^{\gamma_4 l_c} - \frac{e^{\gamma_4 h}}{e^{\gamma_3 h}}\gamma_3^2 e^{\gamma_3 l_c}\right] \end{aligned} \tag{E.21}$$

Considering the first of the boundary conditions at the critical depth, (Equation E.17), provides

$$\frac{-A}{B} = \frac{1}{e^{\gamma_1 l_c}}\left[e^{\gamma_2 l_c} - \frac{C}{B}e^{\gamma_3 l_c} - \frac{E}{B}e^{\gamma_4 l_c}\right] \tag{E.22}$$

Substituting for C from Equation (E.20) and for B from Equation (E.21) into the above leads to

$$\begin{aligned} \frac{-A}{B} &= \frac{1}{e^{\gamma_1 l_c}}\left[e^{\gamma_2 l_c} + e^{\gamma_3 l_c} \times \frac{Ee^{\gamma_4 h}\gamma_3}{e^{\gamma_3 h}\gamma_4} \times \frac{\gamma_4\left[\gamma_2^2 e^{\gamma_2 l_c} - \gamma_1^2 e^{\gamma_1 l_c}\right]}{E\gamma_2\left[\gamma_4^2 e^{\gamma_4 l_c} - \frac{e^{\gamma_4 h}}{e^{\gamma_3 h}}\gamma_3^2 e^{\gamma_3 l_c}\right]}\right. \\ &\quad \left. -Ee^{\gamma_4 l_c} \times \frac{\gamma_4\left[\gamma_2^2 e^{\gamma_2 l_c} - \gamma_1^2 e^{\gamma_1 l_c}\right]}{E\gamma_2\left[\gamma_4^2 e^{\gamma_4 l_c} - \frac{e^{\gamma_4 h}}{e^{\gamma_3 h}}\gamma_3^2 e^{\gamma_3 l_c}\right]}\right] \\ \frac{-A}{B} &= e^{2\psi l_c} + \frac{1}{e^{\gamma_1 l_c}}\left[e^{2\psi_2 h}e^{\gamma_3 l_c} \times \frac{v_z - \psi_2}{v_z + \psi} \times \frac{\left[\gamma_2^2 e^{\gamma_2 l_c} - \gamma_1^2 e^{\gamma_1 l_c}\right]}{\left[\gamma_4^2 e^{\gamma_4 l_c} - e^{2\psi_2 h}\gamma_3^2 e^{\gamma_3 l_c}\right]}\right. \\ &\quad \left. -e^{\gamma_4 l_c} \times \frac{v_z + \psi_2}{v_z + \psi} \times \frac{\left[\gamma_2^2 e^{\gamma_2 l_c} - \gamma_1^2 e^{\gamma_1 l_c}\right]}{\left[\gamma_4^2 e^{\gamma_4 l_c} - e^{2\psi_2 h}\gamma_3^2 e^{\gamma_3 l_c}\right]}\right] \\ \frac{-A}{B} &= e^{2\psi l_c} + e^{2\psi_2 h} \times \frac{v_z - \psi_2}{v_z + \psi} \times \frac{\left[\gamma_2^2 e^{2\psi l_c} - \gamma_1^2\right]}{\left[\gamma_4^2 e^{2\psi_2 l_c} - e^{2\psi_2 h}\gamma_3^2\right]} \\ &\quad - \frac{v_z + \psi_2}{v_z + \psi} \times \frac{\left[\gamma_2^2 e^{2\psi l_c} - \gamma_1^2\right]}{\left[\gamma_4^2 - e^{2\psi_2 h}\gamma_3^2 e^{-2\psi_2 l_c}\right]} \\ \frac{-A}{B} &= e^{2\psi l_c} + \frac{\left[\gamma_2^2 e^{2\psi l_c} - \gamma_1^2\right]}{\left[\gamma_4^2 - e^{2\psi_2 h}\gamma_3^2 e^{-2\psi_2 l_c}\right]} \times \left[\frac{v_z - \psi_2}{v_z + \psi}\frac{e^{-2\psi_2 h}}{e^{-2\psi_2 l_c}} - \frac{v_z + \psi_2}{v_z + \psi}\right] \\ \frac{-A}{B} &= e^{2\psi l_c} + \frac{1}{v_z + \psi} \times \frac{\left[(v_z + \psi)^2 e^{2\psi l_c} - (v_z - \psi)^2\right]}{\left[(v_z + \psi_2)^2 - e^{2\psi_2(h - l_c)}(v_z - \psi_2)^2\right]} \times \\ &\quad \left[e^{2\psi_2(h - l_c)}(v_z - \psi_2) - (v_z + \psi_2)\right] \end{aligned} \tag{E.23}$$

Equation (E.23) is a modified form of the equation stating that the population density at $z_+ = l_c$ is continuous that only involves the constants of integration A and B. The boundary conditions at $z_+ = 0$ and $z_+ = h$ and the condition that the flux of population is a continuous function at $z_+ = l_c$ were used to form the relationships between the constants of integration that allowed elimination of the constants C and D. For a given domain and flow conditions the right hand side of Equation (E.23) consists of known quantities except for λ_z, (contained within ψ and ψ_2). Therefore, a solution that satisfies all the boundary conditions has been found if a value of λ_z can be found which allows the right hand side of Equation (E.23) to equal the right hand side of Equation (E.15). That is if

$$\begin{aligned}\frac{v_z - \psi}{v_z + \psi} &= e^{2\psi l_c} + \frac{1}{v_z + \psi} \times \frac{\left[(v_z + \psi)^2 e^{2\psi l_c} - (v_z - \psi)^2\right]}{\left[(v_z + \psi_2)^2 - e^{2\psi_2(h-l_c)}(v_z - \psi_2)^2\right]} \\ &\quad \times \left[e^{2\psi_2(h-l_c)}(v_z - \psi_2) - (v_z + \psi_2)\right] \end{aligned} \tag{E.24}$$

Check on validity of Equation (E.24)

Considering the region of the water column from the bed to the critical depth, the difference in the solution to the current problem and the one described in Appendix A is that a local per capita growth rate of Λ_{br} replaces the intrinsic growth rate r and the region beyond the critical depth is not assumed to have an infinitely large negative per-capita growth rate. If the assumed growth rate for the upper layer is set to $-\infty$ and Λ_{br} replaced by r then Equation (E.24) should collapse back to the same form found in Appendix A, namely

$$\frac{v_z - \psi}{v_z + \psi} = e^{2\psi l_c} \tag{E.25}$$

where v_z is the equivalent of ν and l_c the equivalent of l of the original equation.

Substituting dimensional terms into the expression for ψ as currently defined gives

$$\psi = \sqrt{\left(\frac{V_z}{2\sqrt{\Phi_z \Lambda_{br}}}\right)^2 + \frac{\Lambda_z}{\Lambda_{br}} - 1} \tag{E.26}$$

On replacing Λ_{br} with r this becomes the direct equivalent of the expression in Appendix A, remembering that V_x and V_z are just any velocity defined positive in the direction of X, Z_+ increasing. Therefore the left hand side and the first term on the right hand side of Equation (E.24) is directly equivalent to the condition found in Appendix A. What remains is to show that the remainder of Equation (E.24) reduces to zero.

The terms v_z, ψ and $e^{2\psi l_c}$ are all finite. Therefore, except when $\psi = -v_z$, the expression

$$\frac{\left[(v_z + \psi)^2 e^{2\psi l_c} - (v_z - \psi)^2\right]}{v_z + \psi}$$

is always finite. For the exceptional case when $\psi = -v_z$, consideration of Equation (E.26) shows this would require $\Lambda_z = r$. The only way this could occur would be if there were no losses at the absorbing boundary, and this in turn would require an infinitely large sinking velocity. The above expression is multiplied by the expression

$$\frac{\left[e^{2\psi_2(h-l_c)}(v_z - \psi_2) - (v_z + \psi_2)\right]}{\left[(v_z + \psi_2)^2 - e^{2\psi_2(h-l_c)}(v_z - \psi_2)^2\right]}$$

which we can label Ψ. On setting $\Lambda_{br} = r$ and $\Lambda_{sr} = -\infty$ the term ψ_2 becomes

$$\begin{aligned} \psi_2 &= \sqrt{\left(\frac{V_z}{2\sqrt{\Phi_z r}}\right)^2 + \frac{\Lambda_z}{r} - \frac{(-\infty)}{r}} \\ \psi_2 &= \infty \end{aligned} \tag{E.27}$$

As $\psi_2 \to \infty$ then

$$\begin{aligned}
\lim_{\psi_2 \to \infty} \Psi &= \frac{\left[e^{\psi_2}(-\psi_2) - (\psi_2)\right]}{[(\psi_2)^2 - e^{\psi_2}(-\psi_2)^2]} \\
\lim_{\psi_2 \to \infty} \Psi &= \frac{-\psi_2(e^{\psi_2}+1)}{-\psi_2^2(e^{\psi_2}-1)} \\
\lim_{\psi_2 \to \infty} \Psi &= \frac{1}{\psi_2} \\
\lim_{\psi_2 \to \infty} \Psi &= 0
\end{aligned} \tag{E.28}$$

E.2 Low velocity case

As stated earlier, for the γs and ψs to be real requires $v_z^2 > 1 - \lambda_z$ and $v_z^2 > \Lambda_{sr}/\Lambda_{br} - \lambda_z$. As this work involves finding the maximum value of Φ_z that allows λ_z to remain non-negative it is useful to restrict considerations to those involving non-negative values of λ_z. The problem can be further restricted by only considering systems that contain a critical depth, such that Λ_{sr} is always negative. As Λ_{br} is always positive then $v_z^2 > \Lambda_{sr}/\Lambda_{br} - \lambda_z$ is guaranteed. For the systems under consideration, the roots γ_3 and γ_4 will always be real.

In contrast it is possible, for systems of interest, for the inequality $v_z^2 > 1 - \lambda_z$ to fail, in particular, when $\lambda_z = 0$ and $|V_z| < 2\sqrt{\Phi_z \Lambda_{br}}$. In these instances the roots γ_1 and γ_2 become complex conjugates and the roots can be written as

$$\begin{aligned}
\gamma_1 &= \xi - ki \\
\gamma_2 &= \xi + ki
\end{aligned}$$

where $\xi \equiv v_z$ and $k \equiv \sqrt{1 - \lambda_z - v_z^2}$. The general solution of $f(z_+)$ in the lower region of the domain can then be written as

$$f(z_+) = Ae^{\xi z_+}\cos(kz_+) + Be^{\xi z_+}\sin(kz_+) \tag{E.29}$$

If this new form of the general solution is substituted into the boundary condition of Equation (E.10) we obtain

$$\begin{aligned} 2v_z(Ae^{\xi 0}\cos k0 + Be^{\xi 0}\sin k0) & \\ -(A[e^{\xi 0}\times -k\sin k0 + \cos k0 \times \xi e^{\xi 0}] & \\ +B[e^{\xi 0}\times k\cos k0 + \sin k0 \times \xi e^{\xi 0}]) &= 0 \\ 2v_z A - v_z A - kB &= 0 \\ \frac{A}{B} &= \frac{k}{v_z} \end{aligned} \tag{E.30}$$

The boundary conditions at $z_+ = l_c$ expressed by Equations (E.12) and (E.14) now have the form

$$Ae^{\xi l_c}\cos kl_c + Be^{\xi l_c}\sin kl_c = Ce^{\gamma_3 l_c} + Ee^{\gamma_4 l_c} \tag{E.31}$$

and

$$\begin{aligned} A[v_z e^{v_z l_c}\cos kl_c - ke^{v_z l_c}\sin kl_c] & \\ +B[v_z e^{v_z l_c}\sin kl_c + ke^{v_z l_c}\cos kl_c] &= C\gamma_3 e^{\gamma_3 l_c} + E\gamma_4 e^{\gamma_4 l_c} \end{aligned} \tag{E.32}$$

Using the results from Equation (E.30) and from Equation (E.20) to back-substitute into Equation (E.32) the relationship between the constants of integration B and E now becomes

$$Be^{v_z l_c}\left[2k\cos kl_c + \frac{v_z^2 - k^2}{v_z}\sin kl_c\right] = \frac{E}{\gamma_4}\left[\gamma_4^2 e^{\gamma_4 l_c} - \frac{e^{\gamma_4 h}}{e^{\gamma_3 h}}\gamma_3^2 e^{\gamma_3 l_c}\right] \tag{E.33}$$

Considering again the condition for the population density to be a continuous function of depth and solving to obtain $-A/B$ again gives

$$
\begin{aligned}
-Ae^{\xi l_c}\cos kl_c &= Be^{\xi l_c}\sin kl_c - Ce^{\gamma_3 l_c} - Ee^{\gamma_4 l_c} \\
-\frac{A}{B} &= \frac{1}{e^{\xi l_c}\cos kl_c}\left[e^{\xi l_c}\sin kl_c - \frac{C}{B}e^{\gamma_3 l_c} - \frac{E}{B}e^{\gamma_4 l_c}\right] \qquad \text{(E.34)}
\end{aligned}
$$

Substituting for C from Equation (E.20) and for B from Equation (E.33) gives

$$
\begin{aligned}
-\frac{A}{B} &= \frac{1}{e^{\xi l_c}\cos kl_c}\left[e^{\xi l_c}\sin kl_c + \frac{e^{\gamma_3 l_c}}{B}\times\frac{Ee^{\gamma_4 h}\gamma_3}{e^{\gamma_3 h}\gamma_4} - \frac{E}{B}e^{\gamma_4 l_c}\right] \\
-\frac{A}{B} &= \frac{1}{e^{v_z l_c}\cos kl_c}\left[e^{v_z l_c}\sin kl_c + e^{\gamma_3 l_c}\times\frac{Ee^{\gamma_4 h}\gamma_3}{e^{\gamma_3 h}\gamma_4}\times\frac{\gamma_4 e^{v_z l_c}\left[2k\cos kl_c + \frac{v_z^2-k^2}{v_z}\sin kl_c\right]}{E\left[\gamma_4^2 e^{\gamma_4 l_c} - \frac{e^{\gamma_4 h}}{e^{\gamma_3 h}}\gamma_3^2 e^{\gamma_3 l_c}\right]}\right. \\
&\quad \left. -e^{\gamma_4 l_c}E\times\frac{\gamma_4 e^{v_z l_c}\left[2k\cos kl_c + \frac{v_z^2-k^2}{v_z}\sin kl_c\right]}{E\left[\gamma_4^2 e^{\gamma_4 l_c} - \frac{e^{\gamma_4 h}}{e^{\gamma_3 h}}\gamma_3^2 e^{\gamma_3 l_c}\right]}\right] \\
-\frac{A}{B} &= \tan kl_c + \left[2k + \frac{v_z^2-k^2}{v_z}\tan kl_c\right]\left[\gamma_3 e^{2\psi_2 h}\times\frac{1}{[\gamma_4^2 e^{2\psi_2 l_c} - e^{2\psi_2 h}\gamma_3^2]}\right. \\
&\quad \left. -\gamma_4\times\frac{1}{[\gamma_4^2 - e^{2\psi_2 h}e^{-2\psi_2 l_c}\gamma_3^2]}\right] \\
-\frac{A}{B} &= \tan kl_c + \frac{\left[2k + \frac{v_z^2-k^2}{v_z}\tan kl_c\right]}{[\gamma_4^2 - e^{2\psi_2(h-l_c)}\gamma_3^2]}\left[\gamma_3 e^{2\psi_2(h-l_c)} - \gamma_4\right] \qquad \text{(E.35)}
\end{aligned}
$$

Substituting for γ_3 and γ_4 gives a final relationship of

$$
\begin{aligned}
-\frac{A}{B} &= \qquad \text{(E.36)} \\
&\tan kl_c + \frac{\left[2k + \frac{v_z^2-k^2}{v_z}\tan kl_c\right]}{[(v_z+\psi_2)^2 - e^{2\psi_2(h-l_c)}(v_z-\psi_2)^2]}\left[(v_z-\psi_2)e^{2\psi_2(h-l_c)} - (v_z+\psi_2)\right]
\end{aligned}
$$

So, via the same arguments used for the case with higher absolute values of v_z, we know a solution has been obtained that satisfies all boundary conditions if

$$
\begin{aligned}
-\frac{k}{v_z} &= \tan kl_c + \frac{\left[2k + \frac{v_z^2-k^2}{v_z}\tan kl_c\right]}{[(v_z+\psi_2)^2 - e^{2\psi_2(h-l_c)}(v_z-\psi_2)^2]} \\
&\quad \times\left[(v_z-\psi_2)e^{2\psi_2(h-l_c)} - (v_z+\psi_2)\right] \qquad \text{(E.37)}
\end{aligned}
$$

Check on validity of Equation (E.37)

As for the case with higher absolute advection, we set $\Lambda_{br} = r$ and $\Lambda_{sr} = -\infty$ to see if Equation (E.37) reduces to an equivalent form of the condition for solutions as that found for the problem of a domain with local per-capita growth rate equalling r and an absorbing boundary, as described in Appendix A, with in this case the absorbing boundary at $z_+ = l_c$. The term v_z obtains the same meaning as for the higher velocity case which has already shown it to be equivalent to the term ν used in Appendix A. With $v_z \equiv \nu$ then the term for k here is also equivalent to the same term used in Appendix A. It remains to show that the final term of Equation (E.37) reduces to zero.

The expression previously labelled Ψ is again present in this final term and this will tend to zero as $\Lambda_{sr} \to -\infty$. The remaining expression present is

$$\left[2k + \frac{v_z^2 - k^2}{v_z} \tan kl_c\right]$$

The terms k, v_z and l_c are all finite, meaning the expression is also finite except when $\tan kl_c = \infty$. To deal with this one case Equation (E.37) is re-cast in the form

$$-\frac{k}{v_z} = \frac{\sin kl_c}{\cos kl_c} + \left[2k + \left(\frac{v_z^2 - k^2}{v_z}\right)\frac{\sin kl_c}{\cos kl_c}\right] \times \frac{\left[(v_z - \psi_2)e^{2\psi_2(h-l_c)} - (v_z + \psi_2)\right]}{\left[(v_z + \psi_2)^2 - e^{2\psi_2(h-l_c)}(v_z - \psi_2)^2\right]} \tag{E.38}$$

Multiplying through by $\cos kl_c$ and v_z Equation (E.38) becomes

$$\begin{aligned} -k\cos kl_c \;\; = \;\; & v_z \sin kl_c + \left[2kv_z \cos kl_c + \left(v_z^2 - k^2\right)\sin kl_c\right] \times \\ & \frac{\left[(v_z - \psi_2)e^{2\psi_2(h-l_c)} - (v_z + \psi_2)\right]}{\left[(v_z + \psi_2)^2 - e^{2\psi_2(h-l_c)}(v_z - \psi_2)^2\right]} \end{aligned} \tag{E.39}$$

$\tan(kl_c) = \infty$ when kl_c becomes any odd multiple of $\pi/2$ such that $\cos kl_c = 0$ and $\sin kl_c = \pm 1$. Substituting these values into Equation (E.39) gives

$$
\begin{aligned}
0 &= \pm v_z + \left[0 \pm \left(v_z^2 - k^2\right)\right] \times [0] \\
0 &= v_z
\end{aligned} \tag{E.40}
$$

Therefore, for any value of v_z other than zero the reduction to the condition for a solution of the previous theory has been achieved. The case where v_z is also the case where $\tan(kl_c) = \infty \rightarrow kl_c = j \times \pi/2$ (where j is an odd number). As before, maximum values of λ_z are given by the smallest possible value of kl_c so $kl_c = \pi/2$ is the value of interest. In seeking a critical vertical diffusion coefficient we require $\lambda_z = 0$. With $\lambda_z = 0$ and $v_z = 0$, $k = 1$. This implies that $l_c = \pi/2$. Substituting back in dimensional terms shows that when $v_z = 0$ the critical vertical diffusion coefficient is given by

$$
\frac{(D - z_c)}{\sqrt{\Phi_{zc}\Lambda_{br}^{-1}}} = \frac{(D - z_c)}{\sqrt{\Phi_{zc} r^{-1}}} = \frac{\pi}{2} \tag{E.41}
$$

This is the same relationship for Φ_{zc} found from the one segment equations.

Bibliography

Abraham, G., M. Karelse, and W. B. P. M. Lases (1975). Data requirement for one-dimensional mathematical modelling of salinity intrusion in estuaries. Technical Report 149, Delft Hydraulics Laboratory.

Allan, J. D. (1995). *Stream Ecology: Structure and Function of Running Waters*. Chapman and Hall.

Allan, J. D. and B. P. Feifarek (1989). Distances travelled by drifting mayfly nymphs: factors influencing return to the substrate. *Journal of the North American Benthological Society 8*(4), 322–330.

Allan, J. D., G. N. Herbst, R. Ortal, and Y. Yegev (1988). Invertebrate drift in the dan river, israel. *Hydrobiologia 160*, 155–163.

Allee, W. C. (1931). *Animal Aggregations: A study in general sociology*. University of Chicago Press, Chicago.

Anholt, B. R. (1995). Density dependence resolves the stream drift paradox. *Ecology 76*, 2235–2239.

Beer, T. and P. C. Young (1983). Longitudinal dispersion in natural streams. *Journal of Environmental Engineering, ASCE 109*, 1049–1067.

Bell, M. J. (1997). Vortex stretching and bottom torque in the bryan-cox ocean circulation model. Applications T. N. 17, The Met. Office, U. K., London Road, Bracknell, Berkshire, RG12 2SY, U. K.

Bencala, K. E. and R. A. Walters (1983). Simulation of solute transport in a mountain pool-and-riffle stream: a transient storage model. *Water Resources Research 9*, 718–724.

Bergey, E. A. and J. V. Ward (1989). Upstream-downstream movements of aquatic invertebrates in a rocky mountain stream. *Hydrobiologia 185*, 71–82.

Blumberg, A. F. and G. L. Mellor (1987). A description of a three-dimensional coastal ocean circulation model.three-dimensional coastal ocean models. In N. S. Heaps (Ed.), *Three-Dimensional Coastal Ocean Models*, Volume 4 of *Coastal and Estuarine Sciences*, pp. 1–16. AGU.

Boehlert, G. W. and B. C. Mundy (1988). Roles of behavioral and physical factors in larval and juvenile fish recruitment to estuarine nursery areas. *American Fisheries Society Symposium 3*, 51–67.

Bothwell, M. L., K. E. Suzuki, M. K. Bolin, and H. F. J. (1989). Evidence of dark avoidance by phototrophic periphytic diatoms in lotic systems. *Journal of Phycology 25*, 85–94.

Bowden, K. F. (1967). Stability effects on mixing in tidal currents. *Physics of Fluids Supplement 10*, S278–S280.

Bowden, K. F. and S. H. Sharaf El Din (1966). Circulation, salinity and river discharge in the mersey estuary. *Geophysical Journal of the Royal Astronomical Society 10*, 383–399.

Brittain, J. E. and T. J. Eikeland (1988). Invertebrate drift - a review. *Hydrobiologia 166*, 77–93.

Brown, A. V., J. C. Limbeck, and M. D. Schram (1989). Trophic importance of zooplankton in streams with alluvial riffle and pool geomorphometry. *Archiv für Hydrobiologie 114*(3), 349–367.

Brussock, P. P., A. V. Brown, and J. C. Dixon (1985). Channel form and stream ecosystem models. *Water Research Bulletin 21*, 859–866.

Burchard, H., O. Petersen, and T. P. Rippeth (1998). Comparing the performance of the mellor-yamada and the k-e two-equation turbulence models. *Journal of Geophysical Research 103*(C5), 10543–10554.

Cameron, W. M. and D. W. Pritchard (1963). Estuaries. In M. N. Hill (Ed.), *The Sea*, Volume 2, pp. 306–324. John Wiley and Sons, New York.

Campbell, R. N. B. (1985). Comparison of the drift of live and dead baetis nymphs in a weakening water current. *Hydrobiologia 126*, 229–236.

Chanson, H. (1999). *The Hydraulics of open channel flow: an introduction*. Arnold.

Chapra, S. C. (1997). *Surface Water-Quality Modeling*. McGraw-Hill.

Chen, Y. H., P. T. Shaw, and T. G. Wolcott (1997). Enhancing estuarine retension of planktonic larvae by tidal currents. *Estuarine, Coastal and Shelf Science 45*, 525–533.

Chow, V. T. (1959). *Open-Channel Hydraulics*. McGraw-Hill.

Christy, J. H. (1989). Rapid development of magalopae of the fiddler crab *Uca pugilator* reared over sediment: implications for models of larval recruitment. *Marine Ecology Progress Series 57*, 259–265.

Ciborowski, J. J. H. (1983). Influence of current velocity, density and detritus on drift of two mayfly species. *Canadian Journal of Zoology 61*, 119–125.

Ciborowski, J. J. H. and L. D. Corkum (1980). Importance of behaviour to the re-establishment of drifting textitEphemeroptera. In J. F. Flanagan and K. E. Marshall (Eds.), *Advances in Ephemeroptera Biology*, pp. 321–330. Plenum Press.

Corkum, L. D. (1978). The influence of density and behavioral type on the active entry of two mayfly species (*Ephemeroptera*) into the water column. *Canadian Journal of Zoology 56*, 1201–1206.

Corkum, L. D. and H. F. Clifford (1980). The importance of species associations and substrate types to behavioural drift. In J. F. Flanagan and K. E. Marshall (Eds.), *Advances in Ephemeroptera Biology*, pp. 331–340. Plenum Press.

Corkum, L. D., P. J. Pointing, and J. J. H. Ciborowski (1977). The influence of current velocity and substrate on the distribution and drift of two species

of mayflies (*Ephemeroptera*). *Canadian Journal of Zoology 55*, 1970–1977.

Cox, D. R. and H. D. Miller (1990). *The Theory of Stochastic processes*. Chapman and Hall.

Creutzberg, F. (1961). On the orientation of migrating elvers (*Anguilla vulgaris* turt.) in a tidal area. *Netherlands Journal of Sea Research 1*, 257–338.

Davis, J. A. and L. A. Barmuta (1989). An ecologically useful classification of mean and near-bed flows in streams and rivers. *Freshwater Biology 21*, 271–282.

Degani, G., G. N. Herbst, R. Ortal, H. J. Bromley, D. Levanon, Y. Netzer, N. Harari, and H. Glazman (1993). Relationships between current velocity, depth and the invertebrate community in a stable river system. *Hydrobiologia 263*, 163–172.

Descy, J. P., V. Gosselain, and F. Evrard (1994). Respiration and photosynthesis of river phytoplankton. *Verh. Internat. Verein. Limnol. 25*, 1555–1560.

Descy, J. P., P. Servais, J. S. Smitz, G. Billen, and E. Everbecq (1987). Phytoplankton biomass and production in the river meuse (belgium). *Water Research 21*(12), 1557–1566.

Dobson, M. and C. Frid (1998). *Ecology of Aquatic Systems*. Longman,Harlow.

Dyer, K. R. (1973). *Estuaries: A Physical Introduction*. John Wiley and Sons, New York.

Dyer, K. R. (1974). The salt balance in stratified estuaries. *Estuarine and Coastal Marine Science 2*, 273–281.

Dyer, K. R. (1977). Lateral circulation effects in estuaries. In *Estuaries, Geophysics and the Environment*, pp. 22–29. National Academy of Science.

Dyer, K. R. (1987). Flushing and dispersal mechanisms in estuaries. In P. J. Coughtrey, M. H. Martin, and M. H. Unsworth (Eds.), *Pollutant transport and fate in ecosystems*, pp. 35–45. Blackwell.

Edwards, A. and F. Sharples (1986). Scottish sea lochs: A catalogue. Technical report, Nature Conservancy Council.

Elliott, J. M. (1971a). The distances travelled by drifting invertebrates in a lake district stream. *Oecologia 6*, 350–379.

Elliott, J. M. (1971b). Upstream movements of benthic invertebrates in a lake district stream. *Journal of Animal Ecology 40*, 235–252.

Everbecq, E., V. Gosselain, L. Viroux, and J. P. Descy (2001). Potamon: A dynamic model for predicting phytoplankton composition and biomass in lowland rivers. *Water Research 35*(4), 901–912.

Ferziger, J. H. and M. Peric (1999). *Computational Methods for Fluid Dynamics*. Springer-Verlag,Berlin.

Figueroa, F. L., F. X. Niell, F. G. Figueiras, and M. L. Villarino (1998). Diel migration of phytoplankton and spectral light field in the ria de vigo (nw spain). *Marine Biology 130*, 491–499.

Fischer, H. B. (1967). The mechanics of dispersion in natural streams. *Journal of the Hydraulics Division, Proceedings, ASCE 93*(HY6), 187–216.

Fischer, H. B. (1972). Mass transport mechanisms in partially stratified estuaries. *Journal of Fluid Mechanics 53*, 671–687.

Fischer, H. B. (1976). Mixing and dispersion in estuaries. *Annual Reviews in fluid Mechanics 8*, 107–133.

Fischer, H. B., E. J. List, R. C. Koh, J. Imberger, and N. H. Brooks (1979). *Mixing in Inland and Coastal Waters*. Academic.

Fofonoff, N. P. (1962). Physical properties of sea-water. In *The Sea*, Volume 1, pp. 3–30. Wiley-Interscience.

Fonseca, D. M. and D. D. Hart (1996). Density dependent dispersal of black fly neonates is mediated by flow. *Oikos 75*, 49–56.

Galperin, B. and G. L. Mellor (1990). A time-dependent, three-dimensional model of the delaware bay and river system. part 1: Description of the model and tidal analysis. *Estuarine, Coastal and Shelf Science 31*, 231–253.

Garvine, R. W. (1977). River plumes and estuary fronts. In *Estuaries, Geophysics and the Environment.*, pp. 30–35. National Academy of Sciences, Washington.

Garvine, R. W. (1999). Penetration of buoyant coastal discharge onto the continental shelf: A numerical model experiment. *Journal of Physical Oceanography 29*(part 2), 1892–1909.

Grindley, J. R. (1964). Effect of low salinity water on vertical migration of estuarine plankton. *Nature 203*, 781–782.

Growns, I. O. and J. A. Davis (1994). Longitudinal changes in near-bed flows and macroinvertebrate communities in a western australian stream. *Journal of the North American Benthological Society 13*, 417–438.

Gurney, W. S. C. and R. M. Nisbet (1975). The regulation of inhomogeneous populations. *Journal of Theoretical Biology 52*, 441–457.

Gurney, W. S. C. and R. M. Nisbet (1998). *Ecological Dynamics*. Oxford University Press.

Gurney, W. S. C., D. C. Speirs, S. N. Wood, E. D. Clarke, and M. R. Heath (2001). Simulating spatially and physiologically structured populations. *Journal of Animal Ecology 70*, 881–894.

Hansen, D. V. and M. Rattray (1966). New dimensions in estuary classification. *Journal of Physical Oceanography 11*, 319–325.

Hart, D. D. and V. H. Resh (1980). Movement patterns and foraging ecology of a stream caddisfly larva. *Canadian Journal of Zoology 58*, 1174–1185.

Hayden, W. and H. F. Clifford (1974). Seasonal movements of the mayfly *Leptophlebia cupida* (say) in a brown-water stream in alberta, canada. *Am. Midl. Natur. 91*(1), 90–102.

Hershey, A. E., J. Pastor, B. J. Peterson, and G. W. Kling (1993). Stable isotopes resolve the drift paradox for *Baetis* mayflies in an arctic river. *Ecology 74*, 2315–2325.

Hill, A. E. (1995). The kinematical principles governing horizontal transport induced by vertical migration in tidal flows. *Journal of the Marine Biological Association of the UK 75*, 3–13.

Holley, E. R., D. R. F. Harleman, and H. B. Fischer (1970). Dispersion in homogeneous estuary flow. *Journal of the Hydraulics Division, ASCE 96*(HY8), 1691–1709.

Horne, A. J. and C. R. Goldman (1994). *Limnology*. McGraw-Hill.

Hughes, F. W. and M. Rattray (1980). Salt flux and mixing in the columbia river estuary. *Estuarine and Coastal marine Science 10*, 479–493.

Jager, Z. (1999). Selective tidal stream transport of flounder larvae (*Platichthys flesus* l.) in the dollard (ems estuary). *Estuarine Coastal and Shelf Science 49*, 347–362.

Kantha, L. H. and C. A. Clayson (1994). An improved mixed layer model for geophysical applications. *Journal of Geophysical Research 99*, 25235–25266.

Knighton, D. (1984). *Fluvial Forms and Processes*. Edward Arnold, London.

Kohler, S. L. (1985). Identification of stream drift mechanisms: an experimental and observational approach. *Ecology 66*, 1749–1761.

Kopp, M., J. M. Jeschke, and W. Gabriel (2001). Exact compensation of stream drift as an evolutionarily stable strategy. *Oikos 92*(3), 522–530.

Lancaster, D. and A. G. Hildrew (1993). Characterising in-stream flow refugia. *Canadian journal of Fisheries and Aquatic Sciences 50*, 1663–1675.

Lancaster, D., A. G. Hildrew, and C. Gjerlov (1996). Invertebrate drift and longitudinal transport processes in streams. *Canadian journal of Fisheries and Aquatic Sciences 53*, 572–582.

Lewis, R. E. (1987). Transfer mechanisms for dissolved pollutants in estuaries. In P. J. Coughtrey, M. H. Martin, and M. H. Unsworth (Eds.), *Pollutant Transport and Fate in Ecosystems*, pp. 47–53. Blackwell.

Longuet and M. S. Higgins (1969). On the transport of mass by time-varying ocean currents. *Deep-Sea Research 16*, 431–447.

Madsen, B. L. A. (1968). A comparative ecological investigation of two related mayfly nymphs. *Hydrobiologia 31*, 337–349.

Malmqvist, B. and P. Sjostrom (1987). Stream drift as a consequence of predator disturbance: field and laboratory experiments. *Oecologia 74*, 396–403.

March, J. G., J. P. Benstead, C. M. Pringle, and F. N. Scatena (1998). Migratory drift of larval freshwater shrimps in two tropical streams, puerto rico. *Freshwater Biology 40*, 261–273.

Marchant, R. and H. B. N. Hynes (1981). The distribution and production of *Gammarus pseudolimnaeus* (crustacea, amphipoda) along a reach of the credit river, ontario. *Freshwater Biology 11*, 169–182.

McDowell, D. M. and B. A. O'Connor (1977). *Hydraulic Behaviour of Estuaries*. The Macmillan Press Ltd, London.

McLay, C. (1970). A theory concerning the distance travelled by animals entering the drift of a stream. *Journal of the Fisheries Research Board of Canada 27*, 359–370.

McNair, J. N., J. D. Newbold, and D. D. Hart (1997). Turbulent transport of suspended particles and dispersing benthic organisms: How long to hit bottom? *Journal of Theoretical Biology 188*, 29–52.

McQuivey, R. S. and T. N. Keefer (1974). Simple method for predicting dispersion in streams. *Journal of the Environmental Engineering Division, ASCE 100*(EE4), 997–1011.

Mellor, D. W., S. Hakkinen, T. Ezer, and R. Patchen (1999). A generalization of a sigma coordinate ocean model and an intercomparison of model vertical grids. In P. N. (Ed.), *Ocean Forecasting: Theory and Practice*. Springer-Verlag.

Mellor, G. L. (1996). *Introduction to Physical Oceanography*. Springer-Verlag.

Mellor, G. L. (1998). Users guide for a three-dimensional, primitive equation, numerical ocean model. Technical report, Princeton University, Princeton, NJ 08544-0710.

Mellor, G. L., T. Ezer, and L. Y. Oey (1994). The pressure gradient conundrum of sigma coordinate ocean models. *Journal of Atmospheric and Oceanic Technology 11*, 1126–1134.

Mellor, G. L., L. Y. Oey, and T. Ezer (1998). Sigma coordinate pressure gradient errors and the seamount problem. *Journal of Atmospheric and Oceanic Technology 15*(5), 1122–1131.

Mellor, G. L. and T. Yamada (1982). Development of a turbulence closure model for geophysical fluid problems. *Reviews of Geophysics and Space Physics 20*, 851–875.

Minshall, G. W. and F. V. Winger (1968). The effect of reduction in stream flow on invertebrate drift. *Ecology 49*, 580–582.

Morisawa, M. (1985). *Rivers*. Longman, London.

Müller, K. (1954). Investigations on the organic drift in north swedish streams. Technical Report 34, Institute of Freshwater Research, Drottningholm.

Müller, K. (1982). The colonisation cycle of freshwater insects. *Oecologia 53*, 202–207.

Nultsch, W. and D. P. Hader (1988). Photomovement in motile organisms. *Photochemistry and Photobiology 47*, 837–869.

Nunn, R. H. (1989). *Intermediate Fluid Mechanics*. Hemisphere.

O'Doherty, E. C. (1985). Stream-dwelling copepods: their life history and ecological significance. *Limnology and Oceanography 30*(3), 554–564.

O'Donnell, J. (1993). Surface fronts in estuaries: a review. *Estuaries 16*(1), 12–39.

Oey, L. Y. (1984). On steady salinity distribution and circulation in partially mixed and well mixed estuaries. *Journal of Physical Oceanography 14*, 629–645.

Oey, L. Y., G. L. Mellor, and R. I. Hires (1985a). A three-dimensional simulation of the hudsen-raritan estuary. part i: Description of the model and model simulations. *Journal of Physical Oceanography 15*, 1676–1692.

Oey, L. Y., G. L. Mellor, and R. I. Hires (1985b). A three-dimensional simulation of the hudsen-raritan estuary. part ii: Comparison with observation. *Journal of Physical Oceanography 15*, 1693–1709.

Orlanski, I. (1976). A simple boundary condition for unbounded hyperbolic flows. *Journal of Computational Physics 21*, 251–269.

Peckarsky, B. L. (1980). Predator-prey interactions between stoneflies and mayflies: behavioral observations. *Ecology 61*, 932–943.

Poff, N. L. and J. V. Ward (1991). Drift responces of benthic invertebrates to experimental streamflow variation in a hydrologically stable stream. *Canadian Journal of Fisheries and Aquatic Sciences 48*, 1926–1936.

Pond, S. and G. L. Pickard (1983). *Introductory Dynamical Oceanography*. Butterworth-Heinemann.

Prandle, D. (1982). The vertical structure of tidal currents and other oscillatory flows. *Continental Shelf Research 1*, 191–207.

Reckendorfer, W., H. Keckeis, G. Winkler, and F. Schiemer (1999). Zooplankton abundance in the river danube, austria: the significance of inshore retention. *Freshwater Biology 41* (3), 583–591.

Reynolds, C. S. (1984). *The Ecology of Freshwater Phytoplankton*. Cambridge.

Reynolds, C. S. (1994a). *Algae and the aquatic environment*, Chapter Potamoplankton: paradigms, paradoxes and prognoses., pp. 285–311. Biopress, Bristol.

Reynolds, C. S. (1994b). *Aquatic Ecology*, Chapter The role of fluid motion in the dynamics of phytoplankton in lakes and rivers, pp. 141–187. Blackwell Science, Oxford.

Reynolds, C. S., P. A. Carling, and K. Beven (1991). Flow in river channels: new insights into hydraulic retention. *Archiv für Hydrobiologie 121*, 171–179.

Reynolds, C. S. and M. S. Glaister (1993). Spatial and temporal changes in phytoplankton abundance in the upper and middle reaches of the river

severn. *Archiv für Hydrobiologie suppl 101*(9), 1–22.

Richards, S. A. (1996). *Mathematical Models of Zooplankton Dispersal*. Ph. D. thesis, The University of Adelaide.

Robertson, A. L., J. Lancaster, and A. G. Hildrew (1995). Stream hydraulics and the distribution of microcrustacea: a role for refugia? *Freshwater Biology 33*, 469–484.

Saunders, J. F. and W. M. Lewis (1988). Zooplankton abundance and transport in a tropical white-water river. *Hydrobiologia 162*, 147–155.

Saunders, J. F. and W. M. Lewis (1989). Zooplankton abundance in the lower orinoco river, venezuela. *Limnology and Oceanography 34*, 397–409.

Skellam, J. G. (1951). Random dispersal in theoretical populations. *Biometrika 38*, 196–218.

Smagorinsky, J. (1963). General circulation experiments with the primitive equations, i. the basic experiment. *Monthly Weather Review 91*, 99–164.

Smith, I. R. (1975). Turbulence in lakes and rivers. Technical Report 29, Freshwater Biological Association.

Smith, I. R. (1982). A simple theory of algal deposition. *Freshwater Biology 12*, 445–449.

Speirs, D. C. and W. S. C. Gurney (2001). Population persistence in rivers and estuaries. *Ecology 82*(5), 1219–1237.

Statzner, B., J. A. Gore, and V. H. Resh (1988). Hydraulic stream ecology: observed patterns and potential applications. *Journal of the North American Benthological Society 7*(4), 307–360.

Sverdrup, H. U. (1953). On conditions of vernal blooming of phytoplankton. *Journal du Conseil. Conseil Permanent International pour l'Exploration de la Mer 18*, 287–295.

Swale, E. M. F. (1963). Notes on *Stephanodiscus hantzschii* grun. in culture. *Arch. Microbiol. 45*, 210–216.

Syvitski, J. P. M., D. C. Burrell, and J. M. Skei (1987). *Fjords; Processes and Products*. Springer-Verlag.

Tritton, D. J. (1988). *Physical Fluid Dynamics*. Oxford.

Vannote, R. L., G. W. Minshall, K. W. Cummins, J. R. Sedell, and C. E. Cushing (1980). The river continuum concept. *Canadian Journal of fisheries and Aquatic Science 37*, 130–137.

Wallis, S. G., P. C. Young, and K. J. Beven (1989). Experimental investigation of the aggregated dead zone model for longitudinal solute transport in stream channels. *Proceedings of the Institution of Civil Engineers, Part 2 87*, 1–22.

Waters, T. F. (1972). The drift of stream insects. *Annual review of Entomology 17*, 253–272.

Waters, T. F. (1981). Seasonal patterns in production and drift of *Gammarus pseudolimnaeus* in valley creek, minnesota. *Ecology 62*, 1458–1466.

West, J. R. and J. S. Mangat (1986). The determination and prediction of longitudinal dispersion coefficients in a narrow, shallow estuary. *Estuarine, Coastal and Shelf Science 22*, 161–181.

Williams, D. D. and N. E. Williams (1993). The upstream/downstream movement paradox of lotic invertebrates: quantitative evidence from a welsh mountain stream. *Freshwater Biology 30*, 199–218.

Wilzbach, M. A. (1990). Nonconcordance of drift and benthic activity in *Baetis*. *Limnology and Oceanography 35*(4), 945–952.

Winterwerp, J. C. (1983). Decomposition of the mass transport in narrow estuaries. *Estuarine, Coastal and Shelf Science 16*, 627–638.

Wolf, P. d. (1973). Ecological observations on the mechanisms of dispersal of barnacle larvae during planktonic life and settling. *Netherlands journal of Sea Research 6*, 1–29.